THE JOURNAL OF

PHYSICAL

CHEMISTRY

THE JOURNAL OF
PHYSICAL CHEMISTRY

Published biweekly by the American
Chemical Society at 20th and Northampton
Sts., Easton, Pennsylvania 18042. Second
class postage paid at Washington, D.C. and
at additional mailing offices.

Editorial Information

Instructions for authors are printed in
the first issue of each volume. Please conform
to these instructions when submitting man-
uscripts.

Manuscripts for publication should be
submitted to *The Journal of Physical
Chemistry*, Department of Chemistry, Uni-
versity of Minnesota. Minneapolis. Minn.
55455. Correspondence regarding **accepted
papers and proofs** should be directed to the

Editorial Department at the ACS Easton
address.

Page charges of $60.00 per page are as-
sessed for papers published in this journal.
Ability to pay does not affect acceptance or
scheduling of papers.

Bulk reprints or photocopies of indi-
vidual articles are available. For information
write to Business Operations. Books and
Journals Division at the ACS Washington
address.

Requests for **permission to reprint**
should be directed to Permissions, Books and
Journals Division at the ACS Washington
address. The American Chemical Society and
its Editors assume no responsibility for the
statements and opinions advanced by con-
tributors.

Subscription and Business Information

1977 Subscription rates—including surface
postage

	U.S.	PUAS	Canada. Foreign
Member	$24.00	$33.00	$34.00
Nonmember	96.00	105.00	106.00
Supplementary material	15.00	19.00	20.00

Air mail and air freight rates are avail-
able from Membership & Subscription Ser-
vices, at the ACS Columbus address.

New and renewal subscriptions should
be sent with payment to the Office of the
Controller at the ACS Washington address.
Changes of address must include both old
and new addresses with ZIP code and a recent
mailing label. Send all address changes to the
ACS Columbus address. Please allow six
weeks for change to become effective. **Claims
for missing numbers** will not be allowed if
loss was due to failure of notice of change of
address to be received in the time specified:

if claim is dated (a) North America—more
than 90 days beyond issue date, (b) all other
foreign—more than 1 year beyond issue date;
or if the reason given is "missing from files".
Hard copy claims are handled at the ACS
Columbus address.

Microfiche subscriptions are available
at the same rates but are mailed first class to
U.S. subscribers, air mail to the rest of the
world. Direct all inquiries to Special Issues
Sales, at the ACS Washington address or call
(202) 872-4554. **Single issues** in hard copy
and/or microfiche are available from Special
Issues Sales at the ACS Washington address.
Current year $4.75. Back issue rates available
from Special Issues Sales. **Back volumes** are
available in hard copy and/or microform.
Write to Special Issues Sales at the ACS
Washington address for further information.
Microfilm editions of ACS periodical pub-
lications are available from volume 1 to the
present. For further nformation, contact
Special Issues Sales at the ACS Washington
address. **Supplementary material** men-
tioned in the journal appears in the microfilm
edition. Single copies may be ordered directly
from Business Operations, Books and Jour-
nals Division, at the ACS Washington ad-
dress.

	U.S.	PUAS, Canada	Other Foreign
Microfiche	$2.50	$3.00	$3.50
Photocopy			
1-7 pages	4.00	5.50	7.00
8-20 pages	5.00	6.50	8.00

Orders over 20 pages are available only on
microfiche, 4 × 6 in., 24X, negative, silver
halide. Orders must state photocopy or mi-
crofiche if both are available. Full biblio-
graphic citation including names of all au-
thors and prepayment are required. Prices
are subject to change.

Notice to Authors printed in this issue

COMMUNICATIONS TO THE EDITOR

■ Supplementary and/or miniprint material for this paper is available separately (consult
the masthead page for ordering information); it will also appear following the paper in the
microfilm edition of this journal.

* In papers with more than one author, the asterisk indicates the name of the author to
whom inquiries about the paper should be addressed.

AUTHOR INDEX

NOTICE TO AUTHORS

I. General Considerations

The Journal of Physical Chemistry is devoted to reporting both experimental and theoretical research dealing with fundamental aspects of physical chemistry. Space limitations necessitate giving preference to research articles dealing with previously unanswered basic questions in physical chemistry. Acceptable topics are those of general interest to physical chemists, especially work involving new concepts, techniques, and interpretations. Research that may lead to reexaminations of generally accepted views is, of course, welcome.

Authors reporting data should include an interpretation of the data and its relevance to the theories of the properties of matter. However, the discussion should be concise and to the point and excessive speculation is to be discouraged. Papers reporting redeterminations of existing data will be acceptable only if there is reasonable justification for repetition: for example, if the more recent or more accurate data lead to new questions or to a reexamination of well known theories. Manuscripts that are essentially applications of chemical data or reviews of the literature are, in general, not suitable for publication in *The Journal of Physical Chemistry*. Detailed comparisons of methods of data analysis will be considered only if the paper also contains original data, or if such comparison leads to a genesis of new ideas.

Authors should include an introductory statement outlining the scientific rationale for the research. The statement should clearly specify the questions for which answers are sought and the connection of the present work with previous work in the field. All manuscripts are subject to critical review. It is to be understood that the final decision relating to a manuscript's suitability rests solely with the editors.

Symposium papers are sometimes published as a group, but only after special arrangement with the editor.

II. Types of Manuscripts

The Journal of Physical Chemistry publishes two types of manuscripts: *Articles* and *Communications*.

A. *Articles* should cover their subjects with thoroughness, clarity, and completeness. However, authors should also strive to make their *Articles* as concise as possible, avoiding unnecessary historical background. Abstracts to *Articles* should be brief—300 words is a maximum—and should serve to summarize the significant data and conclusions. The abstract should convey the essence of the *Article* to the reader.

B. *Communications* are of two types, *Letters* and *Comments*. Both types are restricted to three-quarters of a page (750 words or the equivalent) including tables, figures, and text, and both types of *Communications* are subject to critical review, but special efforts will be made to expedite publication. Communications should be accompanied by an abstract (on a separate sheet of paper).

Letters should report preliminary results whose immediate availability to the scientific community is deemed important, and whose topic is timely enough to justify the double publication that usually results from the publication of a *Letter*.

Comments include significant remarks on the work of others. The editors will generally permit the authors of the work being discussed to reply.

The category of *Notes* has been discontinued since the handling of such manuscripts was precisely the same as that of *Articles* save for the requirement of an Abstract, and since even a short *Article* now needs an Abstract it seems as well to ask the author to provide this. Short *Articles* will of course continue to be welcome contributions.

III. Introduction

All manuscripts submitted should contain brief introductory remarks describing the purpose of the work and giving sufficient background material to allow the reader to appreciate the state-of-knowledge at the time when the work was done. The introductory remarks in an *Article* should constitute the first section of the paper and should be labeled accordingly. In *Communications*, the introductory material should not be in such a separate section. To judge the appropriateness of the manuscript for *The Journal of Physical Chemistry*, the editors will place considerable weight on the author's intentions as stated in the Introduction.

IV. Microform Material

From time to time manuscripts involve extensive tables, graphs, spectra, mathematical derivations, expanded discussions of peripheral points, or other material which, though essential to the specialized reader who needs all the data or all the detail, does not help and often hinders the effective presentation of the work being reported. Such "microform material" can be included in the *microfilm* edition of this Journal, available in many scholarly libraries, and also in the *microfiche* edition. In some instances the microform material may *also* be included in the printed issue as *miniprint*, in which the manuscript pages are reproduced directly in reduced size. All microform material may be obtained directly by the interested reader at nominal cost, either in full size photocopy or in microfiche (in which miniprint material appears at standard reduction, i.e., one manuscript page per microfiche frame). Authors are encouraged to make use of this resource, in the interest of shorter articles (which mean more rapid publication) and clearer more readable presentation.

Microform material should accompany a manuscript at the time of its original submission to an editor. It should be clipped together and attached at the end of the manuscript, along with a slip of paper clearly indicating the material is "microform material". Copy for microform material should preferably be 22 × 28 cm, and in no case on sheets larger than 28 × 43 cm; if typed it should be one and one-half spaced, and in any event the smallest character should be at least 3.5 mm in size; good contrast of black characters against a white background is required for clear photoprocess reproduction (glossies are not suitable for microfilm processing). A duplicate copy is required for indexing purposes.

A paragraph should appear at the end of the paper indicating the nature of the material and the means by which the interested reader may obtain copies directly. The following is an example.

Supplementary Material Available: description of the material (no. of pages). Ordering information is given on any current masthead page.

V. Functions of Reviewers

The editors request the scientific advice of reviewers who are active in the area of research covered by the manuscript. The reviewers act only in an advisory capacity and the final decision concerning a manuscript is the responsibility of the editors. The reviewers are asked to comment not only on the scientific content, but also on the manuscript's suitability for *The Journal of Physical Chemistry*. With respect to *Communications*, the reviewers are asked to comment specifically on the urgency of publication. **Authors are encouraged to suggest, when submitting a manuscript, names of scientists who could give a disinterested and informed and helpful evaluation of the work.** All reviews are anonymous and the reviewing process is most effective if reviewers do not reveal their identities to the authors. An exception arises in connection with a manuscript submitted for publication in the form of a comment on the work of another author. Under such circumstances the first author will, in general, be allowed to review the communication and to write a rebuttal, if he so chooses. The rebuttal and the original communication may be published together in the same issue of the journal. Revised manuscripts are generally sent back to the original reviewers, who are asked to comment on the revisions. If only minor revisions are involved, the editors examine the revised manuscript in light of the recommendations of the reviewers without seeking further opinions. For the convenience of reviewers, authors are advised to indicate clearly, either in the manuscript or in a covering letter, the specific revisions that have been made.

VI. Submission of Manuscripts

All manuscripts must be submitted in triplicate to expedite handling. Manuscripts must be typewritten, double-spaced copy, on 22 × 28 cm paper. Legal sized paper is not acceptable. Authors should be certain that copies of the manuscript are clearly reproduced and readable. **Authors submitting figures must include the original drawings or photographs thereof, plus three xerographic copies for review purposes. These reproductions of the figures should be on 22 × 28 cm paper.** Graphs must be in black ink on white or blue paper. Lettering should be done with a mechanical lettering set or its equivalent. It should be of sufficent size so that after photoreduction to a single-column width (~8 cm) the smallest letter will be 2 mm. Figures and tables should be held to a minimum consistent with adequate presentation of information. All original data which the author deems pertinent must be submitted along with the manuscript. For example, a paper reporting a crystal structure should include structure factor tables for use by the reviewers.

All references and explanatory notes, formerly set up as footnotes on individual pages, are now grouped at the end of the article in a section called "References and Notes". They should be numbered consecutively in the order in which they are first mentioned in the text, and the complete list of notes and literature citations should appear at the end of the manuscript. Nomenclature should conform to that used in *Chemical Abstracts*. Complicated chemical equations, schemes, and structures should be supplied as furnished artwork, ready for photoreproduction. Mathematical expressions and chemical formulas should be typed, with unavailable symbols and letters clearly drawn in ink. Capital, lower case, and Greek letters should be easily discernible, and identified in the margin when ambiguity might result. Avoid complicated superscripts and subscripts. Use fractional exponents instead of root signs.

Papers should not depend for their usefulness on unpublished material, and excessive reference to material in press is discouraged. References not readily available (e.g., private technical reports, preprints, or articles in press) that are necessary for a complete review of the paper must be included with the manuscript for use by the reviewers.

VII. Revised Manuscripts

A manuscript sent back to an author for revision should be returned to the editor within 6 months; otherwise it will be considered withdrawn and treated as a new manuscript when and if it is returned. Revised manuscripts returned to the editor must be submitted in triplicate and all changes should be made by typewriter. **Unless the changes are very minor, all pages affected by revision must be retyped.** If revisions are so extensive that a new typescript of the manuscript is necessary, it is requested that a copy of the original manuscript be submitted along with the revised one.

VIII. Proofs and Reprints

Galley proofs, original manuscript, cut copy, and reprint order form are sent by the printer directly to the author who submitted the manuscript. The attention of the authors is directed to the instructions which accompany the proof, especially the requirement that all corrections, revisions, and additions be entered on the proof and not on the manuscript. Proofs should be checked against the manuscript (in particular all tables, equations, and formulas, since this is not done by the editor) and returned as soon as possible. No paper is released for printing until the author's proof has been received. Substantial changes in an article after it has been set in type are made at the author's expense. The filled-out reprint form must be returned with the proof, and if a price quotation is required by the author's organization a request for it should accompany the proof. Reprint shipments are made a month or more after publication, and bills are issued by the printer subsequent to shipment. Neither the editors nor the Washington office keeps any supply of reprints. Requests for single copies of papers should be addressed to the author concerned.

A page charge is assessed to cover in part the cost of publication. Although payment is expected, it is not a condition for publication. Articles are accepted or rejected only on the basis of merit, and the editor's decision to publish the paper is made before the charge is assessed. The charge per journal page is $60.

Shock-Tube Chemistry.   1.   The Laminar-to-Turbulent Boundary Layer Transition

John A. Bander and George Sanzone*

Department of Chemistry, Virginia Polytechnic Institute and State University, Blacksburg, Virginia 24061 (Received April 7, 1976)

A model is proposed for the determination of the laminar-to-turbulent transition in the boundary layer of a chemical shock-tube flow. The implications of this model for the accurate determination of reaction-rate constants are discussed.

I. Introduction

In a kinetic study in the incident-shock region of a chemical shock tube, the arrival time of the contact surface is an important parameter since it determines the test-time available for the study. The prediction of contact-surface arrival times has been used as a test of a model for the determination of the laminar-to-turbulent transition in the incident-shock flow field. The implications of this model for the accurate determination of reaction rate constants in this flow field will be discussed.

II. Incident Region Test Times

The laboratory test time is the time interval between the passage of the incident shock front and the arrival of the contact surface. In the ideal shock tube, the shock-front-to-contact-surface distance increases uniformly with time. Consequently the laboratory test time also increases with time of flow (or with distance downstream of the shock-tube driver section). The ratio of laboratory test time to actual particle time for observed gas is equal to the ratio of gas densities across the shock front.[1]

In the real shock tube, the shock-treated test gas in contact with the cold shock-tube walls will lose both heat and momentum. This creates a region of thermal, density, and velocity gradients at the walls called a boundary layer. The shock wave can be considered as generated by the pile-up of test gas in front of the expanding driver gas. In other words, the driver gas acts as a piston. However since shock-treated gas is channeled through the boundary layer, the driver acts as a leaky piston.[2] See Figure 1.   As a

consequence of this effect, the contact surface accelerates while the shock front decelerates until gas is being leaked through the boundary layer at the same rate it is being shock treated. When this steady-state condition is attained, the shock-front-to-contact-surface distance remains constant; this is the condition of "limiting flow". The laboratory test time is much shorter than for ideal shock-tube flow and there are pressure and density gradients and therefore temperature gradients between the shock and contact fronts. Also, the laboratory-to-particle time ratio is no longer equal to a simple density ratio.[3]

Since two of the most important kinetic variables, observation time and temperature, are affected, the presence of nonidealities in shock-tube flows has important implications for chemical kinetic studies. There appear to be two schools of thought as to the inclusion of boundary-layer corrections in the treatment of kinetic data. One school recognizes that the corrections have been difficult-to-apply averages over an *assumed* boundary layer flow state. They have opted to ignore the corrections and to treat their data on the assumption that shock-tube flows are ideal.[4,5] These researchers point to what they feel is reasonable agreement with kinetic data obtained by other methods; they have tended to be interested in the determination of reaction mechanisms.

The second school has been more interested in details of the theory of reaction rates or of reactive flows.[6-8] They have opted to apply boundary-layer corrections to their data. However the corrections employed have been approximations based on the assumption that the boundary
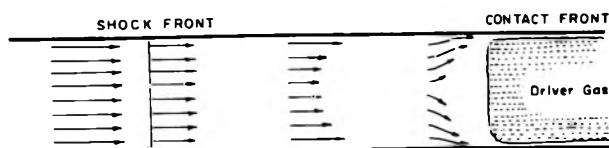
Figure 1. The "leaky-piston" effect. The test gas is channeled around the driver gas.

TABLE I: Reynolds Numbers and Transition Times[a]

Transition Reynolds No.	Flow Reynolds No.		
	$Re_1 = \dfrac{v_s D \rho_2}{\mu_2}$	$Re_2 = \dfrac{v_2 D \rho_2}{\mu_2}$	
$Re_A = \dfrac{v_2{}^2 \tau \rho_2}{\mu_2}$	$\tau_{A1} = \dfrac{v_s D}{v_2{}^2}$	$\tau_{A2} = \dfrac{D}{v_2}$	
$Re_B = \dfrac{v_2{}^2 v_s \tau \rho_2}{(v_s - v_2)\mu_2}$	$\tau_{B1} = \dfrac{D(v_s - v_2)}{v_2{}^2}$	$\tau_{B2} = \dfrac{D(v_s - v_2)}{v_2 v_s}$	

[a] D = hydraulic diameter; ρ_2 = shocked-gas density; μ_2 = shocked-gas viscosity; v_s = shock-wave velocity; v_2 = shocked-gas velocity.

layer is either completely laminar or completely turbulent.[9] Calculated effects of the boundary layer on properties such as the temperature can be significant. However the validity of these corrections might be questioned because of the purely-laminar or purely-turbulent assumption. Kinetic data have not previously been treated for the real case in which a boundary layer undergoes a laminar-to-turbulent transition.

III. The Laminar-to-Turbulent Transition Time

The following model is suggested for the calculation of the laboratory time τ at which the laminar-to-turbulent transition occurs. τ is measured relative to the passage of the shock wave. Under the condition of limiting flow, total laboratory test times can be predicted for either purely laminar or purely turbulent boundary layers.[9] Total test time t is assumed to be the sum of a fraction of a fully-laminar test time L and a fraction of a fully-turbulent test time T. Thus

$$t = (\tau/t)L + (1 - \tau/t)T \tag{1}$$

$$t = \frac{1}{2}T + \frac{1}{2}\{T^2 + 4\tau(L - T)\}^{1/2} \tag{2}$$

Times L and T can be computed with recourse to the original papers[9] or to the very good approximations provided by Strehlow and Belford.[10,11] Note that if $\tau = 0$, the flow is completely turbulent and the test time is T. If the transition occurs just as the contact surface arrives, then $\tau = t = L$. The more general case, which describes most chemical shock-tube studies, involves transition times in the range $0 < \tau < L$.

The above model is viable only if an expression for τ can be found. It is also to be noted that the transition is not instantaneous but occurs over a time interval which is assumed to be a negligible fraction of the test time. Although the transition time also depends on the roughness of the walls,[12] it is well established that the principal factors that affect it define a *transition* Reynolds number.[13,14] We investigated the use of two transition Reynolds numbers based on two measures of boundary-layer thickness. See Table I. The first, Re_A, is based on the distance a free stream particle travels in a transition time. The second, Re_B, is based on the distance a particle travels from its initial position to the transition point. The shocked-gas parameters also define a *flow* Reynolds number. Using the shock-tube hydraulic diameter, we investigated two flow
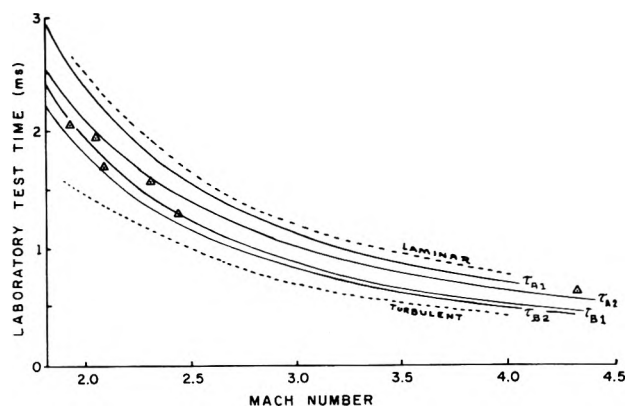
Figure 2. Laboratory test times vs. Mach number. Initial pressure p_1 = 12 Torr. Dotted upper and lower envelopes represent purely laminar and turbulent cases, respectively.
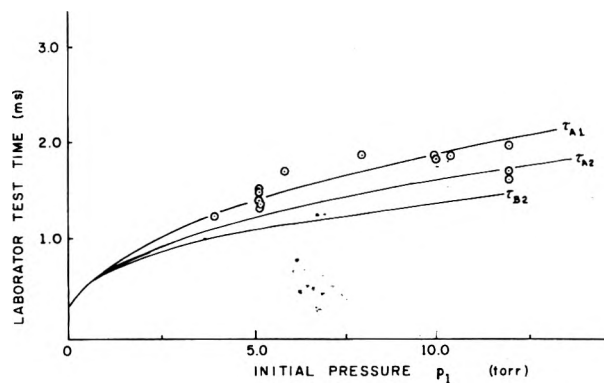
Figure 3. Laboratory test times vs. initial pressure. Mach number for curves is 2.2. For experimental points, $2.0 \leq Ma \leq 2.4$.

Reynolds numbers. The first, Re_1, is based on the velocity of the shock wave; the second, Re_2, is based on the velocity of the shocked gas relative to the wall.

Although the flow and transition Reynolds numbers use different characteristic properties, they are written for the same shock-tube flow state. By equating a flow and a transition Reynolds number, we obtained the four trial expressions for the transition phase given in Table I.

IV. Experimental Results

All shock velocities and laboratory test times for shocks into argon over a range of initial pressures, p_1, and a range of Mach numbers, Ma, were measured with a modified laser-Schlieren system.[15] Experimental test times were compared with theoretical test times as predicted by eq 2 with the four expressions for the laminar-to-turbulent transition time given in Table I. Since the evaluations of the terms L and T in the model assume the condition of limiting flow, it was necessary to reject a considerable number of shock experiments which showed severe attenuation of the velocity of the shock wave with distance along the shock tube. The 2-in. diameter shock tube used in this study has been described elsewhere.[15,16]

From graphs of laboratory observation times as a function of Mach number, (see Figure 2) it was found that transition times τ_{A2} and τ_{B1} fit the data. From graphs of laboratory observation times as a function of initial pressure, (see Figure 3), it was found that transition times τ_{A1} and τ_{A2} fit the data. On the basis of these observations, transition time τ_{A2} was considered to give the best overall agreement between experimental and predicted observation times. Note that the experimental points in Figure 3 correspond to a range of Mach number: $2.0 < Ma < 2.4$. See Figure 4.
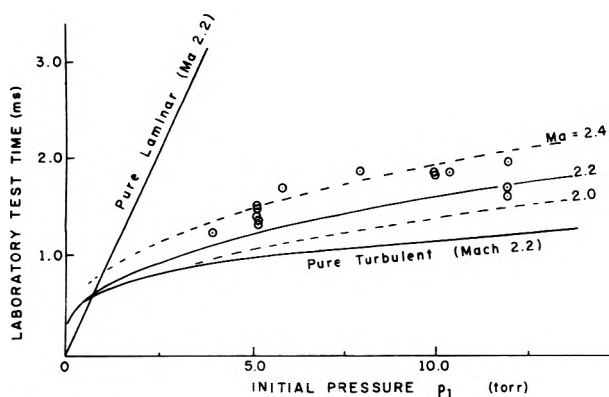
Figure 4. Laboratory test times vs. initial pressure: $\tau = \tau_{A2}$.

V. Conclusions

This work is being extended to a shock tube of larger diameter. Although other expressions for the transition time will be sought, we suggest that the experimental results to date provide a reasonable test of the consistency of the model represented in eq 1. Incidentally, a choice of transition time τ_{A2} implies that the laminar-to-turbulent boundary-layer transition time is simply the time for shocked gas to flow a distance of one shock-tube diameter.

With this model, there now exists a method for the prediction of the laminar-to-turbulent transition time in *any single shock-tube experiment provided the condition of limiting flow is met*. The additional measurement of contact-front arrival time should be made as it provides a consistency check on the data treatment. The density and temperature of any point in the incident-shock flow regime are *determined by the entire flow regime* since the flow in this regime is subsonic. With a knowledge of the

transition time, it should now be possible to more easily obtain these density and temperature profiles and so to definitively determine the effect of shock-tube boundary layers on the measurement of chemical reaction rate constants.

References and Notes

(1) Ideal shock tube flow is described in a number of textbooks. See for example, E. F. Greene and J. P. Toennies, "Chemical Reactions in Shock Waves", Academic Press, New York, N.Y., 1964.
(2) A. Roshko, *Phys. Fluids*, **3**, 835 (1960); W. J. Hooker, *ibid.*, **4**, 1451 (1961).
(3) J. N. Fox, T. I. McLaren, and R. M. Hobson, *Phys. Fluids*, **9**, 2345 (1966).
(4) R. D. Kern et al., *J. Phys. Chem.*, **75**, 171 (1971); **78**, 2549 (1975); **79**, 1483, 2579 (1974).
(5) S. C. Baber and A. M. Dean, *J. Chem. Phys.*, **60**, 307 (1974).
(6) M. Warshay, *J. Chem. Phys.*, **57**, 2223 (1972). Also see *NASA Tech. Note* TN-D-4795 (1970).
(7) R. L. Belford and R. A. Stehlow, *Annu. Rev. Phys. Chem.*, **20**, 247 (1969).
(8) W. E. Trafton, Ph.D. Thesis, University of Illinois, Urbana, Ill., 1973.
(9) H. Mirels, *Phys. Fluids*, **6**, 1201 (1963); **9**, 1265, 1907 (1966). Also see *AIAA J.*, **2**, 84 (1964).
(10) R. A. Strehlow and R. L. Belford, Technical Report No. AAE 69-01, University of Illinois, 1969.
(11) R. J. D'Amato, Ph.D. Thesis, University of Illinois, Urbana, Ill., 1971.
(12) W. P. Thompson and R. J. Emrich, *Phys. Fluids*, **10**, 17 (1967).
(13) A. J. Chabai and R. J. Emrich, *Bull. Am. Phys. Soc., Ser. 2*, **3**, 291 (1958).
(14) R. A. Hartunian, A. L. Russo, and P. V. Marrone, *J. Aerospace Sci.*, **27**, 587 (1960); Also see *Proc. Heat Trans. Fluid Mech. Inst.*, (1958).
(15) J. A. Bander and G. Sanzone, *Rev. Sci. Instrum.*, **45**, 949 (1974).
(16) J. A. Bander, M.Sc. Thesis, Virginia Polytechnic Institute and State University, Blacksburg, Va., 1974.

Absorption Spectrum and Rates of Formation and Decay of the CH_3O_2 Radical

C. J. Hochanadel,* J. A. Ghormley, J. W. Boyle,

Chemistry Division, Oak Ridge National Laboratory, Oak Ridge, Tennessee 37830

and Paul J. Ogren

Central College, Pella, Iowa 50219 (Received May 6, 1976)

Flash photolysis of azomethane was used to produce CH_3 radicals which reacted with O_2 to form CH_3O_2. The CH_3O_2 radical was found to have a broad absorption spectrum centered at 2350 Å, with a maximum extinction coefficient of 870 M^{-1} cm^{-1} based on loss of azomethane. The rate constant at 295 ± 2 K for the formation reaction $CH_3 + O_2 + M \rightarrow CH_3O_2 + M$ (k_2) in the second-order limit was found to be 1.3 ± 0.2 × 10^9 M^{-1} s^{-1}. The rate constant for the combination of peroxy radicals, $CH_3O_2 + CH_3O_2 \rightarrow$ products (k_3), was 2.3 ± 0.3 × 10^8 M^{-1} s^{-1}, and for the combination of methyl radicals, $CH_3 + CH_3 + M \rightarrow C_2H_6 + M$ (k_1), it was 3.1 ± 0.6 × 10^{10} M^{-1} s^{-1}. The reactions were monitored by kinetic spectrophotometry of CH_3 absorption at 2160 Å and CH_3O_2 absorption at 2480 Å.

Introduction

Peroxy radicals are important intermediates in many reaction systems in photochemistry, radiation chemistry, atmospheric chemistry, and combustion. Because of the current emphasis on the production and conversion of energy and the consequences of its usage, there is increased

urgency for establishing mechanisms and accurate rate constants for reactions of radicals of this type. Several years ago the absorption spectrum of the HO_2 radical was observed by us[1] and also by Paukert and Johnston,[2] and rates of its reaction with itself and with OH were measured. This study has now been extended to the CH_3O_2 radical.

The absorption spectrum of the CH_3O_2 radical is reported here along with rate constants for the reactions:

$$CH_3 + CH_3 + M \xrightarrow{k_1} C_2H_6 + M \qquad (1)$$

$$CH_3 + O_2 + M \xrightarrow{k_2} CH_3O_2 + M \qquad (2)$$

$$CH_3O_2 + CH_3O_2 \xrightarrow{k_3} products \qquad (3)$$
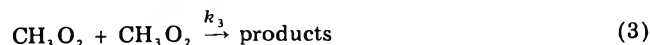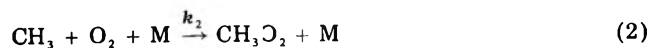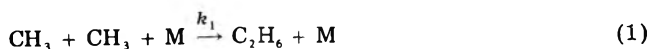
Flash photolysis of azomethane was used to produce CH_3 radicals which absorb in the well-known bands[3] at 2160 Å. In the presence of a small amount of oxygen an additional broad absorption (2050–2900 Å) attributed to CH_3O_2 was produced. Extinction coefficients of both CH_3 and CH_3O_2 were determined from the measured loss of azomethane due to the flash, and by means of kinetic spectrophotometry a self-consistent set of rate constants for the above reactions was obtained.

A spectrum obtained by a molecular modulation technique was reported recently by Parkes et al.,[4] and although the assignment was somewhat tentative because of possible interference by CH_3O, our work clearly supports the CH_3O_2 assignment. Our results for ϵ_{max}, the shape and position of the band, and k_2 agree reasonably well with theirs. We are not aware of any other measured value for k_3.

Several groups have studied the individual reactions 1 and 2, and some have examined both reactions in closely related systems. There have been numerous measurements of k_1.[5] Most of the recent values are in reasonably good agreement except for a value by Bass and Laufer[6] which is about twice as high as the others. Our value agrees with the bulk of these values. The value for k_2 is known with less certainty. Our value for k_2 in the second-order limit at high pressure agrees with the preliminary value of Van den Bergh and Callear[7] and with the value of Laufer and Bass[8] (which is based on their high value for k_1), but is a factor of 3 greater than that of Basco, James, and James.[9]

Experimental Section

Materials. The oxygen was Matheson's ultra high purity grade (99.95%); the nitrogen was oxygen-free grade, with mass spectra analysis indicating 1 ppm O_2. Azomethane was prepared by the method of Renaud and Leitch[10] in which 1,2-dimethylhydrazine is oxidized by HgO. After degassing in a vacuum system the azomethane was distilled through Drierite, and then distilled several times from one trap at dry ice temperature to another at liquid nitrogen temperature. It was finally condensed in a 500-ml stainless steel cylinder and nitrogen was added to a pressure of 200 psi to give a mixture which contained ~1.3% azomethane. Gas mixtures containing azomethane, oxygen, and nitrogen at a total pressure of 1 atm were prepared using calibrated flow meters. Dimethyl peroxide was prepared by the method described by Toth and Johnston.[10b] The absorption spectrum of our product agrees with their spectrum.

Flash System. Most of the features of the flash system have been described.[11] It consists of a high-pressure xenon or Hg–xenon analytical lamp (Hanovia 901C or 901B), a sample cell constructed of Suprasil, a McPherson Model 216 monochromator, an EMI 9558Q photomultiplier, and a Tektronic Model 556 oscilloscope. The two photolysis lamps[11] contained Xe at 15 Torr, and the discharge at 1 μF and 24 kV gave a flash of ~3 μs duration at half-peak height. The lamps were located 2 in. apart, with one on each side of the photolysis cell. These were located inside a cylindrical brass housing which was coated on the inside

with MgO to serve as a reflector. The housing could be purged with various gases to provide filtering; usually, breathing air was used. However, for measurements of CH_3O_2 formation (2480 Å) during and shortly after the flash, oxygen containing ozone was used in order to minimize interference by scattered photolytic light.

Spectrum of Azomethane. Using a Cary Model 15 spectrophotometer purged with nitrogen, the spectrum was measured over part (above 1820 Å) of the strong band centered at 1849 Å. The spectrum shows a strong continuum with superimposed structure, and is very similar to that published by Bass and Laufer.[12] The extinction coefficient at the 1849-Å peak was evaluated using a cell with 0.100-cm optical path containing pure azomethane at 50.7 Torr at 22.0 °C. This gave an optical density of 2.00 and a value for ϵ (1849 Å) of 7257 M^{-1} cm^{-1}, which is 10% lower than the value of Bass and Laufer, ϵ 8102 M^{-1} cm^{-1}. The reason for the difference is not apparent, but is probably not due to a difference in bandwidth or error in wavelength calibration since the resolution in both measurements was adequate, the spectra are very similar, and the comparison is made at the same fine structure peak. We also measured the spectrum over the much weaker and broader band centered at 3400 Å. Using a cell with 10.0-cm path containing azomethane at 349.0 Torr at 22.0 °C, the optical density was 0.95. This gave a value for ϵ (3400 Å) of 4.87 M^{-1} cm^{-1}, in good agreement with the value given in Calvert and Pitts,[13] ϵ 4.75 M^{-1} cm^{-1}. On the basis of the careful method of purification, and the spectral measurements which showed good agreement with published spectra with no indication of other absorbers in the region 1850–5000 Å, we assumed that impurities in the azomethane were insignificant.

Measurements. Measurements of CH_3 absorption were made at 2160 Å using either a 4- or 6-Å bandwidth which overlap both the R and P + Q branches.[3] Measurements of CH_3O_2 kinetics were made at 2480 Å. For some measurements the sample mixture flowed continuously through a 1-cm i.d. Suprasil cell which had a 25.0-cm optical path. Previous experience had shown that the gases, after passing through the flow meters and several mixing regions, were thoroughly dispersed before entering the photolysis cell.

Extinction coefficients of CH_3 and CH_3O_2 were evaluated from the loss of azomethane measured by means of a Cary Model 15 spectrophotometer. It was assumed that each azomethane dissociated by the flash yielded two CH_3 radicals. For these measurements the sample was contained in a 2 cm i.d. Suprasil cell with a 10-cm optical path. Care was taken to minimize photolysis by the analytical light, and a small correction (~1%) was made on the basis of the rate of photolysis and exposure time. Azomethane was measured at 1930 Å (ϵ 3851 M^{-1} cm^{-1}) rather than at the peak in order to minimize interference by O_2 absorption in the Schumann Runge bands ($\epsilon \leq 0.1$ M^{-1} cm^{-1} at 1930 Å). Only a few percent of the azomethane was dissociated in each flash, and in order to achieve sufficient accuracy two identical cells were filled with the same gas mixture. One sample was flashed and the other used as the blank for the Cary measurement. On the next flash the samples were reversed, etc. Using a sensitivity on the Cary spectrophotometer of 0.1 OD unit full scale, the ΔOD values could be measured with an accuracy of ±2% or better.

Results and Discussion

Rate Constant for Reaction 1. Figure 1 shows a typical oscilloscope trace and second-order plot of the decay of absorption by the CH_3 radical at 2160 Å, initiated by the
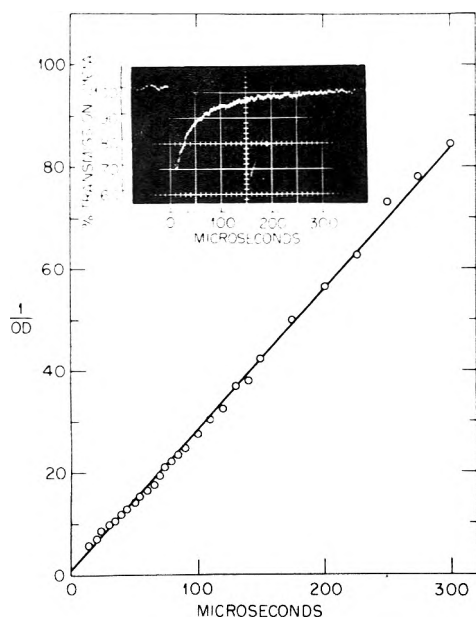
Figure 1. Second-order decay of CH_3 produced by flashing azomethane (1.2×10^{-5} M) in an atmosphere of N_2 (4×10^{-2} M). Optical path 25.0 cm.

Figure 2. Absorption spectrum of the CH_3O_2 radical in the gas phase. The spectrum reported by Parkes et al.[4] is shown as the dashed curve. The HO_2 spectrum, shown for comparison, was reported by us previously.[1]

flash photolysis of azomethane in 1 atm of N_2. In this set of measurements the gas mixture flowed continuously through the cell which had an optical path $l = 25.0$ cm and i.d. = 1.0 cm. The 4-Å band was wide enough to overlap parts of the diffuse R (2157.6 Å) and P + Q (2163.6 Å) branches of CH_3.[3] A test of the Beer-Lambert law was made using a 6-Å bandwidth at 2160 Å by comparing the optical densities at 20 μs after the start of the flash for optical path lengths of 7.8, 16.3, and 25.0 cm (obtained by masking the cell). The optical density was proportional to path length within ±7%. This along with the good second-order kinetics for CH_3 decay was evidence for the validity of the Beer–Lambert law for these conditions. Compliance with the Beer–Lambert law had been observed previously by Van den Bergh et al.[7,14] The second-order plot has slope = $2k_1/\epsilon l$, and assuming an ϵ of 1.02×10^4 M^{-1} cm^{-1},[14-16] a set of three measurements gave $k_1 = 3.46 \pm 0.02 \times 10^{10}$ M^{-1} s^{-1}.

In another set of measurements, both ϵ and k_1 were determined by flashing a static sample and measuring both the CH_3 decay as above, and also the amount of CH_3 produced from the measured loss of azomethane (see Experimental Section). Measurements of CH_3 decay were made using a 6-Å bandwidth in order to improve the signal/noise ratio. From the second-order plots the ratio k_1/ϵ = slope $\times l/2$ was obtained. A preliminary value of ϵ was obtained from the amount of CH_3 produced and the optical density obtained by extrapolating the second-order plot back to the peak of the flash. These values were refined by computer simulation using numerical integration in which the measured amount of CH_3 was introduced over a simulated flash profile and the values for k, and ϵ adjusted (keeping the ratio fixed) to fit the observed decay of CH_3. Seven measurements gave the average values for ϵ of 9000 M^{-1} cm^{-1} and $k_1 = 2.99 \times 10^{10}$ M^{-1} cm^{-1}. Combining all of the measurements the values for k_1 and ϵ are respectively, $3.1 \pm 0.6 \times 10^{10}$ M^{-1} s^{-1} and 9000 ± 800 M^{-1} cm^{-1} (2160- and 6-Å bandwidth). The error limit for the rate constant is expressed as the standard deviation.

The absorption spectrum of CH_3 was measured using several different bandwidths ranging from 1.6 Å (which resolved the two peaks) to 8 Å (which showed a single
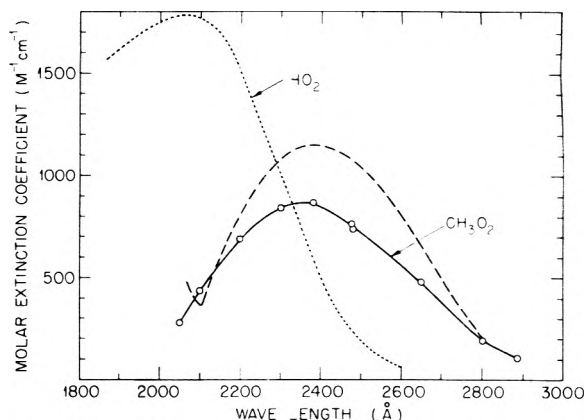
broad band). The absorptions at the peaks for the 4- and 6-Å bandwidths were in the same ratio as the above values for ϵ.

Reaction 1 occurs in the second-order limit under our conditions,[15] and the value we obtained for k_1 agrees very well with the recent value $3.37 \pm 0.46 \times 10^{10}$ M^{-1} s^{-1} reported by James and Simons,[5] and reasonably well with most of the other values listed in their Table I.

It is interesting to note that in liquid water CH_3 absorbs in a broad band at 2130 Å with an ϵ_{max} of 1600 M^{-1} cm^{-1} and with a value for k_1 of $1.6 \pm 0.2 \times 10^9$ M^{-1} s^{-1}.[17]

Absorption Spectrum of CH_3O_2. When a small amount of O_2 is added to the azomethane–N_2 mixture, the CH_3 radicals formed by the flash disappear much more rapidly than predicted by reaction 1, and the decay kinetics are nearly first order. The disappearance is related quantitatively to the simultaneous growth of a new band at 2350 Å with the spectrum shown in Figure 2. This evidence strongly supports the assignment of this band to CH_3O_2 in agreement with the conclusion of Parkes et al.[4] who observed a similar band in a closely related system by means of molecular modulation spectroscopy. We also showed by flashing CH_3OOCH_3 that CH_3O, another possible transient, for which no spectrum has been reported, does not absorb in this region.

The 2350-Å band disappeared by second-order kinetics, and ϵ was determined by comparing the absorption extrapolated to the peak of the flash with loss of azomethane measured on the Cary spectrophotometer as described before. For this purpose a sufficiently high O_2 concentration was used to react with most of the CH_3, but an excess was avoided to minimize O_3 formation. A study of absorption as a function of O_2 concentration indicated an optimum concentration of $\sim 2.5\%$ O_2. For this system the extinction coefficient at 2482 Å was found to be 746 ± 13 M^{-1} cm^{-1} based on 12 measurements. A simple estimate based on relative rate constants and the initial concentration of CH_3 indicated that a small correction for loss of CH_3 by reaction 1 was necessary. By computer simulation the correction was found to be 2%, raising the value for ϵ to 761 ± 13 M^{-1} cm^{-1} at 2482 Å. Loss of CH_3 by reaction with CH_3O_2 is expected to be negligible.[9] The second-order plots sometimes showed a small initial curvature leading to larger OD_0 values than obtained from extrapolation of longer term decay. The curvature might be due to a small amount of ozone interference or to instrumental artifacts. We used the higher OD_0 values, and this could be a systematic error giving an ϵ value as much as 10% too high.
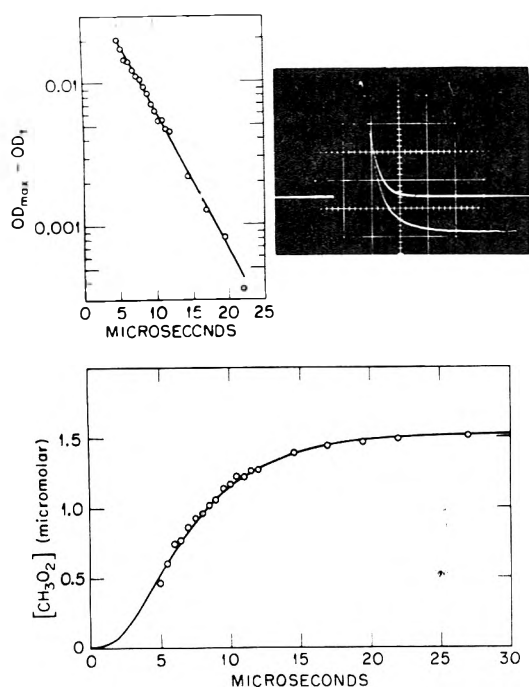
Figure 3. Formation of CH_3O_2 produced by flashing azomethane (1.6 × 10^{-5} M) in the presence of O_2 (1.53 × 10^{-4} M) in an atmosphere of N_2 (4 × 10^{-2} M). The sensitivity and time scales for the inset trace are 5% and 5 μs, respectively, per large division. The quantity on the ordinate of the first-order plot, $OD_{max} - OD_t$, is assumed to be proportional to $[CH_3]_t$ (see text). The solid curve on the lower graph was calculated by computer as described in the test.

The spectrum was determined point by point, with the measurement at each wavelength representing a separate experiment. The measurements were reproducible to ±3%. This method does not allow the resolution required to determine fine structure, and the spectrum is shown as a broad band centered at 2350 Å, with an ϵ_{max} of 870 M^{-1} cm^{-1}. Our spectrum differs slightly from that of Parkes et al.,[4] being somewhat broader, with ϵ_{max} ~ 24% lower. Our spectrum shows no unusual enhancement in the region of HO_2 absorption near 2100 Å indicating that dissociation of azomethane to H and CH_2 amounts to <5% of the total photodecomposition, in agreement with results of Bass and Laufer.[6]

Rate Constant for Reaction 2. Although reaction 2 could be studied by our flash method, it was not possible to achieve high accuracy for several reasons. At a pressure of 1 atm the reaction is close to the second-order limit[9] with reported k_2 values of 1.1 × 10^9,[7] 1.02 × 10^9,[8] and 3.1 × 10^8 M^{-1} s^{-1}.[9] It was necessary to use a low concentration of O_2 in order to slow down the reaction so it could be measured, and yet provide enough O_2 to react with most of the CH_3 radicals in competition with the fast combination reaction 1. Using an O_2 concentration of ~150 μM (~0.4%), the pseudo-first-order time constant $(k_2[O_2])^{-1}$ is ~5 μs, and ~83% of the CH_3 radicals are scavenged by O_2. Typical results for the formation of CH_3O_2 are presented in Figure 3. The radicals are formed in a fast pseudo-first-order reaction and decay by relatively slow second-order combination and thereby reach a maximum concentration ~35 μs after the start of the flash. A preliminary value of k_2 was obtained from first-order plots as shown (inset). Values of OD_t for CH_3O_2 were obtained from the difference between the flash profile and the absorption trace. The quantity on the ordinate, $OD_{max} - OD_t$, assumed to be proportional to $[CH_3]_t$, is slightly inaccurate because of the simultaneous slow decay of CH_3O_2 and because some of the CH_3 radicals combine.
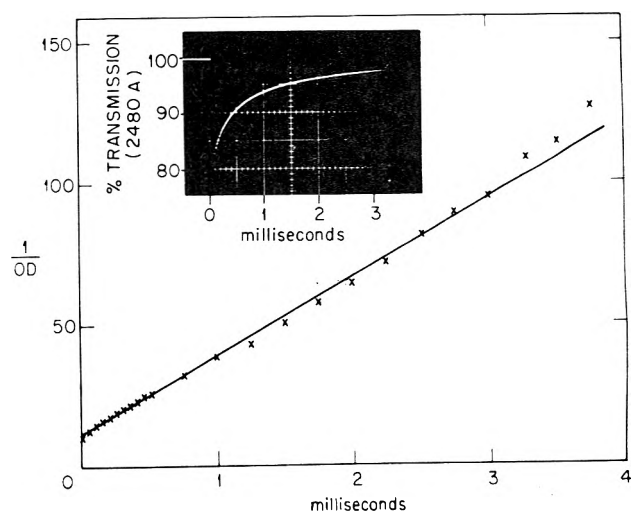
Figure 4. Second-order decay of CH_3O_2 produced by flashing azomethane (6.3 × 10^{-5} M) in the presence of O_2 (1.4 × 10^{-3} M) in an atmosphere of N_2 (4 × 10^{-2} M). Optical path 25.0 cm.

The decay of CH_3O_2 amounts to <1.5% during the period of measurement, and only ~17% of the CH_3 combine, with about half of the combination occuring in the first 5 μs. A set of four measurements gave an average value of k_2 = 1.46 ± 0.08 × 10^9 M^{-1} s^{-1}. A more accurate value was obtained by computer calculation using numerical integration. Known values for k_1 = 3.1 × 10^{10} M^{-1} s^{-1}, k_3 = 2.3 × 10^8 M^{-1} s^{-1}, and $[O_2]$ = 1.53 × 10^{-4} M were introduced. Since appreciable reaction occurs during the flash, it was necessary in the calculation to introduce the CH_3 radicals over a simulated flash profile; about 85% of the radicals were generated within the first 5 μs and 98% within the first 8 μs after the start of the flash. The total amount of CH_3 formed and the value of k_2 were adjusted to give the theroetical curve shown in the lower graph (Figure 3). The total amount of CH_3 produced by photodissociation for these conditions was 1.88 μM, and the value of k_2 was 1.2 × 10^9 M^{-1} s^{-1}. For a pressure of 745 Torr of N_2, we estimate from the pressure dependence observed by Basco, James, and James[9] that our value is 12% below the second-order limit, which brings our value at the second-order limit to 1.34 × 10^9 M^{-1} s^{-1} at 295 K. In estimating the correction, we put a curve through their data since this has more theoretical justification[7,8] than the linear extrapolation indicated (their Figure 3).

Our value for k_2 is based on CH_3O_2 formation, whereas previous workers have followed CH_3 removal. We also studied the latter under conditions in which reaction 2 is dominant, and the results, although less precise, were consistent with the above value. Our value agrees closely with the value of Van den Bergh and Callear[7] and Laufer and Bass,[8] but is about three times larger than that of Basco et al.[9]

In liquid water the CH_3O_2 radical absorbs in a broad band at 2500 Å[17] and reported values of k_2 are 4.7 × 10^9 M^{-1} s^{-1}[18] and 3.2 × 10^8 M^{-1} s^{-1}.[19]

Rate Constants for Reaction 3. The second-order decay of the peroxymethyl radical is illustrated in Figure 4. From the slope of the second-order plot which is equal to $2k_3/\epsilon l$, and from the measured ϵ value, 23 measurements in 4 different runs gave an average value for k_3 of 2.3 ± 0.4 × 10^8 M^{-1} s^{-1}. The measurements were made at 2480 Å; part of them were made in a 1.0-cm i.d. cell with 25.0-cm optical path with the gas flowing continually through the cell, and part were made in a 2.0-cm i.d. cell with 10.0-cm optical path, with a stagnant sample. Our value is in good agreement with that reported by Parkes et al.[4] of 2.6 × 10^8

$M^{-1} s^{-1}$. Part of the difference may reflect the difference in extinction coefficients.

The combination of CH_3O_2 radicals could give CH_2O + CH_3OH + O_2 either directly via a cyclic intermediate,[20] or indirectly via the intermediate formation of CH_3O radicals.[21] We could not observe either CH_3O or CH_2O formation and, therefore, could not distinguish between the two possibilities. In our experiments, direct formation of formaldehyde, for example, would produce <0.3% absorption at 3050 Å and was therefore not measureable. On subjecting a static sample to 15 flashes and then examining it on a Cary spectrophotometer, the expected amount of CH_2O was observed.

References and Notes

(1) C. J. Hochanadel, J. A. Ghormley, and P. J. Ogren, *J. Chem. Phys.*, 56, 4426 (1972).
(2) T. T. Paukert and H. S. Johnston, *J. Chem. Phys.*, 56, 2824 (1972).
(3) G. Herzberg and J. Shoosmith, *Can. J. Phys.*, 34, 523 (1956).
(4) D. A. Parkes, D. M. Paul, C. P. Quinn, and R. C. Robson, *Chem. Phys. Lett.*, 23, 425 (1973).
(5) F. C. James and J. P. Simons, *Int. J. Chem. Kinet.*, VI, 887 (1974).
(6) A. M. Bass and A. H. Laufer, *Int. J. Chem. Kinet.*, V, 1053 (1973).
(7) H. E. Van den Bergh and A. B. Callear, *Trans. Faraday Soc.*, 67, 2017 (1971).
(8) A. H. Laufer and A. M. Bass *Int. J. Chem. Kinet.*, VII, 639 (1975).
(9) N. Basco, D. G. L. James, and F. C. James, *Int. J. Chem. Kinet.*, IV, 129 (1972).
(10) (a) R. Renaud and L. C. Leitch, *Can. J. Chem.*, 32, 545 (1954); (b) L. M. Toth and H. S. Johnston, *J. Am. Chem. Soc.*, 91, 1276 (1969).
(11) C. J. Hochanadel, J. A. Ghormley, and J. W. Boyle, *J. Chem. Phys.*, 48, 2416 (1968); *Rev. Sci. Instrum.*, 39, 1144 (1968).
(12) A. M. Bass and A. H. Laufer, *J. Photochem.*, 2, 465 (1973–1974).
(13) J. G. Calvert and J. N. Pitts, Jr., "Photochemistry", Wiley, New York, N.Y., 1967, p 453.
(14) H. E. Van den Bergh, A. B. Callear, and R. J. Norstrom, *Chem. Phys. Lett.*, 4, 101 (1969).
(15) N. Basco, D. G. L. James, and R. D. Suart, *Int. J. Chem. Kinet.*, II, 215 (1970).
(16) M. Pohjonen, L. Leinonen, H. Lemmetyinen, and J. Koskikallio, *Finn. Chem. Lett.*, 207 (1974).
(17) B. Hickel, *J. Phys. Chem.*, 79, 1054 (1975).
(18) J. K. Thomas, *J. Phys. Chem.*, 71, 1919 (1967).
(19) G. C. Stevens, R. M. Clarke, and E. J. Hart, *J. Phys. Chem.*, 76, 3863 (1972).
(20) G. A. Russell, *J. Am. Chem. Soc.*, 79, 3871 (1957).
(21) W. C. Sleppy and J. G. Calvert, *J. Am. Chem. Soc.*, 81, 769 (1959).

Direct and Sensitized Cis–Trans Photoisomerization of Cyclooctene. Effects of Spin Multiplicity and Vibrational Activation of Excited States on the Photostationary Trans/Cis Ratio[1]

Yoshihisa Inoue,* Setsuo Takamuku, and Hiroshi Sakurai

The Institute of Scientific and Industrial Research, Osaka University, Suita, Osaka 565, Japan (Received May 24, 1976)

The direct and sensitized cis–trans photoisomerizations of cyclooctene were investigated in the liquid phase along with photosensitization in the vapor phase. Upon direct photoisomerization at 1849 Å, an anomalously high photostationary state ratio as obtained for strained cycloalkene, i.e., trans/cis = 0.96, was observed after prolonged irradiation. A number of carbonyl and aromatic additives with triplet energy (E_T) > 72 kcal/mol were effective for sensitizing the cis–trans isomerization and the sensitizers with E_T > 79 kcal/mol gave a definite photostationary trans/cis ratio of 0.049. On vapor-phase photosensitization, some of these same sensitizers and others with E_T > 80 kcal/mol gave higher ultimate trans/cis ratios, which increased up to 0.20 with increasing triplet energy of the sensitizer employed. The effects of spin multiplicity and vibrational activation of the excited states on the photostationary state are discussed and the potential curves for the ground state and the excited singlet and triplet states of cyclooctene which account for the above results are proposed.

Introduction

Photochemical cis–trans isomerization when sterically allowed is a universal photoreaction of alkenes and has been studied in considerable detail.[2] With simple alkenes where direct excitation is difficult because of weak absorption in the UV region above 2300 Å,[3] triplet sensitization and the use of acyclic alkenes as substrates have been adopted in most photoisomerization studies to produce an alkene triplet state. The triplet state of an acyclic alkene thus generated, and probably the singlet state as well, is assumed to decay to the cis or trans isomer with equal probability, since the potential energy curves for the electronically excited singlet and triplet states of ethylene,[4] in which energy minima of the both excited states occur when the methylene groups are orthogonal, can be used as models for those of acyclic alkenes. As demonstrated in the vapor-phase photosensitized cis–trans isomerization of 2-butene,[5] in open-chain alkenes any vibrational excitation in the triplet state is believed to have

no significant influence on the photostationary trans/cis ratio in accord with the above accepted view on the potential surface of the excited states. However, less is known of the cis–trans photoisomerization of cycloalkenes with steric restrictions,[6] and the geometry and the energetics of the excited states of these molecules have not been discussed.

In the present paper, we report a study on the direct and sensitized cis–trans photoisomerization of cyclooctene in the vapor and liquid phases and discuss the drastic effects of spin multiplicity of the excited states involved and of vibrational activation in the triplet state on the photostationary trans/cis ratio, which have not been observed in the photoisomerization of acyclic alkenes.

Experimental Section

Materials. Commercially available *cis*-cyclooctene was purified by fractional distillation through a spinning-band column and preparative gas chromatography to a purity

TABLE I: Liquid-Phase Photosensitized Cis-Trans
Isomerization of Cyclooctene[a]

	Sensitizer	Concn, M	E_T, kcal/mol	(trans/cis)$_{pss}$[b]
1	Benzene	0.4	84.4	0.048
		0.04		0.047
4	Toluene	0.4	82.8	0.052
7	p-Xylene	0.4	80.4	0.047
		0.04		0.046
8	Durene	0.25	80.0	0.041
9	Benzamide	0.005	79.3	0.050
10	Benzonitrile	0.4	76.5	0.031
11	m-Tolunitrile	0.4	75.1	0.024
12	Propiophenone	0.4	74.5	0.033
13	Acetophenone	0.4	73.7	0.032
		0.04		0.030
14	4-Methylacetophenone	0.4	72.9	0.017
15	1-Tetralone	0.4	72.2	0.009
16	Phenylacetylene	0.4	72.0	0
17	Benzaldehyde	0.4	72.0	0
18	Benzophenone	0.25	68.6	0.005
19	Fluorene	0.035	68.0	0

[a] The concentration of cyclooctene was 0.08 M.   [b] Photostationary state trans- to cis-cyclooctene ratio.

of 99.5%. The product contained a small amount (0.5%) of cyclooctane but was free from the trans isomer. trans-Cyclooctene was prepared by a three-step process starting from its cis isomer. The procedure consisted of performic acid oxidation of cis-cyclooctene to trans-cyclooctane-1,2-diol,[7] followed by condensation with benzaldehyde to give the acetal, and subsequent treatment with n-butyllithium.[8] Fractional distillation under a reduced pressure of the product gave the experimental sample of trans-cyclooctene (99.6% trans, 0.38% cis). The sensitizers employed in the vapor- and liquid-phase photosensitizations were purified by fractional distillation or recrystallization. n-Pentane was washed with concentrated sulfuric acid and then fractionally distilled.

Analysis. Gas chromatographic analyses of the reaction mixtures were performed using a 3-m column of 20% β,β'-oxydipropionitrile at 50 °C or, when a sensitizer has a retention time close to that of cis- or trans-cyclooctene, a 6-m column of 15% polyethylene glycol-6000 at 70 °C. The cis-trans isomers of cyclooctene were separated completely under these conditions. As an internal standard, n-octane or cyclooctane was employed for the direct photolysis and the liquid-phase photosensitization.

Direct Photolysis in Liquid Phase. Direct photolyses at 1849 Å (as the effective resonance line of mercury) were run at 17 °C using a 30-W U-shaped low-pressure mercury lamp with an immersion reactor. A pentane solution containing 0.01 M cis- or trans-cyclooctene and 0.002 M n-octane as an internal standard was flushed with nitrogen gas and then irradiated. The product distribution following the direct irradiation was determined by gas chromatographic analysis of aliquots removed from the irradiation mixture.

Liquid-Phase Photosensitization. All experiments of liquid-phase photosensitization were carried out at 17 °C in a quartz or Pyrex tube, 1 cm in diameter, using a 500-W high-pressure mercury lamp. Pyrex tubing was used only for the ketone sensitizers. Pentane solutions of 0.08 M cyclooctene of a given isomer composition containing various sensitizers and 0.002 M cyclooctane or n-octane as an internal standard were flushed with nitrogen gas and then irradiated. The sensitizers are shown in Table I along with their concentrations employed. The isomer compositions following the UV irradiation were determined by periodic analysis of aliquots on gas chromatography. The photostationary states were obtained after prolonged ir-
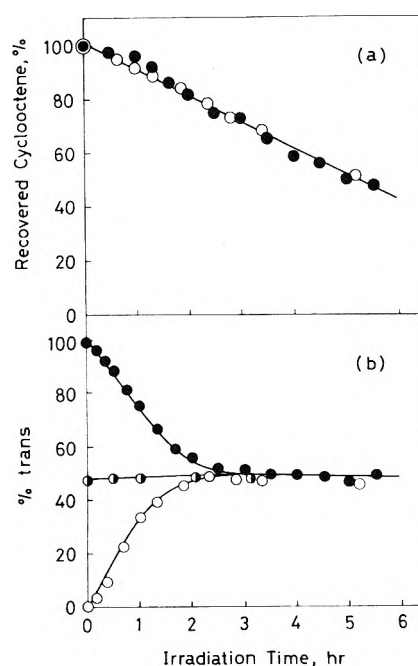
Figure 1. Combined yield (a) and percent of trans-cyclooctenes recovered on direct photoisomerization: (●) initial composition, 99.6% trans: 0.4% cis; (◑) 47:53; (○) 0:100.

radiation: ca. 3–5 h for the aromatics and 1–1.5 h for the ketone sensitizers.

Vapor-Phase Photosensitization. The apparatus and the procedures employed in the vapor-phase photosensitizations were described previously.[9] A mercury-free vacuum system and cylindrical quartz cells, 5 cm long and 5 cm in diameter, were used. The light source was a spiral array of a 30-W low-pressure mercury lamp fitted with a Toshiba UV-25 filter which removes the 1849-Å resonance line of mercury. The vapor-phase photosensitization of a given mixture (3 Torr) of cis- and trans-cyclooctene was run in the presence of the sensitizers, the pressure of which was fixed at 3 Torr with benzene, fluorobenzene, benzotrifluoride, toluene, o-, m-, and p-xylene, and phenylacetylene, or at 1 Torr with benzonitrile. The photostationary state was obtained for each sensitizer by repeated approach from both sides of the final composition. Control runs revealed that no detectable reactions occurred in the absence of either the UV irradiation or the sensitizers.

Results

The direct photolysis at 1849 Å of a pentane solution containing 0.01 M cis- or trans-cyclooctene gave cis-trans isomerization as a major photoreaction. Moderate disappearance of cyclooctenes was observed; after 5 h of irradiation, almost half of the substrate initially used disappeared.[10] The combined yield of cyclooctenes recovered and percent of trans-cyclooctene are plotted as a function of irradiation time in Figure 1. After prolonged irradiation, the pentane solution containing each pure isomer came to a photostationary state, the trans- to cis-cyclooctene ratio of which was 49:51. In order to ensure that the decomposition products did not affect the photostationary ratio, the direct irradiation of a 53:47 mixture of cis- and trans-cyclooctene was examined under similar conditions to give the same photostationary state mixture immediately (within 30 min).

The triplet-sensitized photoisomerization of cyclooctene (0.08 M) in pentane solution was carried out in the presence of a variety of carbonyl and aromatic sensitizers (0.4 M in most cases). Regardless of the sensitizers em-
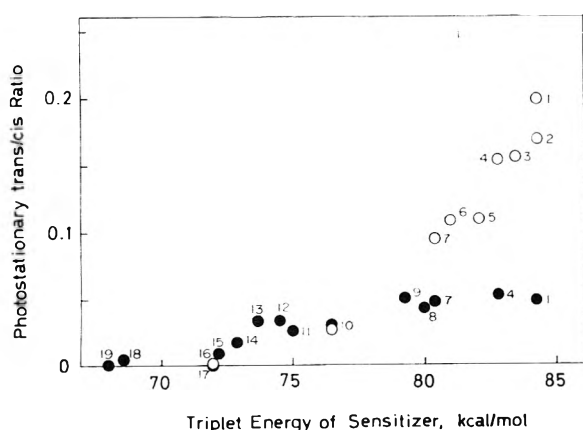
Figure 2. Variations of the photostationary trans/cis ratio with triplet energy of sensitizers, which are shown in Tables I and II, on vapor-phase (O) and liquid-phase (●) photosensitizations.

TABLE II: Vapor-Phase Photosensitized Cis–Trans Isomerization of Cyclooctene[a]

	Sensitizer	Pressure, Torr	E_T, kcal/mol	(trans/cis)$_{pss}$[b]
1	Benzene	3.0	84.4	0.198
2	Fluorobenzene	3.0	84.4	0.168
3	Benzotrifluoride	3.0	83.4	0.156
4	Toluene	3.0	82.8	0.153
5	o-Xylene	3.0	82.1	0.111
6	m-Xylene	3.0	81.0	0.108
7	p-Xylene	3.0	80.4	0.094
10	Benzonitrile	1.0	76.5	0.026
16	Phenylacetylene	3.0	72.0	0.0007

[a] The pressure of cyclooctene was 3 Torr. [b] Photostationary state trans- to cis-cyclooctene ratio.

ployed, slow disappearance (2–5%/h) of the substrate was observed. The photostationary state was determined for each sensitizer by approach from both sides of the final value. The trans/cis ratios at the photostationary state obtained for these sensitizers after prolonged irradiation are presented in Table I and Figure 2. As demonstrated there, a number of sensitizers with triplet energy (E_T)[11] above 72 kcal/mol are effective for the reversible cis ⇌ trans photoisomerization; the photostationary ratios were almost constant for the sensitizers with $E_T > 74$ kcal/mol.[12] Photosensitization of cyclooctene (0.08 M) by benzene, p-xylene, and acetophenone with lower sensitizer concentration (0.04 M) also gave the same photostationary ratios.

Limited experiments revealed that, although the additives with $E_T \leq 72$ kcal/mol, i.e., phenylacetylene (E_T = 72.0 kcal/mol), benzaldehyde (72.0), and benzophenone (68.7), failed to sensitize the cis → trans isomerization, these additives effected irreversible trans → cis isomerization; fluorene (68.0) was no longer completely effective for the photoisomerization.

Photosensitized isomerization of cyclooctene in the vapor phase was also performed in order to examine the effect of vibrational activation in the triplet state on the photostationary state. Since the sensitizers available in the vapor phase are limited by the vapor pressure, nine aromatic compounds were chosen as effective sensitizers.[13] The vapor-phase photolysis of cyclooctene (3 Torr) at 2537 Å in the presence of sensitizers (3 Torr in most cases) gave the cis–trans isomer as a major photoproduct, although prolonged irradiation led to the formation of considerable amounts of 1,7-octadiene and bicyclo[4.2.0]octane as reported previously.[9] The variations of the photostationary ratio with sensitizer triplet energy are shown in Table II and Figure 2. The photostationary trans/cis ratio obtained in the vapor-phase photosensitization intimately depended on the triplet energy of the sensitizer used; the ratio was almost zero (more exactly trans/cis = 0.0007) at E_T = 72.0 kcal/mol (phenylacetylene) and then increased gradually with increasing sensitizer triplet energy in sharp contrast with the result of the liquid-phase photosensitization where the ratios were independent of the sensitizers with $E_T > 79$ kcal/mol.

Discussion

Upon direct irradiation at 1849 Å, a ground state molecule of cyclooctene is promoted spectroscopically to an electronically excited planar singlet state and then suffers fast rotational relaxation to a twisted, not necessarily orthogonal, singlet cyclooctene. Since it is believed

that the large separation in energy causes excited singlet-to-triplet intersystem crossing to be very slow in such a monoolefin, the precursor of the direct cis–trans photoisomerization is inferred to be an excited singlet state of cyclooctene. The considerable disappearance of the substrate on direct photolysis suggests the existence of obscure reactions which give rise to some polymers and, if any, other uncharacterized products.[10] On the assumption of a common twisted singlet intermediate, the cis–trans photoisomerization by direct irradiation can be described by the following simple sequence:

$$c \xrightarrow{h\nu} {}^1p \tag{1}$$

$$t \xrightarrow{h\nu} {}^1p \tag{2}$$

$${}^1p \rightarrow c \tag{3c}$$

$$\rightarrow t \tag{3t}$$

$$\rightarrow \text{other products} \tag{4}$$
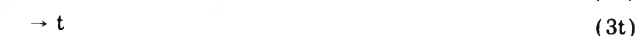
where c and t represent cis- and trans-cyclooctenes in their ground states and ^1p represents the twisted singlet cyclooctene.

A steady-state treatment of the above sequence leads to the following expression for the trans/cis ratio at the photostationary state (pss):

$$([t]/[c])_{pss} = (\epsilon_c/\epsilon_t)(k_{3t}/k_{3c}) \tag{5}$$

where ϵ_c and ϵ_t represent the extinction coefficients of cis- and trans-cyclooctenes at 1849 Å. The reported extinction coefficient for trans-cyclooctene is 5500 M^{-1} cm^{-1} at 1849 Å,[14] while the coefficient of cis-cyclooctene was measured as 6000 M^{-1} cm^{-1}.[15] From these values, the excitation ratio ϵ_c/ϵ_t is calculated as 1.09, and then we can evaluate the decay ratio using eq 5 and the observed photostationary ratio: k_{3t}/k_{3c} = 0.88. It is worth noting that, in spite of the strain energy in the trans form (9.3 kcal/mol),[16] an anomalously high decay ratio of 0.88 is obtained upon direct photoisomerization.

Extremely low trans/cis photostationary ratios were observed on liquid-phase sensitized photoisomerization; the additives with $E_T > 72$ kcal/mol were effective for the cis ⇌ trans photoisomerization. As shown in Figure 2, a definite photostationary ratio of 0.049 was observed for the sensitizers with $E_T > 79$ kcal/mol, while the sensitizers in the triplet energy range 72–77 kcal/mol give rise to somewhat lower photostationary ratios. When the sensitizer is a carbonyl compound, special regard should be paid to the intermediate of the cis–trans isomerization since, as is shown in the Schenck mechanism,[2,17] the 1,4 biradical formed by the addition of a ketone triplet to an acyclic alkene falls apart regenerating the alkene with geometrical isomerization. However, in the case of ketone sensitization of cyclooctene, such a 1,4 biradical, if formed, is considered to decompose preferentially to the cis isomer

because of the strain energy in the trans form.[16] Actually benzophenone, which has fairly low E_T and is known to form a 1,4 biradical with alkenes,[18] photosensitized the irreversible trans → cis isomerization of cyclooctene, probably suggesting the predominant formation of the cis isomer from the 1,4 biradical. It seems, therefore, likely that regarding the ketone sensitizers with $E_T > 72$ kcal/mol, the mechanism involving triplet energy transfer to cyclooctene is operative, although the Schenck mechanism is applicable only for benzophenone sensitization.

Since the benzene-sensitized photostationary ratios for several acyclic alkenes in solution are unity and the triplet energy transfer from benzene triplet to alkenes is sufficiently exothermic,[19] it has been recognized that, when benzene is the sensitizer, the common intermediate for the sensitized cis–trans isomerization is the twisted alkene triplet whose decay ratio is unity.[2,20] In the present system, assuming that the rates of triplet energy transfer from the excited benzene to cis- and trans-cyclooctenes are the same in accord with the above accepted view on the benzene photosensitization, the extremely low trans/cis ratio at the photostationary state is attributable to a low decay ratio (k_t/k_c) from a common twisted, vibrationally relaxed cyclooctene triplet ^3p. Toluene and p-xylene sensitized photoisomerizations gave the same, or nearly so, photostationary ratios as those obtained by benzene sensitization, suggesting that these sensitizers with $E_T > 80$ kcal/mol also excite both isomers of cyclooctene with an equal rate.

The calculated potential curves for the excited states of ethylene,[4] which suggest the same decay ratio for singlet and triplet excited states, are evidently unsuitable for the present system. The extremely low cis → trans isomerization efficiency for the photosensitization of cyclooctene may be attributable to a torsional conversion barrier from the vibrationally relaxed triplet state ^3p into the trans form. Taking into account the strain energy[16] and the torsional angle[21] of trans-cyclooctene in its ground state, the fundamental potential energy curves calculated with ethylene[4] are qualitatively modified to obtain hypothetical potential curves of the ground state (N) and the excited singlet (V) and triplet (T) states of cyclooctene. Since electronically the double bond of cyclooctene is close to that of ethylene and the strain in the trans form, which arises from the steric restrictions of methylene chain, is considered not to be so great compared with the electronic energy, the potential curves for cyclooctene may not be far removed in energy from those for ethylene. Therefore, the crossing of potential curves of the N and T states occurs to give an ethylene-like energy well, although the torsional angle which give the potential minimum of the T state and the maximum of the N state as well, should not be necessarily perpendicular. As shown in Figure 3, a greater activation energy (E_t) is postulated for the decay of ^3p to the trans isomer in order to account for the low decay ratio in the liquid phase photosensitization. The following Arrhenius equations are obtained for the rate constants of the decay from ^3p to the ground-state trans- and cis-cyclooctenes.

$$k_t = A \exp(-E_t/RT) \qquad (6)$$

$$k_c = A' \exp(-E_c/RT) \qquad (7)$$

Assuming the same preexponential factor, i.e., $A = A'$, the logarithm of the decay ratio is represented by the following equation

$$\ln (k_t/k_c) = -\Delta E_a/RT \qquad (8)$$

where $\Delta E_a = E_t - E_c$. Since the experiment was carried
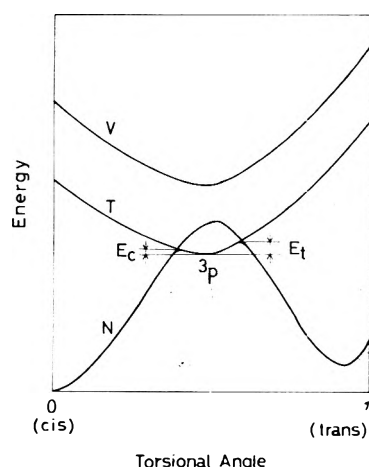
Figure 3. Schematic potential curves for the ground-state (N) and excited singlet (V) and triplet (T) states of cyclooctene.

out at 290 K and the decay ratio (k_t/k_c) observed equals 0.049, then we can evaluate the difference of the activation energies: $E_t - E_c = 1.7_4$ kcal/mol.[22]

The photosensitized cis–trans isomerization in the vapor phase can be used as a test of the speculated potential surface described above, since the triplet state of cyclooctene generated in the vapor-phase photosensitization is considered to have some excess vibrational energy in the absence of fast collisional deactivation by solvent molecules. As shown in Figure 2, the trans/cis photostationary ratios observed in vapor-phase photosensitization are higher than those obtained in liquid-phase photosensitization employing the same sensitizers, and the ratio increases with increasing triplet energy of the sensitizer used, whereas the ratio observed in the liquid phase is independent of the sensitizer with $E_T > 79$ kcal/mol. One might assume the deviation from unity of the excitation ratio on the vapor-phase photosensitization in order to account for the higher trans/cis photostationary ratios and their dependence on the sensitizer triplet energy, although the excitation ratio is regarded as unity in the liquid-phase photosensitization employing sensitizers with $E_T > 79$ kcal/mol. This seems unlikely because the rates of energy transfer from benzene triplet to both cis and trans isomers of simple disubstituted alkenes have been reported to be so close in the vapor phase[5,23] that the higher trans/cis ratios observed in the present work are attributable to the higher decay ratios (k_t/k_c). The higher trans/cis photostationary ratios and their E_T dependence should therefore be interpreted in terms of the excess vibrational energy in the triplet state of cyclooctene. The cyclooctene triplet generated in the vapor-phase photosensitization has some excess vibrational energy, the amount of which increases with rising triplet energy of the sensitizers. According to eq 8, the excess vibrational energy, which is energetically equivalent to thermal activation in the triplet state, enhances the decay ratio (k_t/k_c). Then, the enhanced decay ratio via vibrational activation qualitatively rationalizes the higher photostationary trans/cis ratios and their dependence on the triplet energy in the vapor-phase photosensitization. In this context, the high internal energy of the relaxed singlet state ^1p in itself may account for the anomalously high decay ratio observed on the direct photoisomerization. However, we feel prompted to propose that, since the excited singlet state of alkenes is believed not to undergo intersystem crossing to its triplet state but to suffer rapid internal conversion to its ground state, the twisted ground-state cyclooctene thus formed is deactivated collisionally to give the relaxed cis or trans isomer with almost equal probability, if the correlation between

the potential curves for the V and N states is as shown in Figure 3.

References and Notes

(1) Preliminary report: Y. Inoue, S. Takamuku, and H. Sakurai, *J. Chem. Soc., Chem. Commun.*, 423 (1976).

(2) J. Saltiel, J. D'Agostino, E. D. Megarity, L. Metts, K. R. Neuberger, M. Wrighton, and O. C. Zafiriou, *Org. Photochem.*, **3**, 1 (1973), and references cited therein.

(3) L. C. Jones, Jr., and L. W. Taylor, *Anal. Chem.*, **27**, 228 (1955).

(4) A. J. Merer and R. S. Mulliken, *Chem. Rev.*, **69**, 639 (1969).

(5) R. B. Cundall, *Prog. React. Kinet.*, **2**, 165 (1964); R. B. Cundall and T. F. Palmer, *Trans. Faraday Soc.*, **56**, 1211 (1960); R. B. Cundall, F. J. Fletcher, and D. G. Milne, *J. Chem. Phys.*, **39**, 3536 (1963); S. Sato, K. Kikuchi, and M. Tanaka, *ibid.*, **39**, 239 (1963); M. Tanaka, T. Terumi, and S. Sato, *Bull. Chem. Soc. Jpn.*, **38**, 1645 (1965); S. Tsunashima and S. Sato, *ibid.*, **41**, 284 (1968); E. K. C. Lee, H. O. Denschlag, and G. A. Haninger, Jr., *J. Chem. Phys.*, **48**, 4547 (1968); M. Termonia and G. R. De Mare, *Chem. Phys. Lett.*, **25**, 402 (1974).

(6) The xylene-sensitized photoisomerization of *cis*-cyclooctene has been reported as a synthetic method for preparing *trans*-cyclooctene; J. S. Swenton, *J. Org. Chem.*, **34**, 3217 (1969). This study of Swenton, however, did not provide any quantitative information but demonstrated the extremely low efficiency of the cis → trans photoisomerization of cyclooctene; xylene photosensitization of *cis*-cyclooctene (600 ml) in cyclohexane gave only 2.1–2.4 g (~0.5%) of the trans isomer after 36 h of irradiation.

(7) A. C. Cope, S. W. Fenton, and C. F. Spencer, *J. Am. Chem. Soc.*, **74**, 5884 (1952).

(8) J. N. Hines, M. J. Pergram, G. H. Whitram, and M. Wright, *J. Chem. Soc., Chem. Commun.*, 1593 (1968).

(9) Y. Inoue, K. Moritsugu, S. Takamuku, and H. Sakurai, *J. Chem. Soc., Perkin Trans. 2*, 569 (1976).

(10) A further study for the products which may be produced from the unrecovered cyclooctene was made; formation of methylene-cycloheptane and bicyclo[5.1.0]octane was detected on gas chromatography. In the early stages of photolysis (within 1 h) the combined yield of these two products amounted to almost half of the unrecovered cyclooctene.

(11) D. F. Evans, *J. Chem. Soc.*, 2753 (1959); Y. Kanda and R. Shimada, *Spectrochim. Acta*, **17**, 279 (1961); K. Takei and Y. Kanda, *ibid.*, **18**, 1201 (1962); S. L. Murov, "Handbook of Photochemistry", Marcell Decker, New York, N.Y., 1973.

(12) In another experiment, the photosensitization of cyclooctene by methylbenzoate (E_T = 78.7 kcal/mol) gave a higher trans/cis photostationary ratio of 0.25. It is, however, doubtful whether, as is the case with the other sensitizers, the triplet–triplet energy transfer process is operative. Limited quenching experiments with piperylene suggest that this photoisomerization involves the benzoate singlet rather than the triplet state. The detailed mechanism and the nature of the intermediate involved are under investigation and may be the subject of a separate paper.

(13) S. Hirokami and S. Sato, *Can. J. Chem.*, **45**, 3181 (1967).

(14) M. Yaris, A. Moscowitz, and R. S. Berry, *J. Chem. Phys.*, **49**, 3150 (1968); O. Schnepp, E. F. Pearson, and E. Sharman, *ibid.*, **52**, 6424 (1970); M. G. Mason and O. Schnepp, *ibid.*, **59**, 1092 (1973).

(15) The extinction coefficient of *cis*-cyclooctene was measured with a Hitachi 356 spectrophotometer.

(16) P. v. R. Schleyer, J. E. Williams, and K. R. Blanchard, *J. Am. Chem. Soc.*, **92**, 2377 (1970).

(17) G. S. Schenck and R. Steinmetz, *Bull. Soc. Chim. Belg.*, **71**, 781 (1962).

(18) N. C. Yang, M. Nussim, M. J. Jorgenson, and S. Murov, *Tetrahedron Lett.*, 3657 (1964); N. C. Yang, *Pure Appl. Chem.*, **9**, 591 (1964); G. Porter and P. Suppan, *Trans. Faraday Soc.*, **62**, 3375 (1966); C. Rivas and E. Payo, *J. Org. Chem.*, **32**, 2918 (1967).

(19) The lowest triplet energy of benzene is 84.4 kcal/mol,[11] while the spectroscopic E_T of ethylene has been located near 82 kcal/mol (D. F. Evans, *J. Chem. Soc.*, 1735 (1960)), and alkyl substituted ethylenes are considered to have somewhat lower triplet energies.

(20) M. A. Golub, C. L. Stephens, and J. L. Brash, *J. Chem. Phys.*, **45**, 1503 (1966); H. Morrison, J. Pajak, and P. Peiffer, *J. Am. Chem. Soc.*, **93**, 3978 (1971).

(21) G. Buemi, G. Farini, and F. Zuccarello, *J. Mol. Struct.*, 5, 101 (1970); N. L. Allinger and J. T. Sprague, *J. Am. Chem. Soc.*, **94**, 5734 (1972); P. Ganis, U. Lepore, and E. Martuscelli, *J. Phys. Chem.*, **74**, 2439 (1970); P. C. Manor, D. P. Shoemaker, and A. S. Parkes, *J. Am. Chem. Soc.*, **92**, 5260 (1970).

(22) Although this value may be confirmed by a similar Arrhenius treatment of the photostationary ratio at the elevated temperature, attempted *p*-xylene photosensitization of cyclooctene in cyclohexane at 80 °C failed to get a higher photostationary trans/cis ratio because of significant thermal isomerization in the dark of *trans*-cyclooctene at that temperature.

(23) S. W. Benson, F. R. Cruickshank, D. M. Golden, G. R. Haugen, H. E. O'Neal, A. S. Rodgers, R. Shaw, and R. Walsh, *Chem. Rev.*, 69, 279 (1969); G. A. Haninger, Jr., and E. K. C. Lee, *J. Phys. Chem.*, **71**, 3104 (1967).

Comparative Photophysics of Indolizine and Related Heterocyclics

D. A. Lerner,[1] P. M. Horowitz,[2] and E. M. Evleth*

*Centre de Mécanique Ondulatoire Appliquée, 23 rue du Maroc, 75019, France, and the University of California,
Santa Cruz, California 95064 (Received June 11, 1976)*

The absorption–emission characteristics of six indolizines are reported. Analysis of the fluorescence lifetime-quantum yield data indicates that as a class of materials these substances exhibit slower nonradiative decay than do their indole counterparts and a number of aromatic hydrocarbons. A series of molecular orbital calculations indicate that the spacing and number of triplets states lying below the S_1 states in the indoles are much different than in the indolizines. Calculations indicate that the T_2 states in the indolizines could lie above S_1 so that intersystem crossing from S_1 and T_1 occurs without the benefit of communicating triplets.

Introduction

Indolizine (1) is an isomer of indole (2) conceptually obtained by the transposition of adjacent carbon and nitrogen atoms. There are also several other isomers of indole, 3–5, obtained by the placing of the nitrogen atom in various positions of the basic 5–6 ring structure.[3]

1	2	3
indolizine	indole	1-pyrindine

4	5
2-pyrindine	isoindole
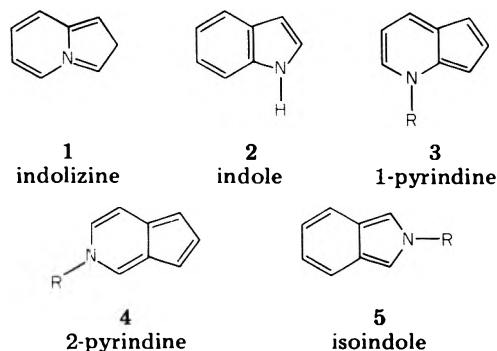
A large number of aza and polyaza derivatives of structures 1–5 are possible. From a photophysical standpoint what makes these systems interesting for study is the wide variation in spectral properties that occurs as a function of the position of these additional nitrogen atoms.[3-5] However, even in the basic series of structures 1–5 the variations of spectral features are dramatic. Indole exhibits two close lying singlet states, S_1 and S_2, transitions to which from S_0 lie in the 260–290-nm region.[6] In contrast to indole the 0–0 bands of 1 for the $S_2 \leftarrow S_0$ and $S_1 \leftarrow S_0$ transitions lie at 295 and 380 nm, respectively. Although aza substitution into indole leaves the positions of the two lowest lying $\pi-\pi^*$ transitions largely in the same energy region[7] the spectra of azaindolizines are strongly dependent on the position of nitrogen substitution.[3] Finally, the S_2-S_1 energy gap in derivatives of 3 and 4 (ca. 1.5 eV)[4] appears even larger than that for 1.

Visually the absorption spectra of 1, 3, and 4 resemble azulene[4,8] even though the magnitude of the S_2-S_1 energy gap is not as large. This resemblance provokes the idea that perhaps these heterocyclics share some of the other photophysical properties of azulene, namely, either $S_2 \rightarrow S_0$ emission[9] or dual fluorescence.[9b] Unfortunately, of this group only the indolizines have extensive preparative literature.[5] Here we report studies on 1, together with 1-azaindolizine (6), 2-azaindolizine (7), 1,8-diazaindolizine (8), and the 2-phenyl derivatives of 1 and 6, these being 9 and 10, respectively.

6	7	8

9	10
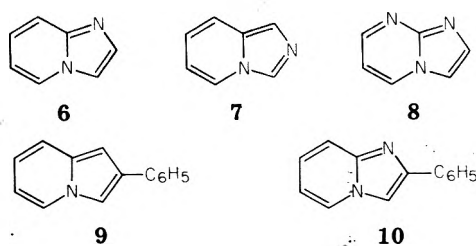
Preliminary reports have been presented on the photophysical properties of 1 and 6–8.[8,10] While no $S_2 \rightarrow S_0$ emission was detected from any of these materials[8] it was determined that the intersystem crossing rate constant and quantum yield had anomalous values.[10] Thus, we will also present theoretical calculations and attempt to rationalize the photophysical properties of the materials dealt with here.

Experimental Section

A. *Materials.* All materials were synthesized by well-established literature methods or obtained from commerical sources. Indolizine (1), known in the older literature as pyrrocoline,[5,11] was synthesized by the given procedure.[11a] The material appears unstable on long storage in the dark but is relatively easily purified by multiple microsublimation to yield a sharp melting point material. It is a colorless volatile material with an odor resembling naphthalene. A gas phase spectrum was easily obtained in a 10-cm gas cell at room temperature.[8]

Compound 6, 1-azaindolizine (imidaza[1,2a]pyridine), is known under the alternate names of [1,3a]diazaindene[5a] and pyrimidazole. It was commercially obtained from Aldrich Chemical Co. under the latter name. However, it was easily synthesized in one step from 2-aminopyridine.[5a] Both synthesized and commerical materials were spectroscopically identical after purification by GLC. The material is a colorless liquid at room temperature. Both 7 and 8, imidaza[1,5a]pyridine and imidaza[1,2a]pyrimidine, respectively, are reported in the literature as [2,3a]diazaindene and [1,3a,7]triazaindene. Their syntheses were easily affected by the given methods.[5a,c] As with indolizine purification of these materials was best achieved by multiple microsublimation immediately before use. Both 9 and 10 were purchased from Aldrich Chemical Co. and purified by recrystallization from ethanol. These latter two materials proved somewhat less soluble in hydrocarbon solvents.

All materials were checked for purity using mass spectral analysis. All physical properties agreed closely with the literature values, especially their rather complex ultraviolet

spectra in hydrocarbon solvents. Either at room temperature or in glassy solvents (EPA, MCH–IP) at 77 K we observed no anomalous emission which could be attributed to either impurity emission or the searched for $S_2 \rightarrow S_0$ fluorescence.

B. *Equipment*. UV–visible spectra were recorded on either a Cary 14 or Beckman Acta V spectrophotometers. Fluorescence–phosphorescence was measured on either Perkin-Elmer-Hitachi MPF-2A or 3A units. Polarization measurements were obtained using Polacoat UV 105 coatings on Suparsil plates and were corrected for using standard procedures.[12] Variable temperature studies were carried out using a Varian variable temperature acessory E-4540 mounted in the fluorimeter. Fluorescence lifetimes were measured from nanosecond flashes using a Tektronix 547 scope with a 1S1 sampling unit.

C. *Techniques*. All lifetime measurements were checked using as standards quinine sulfate, chrysene, biphenyl, and anthracene. The literature values[13] were assumed correct. The quantum yields of fluorescence were obtained using as standards quinine sulfate[14] ($\Phi_f = 0.55$), PPO[12] (1.00), and tryptophane[15] (0.14). Measurements were taken on degassed solutions having optical densities lower than 0.05. An independent check of the quantum yield of anthracene gave a value of 0.31 in n-hexane, identical with the average of the literature values.[7d,16]

Phosphorescence was searched for in these materials both instrumentally and visually under both mild and intense radiation. Unsensitized phosphorescence was only found for **6** and **10** (EPA, 77 K) with yields estimated to be below 0.01. In addition, sensitized phosphorescence was only obtained for **6** and **10** (benzophenone). The quantum yields for photodisappearance for **1** and **6**[10] were found to be less than 0.005.

D. *Theoretical Calculations*. Computational estimates of the spectral features of the materials dealt with here were carried out using both the Pariser–Parr–Pople (PPP–CI)[17] and CNDO/S[18] methods. The latter method generally gave poorer agreement with experiment with regard to the positions of the lowest lying transitions. The CNDO/S calculations did predict that in every structure the lowest lying transition was of the $\pi\pi^*$ type and that $n\pi^*$ states are not the lowest lying even in the case of **8**. A complete analysis of the variation of the $n\pi^*$ states with structure will be published at a later date for the azaindolizines, azaindoles, and related structures. We will only report the results of the PPP–CI computations. These were carried out using 20 single and 17 double excitations. The β integrals were calibrated by fitting the calculations to produce the positions of the 0–0 transitions for indole (**2**), 1-azaindolizine (**6**), and 1-pyrindine (**3**, R = methyl)[4a] to within 0.2 eV. This β parameterization scheme yielded good results for a number of azaindoles and aminonaphthalenes but as will as seen does not reproduce well the spectra of the polyazaindolizines to within 0.2 eV. The resulting β integrals for various bond types were as follows: C–C, -2.07 eV; C=C, -2.20; C–N, -1.84; C=N, -2.55; C=C (aromatic), -2.15; and C=N (aromatic) -2.18 eV. The Coulomb and electron repulsion parameters were as previously used.[3c] For bond distances we used the standard bond distances of Pople and Beveridge.[19] The triplet–triplet spectra were estimated by both CI treatment of the SCF ground state orbitals and by direct minimization of the lowest energy triplet followed by CI using both single and double excitations.

E. *Estimates of Photophysical Constants*. The oscillator strengths of the transitions were estimated from the integrated intensities using the standard equation.[20a]
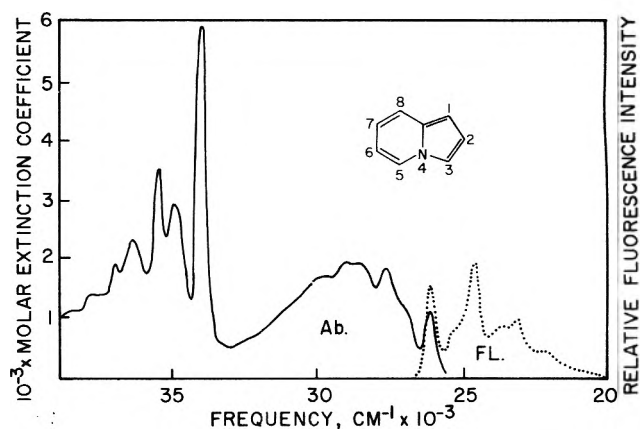
Figure 1. Absorption–emission spectrum of indolizine (**1**) in n-hexane.
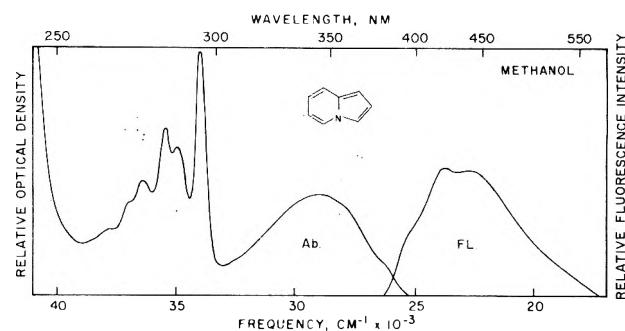
Figure 2. Absorption–emission spectrum of indolizine (**1**) in methanol.
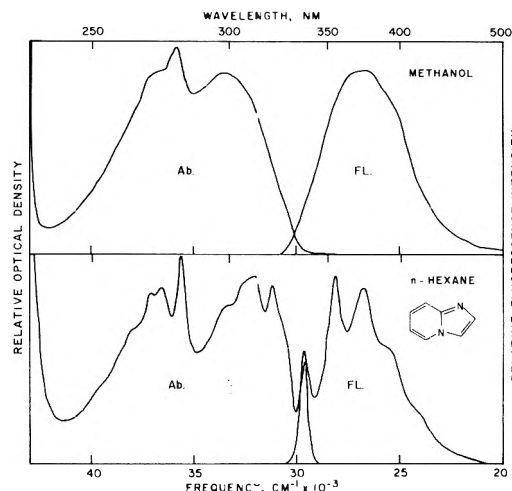
Figure 3. Absorption–emission spectra of 1-azaindolizine (**6**) in n-hexane and methanol.

Likewise, the radiative (natural) lifetimes, τ_{est}, were estimated by direct integration.[20b] The measured radiative lifetime, τ_r, was taken in standard fashion from

$$\tau_r = \tau_f/\Phi_f \tag{1}$$

where τ_f and Φ_f are the measured fluorescence lifetimes and quantum yields.

The radiative rate constant, k_r, is the inverse of τ_r. The nonradiative rate constant, k_{nr}, is estimated from k_r and τ_f using

$$1 - \Phi_f = k_{nr}/(k_r + k_{nr}) \tag{2}$$

Results and Discussion

A. *Absorption and Emission Properties*. Table I and Figures 1–5 show the experimental radiative and nonradiative rate constants and spectral properties of **1** and **6–10**

TABLE I: Computed and Measured Photophysical Properties of Various Indolizines[a]

Compd	Solvent	λ_{00}	f	τ_{est}	Φ_f	τ_f	τ_r	k_r, s^{-1}	k_{nr}, s^{-1}
1	H	383	0.027	42	0.84	42	50	2.0×10^7	4×10^6
	M				0.72	41	57	1.8×10^7	7×10^6
6	H	336	0.037	24	0.80	19	23	4.3×10^7	1×10^7
	M				1.00	21	21	4.8×10^7	$<5 \times 10^6$
7	H	380	0.026	43	0.98	40	40	2.5×10^7	$<3 \times 10^6$
	M				0.98	42	42	2.5×10^7	$<3 \times 10^6$
8	H	368	0.037	28	1.00	25	25	4.0×10^7	$<5 \times 10^6$
	M				0.77	23	30	3.3×10^7	1×10^7
9	H	386	0.039	30	0.60	22	36	1.9×10^7	2.8×10^7
	M				0.67	28	42	2.4×10^7	1.2×10^7
10	H	346	0.10	9	0.73	6	8	1.3×10^8	5×10^7

[a] H = n-hexane; M = methanol; λ_{00}, position of 0–0 band; f, estimated oscillator strength; τ, nanosecond values of the estimated (est), measured (f) or radiative (r) fluorescence lifetimes; Φ_f, measured fluorescence quantum yield; k_r and k_{nr} are the radiative and nonradiative rate constants.
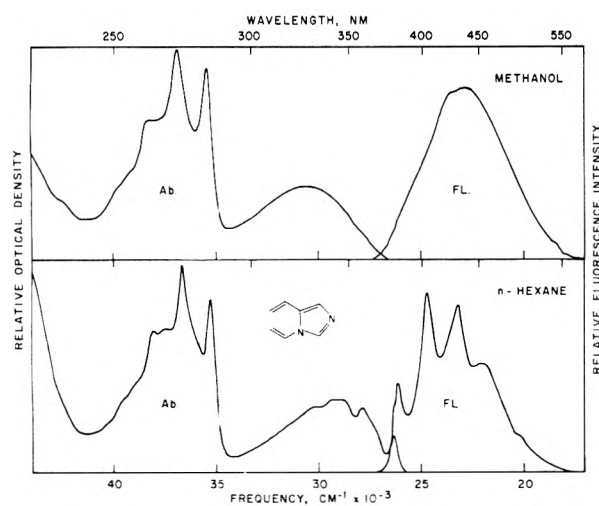
Figure 4. Absorption–emission spectra of 2-azaindolizine (**7**) in n-hexane and methanol.

Figure 5. Absorption–emission spectra of 1,8-diazaindolizine (**8**) in n-hexane and methanol.

in n-hexane and methanol. The absorption–emission spectra of these materials are all similar. The spectra are well defined in n-hexane and blurred in methanol. In the gas phase both 1 and 6[8,21] show a great deal of additional fine structure in the $S_1 \leftarrow S_0$ transition. In 1 there also is displayed unusual sharpness in the $S_2 \leftarrow S_0$ transition. This may be due to the magnitude of the S_2–S_1 energy gap, analogous to the same effect in azulene.[22]

In both methanol and n-hexane the quantum yields of fluorescence at room temperature are uniformly high. Since the molar extinction coefficients for the $S_1 \leftarrow S_0$ transitions are generally weak for indolizines[5] (ϵ_{max} 2000–3000 M^{-1} cm^{-1}) the actual integrated fluorescence lifetimes are moderately long (τ_{est} = 20–50 ns, with the exception of 10). These all approach the actual measured fluorescence lifetimes, τ_f, indicating that the fluorescence quantum yields, Φ_f, are high. Actual measurement of these yields indicated in several cases values approaching unity. Because of these high yields it was not possible to compute accurate values of the nonradiative rate constants, k_{nr}, so we have given estimates of maximum values. A number of these have maximum values in the order of 3–5 × 10^6 s^{-1}. For 1-azaindolizine (6) the measured value[10] of the intersystem crossing quantum yield, Φ_{isc}, in benzene was 0.009. Assuming that both Φ_f and k_{nr} are the same in n-hexane and benzene, this places the actual value of k_{isc} at 5 × 10^5 s^{-1} and a quantum yield for internal conversion at 0.2 with a rate constant in the 10^7 s^{-1} region. We also determined that the quantum yield of phosphorescence for 6 and 10 were less than 0.01 (EPA, 77 K). We were unable to detect phosphorescence under the same conditions for 1, 7, and 8.

From the above results we conclude that the values of Φ_{isc} and k_{isc} are generally low in the indolizines investigated here. The lack of a measured natural phosphorescence even at a very low yield in 1, 7, and 8 was particularly troubling. The phosphorescences displayed by 6 and 10 (τ_p, 5, 2.3 s; and λ_{00} 435, 459 nm, respectively) appeared normal and visually similar to indole. In addition, although the phosphorescenes of 6 and 10 were easily sensitized with benzophenone we could not stimulate emission for 1. Thus, the lack of natural phosphorescences for 1, 7, and 8 does not confirm the hypothesis of extremely low values of k_{isc}. These values must be equal to or less than the values of k_{nr}, however. Finally, in for 9 and 10 the k_{nr} values appear higher than in the cases of the non-phenylated materials. This is in contrast to the effect of phenylation on anthracene and naphthacene[20] in which the quantum yields of fluorescence move toward unity.

The high room temperature values of Φ_f in n-hexane and methanol preclude any large temperature effects on the fluorescence yields as is observed in many materials.[24] No variation of Φ_f (ca. 0.8) was found between 77 and 300 K in MCH–IP or EPA for either 1 or 6. However, 1 did exhibit a large variation in glycerol (4% H$_2$O) between –60 (Φ_f = 0.85) and 30 °C (Φ_f = 0.32). The relation log (Φ_f – 1) was linearly related to $1/T$ giving an activation energy of 3.6 kcal/mol for fluorescence quenching. The emission spectrum of 1 over this temperature range gradually evolves from a moderately structured one at –60 °C to a diffuse one at 30 °C similar to the emission in methanol. Although we did not study the temperature effect on the fluorescence of these materials in water we did examine emission changes with pH. Both the acid and base forms

TABLE II: Ground and Excited State pK's of Indolizines

Compd	λ_{00} IN	λ_{00} INH⁺	$pK_a(S_0)$	$pK_a^*(S_1)$ Calcd	Obsd
1	390ᵃ	327ᵃ	3.94	-6.7	
6	333ᵃ	301ᵃ	6.79	+0.2	+0.7
7	374ᵃ	340	5.54	-0.2	
8	373ᵃ	340	4.81	-0.1	

ᵃ Specie fluoresces; λ_{00}, estimated position of the 0-0 band in the IN (indolizine) or protonated indolizine (INH⁺) as estimated from the overlap region of the absorption and fluorescence or the red edge of the absorption band.

of 1 and 6 fluoresce whereas only the unprotonated forms of 7 and 8 fluoresce strongly. In most cases the protonated forms of the indolizines absorb at higher energies than the base forms.[5] This allows for an estimate of the excited state pK_a's from the Forster cycle.[25] These are shown in Table II. Only in the case of 6 was a definite values of pK_a^* directly measureable. We confirmed the observation of Mason and Smith[26] that, while both the acid and base forms of indolizine fluoresce, proton exchange does not occur within the excited state lifetime of the species. This is probably a consequence of the fact that the protonated form of 1 is a carbon acid and these are known[27] to undergo slow proton exchange in comparison with oxygen or nitrogen protonated species. The acidities of the excited singlet states of the azaindolizines are several pK_a units higher than in the ground state in contrast to the protonated forms of acridine, quinoline, and related heteroaromatics.[28,29] We also found that a hydrogen bonded ground state complex formed when small amounts of 1-butanol are added to n-hexane solutions of 7. However, the fluorescence spectra of these solutions were unchanged in shape and intensity indicating that this complex decomposed within the lifetime of the species we are dealing

with. Our previous theoretical analysis[3c] showed that the indolizines are characterized by a strong shift of electron densities from the five- to the six-member ring on excitation. From a perturbational viewpoint such a shift would show up in an increased acidity for the five-membered ring protonated form of the indolizines in the excited state or a shift toward decomplexation of a hydrogen bonded complex on excitation.

B. *Comparative Photophysics*. Since the indoles and indolizines are structurally related materials an analysis of the latter materials will require some comment on the former. Although the absorption-emission characteristics of indole are well studied[6,7,30-33] direct estimates of the intersystem crossing yield and rate constant have not been made. We estimate from the large mass of quantum yield and lifetime data that the value of k_{nr} is about 5×10^7 s⁻¹ for indole in n-hexane or cyclohexane (300 K). There are insufficient data to make a similar estimate in the cases of the aza- or polyazaindoles. Assuming that $k_{nr} = k_{isc}$, indole undergoes intersystem crossing about 100 times faster than 6. The k_{isc} value in 6 ranks with the lowest values reported for the hydrocarbon pyrene.[23b,34] The lowest value in the case of naphthalene, which is π isoelectronic with 1 and 2, is about 2×10^6 s⁻¹.[23b,35] Thus, the measured value of k_{isc} of 5×10^5 s⁻¹ demonstrates that the indolizines are experimentally differentiated from the indoles in having much slower rates of intersystem crossing. We will now use theoretical calculations to suggest a hypothesis on the reasons for these differences.

Theoretical calculations of the $\pi\pi^*$ singlet and triplet manifolds for 1, 2, and 6-8 are shown in Table III. Because of the low rates for k_{isc} it seems unlikely that the $n\pi^*$ singlet and triplet states are so placed in the azaindolizines so as to play a kinetic role in the photophysics of these materials. The weak nature of the $S_1 \rightarrow S_0$ transitions in all these materials have been well discussed

TABLE III: Computed and Experimental Singlet and Triplet Manifolds ᵃ

Structure	State $n =$	Energy $S_0 \rightarrow S_n$, eV	$f_{0 \rightarrow n}$	Transition moment, θ, deg	State $n =$	Energy $T_1 \rightarrow T_n$, eV	State	Experimental $S_0 \rightarrow X$, eV	$f_{0 \rightarrow n}$
2	0				1	(2.90)	T₁	3.06	
	1	4.33	0.02	-64	2	0.63	S₁	4.32	0.02
	2	4.55	0.10	-35	3	1.15	S₂	4.46	0.13
	3	5.60	0.28		4	1.36	S₃	5.8	0.7
	4	5.90	0.02		5	1.54			
1	0				1	(2.20)	T₁		
	1	3.56	0.05	+46	2	0.81	S₁	3.24	0.027
	2	4.09	0.05	+38	3	1.63	S₂	4.22	0.034
	3	5.21	0.04		4	1.68	S₃	5.2	0.5
	4	5.38	0.55		5	2.29*			
6	0				1	(2.42)	T₁	2.85	
	1	3.95	0.06	+21	2	0.92	S₁	3.70	0.037
	2	4.30	0.03	+76	3	1.29	S₂	4.4	0.034
	3	5.41	0.34		4	1.43	S₃	5.5	0.34
	4	5.62	0.22		5	2.05*			
7	0				1	(2.10)	T₁		
	1	3.49	0.08	+61	2	0.91	S₁	3.27	0.026
	2	4.13	0.13	-12	3	1.75	S₂	4.3	0.057
	3	5.00	0.10		4	2.18	S₃	5.7	0.4
	4	5.60	0.32		5	2.60			
8	0				1	(2.69)	T₁		
	1	3.80	0.07	+15	2	0.71	S₁	3.37	0.037
	2	4.29	0.05	-38	3	0.74	S₂	4.3	0.027
	3	5.52	0.40		4	1.59	S₃	5.3	0.26
	4	5.68	0.12		5	1.98			

ᵃ S and T are the singlet and triplet states; $f_{0 \rightarrow n}$ are the computed or measured oscillator strengths; θ is the transition moment measured counterclockwise with respect to the long axis of the molecule; all f values for the triplet-triplet transitions were computed at less that 0.01, except the values marked by an asterisk, these were 0.01.

in the cases of indole[6] and the indolizines.[3] In indole the lowest energy transition has been refered to[6] as being of the ^1L_b ← A type. This is actually a misapplication of the Platt classification scheme.[3b] Computationally the weak nature of this transition results from a near cancelling of the transition moments of two major configurations in the total configurational wave function, resulting from the promotion of an electron from the HOMO to the LUMO + 1 orbital and the HOMO − 1 to the LUMO. These are the same kind of configurations which give rise to the zero computed moments for the ^1L_b ← A transitions in the alternate hydrocarbons.[37] The higher computational oscillator strength of the S_2 ← S_0 transition in indole results from the fact that it is mainly composed of one configuration of the HOMO → LUMO type and thus is related to the ^1L_a ← A transition in alternate hydrocarbons. Experimentally, it is difficult to resolve these two transitions in indole into separate components so as to obtain an estimate of the integrated fluorescence lifetime.[3c,6e] It seems likely that the oscillator strength of the second transition is in the order of 3 times the first[6e] but the degree of vibronic coupling is not known. In the case of all the indolizines dealt with here we found that the S_1 ← S_0 transition is mostly a single determinant of the type HOMO → LUMO.[38] The weak nature of this transition is mainly the result of charge transfer from the five-member ring to the six-member ring. Computationally speaking, a mismatch in the position and magnitude of the orbital coefficients in the HOMO and LUMO orbitals gives rise in a low computed transition moment for the HOMO → LUMO configuration.

Visually, Figures 1–5 indicate that in 1 and 6–8 two electronic singlet–singlet transitions occur in the region above 250 nm. This is confirmed computationally. In addition, fluorescence polarization measurements were also consistent with this interpretation. These measurements also indicated that there was a 30° difference between the S_2 and S_1 ← S_0 moments in 1, 10–20° in 6, and 40–50° in 8. These are only in partial agreement with the relative moments shown in Table III.

With regard to the triplet manifold computed in Table III there is insufficient experimental information to test the validity of the relative values of the upper triplet states. The experimental S_1–T_1 energy gap in indole is about 1.3 eV. PPP–CI calculations predict that both T_2 and T_3 lie at lower energies than S_1 while T_4 and T_5 lie in the same energy region as the S_1 and S_2 states. We found the same situation in benzimidazole and a number of aza and polyazaindoles. The S_1–T_1 experimental energy gap is 0.85 eV in 6. The closed shell CI estimate of the position of the T_2 state in 6 (Table III) is 0.92 eV. Likewise, in 1, 7, and 8 the T_2 states are placed, respectively, 0.81, 0.91, and 0.71 eV above T_1. We also found that direct SCF minimization of the T_1 state followed by CI (of the same type as in the closed shell case) yielded T_2 states at 1.62, 1.15, 1.20, and 0.94 eV above T_1 in 6, 1, 7, and 8, respectively. In 1-azaindolizine (6) both types of calculation compute the T_2 state at a higher energy than the S_1 state. If so, intersystem crossing in 6 would have to take place directly from S_1 to T_1 without passing through a communicating triplet.

It has been proposed that in naphthalene and a number of aromatic hydrocarbons two different mechanisms control the rate of intersystem crossing.[39] Intersystem crossing can occur directly from S_1 to T_1 without need to invoke other triplet states as aiding this proces. The direct S_1 to T_n process could be much faster if a resonance matching of the initial singlet and intermediate triplet states occurred. This type of resonance mechanism has been invoked to explain the much faster intersystem crossing process in anthracene than in diphenyl-anthracene[20] as well as the temperature dependence of many intersystem crossing processes.

In the indolizines our results suggest that a direct S_1 to T_1 process occurs without the benefit of intermediate triplet states. However, two other hypotheses are possible. The computations also suggested that the density of triplet states in indole may be intrinsically larger than with the indolizines. Thus even if other triplet states beside T_1 lie at lower energies that S_1 the intersystem crossing process in the indolizines are slowed relative to indole. We have also determined that the S_1 states in the indolizines have a larger degree of charge transfer character than in indole. In addition, although not documented here, we have determined that the spin density character of the T_1 states in the indolizines is very much different than with indole. Therefore, while we view the major argument we have presented here as the most likely hypothesis explaining the results other theoretically more indeterminate factors may be operating.

References and Notes

(1) Current address: Ecole Nationale Superieure de Chimie, Montpellier, France.
(2) Current address: Department of Biochemistry, Darmouth College, Hanover, N.H.
(3) (a) S. F. Mason, *J. Chem. Soc.*, 3999 (1960); (b) J. Feitelson, *J. Chem. Phys.*, 43, 2511 (1965); (c) E. M. Evleth, *Theor. Chim. Acta*, 16, 22 (1970).
(4) A. G. Anderson, Jr., and H. L. Ammon, *Tetrahedron*, 23, 3601 (1967), and references cited therein.
(5) (a) J. D. Bower, *J. Chem. Soc.*, 4506, 4510 (1957); (b) J. D. Bower and G. R. Ramage, *ibid.*, 2534 (1955); (c) W. L. F. Armarego, *ibid.*, 4226 (1964); *ibid.*, 2778 (1965).
(6) (a) G. Barth, W. Voelter, E. Bunnenberg, and C. Djerassi, *J. Am. Chem. Soc.*, 94, 1293 (1972); (b) F. M. Sprinkel, C. Shillady, and R. W. Strickland, *ibid.*, 97, 6653 (1975); (c) W. Hug and I. Tinoco, Jr., *ibid.*, 95, 2803 (1973); (d) P.-S. Song and W. E. Kurtin, *ibid.*, 91, 4892 (1969); (e) L. J. Andrews and L. S. Forster, *Photochem. Photobiol.*, 19, 353 (1974); (f) E. H. Strickland, J. Horwitz, and C. Billups, *Biochemistry*, 9, 4914 (1970); (g) E. H. Strickland, C. Billups, and E. Kay, *ibid.*, 11, 3657 (1972); (h) Y. Yamamoto and J. Tanaka, *Bull. Chem. Soc. Jpn.*, 45, 1362 (1972).
(7) (a) M. J. Robey and I. G. Ross, *Photochem. Photobiol.*, 21, 363 (1975); (b) T. K. Alder, *Anal. Chem.*, 34, 685 (1962); (c) R. E. Linder, H. Weiler-Feilchenfeld, G. Barth, E. Bunnenberg, and C. Djerassi, *Theor. Chim. Acta*, 36, 135 (1974); (d) J. W. Eastman, *Spectrochim. Acta, Part A*, 26, 1545 (1970).
(8) D. A. Lerner and E. M. Evleth, *Chem. Phys. Lett.*, 15, 260 (1972).
(9) (a) J. B. Birks, *Chem. Phys. Lett.*, 17, 370 (1972); (b) G. Eber, F. Gruneis, S. Schneider, and F. Dorr, *ibid.*, 29, 397 (1974); (c) S. Murata, C. Iwanga, T. Toda, and H. Kokubun, *Ber. Bunsenges. Phys. Chem.*, 76, 1176 (1972), and references cited therein.
(10) A. Gupta, R. J. Kelly, E. M. Evleth, and G. S. Hammond, *J. Chem. Phys.*, 63, 5496 (1975).
(11) (a) V. Boekelheide and W. Freely, *J. Org. Chem.*, 22, 589 (1957); (b) A. Galbraith, T. Small, R. A. Barnes, and V. Boekelheide, *J. Am. Chem. Soc.*, 83, 453 (1961).
(12) T. Azumi and S. P. McGlynn, *J. Chem. Phys.*, 39, 1186 (1963).
(13) I. B. Berlman, "Handbook of Fluorescence Spectra of Aromatic Molecules", Academic Press, New York, N.Y., 1965.
(14) C. A. Parker and T. W. Rees, *Analyst*, 85, 587 (1960).
(15) J. E. Eisinger and G. Navon, *J. Chem. Phys.*, 50, 2069 (1969).
(16) (a) T. Medinger and F. Wilkinson, *Trans. Faraday Soc.*, 61, 620 (1965); (b) G. Weber and F. W. J. Teale, *ibid.*, 53, 646 (1957); (c) P. G. Bowers and G. Porter, *Proc. R. Soc. London, Ser. A*, 299, 348 (1967); (d) E. J. Bowen and K. West, *J. Chem. Soc.*, 4394 (1955).
(17) (a) J. A. Pople, *Trans. Faraday Soc.*, 49, 1375 (1955); (b) R. Pariser and R. G. Parr, *J. Chem. Phys.*, 21, 466, 767 (1953).
(18) R. L. Ellis, G. Kuehnlenz, and H. H. Jaffe, *Theor. Chim. Acta*, 26, 131 (1972). This paper contains the revised parameterization for estimating

$n\pi^*$ transition energies as well as $\pi\pi^*$ transitions. There are a number of options which can be used to calibrate the computed transitions to the observed ones. We found this was more easily accomplished in the PPP–CI approximation than in the CNDO/S method and therefore opted not to publish the results of the latter method.

(19) J. A. Pople and D. L. Beveridge, "Approximate Molecular Orbital Theory", McGraw-Hill, New York, N.Y., 1970, pp 90–92.
(20) (a) J. B. Birks, "Photophysics of Aromatic Molecules", Wiley-Interscience, London, 1970, p 51, eq 3.49; (b) p 88, eq 4.21.
(21) G. Fischer and R. Naaman, J. Mol. Spectrosc., 57, 284 (1975).
(22) J. Jortner, S. A. Rice, and R. M. Hochstraser, "Advances in Photochemistry", Vol. 7, J. N. Pitts, Jr., G. S. Hammond, and W. A. Noyes, Jr., Ed., Interscience, New York, N.Y., 1969, p 179.
(23) (a) Reference 20, see Tables 5.1 and 5.2, pp 178–181; (b) F. Wilkinson, "Organic Molecular Photophysics", Vol. 2, J. B. Birks, Ed., Wiley, New York, N.Y., pp 127–155.
(24) H. Lami, Chem. Phys. Lett., 21, 140 (1973).
(25) Th. Forster, Z. Elektrochem., 54, 42 (1950).
(26) S. F. Mason and B. E. Smith, J. Chem. Soc. A, 325 (1969).
(27) M. Eigen, W. Kruse, G. Maas, and L. DeMaeyer, Prog. React. Kinet., 2, 283–318 (1964).
(28) (a) H. U. Schutt and H. Zimmermann, Ber. Bunsenges. Phys. Chem., 67, 54 (1963); (b) H. Zimmermann and N. Joop, ibid., 65, 61 (1961).
(29) A. Weller, Z. Elektrochem., 61, 956 (1957).
(30) S. V. Konev, "Fluorescence and Phosphorescence of Proteins and Nucleic Acids", Plenum Press, New York, N.Y., 1967.

(31) (a) M. S. Walker, T. W. Bednar, and R. Lumry, J. Chem. Phys., 45, 3455 (1966); 47, 1020 (1967); (b) M. S. Walker, T. W. Bednar, R. Lumry, and F. Humphries, Photochem. Photobiol., 14, 147 (1971); (c) T. P. Hopkins and R. Lumry, ibid., 15, 555 (1972); (d) I. Tatischeff and R. Klein, ibid., 22, 221 (1975).
(32) C. Cazeau-Dubroca, F. Dupuy, M. Martinaud, and A. Campillo, Chem. Phys. Lett., 23, 397 (1973).
(33) I. B. Berlman, Spectrochim. Acta, Part A, 27, 473 (1971).
(34) (a) J. L. Kropp, W. R. Dawson, and M. W. Windsor, J. Phys. Chem., 73, 1747 (1969); (b) J. B. Birks, B. N. Srinivasan, and S. P. McGlynn, J. Mol. Spectrosc., 27, 266 (1968).
(35) (a) G. Karamos, T. Cole, P. Scribe, J. C. Dalton, and N. J. Turro, J. Am. Chem. Soc., 93, 1022 (1971); (b) M. Stockburger, H. Gattermann, and W. Klusmann, J. Chem. Phys., 63, 4529 (1975); (c) A. Reiser and T. R. Wright, ibid., 59, 3433 (1973).
(36) The CNDO/S calculations predicted in the cases of 6, 7, and 8 that the lowest $n\pi^*$ singlet states were between 0.2 to 1.2 eV above the S_1 state, with the energy separation being well over 1 eV in the cases of 6 and 7.
(37) (a) R. Pariser, J. Chem. Phys., 24, 250 (1956); (b) A. D. McLachlan, Mol. Phys., 2, 361 (1959).
(38) V. Galasso, G. DeAlti, and A. Bigatto, Theor. Chim. Acta, 9, 222 (1968).
(39) (a) B. R. Henry and W. Siebrand, "Organic Photophysics", Vol. 1, J. B. Birks, Ed., Wiley, New York, N.Y., 1973, pp 153–237; (b) S. A. Rice, "Excited States", Vol. 2, E. C. Lim, Ed., Academic Press, New York, N.Y., 1975, pp 235–256.

Characterization of the Hydroxyl Radical in Some Photochemical Reactions

Nalini Jacob, I. Balakrishnan, and M. P. Reddy*

The National Chemical Laboratory, Poona, India (Received May 27, 1976)

Quantitative estimation of OH by measuring its reaction with benzene in the presence of oxygen to give phenol and hydroxymucondialdehyde (HMD) shows that in the photolysis of hydrogen peroxide at 2970–3650 Å OH radicals account for all the primary decomposition. In the photolytic reduction of Fe^{3+} in water, the average quantum yield of OH for 2970–4358 Å is ~0.02, of the same order of magnitude as the earlier estimate of the Fe^{2+} yield for 2537 Å. The oxidation of benzene to phenol by Cu^{2+}, in contrast, yields no HMD, and must be by oxygen uptake not involving an OH intermediate. Inner filter corrections are deduced for the accumulation of product interfering with light absorption.

Introduction

The progress of research touching on the hydroxyl radical has been carefully reviewed in a recent article.[1] OH has been detected earlier by its spectrum in combustion reactions.[2] Pulse radiolysis studies coupled with fast photography followed and the spectra of the OH adduct of benzene and of its hydroxyperoxy radical were obtained.[3] These intermediates in the γ radiolysis of aerated aqueous solution of benzene yield as ultimate products phenol and hydroxymucondialdehyde (HMD), α and β isomers, in a ratio dependent upon temperature.[4] Addition of Fe^{2+} in acid medium produces the Fenton reaction in this system and raises the yield of both products in the same ratio[5,6] proving the occurrence of OH as an intermediate (Weiss–Haber mechanism) in the reaction of H_2O_2 with Fe^{2+}. In view of the unique identifiability of these products a good method is indicated for the detection and estimation of OH in several systems where centimolar concentrations of benzene could be tolerated. Thus, by this device, in the photolysis of H_2O_2 and the photoreduction of Fe^{3+}, these products can be used to measure the primary yields of OH. Recently, p-nitroso-N,N-dimethylaniline has been used for this purpose[7] in the photolysis of H_2O_2.

Experimental Section

Benzene (BDH), distilled, was purified by successive freezing. Water was triply distilled radiolysis grade. 30%

H_2O_2 containing an inorganic stabilizer was diluted for preliminary studies and was later replaced by pure H_2O_2 from BaO_2 (precipitated from strong H_2O_2 using baryta) and sulfuric acid. Excess acid was removed with slight excess of baryta and the pH finally adjusted at 6–7 by titrating with dilute H_2SO_4. Ferric perchlorate and uranyl sulfate were made by dissolving the hydroxides in the acids and evaporating. Other inorganic salts were AR grade.

The decomposition of H_2O_2 was measured by titrating with $KMnO_4$. Perkin-Elmer 350 and Beckman 378E ratio recording spectrophotometers were used. In the ferric systems iron was precipitated with dilute NaOH after the reaction and centrifuged. Several precautions are to be observed to secure reliable estimates of the OH yield. Steady but slow bubbling of air through the solution during photolysis is necessary. Precipitation of DDP occurs long after O_2 depletion and cannot be used as an indicator. Ether extraction and separate estimation of phenol yields low values in general. At the stage of alkali extraction traces of H_2O_2 in the ether layer decompose and destroy some phenol. The best procedure is to obtain the spectrum of the irradiated solution as such against the unirradiated as blank (Figure 2), verify the temperature with the γ value, and use the corresponding ϵ on the 345-nm absorbance (Figure 3). Spectra were run against proper blanks identically treated. Quantum yield determinations were based upon uranyl oxalate value of 0.56 for 2970–3650 Å and the absorbance values for 10^{-3} M ferric nitrate. A
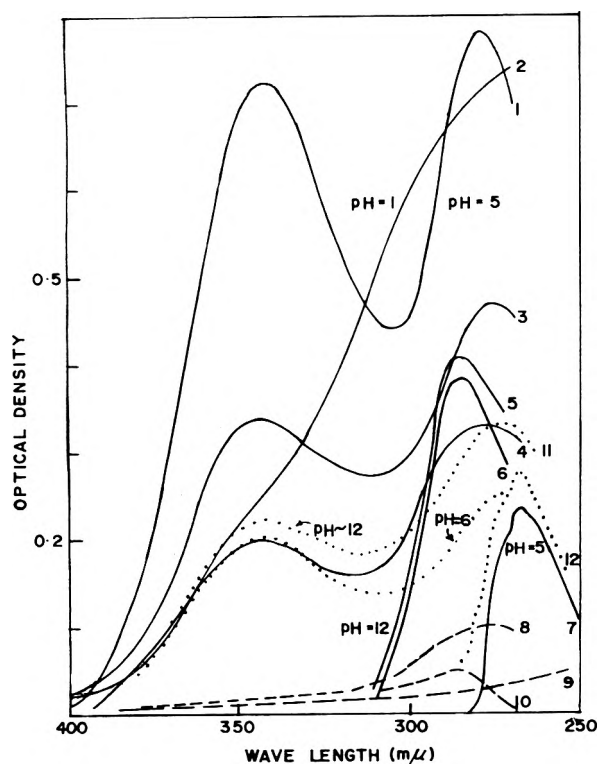
Figure 1. UV spectra of the products of the photolysis of H_2O_2 and of $Fe(NO_3)_3$ in presence of benzene and air: (1,2) HMD in 0.1 M H_2O_2 photolysis at 30 °C (pH effect); (3) HMD in 0.025 M H_2O_2 photolysis at 67 °C; (4) at 30 °C; (5,6) phenate in 67 and 30 °C photolysis of 0.025 M H_2O_2; (7) phenol at 30 °C; (8,9) total product and aqueous layer in the photolysis (2537 Å) of aerated aqueous benzene; (10) unknown phenate in alkali extract of ether layer; (11,12) HMD and phenol from photoreduction of 10^{-3} M ferric nitrate in the presence of benzene and air.

Figure 2. UV spectra of the products of the reaction of OH with benzene in presence of air at room temperature. γ radiolysis of aerated aqueous benzene: (1) total product; (2) HMD (aqueous layer); (3) phenol. Photolysis of H_2O_2 in presence of benzene and air: (4) total product; (5) HMD (aqueous layer); (6) phenol (neutralized alkali extract of ether layer).

medium pressure mercury lamp at 220 V and 3.5 A with maximum emission at 3650 Å was used. A $CuSO_4$ filter (0.1–0.5 M, 1 cm) eliminated wavelengths below 2970 Å. Distilled water circulating in a large quartz jacket served to control the temperature of the filter and the experimental solution dipping in it. A quartz tube bubbler was used to aerate the solutions.

Results and Discussion

Earlier, the mechanism of reaction of OH with benzene in aqueous solutions under γ radiolysis to give phenol and HMD isomers has been explained.[4]

Figure 1 demonstrates qualitatively the occurrence of OH in the photolysis of H_2O_2 ($CuSO_4$ filter; wavelengths not absorbed by benzene) and in the photoreduction of Fe^{3+} in water. Phenol and HMD, α and β, in the expected ratio, are clearly formed in the two systems. UV spectra of the products, separated by ether extraction, are presented. At low pH ($\sim$1) the two peak spectrum of the HMD isomer mixture (ether insoluble part) changes to the familiar broad tail of an absorption[8] whose maximum lies below 2700 Å. In two runs, at 30 and 67 °C, the phenol yield differs only slightly.[4] However the 345-nm peak for 67 °C is vastly enhanced over that for 30 °C, due to the increase in αHMD concentration at the higher temperature.[4] These aldehydes are not ether extractable and also yield slim precipitates of dinitrophenylhydrazone (somewhat reduced because of the presence of H_2O_2) which gives the familiar blue violet color in alkali, like the γ radiolysis product.[9] For the Fe^{3+} ion reaction the spectrum (dotted lines) of the solution after precipitation and ether extraction is shown at pH 6 and 12, and is as expected.[4,8] Also, in both systems prolonged irradiation without

bubbling air produces cloudiness and eventually a precipitate which has the odor characteristic of dihydrated diphenyl (DDP) described[10,11] for γ radiolysis of air-free aqueous benzene. The turbidity, however, appears in all these cases sometime after complete depletion of dissolved oxygen, the compound being soluble in water to $\sim 10^{-3}$ M. The broken curves in Figure 1 are for the products of photolysis of the same solution of benzene in the absence of H_2O_2 (without the $CuSO_4$ filter) resulting from reaction of excited benzene with dissolved O_2. The reaction is of negligible efficiency compared to that of H_2O_2. The phenols formed are a mixture of several. The aldehydic and other products contain no HMD. The precipitate formed in this case has an odor easily distinguishable from that of DDP. These facts are consistent with earlier findings[12] and further prove the role of OH in the formation of phenol, HMD, and DDP from benzene.

In Figure 2 the identity of product formation is conclusively proved by superposition of total product spectra for γ irradiated aerated aqueous benzene and photolyzed H_2O_2 solutions of benzene run against identically treated unirradiated solutions as blanks in order to correct for the substantial absorption background due to H_2O_2 and register the product phenol spectrum clearly. The 345-nm peak represents α HMD and the 270-nm peak is due to all the three products. The ratio 270 nm/345 nm = γ, for solutions at pH 6, determines the temperature at which OH reacts with benzene and can be used in conjunction with an effective extinction coefficient ϵ for the absorption at 345 nm to obtain the concentration of the total product (= OH yield). Figure 3 based upon earlier γ radiolysis studies, has been devised for this purpose.

TABLE I: Photolysis of H_2O_2 in the Presence of Benzene

Series A. H_2O_2 Decomposition Estimated by Polarography

Time, min	$[H_2O_2]$, M	H_2O_2 decomposed, %	
		Benzene absent	Benzene present[b]
30	0.0227	5.7	1.4
30	0.0260	15.4	3.7
Same[f]		15.4	7.1
16	0.0242	18.75	4.5

Series B. H_2O_2 Decomposition Correlated with OH Yield

Filter	Time, min	$[H_2O_2]$, M	Light int, photons/l s	Inner filter corr	$\Delta H_2O_2/OH$
Corning 1 mm[a]	15	0.0500			6.6[c]
0.5 M $CuSO_4$	30	0.0280	2.2×10^{17}		3.6[c]
0.4 M $CuSO_4$	15	0.0121	1.29×10^{17}		3.8[c]
0.2 M $CuSO_4$	15	0.0121	2.38×10^{17}		1.7[c]
0.1 M $CuSO_4$	7.5	0.0250	5.5×10^{17}	0.730	1.21[d]
0.08 M $CuSO_4$	15	0.0121	4.3×10^{17}	0.714	1.03[e]
	10	0.0121	4.3×10^{17}	0.758	1.05[e]

[a] A strong filter. [b] Three runs with random variation of intensity. [c] Chain region. [d] A border line case. [e] Nonchain region. [f] With O_2 depletion and turbity.
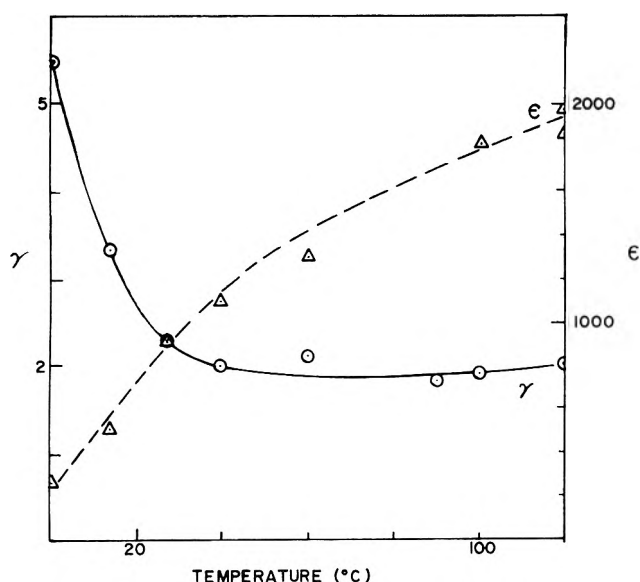
Figure 3. Estimation of products of reaction of OH with benzene in presence of air. γ is the ratio of absorbance of total product spectrum at 270 nm to that at 345 nm. ϵ is the equivalent extinction coefficient on the 345-nm peak for direct estimation of the concentration of OH. (The x axis gives the temperature at which the reaction occurred.)

Photolysis of H_2O_2. The overall quantum yield of ~ 2 obtained by Dainton[13] allows any one of three primary photolytic decomposition mechanisms

$$H_2O_2 \xrightarrow{h\nu} 2OH \quad \text{(ref 13 and 14)}$$
$$\longrightarrow 2OH \rightarrow H_2O + O \quad \text{(ref 15)}$$
$$\longrightarrow H_2O_2^* + H_2O_2 \rightarrow 2H_2O + O_2 \quad \text{(Stern-Volmer[16] type)}$$
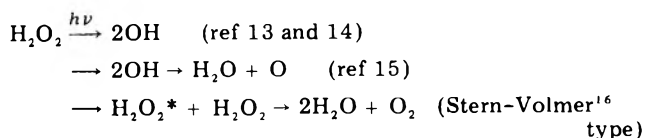
In the present study there is a possibility of distinguishing between them. In one series of experiments the rate of photodecomposition of H_2O_2 in the presence and absence of benzene was determined. A preliminary study by destroying H_2O_2 with a slight excess of $FeSO_4$ and colorimetric assay of the excess (o-phenanthroline) showed that the initial concentration of H_2O_2 was intact in samples photolyzed in presence of benzene, in contrast to high color of the o-phenanthroline complex shown by lowering of H_2O_2 concentration in photolyzed solutions free of benzene. The result was quantitatively confirmed by polarography ($E_{1/2} = -0.94$; comparison of diffusion current was by

superposition of curves). Benzene saturated solutions always indicated a very low value for the decomposition of H_2O_2 (Table I). In the mechanism for the formation of phenol and HMD there is an equivalent restoration[4] of H_2O_2. The present experimental result therefore indicates that the photodecomposition is solely through an OH intermediary. The result is similar to earlier findings[14] for H_2O_2 photolysis in the presence of alcohol.

In the second series the decomposition in pure H_2O_2 solutions was matched with the yield of OH in the corresponding benzene saturated solutions. In low intensity runs (0.2–0.5 M $CuSO_4$ or with a Pyrex filter) the ratio of the H_2O_2 decomposed (ΔH_2O_2) to the yield of phenol and HMD (= OH) in the presence of benzene is significantly higher than unity. The phenol + HMD in these runs seems to represent the OH yield in the primary decomposition step. The range of intensity absorbed corresponding to these runs (Table I) clearly indicates that decomposition is in the chain reaction region (for 0.01 M H_2O_2 solutions at $I_{abs} < 3 \times 10^{17}$ photons/l s).[17] The ratio $\Delta H_2O_2/OH$ then represents the chain length. This interesting result, that benzene suppresses the chain reaction, can be best explained in terms of Dorfman's two mechanisms[3] for the disappearance of hydroxycyclohexadienylperoxy radical, according to which phenol and HMD formation may be visualized as in Scheme I. When the chain decomposition of H_2O_2 due to HO_2 is absent (high intensity), the ΔH_2O_2 in presence of benzene should be nil, and the phenol + HMD yield would be equal to the ΔH_2O_2 in the absence of benzene, whatever the relative proportion of incidence of reactions 1 and 2. In the chain decomposition region (low intensities), however, bimolecular mechanism 2 would completely suppress ΔH_2O_2 and the chain, but unimolecular mechanism 1 would sustain the chain and produce about as much ΔH_2O_2 as phenol + HMD. The small residue of ΔH_2O_2 shown by the polarographic results (Table I) may thus be regarded as an indication of some chain reaction and slight incidence of mechanism 1. In the second series the high $\Delta H_2O_2/OH$ values obtained at low intensities are clear proof of large incidence of mechanism 2. In complete absence of mechanism 1 these values would represent chain lengths. With higher I_{abs} values (0.1 M or less $CuSO_4$ filter) the reaction goes into the nonchain region and the $\Delta H_2O_2/OH$ ratio approaches, but never actually becomes, unity. The discrepancy could be traced to a cut in the energy absorbed by the H_2O_2 in the benzene saturated solutions as a result

Scheme I
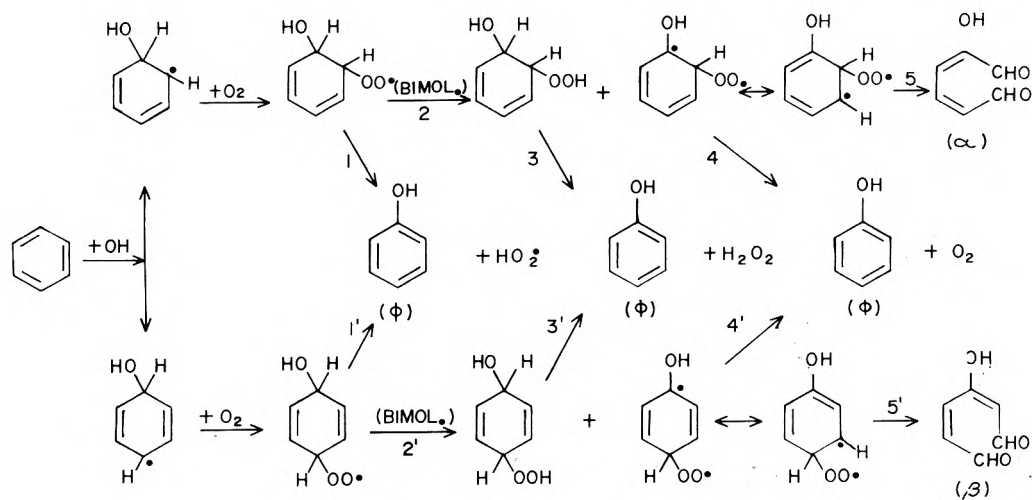
of the growth of absorption in the 2900–3600-Å region due to the αHMD. Correction for this inner filter phenomenon[18] equalises ΔH_2O_2 and phenol + HMD yield (last entries, Table I; the entry for 0.025 M H_2O_2 is evidently a border line case) and verifies the conclusion from the first set of experiments that the primary decomposition of H_2O_2 excited by 3000 Å and above is exclusively into OH radicals.

Earlier,[4–6] phenol and HMD formation was depicted entirely in terms of Dorfman's mechanism 1. The scheme required by the present work, in utilizing mechanism 2, obviates the uncomfortable postulate of a two stage uptake of oxygen for HMD formation, and is evidently more satisfactory. Attributing a higher activation energy to reactions 1 and 1' on the new scheme, one can easily explain the mild increase in phenol yield with temperature. Analysis of much higher temperature results is being done here before advancing an explanation for the observed rise in αHMD and fall in βHMD as the temperature of reaction is increased. At very low intensities, under conditions of high incidence of chain in H_2O_2 photolysis,[18] we do find the increase in relative proportion of phenol required by the present scheme. The effect however is too small to influence drastically the overall analysis and method presented here.

The quantum yield for nonchain decomposition of H_2O_2 obtained in this work is 1.2 and 1.0, respectively, for 0.025 and 0.1 M solutions. The highest measurable yield for the OH quantum yield is 70% of these, in the absence of inner filter correction.[18]

Photoreduction of the Ferric Ion in Water. Together with Fenton's reagent, the aqueous ferric ion photolytic system has been developed as a hydroxylating agent. The species $Fe^{3+}\cdot OH^-$, upon excitation, is said to release the OH radical. This system was a natural choice for testing the present method. The following set of simple observations was made. In initial experiments with $Fe(ClO_4)_3$ in sun light, after extraction of phenol, the aqueous layer showed the spectrum of HMD partially oxidized by the $HClO_4$ in solution, a broad absorption mounting toward 250 nm with indication of maxima at 270 and 345 nm. Photolyzed acid-free ferric sulfate and nitrate, however, showed the two peak spectrum of HMD, in intensity consistent with the requirement of Figure 3 for room temperature. The dotted line spectra of Figure 1, for acid free 10^{-3} M $Fe(NO_3)_3$, of pH 2.8, correspond to an OH quantum yield of 0.022 allowing for the drop in Fe^{3+} concentration and growth in αHMD in the course of the reaction (inner filter correction[18]). Added Fe^{2+} ion at 10^{-2} M competes with

benzene and reduces phenol + HMD yield by 20%, indicating a k value of $5–10 \times 10^8$ for the reaction of OH with Fe^{2+}. Earlier,[19] a quantum yield of 0.05 was obtained for Fe^{2+} from the photoreduction of radioactively labeled $Fe(ClO_4)_3$ in $HClO_4$ at 2537 Å. On the other hand, measurements[20,21] of OH at 3130 Å in Fe^{3+} solutions using benzene or acrylamide as scavengers gave a quantum yield of ~ 0.14. In Baxendale's work,[20] inefficient scavenging of radicals by Fe^{3+} leads to dimer formation, which complicates the study. The present method is more satisfactory for a count of the OH radicals. The lower value of 0.022 obtained here at 3650, 4040, and 4358 Å seems to indicate a dependence of OH yield upon wavelength such as has been reported earlier by Evans, Santappa, and Uri.[22] Also in scavenging experiments using benzoic acid, Bates and Uri[23] obtained, for 3650 Å, a yield of salicyclic acid of 0.01, in essential agreement with the present value (products other than salicylic acid have been missed). Dainton's value[19] for reduction of ferric to ferrous (direct measure) of 0.05 is for 2537 Å. This value, again, on the assumption of a wavelength dependence, appears to be consistent with the 3650-Å values. One is tempted to think that the values for 3130 Å are too high[20,21] and need to be redetermined. Ultimately it may not be necessary to visualize a different and distinct mechanism for the reduction of the ferric ion, involving an intermediate capable of being deactivated in a reaction with Fe^{2+}, as Dainton[19] has suggested.

Cu^{2+} Catalyzed Oxidation of Benzene to Phenol. Since the oxidation of benzene to phenol using O_2 in the presence of metal ions was one of the earlier preoccupations of the present program, the cupric ion system in particular was tested by the present method. Aqueous benzene solutions containing 10^{-3} M $CuSO_4$ do not show any immediate phenol formation upon photolysis (wavelengths below 3000 Å). On standing for several days with occasional shaking, large yields of phenol are noted. The spectrum, however, does not show any trace of HMD. Clearly, therefore, the OH is not an intermediate in this dark reaction.

In the metal ion induced hydroxylation of substituted aromatic compounds the ratio of the isomeric products is dependent on the metal ion concentration and significantly different from that in the Fenton hydroxylation. Also there is no dimeric biproduct formed. These findings were suggestive of a mechanism not involving OH and indicated active involvement of a metal ion–oxygen complex in the reaction with the aromatic compound.[24] The present result is a further confirmation of these ideas. On the other hand, a negative result in a situation, where much phenol is

TABLE II: Inner Filter Correction in Photochemical Reactions
(A) Photolysis of H_2O_2 in the Presence of Benzene

λ, A	t, min	c, M	ε	2.303a	b/a	2.303p	ΔE/N II[a]	ΔE/N IV[b]	Corr
2800	10	0.012	4.00	0.1105	0.0072	0.25085	1.0450	0.6397	0.612
2890	10	0.012	2.16	0.0597	0.0132	0.1525	0.5800	0.4188	0.722
2970	10	0.012	1.31	0.0362	0.0220	0.1084	0.3600	0.2722	0.770
3020	10	0.012	0.86	0.0238	0.0330	0.0993	0.2376	0.1874	0.789
3120	10	0.012	0.39	0.0108	0.0725	0.0933	0.1077	0.0904	0.804
3340	10	0.012	0.063	0.0017	0.4641	0.1204	0.0174	0.0133	0.764
2800	15	0.012	4.00	0.1105	0.0071	0.2156	1.5675	0.8828	0.563
2890	15	0.012	2.16	0.0597	0.0130	0.1311	0.8700	0.5859	0.674
2970	15	0.012	1.31	0.0362	0.0217	0.0930	0.5400	0.3915	0.725
3020	15	0.012	0.86	0.0238	0.0326	0.0853	0.3570	0.2660	0.745
3120	15	0.012	0.39	0.0108	0.0716	0.0801	0.1620	0.1234	0.762
3340	15	0.012	0.063	0.0017	0.4580	0.1034	0.0261	0.0187	0.717

(B) Photoreduction of Ferric Nitrate in the Presence of Benzene

λ, A	t, min	c, M	ε	a	b	p	ΔE/N V (i)[c]	ΔE/N V (ii)[d]	ΔE/N V (i) + (ii)	I	Corr
3650	10	10^{-3}	1000	1.00	0.022	0.016	9.224[e]	−1.266[f]	7.958	9.000	0.884
3340	10	10^{-3}	1500	1.50	0.033	0.016	10.197[g]	−1.151[h]	9.046	9.684	0.935
3120	10	10^{-3}	2000	2.00	0.044	0.012	10.759[i]	−1.364[j]	9.395	9.900	0.949
3020	10	10^{-3}	2170	2.17	0.048	0.011					} ~0.96
2970	10	10^{-3}	2200	2.20	0.048	0.012					

[a] Value of integral (II) in text. [b] Value of integral (IV) in text. [c] First bracket in (V). [d] Sum of integrals in second bracket in (V). [e] To 13 terms. [f] To 8 integrals. [g] To 14 terms. [h] To 11 integrals. [i] To 15 terms. [j] To 14 integrals.

formed, further proves the soundness of the present test for OH.

Inner Filter Correction for Growth of Product Interfering with Light Absorption.[25,26] If N is the number of photons falling on the system per unit time, and a the absorbance of the solution, the absorption in time t by a substance of extinction coefficient ϵ at concentration c, in unit path length, is

$$E = N(1 - 10^{-\epsilon c})t = N(1 - e^{-2.303a})t \qquad (I)$$

For a linear drop in absorbance, at a rate b, as a result of decomposition of reactant

$$E = \int_0^t N[1 - e^{-2.303(a-bt)}]\,dt$$
$$= N[t - e^{-2.303a}(e^{2.303bt} - 1)/2.303b] \qquad (II)$$

When two substances (or groups) absorb at the same wavelength the individual absorbances add up but the total energy absorbed is less than the sum of the energies absorbed individually if each were present alone in that solution. This energy is distributed between the two members, 1 and 2, in the ratio of their absorbances A_1 and A_2.

The total energy absorbed by the mixture per unit time, in unit path length, is

$$\Delta E = N[1 - e^{-2.303(A_1+A_2)}]$$

of which

$$\Delta E_1 = N[1 - e^{-2.303(A_1+A_2)}]A_1/(A_1 + A_2) \qquad (III)$$

goes to constituent 1.

Applying this to an inner filter action due to product accumulating linearly in time, at a rate of growth of absorbance, p, where the reactant retains its initial concentration, and absorbance, a, the energy absorbed in time t by the reactant is given by

$$\Delta E = \int_0^t N[1 - e^{-2.303(a+pt)}][a/(a + pt)]\,dt$$
$$= [Na/p][2.303pt - 2.303^2\{(a + pt)^2$$
$$- a^2\}/2.2! + 2.303^3\{(a + pt)^3 - a^3\}/$$
$$3.3! - \ldots] \qquad (IV)$$

The most complicated case is one in which the reactant also decreases as a result of reaction, linearly in time, at a rate of drop of absorbance, b. In this case

$$\Delta E_1 = \int_0^t N[1 - e^{-2.303[a-(b-p)t]}][(a - bt)/\{a$$
$$- (b - p)t\}]\,dt$$
$$= [Na/(p - b)][2.303(p - b)t$$
$$- (2.303^2/2.2!)\{[a + (p - b)t]^2 - a^2\}$$
$$+ (2.303^3/3.3!)\{[a + (p - b)t]^3 - a^3\} - \ldots]$$
$$- N[2.303bt - (2.303^2/2!)\int_0^t[a + (p - b)t]$$
$$\times bt\,dt + (2.303^3/3!)\int_0^t[a + (p - b)t]^2$$
$$\times bt\,dt - \ldots] \qquad (V)$$

Any one of eq II, IV, or V may be normalized by dividing with eq I to eliminate N and the correction factor for occurrence of the particular effect ascertained.

In the photolysis of H_2O_2 solutions containing p-nitroso-N,N-dimethylaniline scavenger[7] the energy absorbed by H_2O_2 has been evaluated with the eq III. With benzene as scavenger, one has a case for testing eq II and IV. The photoreduction of Fe^{3+} in the presence of benzene provides an opportunity for testing eq V. Although the benzene scavenger does not itself interfere at 2900–3650 Å, the product, α-hydroxymucondialdehyde, does, as it increases in concentration. Typical experimental results and estimates of correction based upon these equations are indicated in Table II. These have been incorporated in the discussion of the mechanism given earlier.

References and Notes

(1) C. Walling, *Acc. Chem. Res.*, 8, 125 (1975).
(2) P. Harteck, "Free Radicals", 59th General Discussion of the Faraday Society, 1934, p 139.
(3) L. M. Dorfman, I. A. Taub, and F. E. Buhler, *J. Chem. Phys.*, 36, 3051 (1962).
(4) I. Balakrishnan and M. P. Reddy, *J. Phys. Chem.*, 76, 1273 (1972).
(5) T. K. K. Srinivasan, I. Balakrishnan, and M. P. Reddy, *J. Phys. Chem.*, 73, 2071 (1969).
(6) I. Balakrishnan and M. P. Reddy, *J. Phys. Chem.*, 74, 850 (1970).
(7) M. Hatada, I. Kraljic, A. El Samahy, and C. N. Trumbore, *J. Phys. Chem.*, 78, 888 (1974).
(8) J. Goodman and J. Steigman, *J. Phys. Chem.*, 62, 1020 (1958).
(9) M. Daniels, G. Scholes, and J. Weiss, *J. Chem. Soc.*, 832 (1956).

(10) L. I. Kartasheva, E. V. Barelko, and M. A. Proskurnin, *Dokl. Akad. Nauk. SSSR*, **116**, 74 (1957).

(11) L. I. Kartasheva, Z. S. Boulanovskaya, E. V. Barelko, Ya M. Varshavskii, and M. A. Proskurnin, *Dokl. Akad. Nauk. SSSR*, **136**, 143 (1961).

(12) I. Loeff and G. Stein, *J. Chem. Soc.*, 2623 (1963).

(13) F. S. Dainton and J. Rowbottom, *Trans. Faraday Soc.*, **49**, 1160 (1953).

(14) J. H. Baxendale and J. A. Wilson, *Trans. Faraday Soc.*, **53**, 343 (1957).

(15) J. P. Hunt and H. Taube, *J. Am. Chem. Soc.*, **74**, 5999 (1952).

(16) M. Stern and O. Volmer, *Z. Wiss. Photogr., Photophys., Photochem.*, **19**, 275 (1920). See also G. K. Rollefson and M. Burton, "Photochemistry and Mechanism of Reactions", Prentice-Hall, Englewood Cliffs, N.J., 1939, p 190; ref 2, p 122; G. B. Kistiakowsky, "Photochemical Processes", Chemical Catalogue Company, New York, NY., 1928, pp 20–21.

(17) D. E. Lea, *Trans. Faraday Soc.*, **45**, 81 (1949).

(18) See last section of the discussion. The authors are grateful to the referee for pointing out the intensity dependence of the phenol yield.

(19) M. G. Adamson, D. L. Baulch, and F. S. Dainton, *Trans. Faraday Soc.*, **58**, 1388 (1962).

(20) J. H. Baxendale and J. Magee, *Trans. Faraday Soc.*, **51**, 205 (1955).

(21) F. S. Dainton and M. Tordoff, *Trans. Faraday Soc.*, **53**, 666 (1957).

(22) M. G. Evans, M. Santappa, and N. Uri, *J. Polym. Sci.*, **7**, 252 (1951).

(23) H. G. C. Bates and N. Uri, *J. Am. Chem. Soc.*, **75**, 2754 (1953).

(24) M. B. Dearden, C. R. E. Jeffcoate, and J. R. L. Smith, *Adv. Chem. Ser.*, **No. 77**, Vol. III, p 261, (1968).

(25) W. A. Noyes and P. A. Leighton, "Photochemistry of Gases", Reinhold, New York, N.Y., 1941, p 152.

(26) E. J. Bowen, "The Chemical Aspects of Light", Oxford University Press, London, 1949, p 195.

Diffusion-Limited Solvated Electron Reactions in Ethanol and Water

Harold A. Schwarz*

Chemistry Department, Brookhaven National Laboratory, Upton, New York 11973

and Piara S. Gill

Chemistry Department, Tuskegee Institute, Tuskegee, Alabama 36088 (Received July 26, 1976)

The rate constants for reaction of solvated electrons with Ag^+, $CuCl^+$, $CdNO_3^+$, NH_4^+, and I_2 have been measured in ethanol solution. The state of ionization and diffusion constants of the ions were established by conductivity measurements. The rare constants for the reactions with positive ions are all equal to the calculated diffusion-limited constant within 10%. The reaction with NH_4^+ is orders of magnitude larger in ethanol than in either water or liquid ammonia. Rate constants for hydrated electron reactions with I_2, I_3^-, Br_2, and Br_3^- have also been measured. The reaction radii for reaction with the halogens are large (9–15 Å). A reaction probability varying exponentially with the distance between the reactants is incorporated into diffusion theory to explain the results.

Relatively little work has been done on solvated electron reaction rates in nonaqueous solvents[1] compared to the vast amount of data gathered on the hydrated electron in water.[2] A study of reactions of the solvated electron in ethanol was undertaken with the hope that it might shed some additional light on the mechanisms of such reactions.

Experimental Section

USI ethanol (200 proof) was refluxed for 2 h with 10 g Mg metal/l[3] and distilled in a 30-plate column. Cd-$(NO_3)_2 \cdot 4H_2O$, $CuCl_2 \cdot 2H_2O$, and 12 M HCl were used without removal of water. (The additional water content introduced into the solutions from these sources was small compared to the water content of the ethanol.) Other salts used were anhydrous.

Oxygen was removed from the solutions by argon bubbling. Iodine was introduced into some solutions by passing the argon over iodine crystals. Bromine was added by passing the argon over Br_2 held at dry ice temperature. The iodine or bromine concentrations in the pulse-irradiated solutions were determined by mixing 5 cm³ of aqueous solutions with 5 cm³ of 0.2 M KI, or 2 cm³ of ethanolic solutions with 3 cm³ of 0.2 M KI, and measuring the optical density at 350 nm. The extinction coefficient of the I_3^- was taken to be 2.50×10^4 M^{-1} cm^{-1}.[4]

The pulse radiolysis was accomplished in cells with a 4.0-cm optical pathlength using a 2-MeV Febetron as the pulsed electron source. Approximately 1.5×10^{20} eV l^{-1} were delivered to the sample in each pulse. The samples were not thermostatted, but room temperature was recorded. The rise time of the light measuring system was 10 ns.

Conductivity measurements of ethanolic solutions were made at 25.0 °C using a stoppered cell with shiny Pt electrodes and a Beckmann Model RC 16B2 conductivity bridge. The cell constant was determined to be 0.141 cm from resistance measurements of an aqueous 0.02 M KCl solution.

The water content of the ethanol was estimated to be 0.4 wt % by comparing the specific resistance of a 1.25×10^{-4} M $MgCl_2$ solution in ethanol with measurements by El-Aggan et al.,[5] on ethanolic solutions at the same concentration as a function of water concentration.

Results

It is necessary to know the state of ionization in ethanol of the salts used, and to know the diffusion constants (or ionic conductivities) of the reactive ions in order to interpret the rate constant data. Conductivities of $Cd(NO_3)_2$, $CuCl_2$, and NH_4NO_3 were measured at various concentrations (between 8×10^{-5} and 6×10^{-4} M) and plotted as suggested by the Ostwald equation

$$\frac{1}{\Lambda_m} = \frac{1}{\Lambda_m^{\,0}} + Sc\Lambda_m \tag{1}$$

where Λ_m is the measured molar conductance, $\Lambda_m^{\,0}$ is the limiting molar conductance, c is the concentration, and S is the slope. Measurements of Λ_m were reproducible to 1%. Values determined for $\Lambda_m^{\,0}$ and S are given in Table I, along with literature values of $\Lambda_m^{\,0}$ for $AgNO_3$ and KOEt.

TABLE I: Conductivity of Salts in 99.6% Ethanol at 25 °C

Salt	Λ_m^0	S^a	Ref
$Cd(NO_3)_2 \cdot 4H_2O$	47	1.6	b
$CuCl_2 \cdot 2H_2O$	34	4.0	b
NH_4NO_3	46	0.04	b
$AgNO_3$	42		c
KOEt	47		d

^{a} Slope of Ostwald plot, eq 1. Concentration range is 8×10^{-5} to 6×10^{-4} M. ^{b} This work. ^{c} M. Kikindai, *C. R. Acad. Sci.*, 246, 412 (1958). ^{d} J. Barthel, H. J. Gores, and G. Engel, *Z. Phys. Chem.*, 72, 50 (1970).

TABLE II: Ionic Conductances and Diffusion Constants in 99.6% Ethanol at 25 °C

Species	λ^0	$10^5 D$, cm^2 s^{-1}
NH_4^+	21	0.58
Ag^+	18	0.48
$CuCl^+$	12	0.32
$CdNO_3^+$	22	0.58
e_{Et}^-	23^a	0.61
I_2		1.3^b

^{a} Fowles finds $\lambda^0(e_{Et}^-) = \lambda^0(OEt^-)$, ref 7. ^{b} P. Chang and C. R. Wilke, *J. Phys. Chem.*, 59, 592 (1955).

The value of 46 for NH_4NO_3 may be compared with a literature value of 47 determined by Barack and Hartley.[6] The limiting conductivity of KOEt is of interest because Fowles[7] has determined that the ionic conductance of the solvated electron in ethanol is equal to that of OEt$^-$ within experimental error (stated to be 20%).

The ionic conductivities, λ^0, of Cl$^-$, NO$_3^-$, and K$^+$ are 22, 25, and 24 cm^4 Ω^{-1} mol^{-1} in ethanol.[8] It may be seen that Λ_m^0 for $Cd(NO_3)_2$ is less than twice λ^0 for NO$_3^-$ and Λ_m^0 for $CuCl_2$ is less than twice λ^0 for Cl$^-$, demonstrating that these salts are not fully dissociated at these concentrations, but ionize to $CdNO_3^+$ and $CuCl^+$.

The ionic conductivities of the ions may be found from the molar conductivities in Table I and the values of λ_0 for the corresponding counterions. The diffusion coefficients of the ions may be determined from

$$D = \frac{RT}{F}\lambda_0 = 2.7 \times 10^{-7}\lambda_0 \text{ at } 25 \text{ °C}$$

The ionic conductivities and diffusion coefficients are given in Table II.

Rate constants for reactions of the electron in ethanol solution were measured by following the change in absorbance at 600 nm with time after the electron pulse. The absorbance decayed by first order in all cases

$$A = (A_0 - A_\infty)e^{-k_{obsd}t} + A_\infty$$

and A_∞ at 600 nm was negligible except in solutions of iodine in ethanol, in which there was a long-lived product.

In experiments with iodine in ethanol the observed rate constant is related to k, the second-order rate constant, by

$$k_{obsd} = k_0 + k[I_2]$$

where k_0 describes electron disappearance without iodine. We found k_0 to be 3.2×10^5 s^{-1}, somewhat greater than the value of 2.5×10^5 found by Fletcher et al.[9] at the same dose. The difference is likely due to traces of oxygen in our solutions. The I_2 concentration was varied up to 2×10^{-4} M (k_{obsd} values up to 4.5×10^6). The value of k found in this set of experiments was 2.0×10^{10} M^{-1} s^{-1}. Another set of experiments was performed in iodine solutions containing approximately 10^{-5} M HCl ($k_0 = 5 \times 10^5$ s^{-1}) to eliminate concern about possible solvolysis of the iodine.

TABLE III: Rate Constants for Solvated Electron Reactions in Ethanol at 28 °C

Reactant	$k \times 10^{-10}$, M^{-1} s^{-1}	$10^{-10} k_{diff}{}^a$
Ag^+	2.0	1.9
$CuCl^+$	1.8	1.7
$CdNO_3^+$	2.0	2.1
NH_4^+	2.0	2.1
I_2	2.1	

^{a} Calculated from eq 2 and 3.

The value of k was 2.2×10^{10} M^{-1} s^{-1} in these experiments and the average of the two values is reported in Table III.

The pseudo-first-order rate constant k_{obsd} was found to increase somewhat less than linearly with concentration in ethanolic solutions in which the reactant was a positive ion. This effect is due to the fact that ionic strength, μ, was not kept constant. The rate constant $k(\mu)$ for reactions between ions, at low ionic strength, varies as[10]

$$k(\mu) = k \exp\left[\frac{Z_a Z_b e^2}{DkT}\left(\frac{8\pi e^2 Nd}{1000DkT}\right)^{1/2}\mu^{1/2}\right]$$

where Z_a and Z_b are the number and sign of charges on the reactant, e, D, k, d, and N are the charge on an electron, the dielectric constant, Boltzmann's constant, the density, and Avogadros' number. In ethanol at 28 °C $D = 23.9$, $d = 0.783$ g cm^{-3}, and $\mu = c$, so

$$k(c) = ke^{-12.2c^{1/2}}$$

or

$$k_{obsd} = k_0 + kc \exp(-12.2c^{1/2})$$

The exponential term varied from 1 to 0.83. The concentration of reactive ion was varied up to 2×10^{-4} M and k was found as the slope of k_{obsd} vs. c $\exp(-12.2c^{1/2})$; so the rate constants reported in Table III are corrected to zero ionic strength.

The counterion in the $CdNO_3^+$ rate measurement was NO_3^-, which reacts rapidly with hydrated electrons in water. The reaction is much slower in ethanol because of the increased charge repulsion. Barat et al.[11] report a value of 3×10^7 M^{-1} s^{-1} for the NO_3^- reaction in ethanol. We find $k = (4 \pm 2) \times 10^7$ in ethanolic LiNO$_3$ solution. The counterion for NH_4^+ was NO_3^- in one case and Cl$^-$ in another with no difference in results.

Rate constants for reaction of the hydrated electron with I_2,I$^-$ solutions and Br_2,Br$^-$ solutions were measured in aqueous solution. The electrons can react with either X_2 or X_3^- (X = I or Br) which exist in equilibrium

$$X_2 + X^- \rightleftharpoons X_3^- \qquad K$$
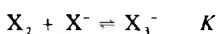
The measured second-order rate constant is a composite

$$k = k_{X_2} + (k_{X_3^-} - k_{X_2})f$$

where f is the fraction of total halogen present as X_3^-:

$$f = K[X^-]/(1 + K[X^-])$$

The equilibrium constant is 714 M^{-1} for iodine[12] and 17 M^{-1} for bromine.[13] The dependence of k on f is shown in Figure 1.

Discussion

The diffusion limit for reaction rate constants of solvated electron reactions may be expressed as[14]

$$k_{diff} = 4\pi(D_e + D_s)RN/1000 \qquad (2)$$

where D_e and D_s are the diffusion coefficients, N is
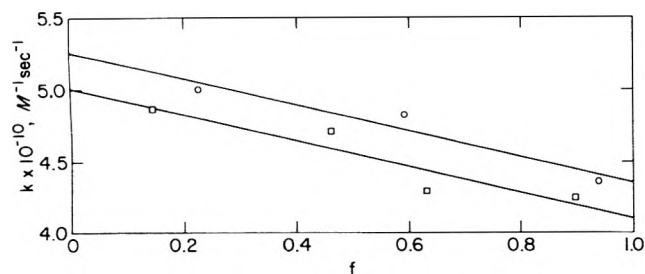
Figure 1. Variation of rate constant for reaction of hydrated electron with iodine (circles) or bromine (squares) with fraction of total halogen present as X_3^-.

Avogadros' number, and R is a reaction radius. If the reactant is an ion

$$R = r_c/[1 - \exp(-r_c/r_0)] \tag{3}$$

$$r_c = Ze^2/DkT$$

where r_0 is the separation of the reactants in contact and Z is the sign and number of charges on the reactant.

In ethanol, the value of r_c is 23.2 Å at 28 °C. Values of k_{diff}, calculated from eq 2 and 3 with the diffusion constants of Table II and $r_0 = 0$, are given in Table III. Any choice of r_0 less than 11 Å would lead to values of k_{diff} within 10% of these values. The excellent agreement with the observed rate constants is pleasing but not surprising, inasmuch as similar agreement (to ±20%) is common in aqueous solution.[15] The assumption of a continuous medium in the derivation of eq 2 becomes even more valid in liquids of low dielectric constant, in which r_c is large compared to molecular dimensions. Barat et al.[11] have demonstrated the dielectric constant dependence of some solvated electron reactions in ethanol–water mixtures. Fowles[7] has shown that the rate constant for reaction of the solvated electron with $C_2H_5OH_2^+$ agrees well with the calculated diffusion limit.

The fact that the reaction of the solvated electron with NH_4^+ is diffusion limited in ethanol is surprising. The rate constant is 2×10^6 M^{-1} s^{-1} in water[16] and 3×10^7 in liquid ammonia at 25 °C[17] or 1.2×10^6 at −35 °C.[18] Of course the lower dielectric constant of ethanol (24) would favor the ionic reaction relative to water ($l = 78$), but the reaction in ammonia should also be favored by dielectric constant ($l = 17$). The low rate constant in ammonia must be due to structural differences between ethanol and ammonia solutions for either the solvated electron or the ammonium ion.

The reactions of solvated electrons with halogens was chosen for further study because the rate constant for reaction with iodine in water was reported to be unusually large.[19] We find the rate constant for reaction with I_2 and Br_2 in water to be 5.6×10^{10} and 5.3×10^{10} M^{-1} s^{-1} (the intercepts at $f = 0$ of Figure 1). The rate constant for I_2 agrees well with the value of 5.1×10^{10} found by Thomas et al.[19] In order to obtain reaction radii for these reactants it is necessary to know their diffusion coefficients in water. An estimate of 1.6×10^{-5} cm^2 s^{-1} for I_2 can be made using the literature value for I_2 in ethanol (Table II) and the ratio of viscosities of ethanol and water. It was further assumed that the diffusion coefficient of bromine was equal to that of iodine. Fortunately, high precision is unnecessary for these diffusion coefficients because D for the hydrated electron is much larger, 4.9×10^5 cm^2 s^{-1}.[20] The use of these values leads to 11 and 10 Å for the reaction radii in the iodine and bromine reactions. A similar calculation for reaction of the solvated electron with iodine in ethanol gives a reaction radius of 15 Å (using the data of Tables II and III).

The other intercepts, at $f = 1$, represent rate constants k_μ for the I_3^- and Br_3^- reactions at appreciable ionic strength, 0.02 M I⁻ or 0.5 M Br⁻. The ionic strength dependence may be taken to be[14]

$$\log k_\mu = \log k + \frac{1.02\mu^{1/2}}{1 + 3\mu^{1/2}}$$

where the constant 3 in the denominator reflects the abnormally large reaction radii in the iodine and bromine reactions. Rate constants reduced to zero ionic strength with this equation are 3.5×10^{10} for I_3^- and 2.7×10^{10} M^{-1} s^{-1} for Br_3^-. The diffusion constant of I_3^- is 1.3×10^{-5} cm^2 s^{-1}[21] and that of Br_3^- may be assumed to be the same. The values of r_0 calculated from eq 2 and 3 are 12 and 9 Å.

These reaction radii are considerably larger than normal ionic radii. Such large reaction radii have been noted before by Anbar and Hart[15] who suggested that tunneling might be involved in the explanation of the effect. Most of their examples were reactions with negatively charged ions, however, which are very sensitive to the choice of R (see eq 2), but for which diffusion theory is perhaps most shaky. More recently, Miller[22] has shown that solvated electrons produced in glasses do not exhibit a normal exponential reaction with solutes but require the reaction rate constant to be a function of the distance between the reactants. He postulated that the electrons were, in fact, tunneling to the reactants and found for certain very effective solutes that his results fit well with a reaction probability $\beta(r)$ given by

$$\beta(r) = \nu e^{-b(r-r_0)} \tag{4}$$

where ν is 10^{15} s^{-1}, b is 1.0×10^8 cm^{-1}, and r_0 is 4×10^{-8} cm. These parameters are those expected for an electron on the basis of simple tunneling theory if the barrier height is 1.2 eV.[22] The applicability of the theory to solvated electron reactions is questionable because there are other pathways for the reaction (the electron exchanges with all surrounding valence electrons, for instance). Nevertheless, the experimentally determined electron transfer probability varies with distance in a fashion similar to eq 4 and Miller suggested that the same effect would explain the large reaction radii in liquids.

Equation 4 can be incorporated into diffusion theory for reactions in which at least one of the species is uncharged. The rate of change with time of w, the probability of finding the reactant at a radius r from the solvated electron, is

$$\partial w/\partial t = (D_e + D_s)\nabla^2 w - \beta(r)w$$

We are concerned here only with the steady-state solution in which the diffusion-limiting probability gradient has been established, so

$$(D_e + D_s)\nabla^2 w - \beta(r)w = 0$$

or, in spherical coordinates

$$\frac{d^2 w}{dr^2} + \frac{2}{r}\frac{dw}{dr} - \beta(r)w/(D_e + D_s) = 0 \tag{5}$$

In the normal diffusion-limited rate constant derivation $\beta(r)$ is assumed to be zero everywhere except at the boundary $r = r_0$, which leads to the solution that the reaction radius equals r_0. If instead $\beta(r)$ is given by eq 4, then the substitutions

$$y = wr$$

and

$$Z = Z_0 \exp\left(-\frac{b(r - r_0)}{2}\right)$$

where

$$Z_0 = 2\nu^{1/2}/b(D_e + D_s)^{1/2} \tag{6}$$

will convert eq 5 into a modified Bessel equation

$$Zy'' + y' - Zy = 0$$

the solution of which is

$$y = C_1 I_0(Z) + C_2 K_0(Z)$$

where I_0 and K_0 are the two zero-order modified Bessel functions and C_1 and C_2 are the constants of integration, to be evaluated as follows: as $r \to \infty$, $Z \to 0$ and $K_0(Z) \to -\ln Z \to br/2$, $y \to rc$ where c is the average bulk concentration of the reactant, and $I_0(Z) \to 1$. Consequently, $C_2 = 2c/b$. To evaluate C_1 we will make the usual assumption of diffusion-limited reaction rate theory that $w = 0$ at $r = r_0$, so that

$$C_1 = \frac{-2cK_0(Z_0)}{bI_0(Z_0)}.$$

The solution becomes

$$y = \frac{2c}{b}\left[K_0(Z) - \frac{K_0(Z_0)}{I_0(Z_0)}I_0(Z)\right]$$

The diffusion-limited reaction rate constant could be determined by integrating the function $w\beta(r)$ over all volume. A simpler method is to note that $4\pi r^2 \beta(r)$ goes to zero as $r \to \infty$ while the total number of reactants diffusing across a spherical boundary of radius, r, $-4\pi r^2 \phi$, does not. Consequently the rate of reaction of a solvated electron with the reactant is

$$R = \lim_{r \to \infty} (-4\pi r^2 \phi)$$

The diffusion-limited rate constant is R/c, and the flux, ϕ is $-(D_e + D_s)(\partial w/\partial r)$, so

$$k = 4\pi(D_e + D_s)\left[\lim_{r \to \infty}\left(\frac{r^2}{c}\frac{dw}{dr}\right)\right]$$

Comparison of this equation with eq 2 (ignoring $N/1000$, which converts units) shows that

$$R = \lim_{r \to \infty}\left(\frac{r^2}{c}\frac{dw}{dr}\right)$$

Performing the differentiation and taking the limit[23] gives

$$R = r_0 + \frac{2}{b}(\ln Z_0 + \gamma + K_0(Z_0)/I_0(Z_0)) \tag{7}$$

where γ is Euler's constant, 0.577.... The right-hand side

of eq 7 goes to r_0 when Z_0 approaches 0, which is the correct solution for the case in which there is no reaction beyond $r = r_0$.

Inserting into eq 6 the values $\nu = 10^{15}$ s^{-1}, $b = 10^8$ cm^{-1}, $r_0 = 4 \times 10^{-8}$ cm, along with $D_e + D_{I_2} = 6.5 \times 10^{-5}$ cm^2 s^{-1} (appropriate for water) gives $Z_0 = 580$. $K_0(Z_0)/I_0(Z_0)$ is approximately πe^{-2Z_0} for large values of Z_0 and consequently is negligible. This term contains the assumption that $w = 0$ at $r = r_0$ and is completely negligible under any other reasonable assumption. The result, then, is

$$R \approx r_0 + \frac{2}{b}(\ln Z_0 + 0.577)$$

or $R = 12.5$ Å for reactions in water. The same values of ν, b, and r_0 with $D_e + D_{I_2} = 1.9 \times 10^{-5}$ cm^2 s^{-1} (appropriate for ethanol) give $R = 13.7$ Å. It appears, then, that the introduction of a distance-dependent reaction probability for solvated electron reactions does correlate the liquid-phase results with the work on glasses. This conclusion, reached by Miller, is on a firmer basis with the derivation of eq 7.

References and Notes

(1) E. Watson, Jr., and S. Roy, *Natl. Stand. Ref. Data Ser., Natl. Bur. Stand.*, No 42 (1972).
(2) M. Anbar, M. Bambenek, and A. B. Ross, *Natl. Stand. Ref. Data Ser., Natl. Bur. Stand.*, No. 43 (1973).
(3) D. W. Johnson and G. Arthur Salmon, *J. Chem. Soc., Faraday Trans. 1*, 71, 583 (1975).
(4) A. O. Allen, C. J. Hochanadel, J. A. Ghormley, and T. W. Davis, *J. Phys. Chem.*, 56, 575 (1952).
(5) A. M. El-Aggan, D. C. Bradley, and W. Wardlaw, *J. Chem. Soc.*, 2092 (1958).
(6) M. Barach and H. Hartley, *Z. Phys. Chem.*, A165, 272 (1933).
(7) P. Fowles, *Trans. Faraday Soc.*, 67, 428 (1971).
(8) B. Kratochvil and H. L. Yeager, *Fortschr. Chem. Forsch.*, 27, 1 (1972).
(9) J. W. Fletcher, P. J. Richards and W. A. Seddon, *Can. J. Chem.*, 48, 1645 (1970).
(10) S. W. Benson, "The Foundation of Chemical Kinetics", McGraw-Hill, New York, N.Y., 1960, p 525.
(11) F. Barat, L. Gilles, B. Hickel, and B. Lesigne, *J. Phys. Chem.*, 77, 1711 (1973).
(12) A. I. Popoff, R. H. Rygg, and N. E. Skelly, *J. Am. Chem. Soc.*, 78, 5740 (1956).
(13) D. B. Scaife and H. J. V. Tyrrell, *J. Chem. Soc.*, 386 (1958).
(14) P. Debye, *Trans. Electrochem. Soc.*, 82, 265 (1942).
(15) M. Anbar and E. J. Hart, *Adv. Chem. Ser.*, No. 81, 79 (1968).
(16) J. Jortner, M. Ottolenghi, J. Rabani, and G. Stein, *J. Chem. Phys.*, 37, 2488 (1962).
(17) G. I. Khaikin, V. A. Zhigunov, and P. I. Dolin, *High Energy Chem. (Eng. Trans.)*, 5, 72 (1971).
(18) R. R. Dewald and R. V. Tsina, *J. Phys. Chem.*, 72, 4520 (1968).
(19) J. K. Thomas, S. Gordon, and E. J. Hart, *J. Phys. Chem.*, 68, 1524 (1964).
(20) K. H. Schmidt and W. L. Buck, *Science*, 151, 70 (1966).
(21) G. Edgar and S. H. Diggs, *J. Am. Chem. Soc.*, 38, 253 (1916).
(22) J. R. Miller, *J. Phys. Chem.*, 79, 1070 (1975).
(23) F. W. J. Olver in "Handbook of Mathematical Functions", M. Abramowitz and I. A. Stegun, Ed., U.S. National Bureau of Standards, Applied Mathematics Series 55, 1964.

Formation of Radical Zwitterions from Methoxylated Benzoic Acids. 1. One Electron Oxidation by Tl²⁺, Ag²⁺, and SO₄⁻

S. Steenken,* P. O'Neill, and D. Schulte-Frohlinde

Institut für Strahlenchemie im Max-Planck-Institut für Kohlenforschung, Stiftstrasse 34-36, D-4330 Mülheim/Ruhr, West Germany (Received March 29, 1976)

In aqueous solution 2-, 3-, and 4-methoxybenzoic acid; 2,3-, 2,4-, 2,6-, 3,4-, and 3,5-dimethoxybenzoic acid; and 2,3,4-, 2,4,5-, 2,4,6-, and 3,4,5-trimethoxybenzoic acid react with Tl²⁺, Ag²⁺, and SO₄⁻ by electron transfer to yield radical zwitterions. The radical zwitterions were identified using in situ radiolysis and photolysis electron spin resonance and spectrophotometric pulse radiolysis techniques. The coupling constants of the radical zwitterions are very similar to those of radical cations from structurally related methoxylated benzenes, indicating that the carboxyl group has very little influence on spin distribution. The radical zwitterions, with the exception of that from 3-methoxybenzoic acid, decay by second-order kinetics with rate constants ranging from 6×10^4 to 3×10^9 M⁻¹ s⁻¹, depending on the number and on the positions of the methoxyl groups relative to each other. Decarboxylation of the radical zwitterions does not occur.

Introduction

Formation of radical cations in aqueous solution by reaction of organic compounds with radical species has recently received considerable attention. Both product studies[1-4] and fast response techniques[5-11] have been applied. Except for the radical cation of biphenyl,[7] the radical cations of benzene derivatives so far identified by pulse radiolysis[6,8,10,11] or ESR[10,11] are derived from benzenes carrying electron-donating substituents such as methyl,[6] amino,[8] or methoxyl[10,11] groups. With methoxylated benzenes radical cations could be produced[10,11] by electron transfer to SO₄⁻, Tl²⁺, and Ag²⁺. While SO₄⁻ seems to be a very powerful oxidant,[4,12] the reactions of Tl²⁺ and Ag²⁺ were suspected to be sensitive to alterations in the ionization potential of methoxylated benzenes induced by electron-withdrawing substituents such as CO₂H. On the other hand, the reaction of benzoic acid and carboxylated benzoic acids with SO₄⁻ has been shown to result in decarboxylation to yield phenyl radicals.[13,14] It was therefore also considered of interest to investigate whether by substitution of ring hydrogens by methoxyl groups one-electron oxidation products of benzoic acids can be stabilized with respect to decarboxylation.

Experimental Section

The 3-MeV van de Graaff accelerator and the optical detection system have been described previously.[15] Solutions were irradiated at 20 ± 2 °C with electron pulses of 1-μs duration. The pH of the solutions was adjusted using HClO₄ or NaOH. Dosimetry was carried out using the modified Fricke solution (10⁻¹ M FeSO₄ in 0.8 N H₂SO₄). Doses were in the range 0.5-1 krad. The optical density values used to plot the spectra have been normalized to 3 krads and refer to a 1-cm pathlength. Carbon dioxide was determined from γ-irradiated 10-ml samples saturated with argon and containing 20 mM K₂S₂O₈ and 1 mM methoxylated benzoic acid at pH 4, using the analytical method described by Weeke et al.[16] The dose rate was ~8 × 10¹⁷ eV g⁻¹ min⁻¹.

The in situ radiolysis ESR experiments were performed at ~5 °C using the method described by Eiben and Fessenden.[17] Magnetic field measurements were made with a field-tracking NMR unit and frequency counter. The g factors were determined from simultaneous measurements of field and microwave frequency taking account of the magnetic field difference between the ESR cell and

NMR probe positions. The coupling constants and g factors are estimated to be accurate to 30 mG and 5×10^{-5}, respectively.

Except for 2,4,6- (Aldrich) and 3,4,5-trimethoxybenzoic acid (Merck) the substrates were obtained from Fluka. They were of the highest purity available and were used as received.

Results and Discussion

ESR Studies. Reaction with Tl²⁺ and Ag²⁺. On in situ electron irradiation at pH 4 of N₂O saturated aqueous solutions of 1-2 mM Tl⁺ or Ag⁺, respectively, and containing 0.1-0.2 mM 2- or 4-methoxybenzoic acid (MBA) or 2,3-, 2,4-, 2,6-, 3,4-, or 3,5-dimethoxybenzoic acid (DMBA) or 2,3,4-, 2,4,5-, or 3,4,5-trimethoxybenzoic acid (TMBA), ESR spectra were obtained (Figure 1) that can be identified consistently as due to one-electron oxidation products of the substrates. In the case of 3-MBA no lines were detected and for 2,4,6-TMBA only very weak lines were observed that could not be fully analyzed.

Under the experimental conditions described the radiolytically formed OH radicals predominantly react with Tl⁺ or Ag⁺ to yield Tl²⁺ [18,19] and Ag²⁺ [20,21] respectively. As in the case of the corresponding methoxylated benzenes,[11] Tl²⁺ and Ag²⁺ subsequently react with the substrates by electron transfer, e.g.

$$Tl^+ + OH \rightarrow Tl^{2+} + OH^- \quad (1)$$

$$2\text{-MBA} + Tl^{2+} \rightarrow (2\text{-MBA})^{\cdot+} + Tl^+ \quad (2)$$
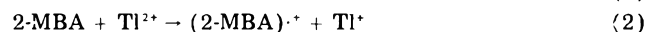
The pH dependence of the stationary concentration of the radicals shows a maximum between pH 3.5 and 5. Below pH ~3 the concentration is reduced by far more than expected on the basis of competition between N₂O and H⁺ for the hydrated electron. This is explained by removal of the one-electron oxidation products by fast reaction with the H adducts formed.[22] In the Tl⁺ system the decrease in the stationary concentration of the radicals observed above pH ~5 is suggested to be due to formation of Tl(OH)⁺ [19] and Tl(OH)₂,[23] which do not seem[10] to react quantitatively with the substrates by electron transfer. In the Ag⁺ system at pH >5 the complex Ag(OH)⁺ is formed[24] which likewise shows a reduced electron transfer efficiency as compared to Ag²⁺.

Identification of the Radicals. The coupling constants and g factors of the observed radicals were found to be
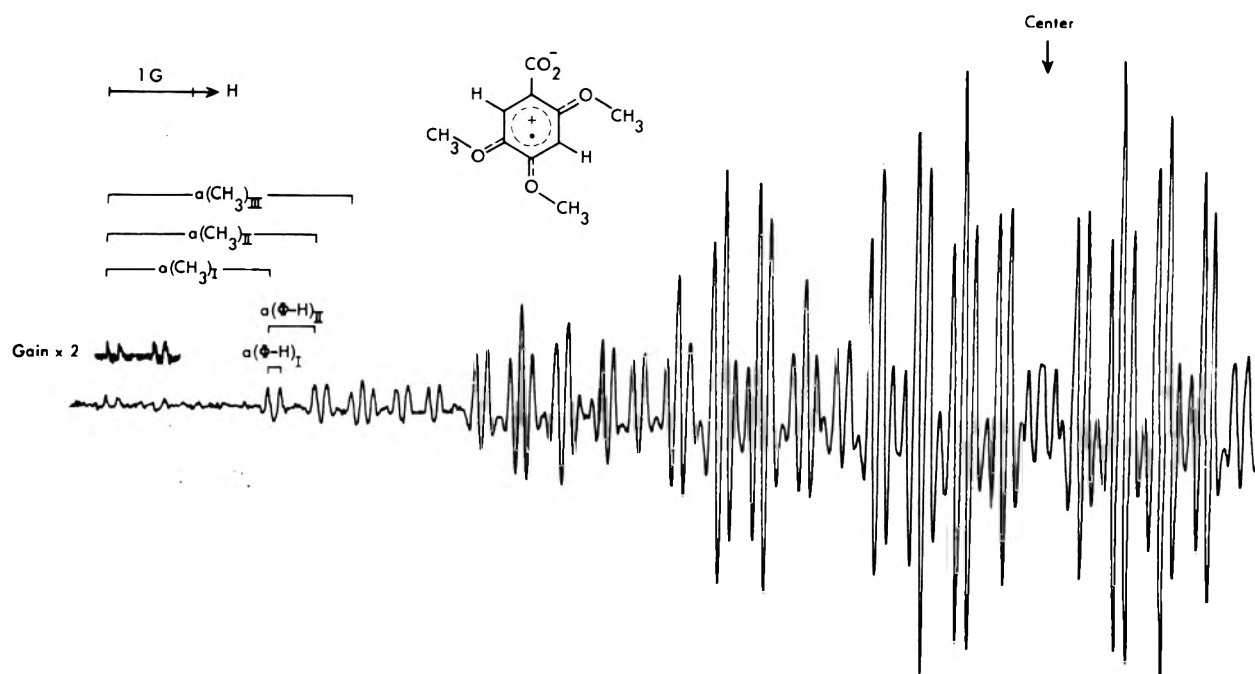
Figure 1. Low field part of the second derivative spectrum obtained on irradiation of a N_2O saturated 2 mM $AgNO_3$ solution containing 0.2 mM 2,4,5-TMBA at pH 4.5 and $\sim$5 °C. The Roman numeral subscripts refer to the (unassigned) individual methyl or ring protons, respectively.

TABLE I: Coupling Constants[a] (Gauss) and g Factors of Radical Zwitterions in Aqueous Solution at $\sim$5 °C

$g = $ 2.00351[b]	2.00350	2.00338	
$g = $ 2.00374[b]	2.00368	2.00357	
$g = $ 2.00354[b]	2.00331	2.00320	2.00349
$g = $ 2.00398[b]	2.00391	2.00372	2.00381

[a] In those cases where a ring proton or a methyl group is assigned more than one coupling constant, the comma separating different coupling constants should be read as "or". [b] Coupling constants and g factors are from ref 11.

constant between pH $\sim$2 and 10 indicating that the ionization state of the radicals remains the same over this pH range. It is very likely that the removal of an electron from the aromatic system results in an increase of the acid strength. It is therefore suggested that the carboxyl group of the radicals is ionized at pH $\geq$2, i.e., that the net charge of the radicals is zero at pH $\geq$2. As shown later, this conclusion is in agreement with results obtained by pulse radiolysis. Since the pK_a values of the methoxylated benzoic acids are between 3.5 and 4.5, the removal of an electron from the aromatic system results in an increase of the acid strength by a factor $\geq 10^2$.

As can be seen from Table I, the coupling constants of the radicals from the methoxylated benzoic acids are very similar to those obtained[11] from the corresponding methoxylated benzenes indicating that substitution of a ring proton by the carboxyl group has little effect on the distribution of the unpaired spin. An analogous situation exists in the case of phenyl[14] and phenoxyl[25] radicals. The similarity of the coupling constants of the radicals from methoxylated benzoic acids with those of corresponding radical cations is particularly pronounced in those cases where there is no steric interaction possible between carboxyl and methoxyl groups. From the similarity it

S. Steenken, P. O'Neill, and D. Schulte-Frohlinde
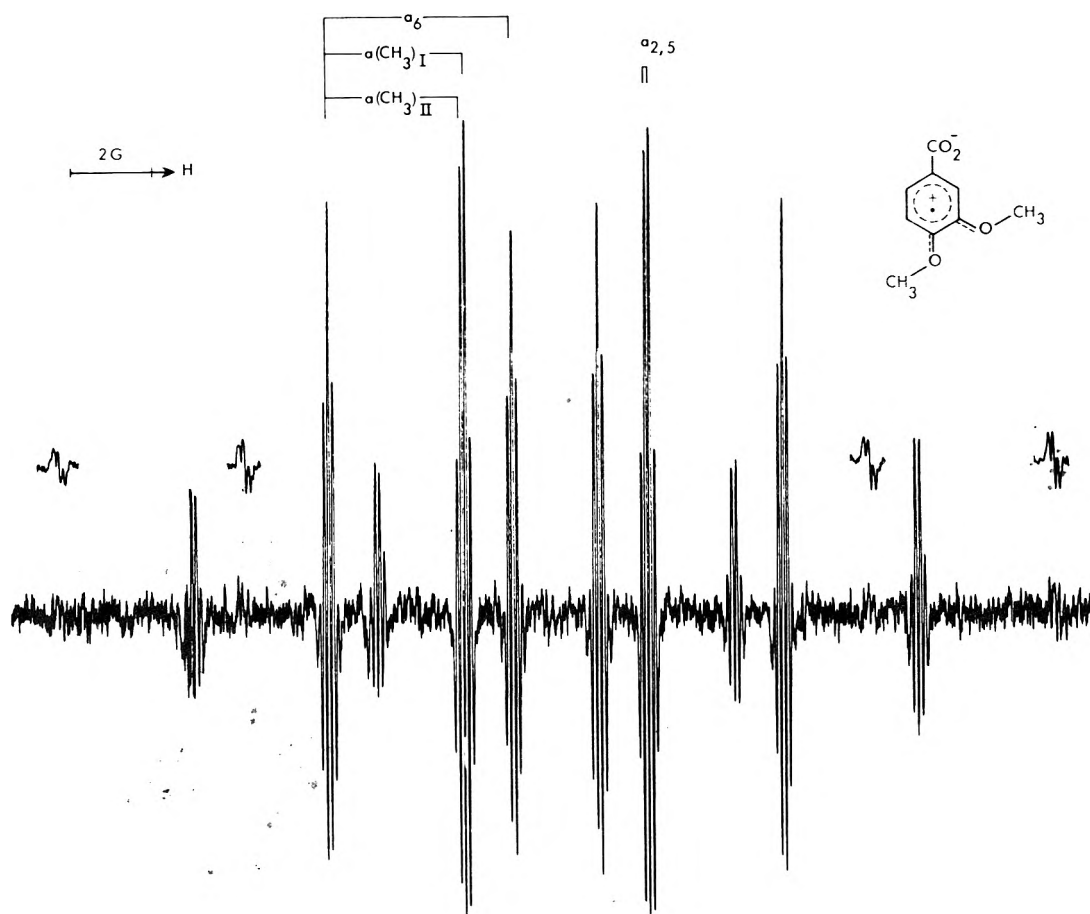
Figure 2. Second derivative (insert, first derivative) spectrum obtained on photolyzing a 20 mM $K_2S_2O_8$ solution containing 0.5 mM 3,4-DMBA at pH 3.3 and $\sim$3 °C. The indices of the coupling constants a refer to ring positions.

follows that the distribution of the unpaired spin and therefore[26] that of the positive charge in the one electron oxidation products from methoxylated benzoic acids is nearly the same as that in radical cations from structurally related methoxylated benzenes. Thus resonance structures such as
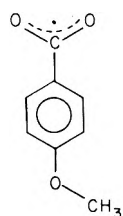
can only contribute to a minor extent to the overall electron distribution, i.e., the radicals must be zwitterionic in nature involving separation of the positive and negative charges as depicted in Table I.

The g factors of the radical zwitterions are lower by, on the average, $\sim$15 $\times$ 10^{-5} than those of radical cations from methyloxylated benzenes.

Reaction with SO_4^{-}. Radical zwitterions of the methoxylated benzoic acids were also obtained by in situ radiolysis or photolysis (Figure 2) of argon saturated 5–50 mM $K_2S_2O_8$ solutions containing 0.1–2 mM substrates. In the radiolysis case, relative concentrations of $S_2O_8^{2-}$ and of the substrates were chosen to ensure reaction of the hydrated electron with $S_2O_8^{2-}$ to yield[27,28] SO_4^{-} and SO_4^{2-}; with the photolytic system, SO_4^{-} is produced by homolytic rupture of the peroxidic bond in $S_2O_8^{2-}$.[29] SO_4^{-} subsequently reacts with the substrates by electron transfer to yield radical zwitterions and SO_4^{2-}. In the radiolytic $S_2O_8^{2-}$ system, the stationary concentration of the radicals was
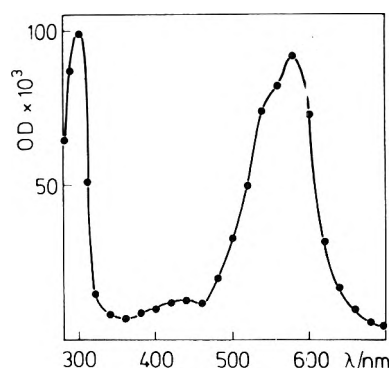
Figure 3. Optical absorption spectrum measured in a N_2O saturated 0.1 mM 2,4,6-TMBA solution containing 1 mM Tl_2SO_4 at pH 3 after 35 μs.

considerably lower than in the Tl^+ or Ag^+ systems. This is explained by removal of the radical zwitterions by fast reaction with OH adducts which are produced by reaction of the substrates with OH (see below).

Optical Investigations. Reaction with Tl^{2+} *and* Ag^{2+}. On pulse irradiation of 1 mM Tl_2SO_4 solutions saturated with N_2O and containing 0.1 mM methoxylated benzoic acids at pH 3–5, optical absorptions, which are not present in the absence of the aromatics and which are not due[22] to OH adducts, were observed at $\lambda \sim$300 nm and $\lambda \geq$400 nm. On the basis of the similarity of the spectral characteristics of the transients (Table II) with those[11] of radical cations of corresponding methoxylated benzenes and on the basis of the observations from ESR the absorptions are assigned to radical zwitterions, formed by reactions 1 and 2. In support of reaction 2, the rate of decay of Tl^{2+} was found to be identical with the rate of

TABLE II: Spectral Characteristics and Rate Constants for the Formation and Decay of Radical Zwitterions

Substrate	Radical zwitterion λ_{max}, nm	ϵ, M^{-1} cm^{-1}	$k(SO_4^- +$ substrate), M^{-1} s^{-1}	$k(Tl^{2+} +$ substrate),[a] M^{-1} s^{-1}	$k(Ag^{2+} +$ substrate),[a] M^{-1} s^{-1}	$k(Ag^{2-} +$ substrate),[b] M^{-1} s^{-1}	$2k$(decay), M^{-1} s^{-1} in Tl system	k(OH adduct + rad. zwitterion),[c] M^{-1} s^{-1}
2-MBA	<300 420	2 970	7.0×10^9	1.2×10^9	6.8×10^8	4.0×10^9	3.0×10^9	2.0×10^9
3-MBA	<300 420	2 970	7.6×10^9	1.6×10^9	3.0×10^8	1.4×10^9	$\sim 1.0 \times 10^{4\,d}$	
4-MBA	290 400–700	11 500 1 490[e]	7.6×10^9	5.3×10^8	3.8×10^8	1.6×10^9	3.4×10^9	1.5×10^9
2,3-DMBA	290 390	7 750 1 800	8.5×10^9	2.1×10^9	6.7×10^8	8.4×10^8	1.4×10^9	9.1×10^8
3,4-DMBA	300 400	7 200 1 900	4.5×10^9	1.7×10^9	4.2×10^8	2.2×10^9	1.4×10^9	1.6×10^9
2,4-DMBA	<280 500	3 700	3.8×10^9	9.1×10^8	4.5×10^8	1.9×10^9	3.9×10^9	1.8×10^9
2,6-DMBA	<260 480	3 000	2.5×10^9	1.8×10^9	2.2×10^9	2.4×10^9	4.8×10^8	1.4×10^9
3,5-DMBA	280 480	9 500 2 600	4.4×10^9	2.4×10^9	6.0×10^8	2.3×10^9	3.5×10^8	2.4×10^9
2,3,4-TMBA	300 460	10 900 1 730	2.5×10^9	1.6×10^9	4.7×10^8	2.1×10^9	3.5×10^7	1.8×10^9
3,4,5-TMBA	310 400–600	10 000 1 400[f]	5.0×10^9	8.4×10^8	4.0×10^8	1.2×10^9	3.4×10^9	2.7×10^9
2,4,5-TMBA	300 460	8 900 5 500	4.4×10^9	8.2×10^8	2.6×10^8	1.2×10^9	5.5×10^4	$\sim 8.0 \times 10^8$
2,4,6-TMBA	300 580	6 000 5 480[g]	2.6×10^9	1.5×10^9	1.1×10^9	2.4×10^9	3.6×10^8	1.0×10^9

[a] At pH ~3. [b] At pH 5-6. [c] Determined in argon saturated 0.1 mM substrate solutions containing 10 mM $K_2S_2O_8$ at pH >5. [d] Dimensions: s^{-1}; see text. [e] Determined at λ 440 nm. [f] Determined at λ 480 nm. [g] Corrected for contribution of radical zwitterions formed from OH adducts.[22]

formation of the radical zwitterions. Analogous reactions were observed to occur when Tl^+ was replaced by Ag^+.

The rate constants for reaction of Tl^{2+} with the aromatics are roughly independent of pH between pH 3 and 5 indicating that the dissociation state of the acids (pK's 3.5–4.5) does not have much influence on the reaction rates. The average rate constant (Table II) for reaction of Tl^{2+} with the methoxylated benzoic acids is a factor of ~2 larger than that[11] with methoxylated benzenes. In comparison, the rate constants for reaction of the substrates with Ag^{2+} (Table II) seem to depend on the ionization state of the acids: the rate constants for reaction of Ag^{2+} with the ionized acids are greater by a factor of ~4 than those with the undissociated acids although there are considerable individual differences. The average rate constant for reaction of Ag^{2+} with the un-ionized or ionized methoxylated benzoic acids is larger by a factor of ~12 or 50, respectively, than that[11] for reaction of Ag^{2+} with corresponding methoxylated benzenes. This indicates that conditions for efficient electron transfer are more complex than estimated from a simple redox potential picture.

Reaction with e_{aq}^-. Electron adducts, formed on irradiation of argon saturated 0.1 mM solutions of methoxylated benzoic acids containing 100 mM *tert*-butyl alcohol at pH >6, have spectral characteristics different from those of the radical zwitterions. The electron adducts have absorption bands in the region 290–330 nm ($\epsilon \approx 6000$–17000 M^{-1} cm^{-1}) and at ~440 nm ($\epsilon \approx 1000$–4000 M^{-1} cm^{-1}) similar to those observed[30] for reaction of e_{aq}^- with benzoic acid at pH >6. With 2,6-DMBA and 2,4,6-TMBA considerably weaker absorptions were observed at $\lambda_{max} \approx$ 320–330 nm. The difference in the absorptions of the electron adducts from 2,6-DMBA and 2,4,6-TMBA and those from the other methoxylated benzoic acids may be due to differences in the electronic structure of the respective electron adducts resulting from the noncoplanarity[31] of the carboxyl group with the ring in 2,6-DMBA and 2,4,6-TMBA. The rate constants for formation of the electron adducts, obtained from both the

decay of e_{aq}^- absorption at 720 nm and from the formation of the transients at 290–330 nm, are in the range (1.5–4) $\times 10^9$ M^{-1} s^{-1}. The decay of the electron adducts follows second-order kinetics for approximately two half-lives; the rate constants ($2k$) are ~(3–7) $\times 10^8$ M^{-1} s^{-1}.

Mode of Decay of the Radical Zwitterions. The zwitterions, except that of 3-MBA, decay at pH <7 by second-order kinetics (Table II). The rate constants for decay of the zwitterions of 2- and 4-MBA and those of 2,4-, 2,6-, and 3,5-DMBA and 2,4,6-TMBA, in which the methoxyl groups are in meta positions relative to each other, are at least an order of magnitude larger than those of the other zwitterions, which carry methoxyl groups ortho and/or para to each other. The relative steady state concentrations of the zwitterions measured by ESR are in agreement with these kinetic results. The differences in the lifetimes between the two groups probably reflect differences in the thermodynamic stability of the zwitterions, as was also found[11] for radical cations of methoxylated benzenes.

The effect of ionic strength on the decay rates of the transients from 2-MBA and 2,4,5-TMBA was investigated at pH 3 in N_2O saturated solutions containing 0.1 mM substrate, 1 mM $AgNO_3$, and 50–500 mM $NaClO_4$. The rate constants for decay of the transients were found to be independent of ionic strength confirming their assignment to radical zwitterions, whose net charge is zero, and not to radical cations for which an increase in decay rate would be observed with increasing ionic strength.

The radical zwitterion of 3-MBA decays by first-order kinetics while a new absorption with a λ_{max} of 370 nm "grows in" on the same timescale as the decay of the zwitterion. This transient has an absorption spectrum similar to that[22] of the OH adduct of 3-MBA. Since the rate of formation of the transient is independent of the concentration of 3-MBA, the absorption cannot be due to an intermediate produced by reaction of the substrate with the zwitterion or any species derived from zwitterion, e.g.. addition of 3-MBA to 3-methoxyphenyl radical, produced

by decarboxylation[14,32] of the zwitterion. The absence of decarboxylation was confirmed by determining the amount of CO_2 produced on reaction of SO_4^- with 3-MBA. $G(CO_2)$ was found to be <0.2 (for 2-MBA <0.2) as compared to ~2.0 for benzoic acid. The transient cannot be due to the 3-methoxyphenyl radical either, since the related hydroxyphenyl radical absorbs below 300 nm.[33] It is therefore concluded that the zwitterion decays by electrophilic reaction with water to yield the OH adduct as shown in reaction 3. This reaction is analogous to that

(3)
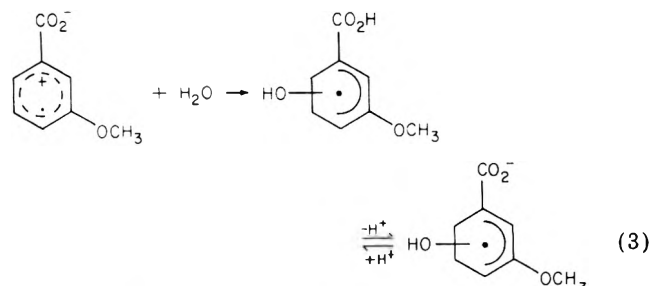
proposed[5,12,34] for the radical cation of benzene.

Whereas the radical zwitterion of 3-MBA is the only one which undergoes reaction with water, all zwitterions react with the stronger nucleophile OH^-. This reaction was investigated at pH values >10 using the persulfate system (see below). Under these conditions the zwitterions decay by (pseudo) first-order kinetics and an increase of optical absorption at λ <400 nm, the region in which OH adducts absorb,[22] occurs on the same timescale as the decay of the zwitterions. This is suggested to be due to reaction of radical zwitterions with OH^- to yield OH adducts, e.g.

$$(2\text{-MBA})^{\pm} + OH^- \rightarrow (2\text{-MBA-OH})^- \qquad (4)$$
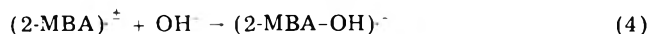
The rate constant for reaction 4 was estimated to be 1.9 $\times 10^8$ M^{-1} s^{-1}.

Reaction with SO_4^-. The reactions of the substrates with SO_4^- were investigated by pulse irradiating argon saturated 10 mM $K_2S_2O_8$ solutions containing 0.1 mM substrate at pH >3. Under these conditions, persulfate scavenges the electrons to yield[27,28] SO_4^- but not the OH radicals which react with the substrates to yield the corresponding OH adducts. The spectra of the transients observed after the pulse are composites of the spectra of the radical zwitterions and those[22] of the OH adducts. The extinction coefficients of the zwitterions (Table II) were calculated by assuming that at pH >5 $G(e_{aq}^-) = G(SO_4^-)$ = $G(\text{zwitterion}) = 2.7$. Since the rates of formation of the zwitterions depend on substrate concentration and since the rate constants are approaching the diffusion controlled limit (Table II), it is suggested that SO_4^- reacts with the substrates by direct electron transfer rather than by intermediate addition to the ring. A similar conclusion, concerning the reaction of SO_4^- with other aromatics, has been drawn previously.[11,12,14]

In the persulfate system at pH >5, the lifetimes of the zwitterions, with the exception of that from 3-MBA, are smaller than those measured in the Tl^+ or Ag^+ systems. In analogy with the methoxylated benzene system,[11] this is explained by an additional reaction occurring, which involves radical zwitterions and OH adducts (Table II).

Summary

The radical zwitterions are produced from the substrates by one-electron oxidation processes followed by depro-

tonation if $pK_a(\text{zwitterion}) < pH < pK_\epsilon(\text{substrate})$. The rate constants for reaction of Tl^{2+} and Ag^{2+} with the substrates are larger than those[11] for reaction with methoxylated benzenes whereas SO_4^- reacts as fast with methoxylated benzoic acids as[11] with methoxylated benzenes. The lifetimes of the zwitterions depend in a systematic fashion on the positions of the methoxyl groups relative to one another. With the exception of that from 3-MBA, hydration of the radical zwitterions, similar to that observed for the radical cation of benzene,[3,5,12] is slower than their bimolecular decay by at least a factor of 10, and decarboxylation to yield phenyl radicals, as recently suggested for benzoic acid and carboxylated benzoic acids,[13,14] does not take place. Thus the presence of even one methoxyl group is sufficient to stabilize one electron oxidation products of benzoic acids with respect to decarboxylation.

References and Notes

(1) R. O. C. Norman and P. M. Storey, *J. Chem. Soc. B*, 1099 (1970).
(2) M. E. Snook and G. A. Hamilton, *J. Am. Chem. Soc.*, **96**, 860 (1974).
(3) C. Walling and R. A. Johnson, *J. Am. Chem. Soc.*, **97**, 363 (1975).
(4) A. Ledwith, P. J. Russell, and L. H. Sutcliffe, *Chem. Commun.*, 964 (1971); A. Ledwith and P. J. Russell, *J. Chem. Soc., Perkin Trans. 2*, 582 (1974); 1503 (1975).
(5) R. O. C. Norman, P. M. Storey, and P. R. West, *J. Chem. Soc. B*, 1087 (1970).
(6) K. Sehested, H. Corfitzen, H. C. Christensen, and E. J. Hart, *J. Phys. Chem.*, **79**, 310 (1975).
(7) K. Sehested and E. J. Hart, *J. Phys. Chem.*, **79**, 1639 (1975).
(8) P. S. Rao and E. Hayon, *J. Phys. Chem.*, **79**, 1063 (1975).
(9) M. Bonifacic, K. Schafer, H. Mockel, and K.-D. Asmus, *J. Phys. Chem.*, **79**, 1496 (1975).
(10) P. O'Neill, S. Steenken, and D. Schulte-Frohlinde, *Angew. Chem.*, **87**, 417 (1975); *Angew. Chem., Int. Ed. Engl.*, **14**, 430 (1975).
(11) P. O'Neill, S. Steenken, and D. Schulte-Frohlinde, *J. Phys. Chem.*, **79**, 2773 (1975).
(12) O. P. Chawla and R. W. Fessenden, *J. Phys. Chem.*, **79**, 2693 (1975).
(13) B. C. Gilbert, L. P. Larkin, and R. O. C. Norman, *J. Chem. Soc., Perkin Trans. 2*, 1272 (1972).
(14) H. Zemel and R. W. Fessenden, *J. Phys. Chem.*, **79**, 1419 (1975).
(15) N. Getoff and F. Schworer, *Radiat. Res.*, **41**, 1 (1970).
(16) F. Weeke, E. Bastian, and G. Schomburg, *Chromatographia*, **7**, 163 (1974).
(17) K. Eiben and R. W. Fessenden, *J. Phys. Chem.*, **75**, 1186 (1971).
(18) H. A. Schwarz, D. Comstock, J. K. Yandell, and R. W. Dodson, *J. Phys. Chem.*, **78**, 448 (1974).
(19) P. O'Neill and D. Schulte-Frohlinde, *Chem. Commun.*, 387 (1975).
(20) J. Pukies, W. Roebke, and A. Henglein, *Ber. Bunsenges. Phys. Chem.*, **72**, 842 (1968).
(21) J. H. Baxendale, E. M. Fielden, and J. P. Keene, "Pulse Radiolysis", M. Ebert, J. P. Keene, and A. J. Swallow, Ed., Academic Press, London, 1965, p 207.
(22) P. O'Neill, S. Steenken, and D. Schulte-Frohlinde, *J. Phys. Chem.*, following paper in this issue.
(23) (a) P. O'Neill, unpublished; (b) M. Bonifacic and K.-D. Asmus, *J. Chem. Soc., Dalton Trans.*, in press.
(24) P. O'Neill, and K.-D. Asmus, to be submitted for publication.
(25) P. Neta and R. W. Fessenden, *J. Phys. Chem.*, **78**, 523 (1974).
(26) This argument applies only to π type radicals of which the zwitterions are examples.
(27) W. Roebke, M. Renz, and A. Henglein, *Int. J. Radiat. Phys. Chem.*, **1**, 29 (1969).
(28) E. Hayon, A. Treinin, and J. Wilf, *J. Am. Chem. Soc.*, **94**, 47 (1972).
(29) M. S. Tsao and W. K. Wilmarth, *J. Phys. Chem.*, **63**, 346 (1959).
(30) M. Simic and M. Z. Hoffman, *J. Phys. Chem.*, **76**, 1398 (1972).
(31) This is concluded by analogy from X-ray data concerning 2-ethoxybenzoic acid (E. M. Gopalakrishna and L. Cartz, *Acta Crystallogr., Sect. B*, **28**, 2917 (1972)), 2,6-dimethylbenzoic acid (R. Anca, S. Martinez-Carrera, and S. Garcia-Blanco, *Acta Crystallogr.*, **23**, 1010 (1967)), and 2,4,6-trimethylbenzoic acid (F. Florencio and P. Smith, *Acta Crystallogr., Sect. B*, **26**, 659 (1970)).
(32) A. L. J. Beckwith and R. O. C. Norman, *J. Chem. Soc. B*, 403 (1969).
(33) B. Cercek and M. Kongshaug, *J. Phys. Chem.*, **74**, 4319 (1970).
(34) C. Walling and D. M. Camaioni, *J. Am. Chem. Soc.*, **97**, 1603 (1975).

Formation of Radical Zwitterions from Methoxylated Benzoic Acids. 2. OH Adducts as Precursors

P. O'Neill, S. Steenken, and D. Schulte-Frohlinde

Institut für Strahlenchemie im Max-Planck-Institut für Kohlenforschung, D-4330 Mülheim a.d. Ruhr, West Germany
(Received March 29, 1976)

Using spectrophotometric and conductometric pulse radiolysis and in situ electron spin resonance techniques it was found that OH adducts, formed from mono-, di-, and trimethoxylated benzoic acids by attachment of OH to nonsubstituted ring positions, react with H^+ ($k = 10^8$–10^9 M^{-1} s^{-1}) to yield radical zwitterions via elimination of H_2O from the protonated OH adduct. With OH adducts from 2,4- and 2,6-dimethoxybenzoic acid and 2,4,5- and 2,4,6-trimethoxybenzoic acid radical zwitterions are additionally produced by a pH independent process involving elimination of OH^- ($k \approx 4 \times 10^4$ s^{-1}). The radical zwitterions react with H adducts with rate constants of $(8$–$40) \times 10^8$ M^{-1} s^{-1}.

Introduction

Radical cations have been proposed as transient products from reactions in aqueous solution of the hydroxyl radical with a variety of solutes.[1-9] In the case of benzene and its derivatives the available evidence[3-6,8,9] indicates that, in contrast to an earlier suggestion,[1] formation of one electron oxidation products proceeds via addition of OH followed by protonation of the OH adduct and subsequent elimination of water. This mechanism is possibly of a more general importance since it also applies to electron transfer reactions between OH and metal ions such as Tl^{+}[10] and Ag^{+}.[11] As pointed out by Walling,[3] the addition–protonation–dehydration mechanism is probably preferred as compared to direct electron transfer since in the former case the heat of formation of water contributes to the driving force of the overall reaction.

In the majority of cases, radical cation formation from benzene derivatives has been observed with benzenes carrying electron-donating substituents. The present investigation was undertaken to elucidate the mechanism of radical cation formation in the reaction of OH with aromatics substituted by both electron-donating and electron-withdrawing groups.

Experimental Section

The pulse radiolysis and in situ radiolysis ESR systems were as described.[9,12] With the conductivity method, measurements were limited to $3.5 \leq pH \leq 11$. The optical density values used for plotting the spectra refer to a dose of 3 krads and an optical path length of 1 cm. The substrates were obtained from Fluka, Merck, and Aldrich and were used as received.

Results and Discussion

Optical Studies. Reaction of Substrates with OH. The optical absorption spectra of the products of the reaction of OH with 2-, 3-, or 4-methoxybenzoic acid (MBA) or 2,3-, 2,4-, 2,6-, 3,4-, or 3,5-dimethoxybenzoic acid (DMBA) or 2,3,4-, 2,4,5-, 2,4,6-, or 3,4,5-trimethoxybenzoic acid (TMBA), measured using N_2O saturated 0.1 mM solutions at pH $\sim$7, have absorption bands at $\lambda \approx 300$–400 nm (Table I), in agreement with OH adduct spectra[9,13,14] of related aromatics. The rate constants for bimolecular decay of the OH adducts (Table I) are similar to that reported[14] for the OH adduct of benzoate.

In comparison with the other methoxylated benzoic acids, 3,4-DMBA and 2,4,5- and 2,4,6-TMBA show some

TABLE I: Spectral Characteristics and Rate Constants for Formation and Decay of OH Adducts at pH 7–8

Substrate	OH adduct λ_{max}, nm	ϵ, M^{-1} cm^{-1}	k(OH + substrate),[a] M^{-1} s^{-1}	$2k$(OH adduct), M^{-1} s^{-1}
2-MBA	330	2900	3.7×10^9	2.3×10^8
3-MBA	350	4270	4.5×10^9	2.3×10^8
4-MBA	370	3410	4.9×10^9	2.5×10^8
2,3-DMBA	320	3400	6.8×10^9	2.1×10^8
3,4-DMBA	310	3390	8.3×10^9	6.0×10^8
	370	3100		
2,4-DMBA	350	4090	6.9×10^9	4.3×10^8
2,6-DMBA	350	4320	4.5×10^9	3.9×10^8
3,5-DMBA	340[b]	4030	4.8×10^9	5.0×10^8
	390	5500		
2,3,4-TMBA	350	3050	6.8×10^9	1.5×10^8
3,4,5-TMBA	390	6000	9.0×10^9	1.6×10^8
2,4,5-TMBA	310[c]	6400	4.8×10^9	5.0×10^8
2,4,6-TMBA	350	4910	8.1×10^9	

[a] Determined at pH $\sim$7 using competition method with KSCN. Using a value[19] for k_{OH+SCN^-} of 7.5×10^9 M^{-1} s^{-1} gives good agreement with the directly measured rate constants. [b] Shoulder. [c] An additional absorption maximum at λ 420 nm was observed and is assigned to phenoxyl radical.[15]

anomalies in their reactions with OH. With 2,4,5-TMBA and 3,4-DMBA increases in absorption were observed after the pulse at 420 and 360–400 nm, respectively, extending over 30–50 μs. These absorptions are not due to OH adducts, the formation of which is complete after $\sim$5 μs, or to radical zwitterions, since the absorptions differ from those of the zwitterions as measured[12] in the Tl^+, Ag^+, or $S_2O_8^{2-}$ systems. A similar observation has previously been reported[9] concerning the reaction of OH with 1,4-dimethoxybenzene. The absorptions are assigned to phenoxyl radicals produced[15] by oxidative demethoxylation by the OH radical. In the case of 2,4,6-TMBA the decay of the OH adduct is mixed order and a further absorption, which is assigned to the radical zwitterion, "grows in" at λ_{max} 580 nm. In the pH range 7–10 its rate of formation follows first-order kinetics ($k \approx 4 \times 10^4$ s^{-1}) and is independent of 2,4,6-TMBA concentration (0.1–1 mM). This excludes production of the zwitterion by direct electron transfer between OH and 2,4,6-TMBA. The yield of zwitterion observed at pH 9 is $\sim$20% of G(OH).

Reaction of OH Adducts with H^+. When the pH of the substrate solutions was decreased to <7, further ab-
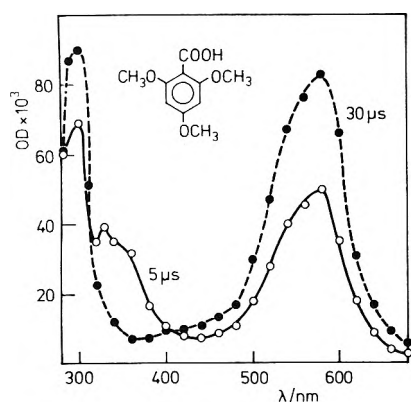
Figure 1. Optical absorption spectra measured in a N_2O saturated 0.1 mM 2,4,6-TMBA solution at pH 3.0 after 5 and 30 μs.
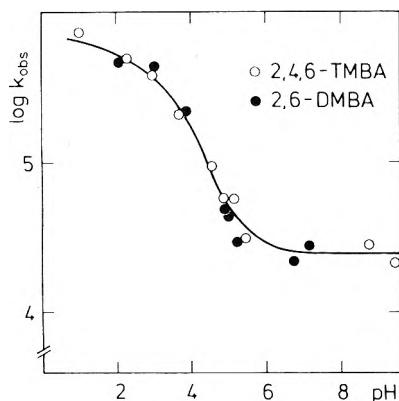

Figure 2. Dependence of log k_{obsd} on pH for formation of radical zwitterion determined optically using 0.1 mM substrate solutions saturated with either argon (pH <3) or N_2O (pH >3).

Figure 3. (a) Dependence of G_{max}(radical zwitterion)/G(OH) on pH determined optically for 2,4- and 2,6-DMBA and 2,4,6- and 3,4,5-TMBA; (b) dependence of maximum conductivity decrease on pH for 2,6-DMBA and 2,4,6- and 3,4,5-TMBA. The changes observed at pH >7 have been multiplied by μ_{H^+}/μ_{OH^-} and are represented as decreases instead of increases. The changes are constant in the pH region 7–10. Both dependences were determined using ~600 rads/1 μs pulse.

sorptions, which were absent in neutral solutions with the exception of those of 2,4,6-TMBA, were observed at λ ~300 nm and $\lambda \geq 400$ nm (Figure 1). These new absorptions "grow in" while those due to the OH adducts decay with an enhanced initial rate as compared to the situation at pH 7. From the agreement of the absorption spectra at $\lambda \geq 400$ nm with those observed[12] in the Tl^+, Ag^+, and $S_2O_8^{2-}$ systems it is concluded that the absorptions are due to radical zwitterions, the presence of which was confirmed by the in situ ESR method using N_2O saturated 1 mM solutions at pH ~3. Under these conditions, with the exception of that from 2,6-DMBA, the stationary concentrations of the zwitterions are however considerably lower than[12] in the Tl^+ or Ag^+ systems.

With 2,4,6-, 2,3,4-, and 3,4,5-TMBA and 2,4- and 2,6-DMBA the optical absorption spectra of the OH adducts and those of the zwitterions are sufficiently separated to compare the initial rates of decay of the former with the rates of formation of the latter. Within the limits of experimental error, these rates were found to be the same. The rates of production and the yields of radical zwitterion increase with increasing [H^+] in the pH range ~5 to ~2 (Figures 2 and 3) indicating that the OH adducts are converted to radical zwitterions by reaction with protons. The rate constants for reaction of the OH adducts with H^+, as determined in the pH range 5–4, are ~10^8–10^9 M^{-1} s^{-1}. This value is comparable to those[9] observed with methoxylated benzenes. At pH ≤ 2 the rates of formation of radical zwitterions approach those for addition of OH to the aromatic ring.

At pH 1 the yields of radical zwitterion are $\geq 90\%$ of G(OH) for 2,4-, 2,6-, and 3,5-DMBA and 2,4,6-TMBA, which are all characterized by methoxyl groups in meta

positions to each other, whereas for the remaining di- and trimethoxylated substrates, which carry methoxyl groups in ortho or para positions relative to one another, the yields are estimated to be $\leq 60\%$ of G(OH). Completely analogous results have been reported[9] using di- and trimethoxylated benzenes; with these the maximum yields of radical cation, produced by reaction of protons with the OH adducts, also depend on whether the methoxyl groups are in an ortho/para or in a meta position relative to each other. The differences in yields are explained by selective addition of OH to ring positions followed by either radical zwitterion formation or elimination of methanol.[15] With the exception of 2,6-DMBA and 2,4,6-TMBA the H^+ concentration needed to produce 50% of the maximum obtainable yield of radical zwitterion is ~10 times higher than that[9] necessary with the corresponding methoxylated benzenes. The exceptional behavior of 2,6-DMBA and 2,4,6-TMBA may be related to the noncoplanarity[16] of the carboxyl group with the ring by which the electron-withdrawing effect of the carboxyl group, which should lower the basicity of the OH adducts, becomes less effective.

Due to formation of radical zwitterions, the pK_a values of the OH adducts are difficult to determine. However, on the basis of ~10–20-nm spectral shifts of the OH adduct absorptions on lowering the pH, the pK_a values are estimated to be in the same region as the pK_a values of the substrates. The pK_a of the OH adduct of benzoic acid is 0.2 units above that of benzoic acid itself.[14]

Decay of Radical Zwitterions. The rates of decay of the radical zwitterions formed in acid solutions depend on pH and on the individual methoxylated benzoic acid. At pH >5 with all the substrates the rates tend toward first order

Scheme I
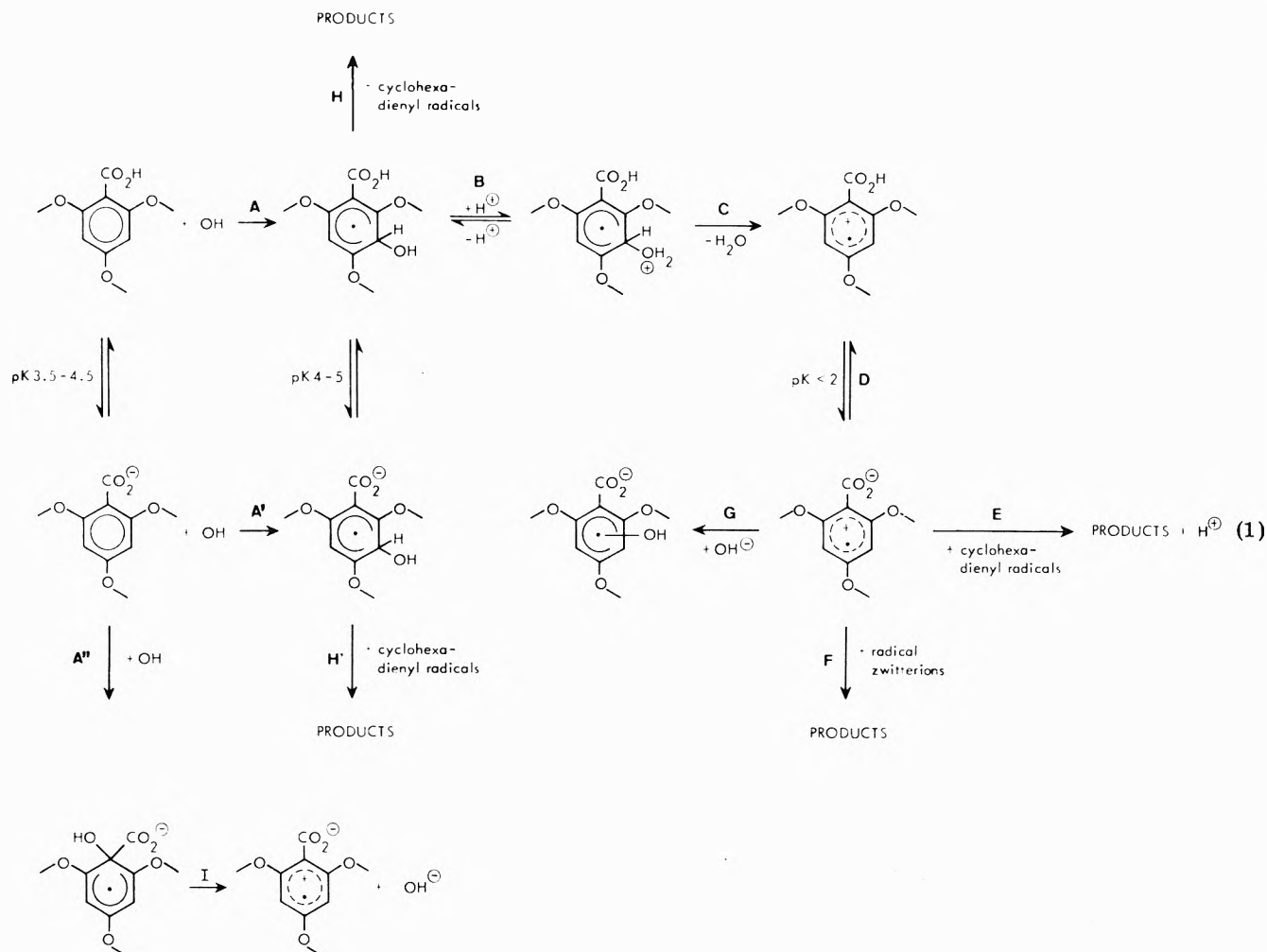
and are different from the decay rates of the OH adducts. Due to overlap of the OH adduct spectra with those of the radical zwitterions and due to differences in yields of zwitterion (Figure 3) from individual methoxylated benzoic acids, below pH 5 the kinetic behavior of the majority of the transients is complicated. The kinetic behavior can however be explained by reaction of radical zwitterions with OH or H adducts. The rate constants for the former reaction were determined in the pH range 3–5 and are in agreement with those[12] measured in the $S_2O_8^{2-}$ system. The rate constants for reaction of zwitterions with H adducts were measured at pH 1–2 and were found to be in the region $(8-40)$ 10^8 M^{-1} s^{-1}. With 2,6-DMBA and 2,4,6-TMBA the rate of decay of the zwitterions at pH 3 is second order and the respective rate constants are the same as those[12] measured in the Tl^+ or Ag^+ systems.

Conductometric Studies. In order to support the conclusions drawn from ESR and optical measurements concerning formation of radical zwitterions by reaction of OH adducts with H^+, conductivity experiments were performed in the pH range 3.5–9 using N_2O saturated solutions containing 0.1 mM substrate. At pH 5–7 a decrease in conductivity within the first 100 μs after the pulse was observed with all the substrates. This decrease is explained by assuming that H^+ (μ = 34 × 10^{-4} V^{-1} cm^2 s^{-1}) is replaced by nonconducting radical zwitterions. In order to support this concept, the extinction coefficients of the radical zwitterions from 2,6-DMBA and 3,4,5- and 2,4,5-TMBA were determined, for solutions at pH ~6, by combining G(radical zwitterion) measured by conductivity and G(radical zwitterion) × ϵ obtained optically. The

extinction coefficients thus calculated are in agreement to within ±10% with those[12] determined using the persulfate system.

The dependence on pH of G(maximum conductivity decrease) at pH <5 is different from the dependence of G(radical zwitterion) on pH measured optically (Figure 3). The "drop off" of the conductivity decrease at pH 4–5, which is the region of the pK values of the OH adducts, is additional evidence that radical zwitterions rather than radical cations are formed: when the carboxyl group is un-ionized, the proton removed by reaction with the OH adducts to yield one-electron oxidation products and water is regenerated by deprotonation from the carboxyl group resulting in a zero net change of conductivity. The pH region for this process is characterized by pK_a(OH adduct) > pH > pK_a(zwitterion) ≤ 2.[12]

At pH 4–7, the rate of decrease of conductivity is the same as the rate of formation of the radical zwitterions, observed optically at the same pH value, demonstrating that with both methods the same process is measured. The conductivity decrease is followed by a return of conductivity on the millisecond timescale, but not to the original value prior to the pulse as was observed[9] using methoxylated benzenes. At pH >5 the rate of return of conductivity follows first-order kinetics with the same rate constants as those for decay of the radical zwitterions measured optically.

With 2,4- and 2,6-DMB and 2,4,5- and 2,4,6-TMBA at pH >7, an *increase* of conductivity was observed extending over the first 100 μs after the pulse. The reaction responsible for this conductivity increase is much slower than

that between OH and substrate, in agreement with the kinetic observations obtained optically. The conductivity increase is assumed to be due to reaction of a fraction of the OH adducts to yield OH$^-$ and radical zwitterion (reaction 1I). Using $\mu = 1.8 \times 10^{-3}$ V^{-1} cm^2 s^{-1} for OH$^-$, G(radical zwitterion) at pH 7–9 is equal to ~5% of G(OH) for 2,4- and 2,6-DMBA and 2,4,5-TMBA and 21% for 2,4,6-TMBA.

Reaction Scheme for Formation of Radical Zwitterions. Reaction scheme 1, which is similar to those previously proposed for methoxylated benzenes[9] and other aromatics,[3,5] summarizes the experimental observations using 2,4,6-TMBA as an example. The initial attack of OH radicals is by addition to the aromatic ring to produce hydroxycyclohexadienyl radicals which were observed optically. Only those OH adducts are assumed to yield radical zwitterions where OH is not attached[15] to a ring position which carries a methoxyl group. The main path leading to radical zwitterion involves steps A(A′)–D. This reaction sequence accounts for >95% of the total zwitterion yield for all solutes with the exception of 2,4- and 2,6-DMBA and 2,4,5-TMBA, for which the contribution from steps A(A′)–D is ~95% and of 2,4,6-TMBA, for which steps A(A′)–D contribute 80% to the total zwitterion yield. At pH <2 the rate of radical zwitterion formation by steps A(A′)–D becomes independent of H$^+$ concentration but dependent on substrate concentration since k_A [aromatic] < k_B[H$^+$]; i.e., the OH addition reaction rather than the reaction with protons becomes rate determining.

Formation of radical zwitterions by reactions A″–I is of importance only for 2,4- and 2,6-DMBA and 2,4,5- and, especially, 2,4,6-TMBA whereas for the other substrates this sequence or direct electron transfer between the substrates and OH contributes <5% to the total zwitterion yield. A common feature of the former compounds is that all have methoxyl groups ortho and/or para to the carboxyl group. Since methoxyl groups are ortho–para directive and OH radicals are electrophilic,[17] a larger percentage of OH radicals will add to the ring carbon carrying the carboxyl group (C$_1$) with 2,4- and 2,6-DMBA and 2,4,5- and 2,4,-6-TMBA than with the remaining substrates. From a comparison at pH ~7 of the radical cation yield[9] from 1,3,5-trimethoxybenzene ($\leq$3%) with the radical zwitterion yield from 2,4,6-TMBA (20%), it is concluded that elimination of OH$^-$ only occurs from intermediates in which OH is attached to C$_1$ of the aromatic acid. This elimination is suggested to be facilitated by considerable steric crowding at C$_1$. The importance of electronic factors on the amount of OH addition at C$_1$ or on the tendency for OH$^-$ elimination may be estimated from the difference in radical zwitterion yields between 2,6-DMBA (5%) and 2,4,6-TMBA (20%). With the latter compound, C$_1$ is additionally activated by the methoxyl group at C$_4$. The possibility that formate ($\mu = 5 \times 10^{-4}$ V^{-1} cm^2 s^{-1}) is eliminated from the C$_1$ intermediate instead of OH$^-$ is compatible with the conductivity results only if it is assumed that ~80% of the OH radicals add at C$_1$; this is unreasonable. With benzoic acid, the yield of decarboxylation by OH has been estimated[18] to be 7%.

In order to explain the enhanced rate of decay of the radical zwitterions in the presence of H and/or OH adducts, step E is introduced. To a first approximation, the first-order decay of the zwitterions at pH >5 may be explained by the fact that under these conditions, the concentration of OH adducts is approximately an order of magnitude greater than that of the zwitterions whereas at pH <5 the changes in the kinetics observed result from an increase of the concentrations of radical zwitterions on decreasing pH. Since for the individual methoxylated benzoic acids d[radical zwitterion]/d[H$^+$] and the maximum obtainable radical zwitterion yield differ (Figure 3a), the changes occurring in the zwitterion decay kinetics at pH <5 depend on the individual substrate. With 2,6-DMBA and 2,4,6-TMBA at pH ~3 conversion of the OH adducts to radical zwitterions is nearly quantitative which results in second-order rate constants of decay approximately equal to those[12] observed in the Tl$^+$ and Ag$^+$ systems. With the remaining solutes conversion of OH adducts to radical zwitterions is not quantitative at pH 3 and below pH 3 the kinetic situation is further complicated due to additional reaction with the H adducts formed. The latter reaction also explains the pronounced reduction of the stationary concentration of the radical zwitterions observed[12] by ESR in the Tl$^+$ and Ag$^+$ systems at pH <3. Step E results in the regeneration of H$^+$. Thus a process analogous to that observed[9] with methoxylated benzenes occurs. The apparent nonquantitative production of H$^+$ in step E is expected if the final products have pK_a values larger than those of the substrates.

References and Notes

(1) M. E. Snook and G. A. Hamilton, *J. Am. Chem. Soc.*, **96**, 860 (1974).
(2) R. L. Willson, P. Wardman, and K.-D. Asmus, *Nature (London)*, **252**, 323 (1974).
(3) C. Walling and R. A. Johnson, *J. Am. Chem. Soc.*, **97**, 363 (1975).
(4) K. Sehested, H. Corfitzen, H. C. Christensen, and E. J. Hart, *J. Phys. Chem.*, **79**, 310 (1975).
(5) K. Sehested and E. J. Hart, *J. Phys. Chem.*, **79**, 1639 (1975).
(6) P. S. Rao and E. Hayon, *J. Phys. Chem.*, **79**, 1063 (1975).
(7) M. Bonifacic, K. Schafer, M. Mockel, and K.-D. Asmus, *J. Phys. Chem.*, **79**, 1496 (1975).
(8) P. O'Neill, S. Steenken, and D. Schulte-Frohlinde, *Angew. Chem.*, **87**, 417 (1975); *Angew. Chem., Int. Ed. Engl.*, **14**, 430 (1975).
(9) P. O'Neill, S. Steenken, and D. Schulte-Frohlinde, *J. Phys. Chem.*, **79**, 2773 (1975).
(10) P. O'Neill and D. Schulte-Frohlinde, *Chem. Commun.*, 387 (1975).
(11) P. O'Neill and K.-D. Asmus, to be submitted for publication.
(12) S. Steenken, P. O'Neill, and D. Schulte-Frohlinde, *J. Phys. Chem.*, preceeding paper in this issue.
(13) For a review see A. Habersbergerova, I. Janovsky, and P. Kourim, *Radiat. Res. Rev.*, **4**, 123 (1972).
(14) M. Simic and M. Z. Hoffman, *J. Phys. Chem.*, **76**, 1398 (1972).
(15) P. O'Neill, D. Schulte-Frohlinde, and S. Steenken, *Faraday Discuss., Chem. Soc.*, submitted for publication.
(16) This is concluded by analogy from X-ray data concerning 2-ethoxybenzoic acid (E. M. Gopalakrishna and L. Cartz, *Acta Crystallogr. Sect. B*, **28**, 2917 (1972)), 2,6-dimethylbenzoic acid (R. Anca, S. Martinez-Carrera, and S. Garcia-Blanco, *Acta Crystallogr.*, **23**, 1010 (1967)), and 2,4,6-trimethylbenzoic acid (F. Florencio and P. Smith, *Acta Crystallogr., B*, **26**, 659 (1970)).
(17) M. Anbar, D. Meyerstein, and P. Neta, *J. Phys. Chem.*, **70**, 2660 (1966).
(18) G. W. Klein, K. Bhatia, V. Madhavan, and R. H. Schuler, *J. Phys. Chem.*, **79**, 1767 (1975).
(19) C. L. Greenstock, M. Ng, and J. W. Hunt, *Adv. Chem. Ser.*, **No. 81**, 397 (1968).

Partial Molal Volumes of Monovalent Ions in Ethylene Glycol, Formamide, and Formic Acid

Utpal Sen[1]

Physical Chemistry Division, Jadavpur University, Calcutta 700032, India (Received July 24, 1975; Revised Manuscript Received June 1, 1976)

The partial molal volumes of some alkali-metal halides in ethylene glycol and of hydrochloric acid in formamide and formic acid solution have been determined from density measurements. From these and previously reported data the ionic volumes of the proton ($\bar{V}^0_{H^+}$) and of other monovalent ions ($\bar{V}^0_{ion}$) in these three solvents have been determined by applying Mukerjee's method. Taking into account other works it has been found that the value of $\bar{V}^0_{H^+}$ in different solvents decreases in order of formic acid > formamide > N-methylpropionamide > water > ethylene glycol > ethanol > methanol. Moreover, $\bar{V}^0_{H^+}$ is negative in all the hydroxylic solvents for which data are available today. Hepler's equation has been used to split the geometric and electrostrictive contributions of ionic partial molal volumes, and a comparative study has been made with other previously reported results with respect to the structural aspects of different interactions in electrolytic solutions. The relationship of the electrostrictive decrease in volumes in different solvents with the corresponding dielectric constants has been examined.

Introduction

In an effort to have a better understanding of ion–solvent interactions in water and other solvents, studies of the partial molal volumes of electrolytes in nonaqueous solvents have become important,[2-8] and the need for more data in this field has been felt. Recently, Kawaizumi and Zana[7,8] determined the ionic volumes of monovalent ions in methanol, ethanol, and dimethylformamide (DMF) using the ultrasonic vibration potential method[9] and showed that for both methanol and ethanol solutions their experimental results are in excellent agreement with the values obtained by Mukerjee's empirical method.[10] Earlier[3-5] this method was also applied to ions in N-methylpropionamide (NMP), methanol, and sea water. In the present work the partial molal volumes of several alkali-metal halides in ethylene glycol (EG) and of hydrochloric acid in formamide and formic acid solutions have been determined from density measurements. From these data and the previously reported data in these three solvents,[11-14] partial molal volumes of monovalent ions have been obtained using Mukerjee's method.

Millero[15] proposed that the partial molal volume of an ion at infinite dilution, $\bar{V}^0_{ion}$, can be attributed to

$$\bar{V}^0_{ion} = \bar{V}^0_{cryst} + \bar{V}^0_{elect} + \bar{V}^0_{disord} + \bar{V}^0_{caged} \quad (1)$$

where $\bar{V}^0_{cryst}$ is the crystal partial molal volume, $\bar{V}^0_{elect}$ is the electrostrictive partial molal volume (the decrease in volume due to ion–solvent interactions), $\bar{V}^0_{disord}$ is the disorder partial molal volume (due to void space around the ion in solution), and $\bar{V}^0_{caged}$ is the caged partial molal volume (due to formation of caged or structured water around ions with hydrocarbon tails). It has also been reported[5] that this model (multilayer hydration[16-18]) for ion–water interaction appears to hold in other solvents. However, detailed calculations have not yet been made in different nonaqueous solvents. In the present work the above equation has been used to calculate different contributions to the ionic partial molal volumes at infinite dilution and a comparative study of their values in various solvents has been attempted. It is also the purpose of this work to examine the usefulness of Hepler's semiempirical equation[19] for nonaqueous solutions in estimating the geometric as well as the electrostrictive parts of the ionic partial molal volumes in different solvents.

Experimental Section

Purifications of the solvents and solutes have been performed according to the standard procedures used by previous workers.[12,14,20] Preparation of solutions and other experimental details have been described elsewhere.[11,20-23] It was suggested[22,23] earlier that formamide may not be very stable in the presence of HCl in solution particularly at higher concentrations. As a consequence, freshly prepared solutions were used for the density measurements and no appreciable change in density readings was noticed during the period of experiment. One may, therefore, conclude that the instability of formamide–HCl system did not significantly affect the values of apparent molal volumes. Freshly prepared HCl solutions were also used for density measurements in ethylene glycol and formic acid solutions. Concentrations of the hydrochloric acid solutions in formamide and formic acid were determined by conductometric titrations. A pycnometer was used for density measurements and the reproducibility of the measurements has been discussed elsewhere.[11] The precision of density readings is within ±0.000 02 g cm^{-3}. All measurements have been performed at 25 ± 0.05 °C.

Results

Apparent molal volumes (ϕ_v) for the electrolytes at different concentrations have been calculated from the corresponding density data by the equation[24]

$$\phi_v = \frac{M}{d_0} - \frac{1000(d - d_0)}{d_0 c} \quad (2)$$

where d_0 and d are the densities of the solvent and of the solution, M is the molecular weight of the electrolyte, and c is the molar concentration.

The recommended procedure[5,15,25] for extrapolation of ϕ_v to infinite dilution employs the Redlich–Meyer equation[25]

$$\phi_v = \phi_v^0 + S_v c^{1/2} + q_v c \quad (3)$$

where S_v is the theoretical limiting slope and q_v is a constant. The calculation of a numerical value for S_v requires among other things a knowledge of the pressure dependences of the dielectric constants, which are not available for the solvents under investigation. For this
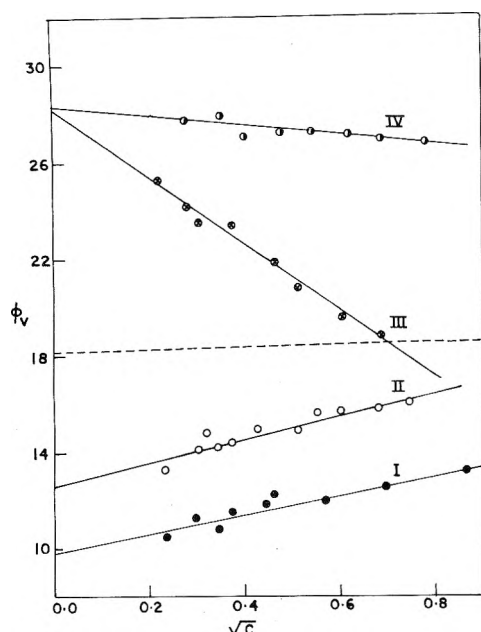
Figure 1. Apparent molal volumes (ϕ_v) of hydrochloric acid plotted vs. the square root of molar concentration ($c^{1/2}$) in propylene glycol (I), ethylene glycol (II), formamide (III), and formic acid (IV) at 25 °C. The broken line represents HCl in aqueous solution (ref 24).
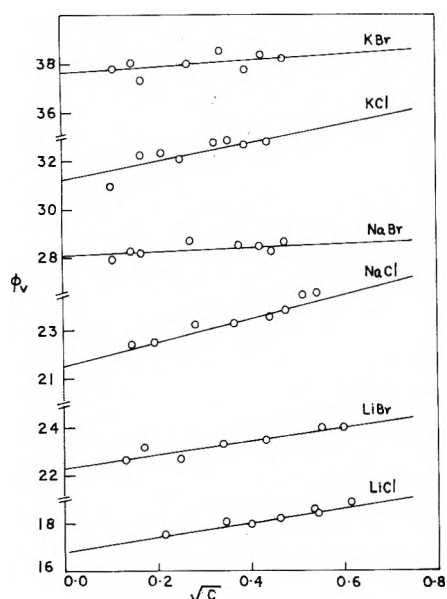

Figure 2. Apparent molal volumes (ϕ_v) of alkali-metal halides plotted vs. the square root of the molar concentration ($c^{1/2}$) in ethylene glycol at 25 °C.

reason the Masson equation[26]

$$\phi_v = \phi_v{}^0 + S_v{}^* c^{1/2} \qquad (4)$$

in which $S_v{}^*$ is an experimental slope, has been used for extrapolating the data to infinite dilution. However, ϕ_v's at the various concentrations are listed in Table I so that the data may be reextrapolated at a later time when accurate theoretical slopes are available (Table I is available as supplementary material; see paragraph at end of text regarding supplementary material). Figure 1 shows the plot of ϕ_v values of a hydrochloric acid solution in five different solvents as a function of $c^{1/2}$, and Figures 2 and 3 show plots of ϕ_v values of different electrolytes in ethylene glycol solution against $c^{1/2}$. The corresponding extrapolated $\phi_v{}^0$ (= $\bar{V}_2{}^0$) values of the different electrolytes and the experimental slopes, $S_v{}^*$, are presented in Tables II and III.
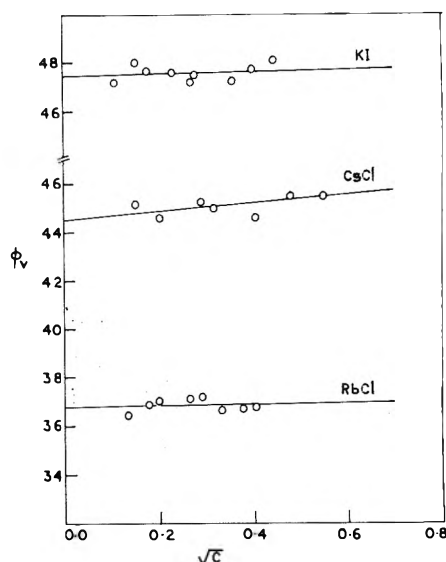
Figure 3. Apparent molal volumes (ϕ_v) of alkali-metal halides plotted vs. the square root of the molar concentration ($c^{1/2}$) in ethylene glycol at 25 °C.

TABLE II: Partial Molal Volume at Infinite Dilution of Hydrochloric Acid ($V^0{}_{HCl}$) and the Concentration Dependence Constant of the Apparent Molal Volumes ($S_v{}^*$) in Various Solvents at 25 °C

Solvent	$V^0{}_{HCl}$, cm^3 mol^{-1}	$S_v{}^*$, cm^3 mol$^{-3/2}$
Water	18.1[a]	0.83[a]
Methanol	-1.5,[b] -2.7,[b] -4.0[c]	
Ethanol	3.0,[b] -3.0[c]	
Propanol	9.6[b]	
Ethylene glycol	12.5[d]	5.1[d]
Propylene glycol	9.8[d]	5.0[d]
Formamide	28.1	-13.7
Formic acid	28.3	-1.8
NMP	28.1[e]	

[a] Reference 24. [b] Reference 5. [c] Reference 8 (by additivity rule). [d] Reference 11. [e] Reference 3 (by additivity rule).

TABLE III: Partial Molal Volume ($\bar{V}_2{}^0$) of Some 1:1 Electrolytes in Ethylene Glycol at Infinite Dilution and the Concentration Dependence Constant of the Apparent Molal Volume ($S_v{}^*$) at 25 °C

Electrolyte	$\bar{V}_2{}^0$, cm^3 mol^{-1}	$S_v{}^*$, cm^3 mol$^{-3/2}$
HCl	12.5	5.1
HBr	19.5[a]	
HI	29.0[a]	
LiCl	16.8	1.6
LiBr	22.3 (21.7)[b]	1.5
LiI	33.2[a]	
NaCl	21.5	2.5
NaBr	28.1 (27.3)[b]	0.4
NaI	38.0[a] (38.4)[b]	
KCl	31.2	2.0
KBr	37.8	0.5
KI	47.5 (47.2)[b]	0.4
RbCl	36.8	0.3
RbBr	43.8[a]	
RbI	53.3[a]	
CsCl	44.5	1.7
CsBr	51.5[a]	
CsI	61.0[a]	

[a] Values obtained by using the additivity rule. [b] Reference 2.

Ionic Partial Molal Volumes. Mukerjee's method[10] assumes that for spherical, large monovalent ions, such as

TABLE IV: Partial Molal Volume (cm^3 mol^{-1}) of Monovalent Ions in Various Solvents (Calculated by Mukerjee's Method) at 25 °C

Ion	Water[a]	Methanol[b]	Methanol[c]	Ethanol[c]	Ethylene glycol	Formamide	Formic acid	NMP[e]	DMF[d,f]
H$^+$	−4.5	−14.5	−17.0[f]	−15.5[f]	−12.0	4.5	9.0	3.4	
Li$^+$	−5.2	−14.0	−17.9[f]	−20.2	−7.8	−4.0			−19.4
Na$^+$	−5.7	−12.6	−16.1	−10.5	−3.0	−2.5	−3.8	6.0	−9.1
K$^+$	4.5	−2.6	−6.3	−1.9	6.5	8.4	0.8	11.1	−2.0
Rb$^+$	9.5		−0.7	3.9	12.3	12.4	9.0		2.0
Cs$^+$	16.9		5.8	11.7	20.0	18.7	14.1		8.5
Cl$^-$	22.3	9.3	12.0	15.0	24.5	23.6	19.3	24.7	15.0
Br$^-$	29.2	16.6	17.3	16.6	31.5	30.0	24.2	29.8	15.9
I$^-$	40.8	24.3	27.2	27.7	41.0	42.4	35.3		32.3

[a] Reference 10. [b] Reference 5. [c] Reference 7. [d] Reference 8. [e] Reference 4. [f] Not calculated by Mukerjee's method.

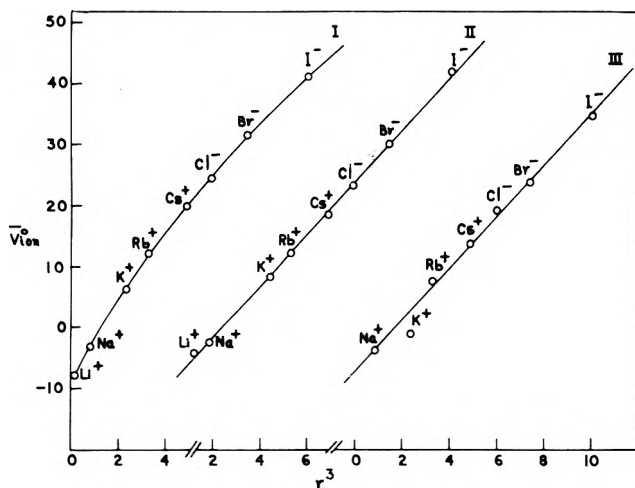Figure 4. The partial molal volume of ions (V^0_{ion}) calculated by Mukerjee's method plotted vs. the cube of the crystallographic radius (r^3) in ethylene glycol (I), formamide (II), and formic acid (III) at 25 °C.

the alkali-metal cations and the halide anions, the partial molal volumes should be a smooth monotonic function of the crystallographic radius (r) quite independently of the sign of the charge. The method has been used in the present study for the three solvents, ethylene glycol, formamide, and formic acid. Figure 4 shows the plot of ionic volumes obtained by this method against r^3 (r = Pauling's radius). The values of partial molal volumes at infinite dilution of different monovalent ions in various solvents are presented in Table IV.

Criss and co-workers[27] used a correspondence method[28] to estimate partial molal entropies of ions in various nonaqueous solvents from their values in water. This method has been found useful for obtaining values of the $\bar{V}^0_{ion}$ in nonaqueous solvents when $\bar{V}^0_{ion}$ in water is known. The correspondence equation is

$$\bar{V}^0_{ion}(S) = a\bar{V}^0_{ion}(W) + b \tag{5}$$

where a and b are constants and S and W indicate $\bar{V}^0_{ion}$ in nonaqueous solvents and in water, respectively. It has been found in the present work with the three solvents that the correspondence principle holds reasonably well. Figure 5 shows the correspondence plots. In Table V the values of the constants a and b for different solvents are listed. While it has been reported[8] that in DMF solutions Mukerjee's method of dividing $\bar{V}^0_{salt}$ does not hold well, in formamide and formic acid solutions no such problem has been encountered.

Volume of Transfer. Volumes of transfer[3,7] ($\Delta\bar{V}^0_T$) defined by the equation

$$\bar{V}^0_{ion}(S) - \bar{V}^0_{ion}(W) = \Delta\bar{V}^0_T \tag{6}$$
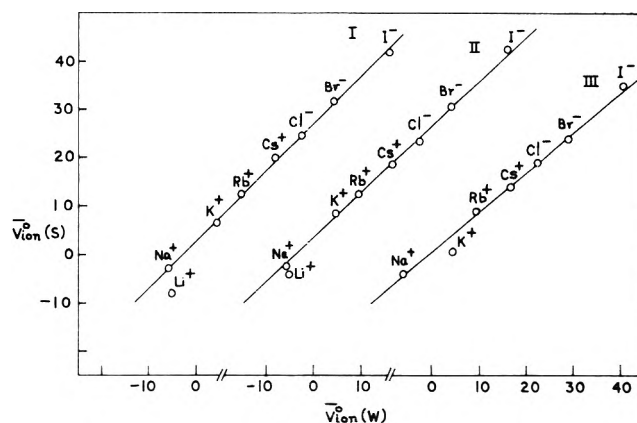
Figure 5. The partial molal volume of an ion in solvent $\bar{V}^0_{ion}(S)$, plotted vs. the partial molal volume of an ion in water, $\bar{V}^0_{ion}(W)$: ethylene glycol (I), formamide (II), and formic acid (III).

TABLE V: Values of the Constants a and b of Eq 5 for Various Solvents

Solvent	a	b
Sea water[a]	0.97	1.5
Methanol[a]	0.81	−9.0
Ethanol[b]	0.72	−3.0
Ethylene glycol	0.98	2.7
Formamide	0.92	3.5
Formic acid	0.96	0.5
NMP[a]	0.76	8.0

[a] Taken from ref 4. [b] Taken from ref 8.

have been calculated for the ions in the three solvents and are presented along with the results in other solvents[4,8] in Table VI. It is interesting to notice from the table that though in methanol[3] and ethanol,[8] values of $\Delta\bar{V}^0_T$ are all negative, in glycol solution they are all positive except for H$^+$ and Li$^+$ ions. In DMF[8] solutions $\Delta\bar{V}^0_T$ values are negative for all the ions, while they are always positive in formamide and NMP.[3] In formic acid, however, $\Delta\bar{V}^0_T$ is negative for all the ions except for H$^+$ and Na$^+$ (Li$^+$ is not available).

Discussion

Volume of a Proton in Various Solvents. The partial molal volume of an ion can be assumed to be the sum of two parts: (i) the intrinsic volume of the ion and (ii) the volume change due to the alteration of the structure of the system by the addition of the ion. The negative partial molal volume of an ion means that, with the addition of the ion, the solvent molecules form a more compact structure around the incorporated ion resulting in the decrease in the net volume of the system.[15] This is directly related to the solvation of the ion. In the case of a proton in solution, when the intrinsic volume is zero, solvation

TABLE VI: Volume of Transfer ($\Delta \bar{V}^0{}_T$) from Water to Various Solvents (cm³ mol⁻¹) at 25 °C

Ion	Methanol[a]	Ethanol[b]	Ethylene glycol	Formamide	Formic acid	NMP[a]	DMF[b]
H⁺	−11.3	−9.8	−7.5	9.0	13.5	3.4	
Li⁺	−11.3	−12.6	−2.6	1.2			−19.8
Na⁺	−10.2	−2.7	2.7	3.2	1.9	6.0	−9.4
K⁺	−10.6	−3.7	2.0	3.9	−3.7	11.1	−12.3
Rb⁺	−10.1	−2.9	2.8	2.9	−0.5		−13.4
Cs⁺	−10.8	−2.3	3.1	1.8	−2.8		−14.1
Cl⁻	−10.5	−11.0	2.2	1.3	−3.0	24.7	−1.5
Br⁻	−12.1	−15.3	2.3	1.3	−5.0	29.8	−7.5
I⁻	−13.7	−15.2	0.2	1.6	−5.5		−2.9

[a] Reference 4.   [b] Reference 8.

TABLE VII: Difference of $\bar{V}^0{}_{ion}$ and $\bar{V}^0{}_{cryst}$ in Various Solvents at 25 °C

| Ion | $\bar{V}^0{}_{cryst}{}^a$ | $\bar{V}^0{}_{ion} - \bar{V}^0{}_{cryst}$, cm³ mol⁻¹ | | | | | | | | |
		Water	Methanol[b]	Methanol[c]	Ethanol[c]	Ethylene glycol	Form-amide	Formic acid	NMP[b]	DMF[d]
H⁺	0.0	−4.5	−14.6	−17.0	−15.5	−12.0	4.5	9.0	3.4	
Li⁺	0.5	−5.7	−14.5	−18.4	−20.7	−8.3	−4.9			−19.9
Na⁺	2.1	−7.8	−14.7	−18.2	−16.4	−5.1	−4.6	−5.9	3.9	−11.3
K⁺	5.9	−1.4	−8.5	−12.2	−7.8	1.6	2.5	−5.1	5.2	−7.9
Rb⁺	8.2	1.3		−8.9	−4.3	4.1	4.2	0.8		−6.2
Cs⁺	12.2	4.7		−6.4	−0.5	7.8	6.5	1.9		−3.7
Cl⁻	14.9	7.4	−5.6	−2.9	0.1	9.6	8.7	4.4	9.8	0.1
Br⁻	18.7	10.5	−2.1	−1.4	−2.1	12.8	11.8	5.5	11.1	−2.8
I⁻	25.4	15.4	−1.1	1.8	2.3	14.6	17.0	9.9		6.9

[a] Reference 15.   [b] $\bar{V}^0{}_{ion}$ values taken from ref 4.   [c] $\bar{V}^0{}_{ion}$ values taken from ref 7.   [d] $\bar{V}^0{}_{ion}$ values taken from ref 8.

alone is important to determine the $\bar{V}^0{}_{H^+}$. The volume of a proton ($\bar{V}^0{}_{H^-}$) in ethylene-glycol is more negative than in water (see Table V). In methanol and ethanol $\bar{V}^0{}_{H^+}$ is still more negative. This suggests that solvation of a proton, which may be considered as an indication of the base strength[29] of the solvent, is stronger in these three solvents, and probably that the base strength of the solvents is in the following order: MeOH > EtOH > ethylene glycol > water. $\bar{V}^0{}_{H^+}$ is positive in NMP (=3.4), formamide (=4.5), and formic acid (=9.0). Recently,[30] it has been shown that the effect of solvent internal pressure on partial molal volumes might become important in the absence of electrostriction. The positive values of $\bar{V}^0{}_{H^+}$ in NMP, formamide, and formic acid probably indicate that in determining partial molal volumes in nonaqueous systems the ability of the solvent to prevent electrostriction can be significant and should be considered along with the ability of the solute to cause electrostriction of the solvent.

It is interesting to note from Tables II and IV that the partial molal volumes of HCl at infinite dilution in all three nonhydroxylic solvents (i.e., formamide, formic acid, and NMP) are almost equal ($\simeq 28.2$) although the ionic volumes of the proton and the chloride ion in the respective solvents are very different.

Ion–Solvent Interactions. For ions in aqueous solutions it has been suggested[15] that when the difference between the ionic volume and the crystal volume ($\bar{V}^0{}_{ion} - \bar{V}^0{}_{cryst}$) is positive the $\bar{V}^0{}_{disord}$ region is greater than $\bar{V}^0{}_{elect}$ region and the ion can be classified as a structure breaking ion[17] or a negative hydrating ion.[31] Assuming that this classification will be valid also in nonaqueous solutions, $\bar{V}^0{}_{ion} - \bar{V}^0{}_{cryst}$ for different ions have been calculated to determine the structure-making character of the ions in various solvents. Table VII contains the values of ($\bar{V}^0{}_{ion} - \bar{V}^0{}_{cryst}$) in different solvents. In aqueous solution the potassium ion (K⁺) is on the border line of the above classification and is generally assumed to have a slight net structure-breaking effect.[32] Larger simple monovalent ions are all structure breakers. Such is the case with ethylene glycol

and formamide. In formic acid solution Rb⁺ is probably on the border line. However in methanol, ethanol, and DMF, all the simple monovalent ions with the exception of I⁻ are structure makers while in NMP all ions are structure breakers. This suggests that in NMP all the simple monovalent ions increase the fluidity of the solvent and the non-nearest-neighbor solvent molecules in the vicinity of the ions become more mobile[32] than those in pure NMP. Exactly the opposite is the case with solvents such as methanol, ethanol, and DMF. The behavior of ions in ethylene glycol, formamide, and formic acid, however, is about the same as in water as far as the structure-breaking and structure-making property is concerned.

Hepler's semiempirical equation[19]

$$\bar{V}^0{}_{ion} = Ar^3 - BZ^2/r \qquad (7)$$

where A and B are constants, Z is the charge on the ion, and r is the crystallographic radius of the ion, has been used to separate the geometric part[7] from the electrostrictive part of the ionic volume. The first term of eq 7, the geometric part, is a combination of $\bar{V}^0{}_{int}$ and $\bar{V}^0{}_{disord}$ and the second term is $\bar{V}^0{}_{elect}$. For monovalent ions eq 7 can be rearranged as

$$\bar{V}^0{}_{ion}r = Ar^4 - B \qquad (8)$$

Equation 8 has been tested with the three solvents in the present work. Figure 6 shows the plot of ($\bar{V}^0{}_{ion}r$) against r^4. From the graph the values of A and B are determined. To separate the intrinsic size of an ion and the void space effect (i.e., to calculate $\bar{V}^0{}_{int}$ and $\bar{V}^0{}_{disord}$, respectively) the following semiempirical equations[15] have been used:

$$\bar{V}^0{}_{ion} = 2.52r^3 + (A - 2.52)r^3 - BZ^2/r \qquad (9)$$

$$\bar{V}^0{}_{ion} = 2.52r^3 + A'r^2 - B'Z^2/r \qquad (10)$$

Equation 9 is actually equivalent to eq 7. In eq 10 the void space is assumed to be proportional to the surface of the ion. A' and B' have been determined graphically from eq

Solvent	D^a	$A \pm$ 0.2	$B \pm$ 2	$A' \pm$ 0.2	$B' \pm$ 2
Water^b	78.3	4.5	8.0 ± 1	4.0	10.0 ± 1
Methanol^b	32.6	3.5	16.0	1.7	16.0
Ethanol^c	24.3	3.3	12.0	3.4	17.6
Ethylene glycol	37.7^d	4.7	6.0	4.5	9.0
Formamide	111.3	4.3	2.5	4.0	7.0
Formic acid	57.0	3.5	3.5	2.6	8.5
NMP^b	176.0	4.0	3.0	3.2	2.0

^{a} Reference 6. ^{b} Reference 4. ^{c} Reference 8. ^{d} Reference 24.

10 by plotting ($\bar{V}^0_{ion}r - 2.52r^4$) against r^3. The values of A, A' and B, B' in various solvents are listed in Table VIII. Table IX contains the values of $\bar{V}^0_{disord}$ (equal to the second term of eq 9 and 10).

Table VIII shows that with the exception of ethylene glycol the values of A and A' are always less than those in water. However A is always larger than the theoretical value calculated by assuming that the ion is a perfect hard sphere ($4/3\pi N10^{-24} = 2.52$). The apparent increase in $\bar{V}^0_{ion}$ is 86% in ethylene glycol, 71% in formamide, 32% in formic acid, and 29% in ethanol.[8] The magnitude and order of the constants A and A' show no apparent simple correlation to common physical properties such as die-
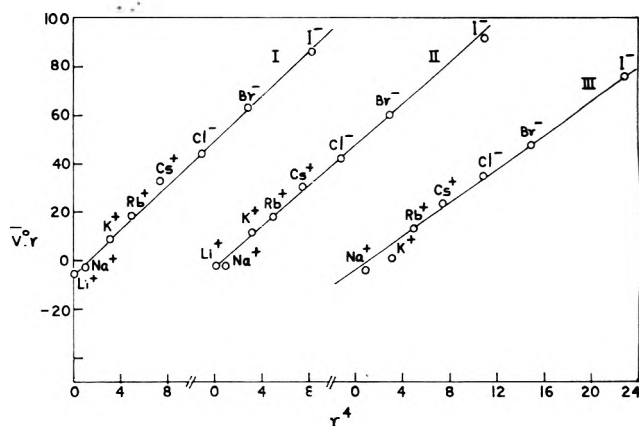

Figure 6. Plot of $V^0_{ion}r$ vs. r^4 in ethylene glycol (I), formamide (II), and formic acid (III) at 25 °C.

lectric constant. The cause of the increase of $\bar{V}^0_{int}$ in water has been attributed to void space packing effect.[33-35] Results in these nonaqueous solvents indicate that the void space packing effect are also important. Millero[4] suggested that because of the large size of the nonaqueous solvent molecules, the increase in $\bar{V}^0_{int}$ may be related, not to void space effect, but to the disorder region surrounding the solvated ion, $\bar{V}^0_{disord}$. It was found earlier that $\bar{V}^0_{disord}$ is the largest in the most highly ordered solvent, i.e., water,

TABLE IX: Disorder or Void-Space Partial Molal Volumes ($\bar{V}^0_{disord}$) of Monovalent Ions in Various Solvents at 25 °C

Ion	Water	Methanol	Ethanol	Ethylene glycol	Formamide	Formic Acid	NMP	DMF
			$\bar{V}^0_{disord} = (A - 2.52)r^3$, cm^3 mol^{-1}					
Li$^+$	0.4	0.2	0.2	0.5	0.4	0.2	0.3	0
Na$^+$	1.7	0.9	0.7	1.9	1.5	0.9	1.3	0
K$^+$	4.7	2.4	1.9	5.2	4.2	2.4	3.5	0
Rb$^+$	6.5	3.2	2.6	7.1	5.8	3.2	4.9	0
Cs$^+$	9.7	4.8	3.9	10.6	8.7	4.8	7.2	0
Cl$^-$	11.9	5.9	4.7	13.1	10.7	5.9	8.9	7.7
Br$^-$	14.8	7.4	5.9	16.3	13.3	7.4	11.1	9.6
I$^-$	20.2	10.1	8.1	22.2	18.1	10.1	15.1	13.1
			$\bar{V}^0_{disord} = A'r^2$, cm^3 mol^{-1}					
Li$^+$	1.4	0.6	1.2	1.6	1.4	0.9	1.2	
Na$^+$	3.6	1.5	3.0	4.1	3.6	2.3	2.9	
K$^+$	7.1	3.0	6.0	8.0	7.1	4.6	5.7	
Rb$^+$	8.8	3.7	7.4	9.8	8.8	5.7	7.0	
Cs$^+$	11.5	4.9	9.8	12.9	11.5	7.4	9.1	
Cl$^-$	13.1	5.6	11.2	14.8	13.1	8.5	10.5	
Br$^-$	15.2	6.5	13.0	17.1	15.2	9.9	12.2	
I$^-$	18.7	7.9	15.8	21.0	18.7	12.1	14.9	

TABLE X: Electrostrictive Decrease in Volume ($\bar{V}^0_{elect}$) of Monovalent Ions in Various Solvents at 25 °C

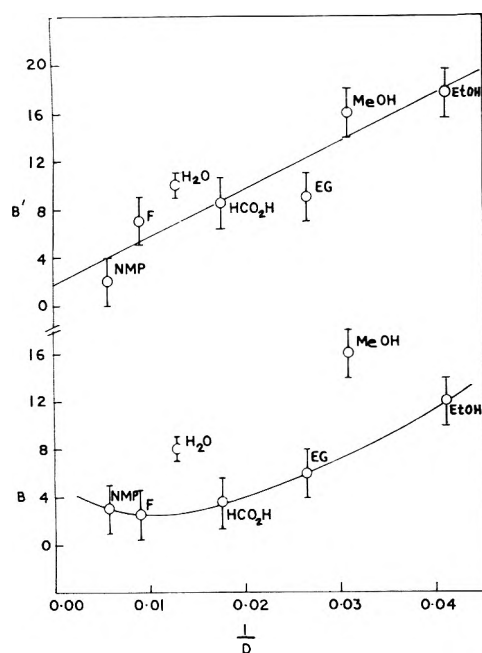| Ion	Water	Methanol	Ethanol	Ethylene glycol	Formamide	Formic acid	NMP	DMF
			$\bar{V}^0_{elect} = B/r$, cm^3 mol^{-1}					
Li$^+$	13.3	26.7	20.0	10.0	4.2	5.8	5.0	30.0
Na$^+$	8.4	16.8	12.6	6.3	2.6	3.7	3.2	18.9
K$^+$	6.0	12.0	9.0	4.5	1.9	2.6	2.3	13.5
Rb$^+$	5.4	10.8	8.1	4.1	1.7	2.4	2.0	12.2
Cs$^+$	4.7	9.5	7.1	3.6	1.5	2.1	1.8	10.7
Cl$^-$	4.4	8.8	6.6	3.3	1.4	1.9	1.7	1.1
Br$^-$	4.1	8.1	6.2	3.1	1.3	1.8	1.5	1.0
I$^-$	3.7	7.4	5.6	2.8	1.2	1.6	1.4	0.9
			$\bar{V}^0_{elect} = B'/r$, cm^3 mol^{-1}					
Li$^+$	16.7	26.7	29.3	15.0	11.7	14.2	3.3	
Na$^+$	10.5	16.8	18.5	9.5	7.4	8.9	2.1	
K$^+$	7.5	12.0	13.2	6.8	5.3	6.4	1.5	
Rb$^+$	6.8	10.8	11.9	6.1	4.7	5.7	1.4	
Cs$^+$	5.9	9.5	10.4	5.3	4.1	5.0	1.2	
Cl$^-$	5.5	8.8	9.7	5.0	3.9	4.7	1.1	
Br$^-$	5.1	8.1	9.0	4.6	3.6	4.4	1.0	
I$^-$	4.6	7.4	8.1	4.2	3.2	3.9	0.9	

Figure 7. The semiempirical constants B and B' for the $\bar{V}^0_{elect}$ term of eq 9 and 10 plotted vs. the reciprocal of the dielectric constant of the solvents ($1/D$).

the solvents studied in this work (Table X).

Acknowledgment. The author thanks Professor M. N. Das, Head, Physical Chemistry Division, Jadavpur University, Calcutta, for Laboratory facilities.

Supplementary Material Available: Tables IA and IB containing apparent molal volumes of HCl and alkali metal halides at different molalities (2 pages). Ordering information is available on any current masthead page.

References and Notes

(1) Present address: Central Electro-Chemical Research Institute, Karaikudi 623006, Tamil Nadu, India.
(2) R. E. Gibson and J. F. Kincaid, *J. Am. Chem. Soc.*, **59**, 579 (1937).
(3) F. J. Millero, *J. Phys. Chem.*, **72**, 3208 (1968).
(4) F. J. Millero, *J. Phys. Chem.*, **73**, 2418 (1969).
(5) F. J. Millero, *Chem. Rev.*, **71**, 147 (1971).
(6) J. Padova, "Water and Aqueous Solutions", R. A. Horne, Ed., Wiley, New York, N.Y., 1972.
(7) F. Kawaizumi and R. Zana, *J. Phys. Chem.*, **78**, 627 (1974).
(8) F. Kawaizumi and R. Zana, *J. Phys. Chem.*, **78**, 1099 (1974).
(9) R. Zana and E. B. Yeager, *J. Phys. Chem.*, **71**, 521, 4241 (1967).
(10) P. Mukerjee, *J. Phys. Chem.*, **65**, 740 (1961).
(11) U. Sen, *J. Phys. Chem.*, **80**, 1566 (1976).
(12) R. Gopal and R. K. Srivastava, *J. Phys. Chem.*, **66**, 2704 (1962).
(13) R. Gopal and R. K. Srivastava, *J. Ind. Chem. Soc.*, **40**, 99 (1963).
(14) V. N. Fesenko, E. F. Ivanova, and G. P. Kotlyarova, *Russ. J. Phys. Chem.*, **42**, 1416 (1968).
(15) F. J. Millero in ref 6.
(16) R. W. Gurney, "Ionic Processes in Solution", McGraw-Hill, New York, N.Y., 1953.
(17) H. S. Frank and W. Y. Wen, *Discuss. Faraday Soc.*, **24**, 133 (1957).
(18) M. Eigen and E. Wicke, *J. Phys. Chem.*, **58**, 702 (1954).
(19) L. G. Hepler, *J. Phys. Chem.*, **61**, 1426 (1957).
(20) U. Sen, K. K. Kundu, and M. N. Das, *J. Phys. Chem.*, **71**, 3665 (1967).
(21) U. Sen, *J. Chem. Soc., Faraday Trans 1*, **69**, 2006 (1973).
(22) R. K. Agarwal and B. Nayak, *J. Phys. Chem.*, **70**, 2568 (1966).
(23) R. K. Agarwal and B. Nayak, *J. Phys. Chem.*, **71**, 2062 (1967).
(24) H. S. Harned and B. B. Owen, "The Physical Chemistry of Electrolytic Solutions", 3d ed., Reinhold, New York, N.Y., 1958.
(25) O. Redlich and D. M. Meyer, *Chem. Rev.*, **64**, 221 (1964); O. Redlich, *J. Phys. Chem.*, **67**, 496 (1963).
(26) D. O. Masson, *Phil. Mag.*, (7), **8**, 218 (1929).
(27) C. M. Criss, R. P. Held, and E. Luska, *J. Phys. Chem.*, **72**, 2970 (1968).
(28) C. M. Criss and J. W. Cobble, *J. Am. Chem. Soc.*, **86**, 5385 (1964).
(29) W. Gerrard and E. D. Macklin, *Chem. Rev.*, **59**, 1105 (1959).
(30) M. R. J. Dack, *Chem. Soc. Rev.*, **4**, 211 (1975).
(31) O. Y. Samailov, *Discuss. Faraday Soc.*, **24**, 141 (1957).
(32) J. L. Kavanau, "Water and Solute-Water Interactions", Holden Day, San Francisco, Calif., 1964.
(33) B. E. Conway, R. E. Verral, and J. F. Desnoyers, *Z. Phys. Chem.*, **230**, 157 (1965).
(34) E. Glueckauf, *Trans. Faraday Soc.*, **61**, 914 (1965).
(35) S. W. Benson and C. S. Copeland, *J. Phys. Chem.*, **67**, 1194 (1963).
(36) P. Drude and W. Nernst, *Z. Phys. Chem.*, **15**, 79 (1894).

but in the present work $\bar{V}^0_{disord}$ in ethylene glycol is almost same as that in water, if not slightly higher (Table IX).

Values of the constants B and B' (eq 9 and 10) in different solvents (Table VIII) have been plotted against the reciprocal of the corresponding dielectric constants ($1/D$) in Figure 7. It can be seen that the values of B and B' in general increase with decrease in the dielectric constant. This trend is expected from the theoretical relation of Drude–Nernst.[36] No attempt has, however, been made to calculate theoretically $\bar{V}^0_{elect}$ due to lack of necessary data for the systems under investigation. Figure 7 shows that the values of B' in different solvents fit a straight line ($B' = 2 + 400/D$) better than the corresponding B values when plotted against $1/D$. $\bar{V}_{elect}^0$ values (i.e., the decrease in volume due to electrostriction) of monovalent ions in different solvents have been calculated from both the values of B and B' and are presented in Table X. As in water the electrostriction is smaller for larger ions in all

Potentiometric Determination of Solvation Numbers and Hydration Constants for Cations

Craig E. Van Uitert, Leonard D. Spicer,

Chemistry Department, University of Utah, Salt Lake City, Utah 84112

and LeGrand G. Van Uitert*

Bell Telephone Laboratories, Murray Hill, New Jersey 07974 (Received July 1, 1976)

A technique is developed for determining solvation numbers and hydration constants for metal ions. Stability constants are obtained that are essentially independent of the solution composition for a wide range of solvents. It is shown that two ROH molecules can take part in hydronium(-like) complex formation. Solvation numbers are obtained for H^+, OH^-, and organic acid anions as well as for divalent metal ions and their monochelates.

Introduction

Most of the stability constant data in the literature for the formation of metal chelates has been measured in

aqueous solvents.[1-3] The constants so obtained are more complex than expected as the cations are hydrated and must lose H_2O molecules from their coordination spheres

before they can accept a ligand.[4,5] If one could correct fully for the extent of solvation, it would be possible to obtain a stability constant for the formation of the complex from entities that are the same as its immediate products of dissociation. Such values will be shown to be essentially independent of the solvent medium and therefore should show significant relationships to rate constants and be helpful in understanding ionophore processes for ion diffusion through membranes. The suitably stripped cations (partially solvated or unsolvated) are termed *particles*, P*, herein and the constants derived using their concentrations will be termed *particle constants*. Both the species and the constants will be identified by an asterisk.

The problem of measuring hydration constants by the present method can be divided into four parts: *First*, a measurement technique that is not subject to electrode poisoning by metal ions or ligands must be employed; *Second*, the dependence of hydrogen ion activity upon water content over the entire range of mixed solvents (H_2O–ethanol here) must be determined; *Third*, the ratio of the hydration tendencies of the metal ion species of interest to that of the hydrogen ion in the same solvent mixtures must be established; and *Fourth*, solvation by nonaqueous components of the solution must be taken into account. Correction of the *third* item by the *second* and the *fourth*, where necessary, provides a measure of the strength of certain hydration steps involving the metal ion.

These requirements have been met for the H_2O–ethanol system by: *First*, making the requisite chelation measurements using a pH meter that has been calibrated to read hydrogen ion *concentration* over the entire H_2O–ethanol range; *Second*, correlating electrode potential data for the activity of HCl in liquid junction free cells[6,7] and applying the results to a simple model for the formation of hydronium(-like) complexes; *Third*, analyzing the relative complexing tendencies of the anion of a proton-donating chelating agent (HCh = ethyl acetoacetate here) with the hydrogen ion and the metal ion species (M^{2+} or its monochelate M^+Ch); and *Fourth*, by analyzing the hydration data for an extended series of M^{2+} ions in the H_2O–ethanol system to sort out the effects of solvation by ethanol.

Experimental Section

All measurements were carried out at an ambient temperature of 25 °C using a Beckman Model G pH meter equipped with extension electrodes, i.e., a No. 40498 pH 0–11 glass electrode and a No. 1170 fiber junction calomel electrode. The electrodes fitted into the side arms of a 100-ml three-necked flask and reached 3/4 of the way to the bottom. The contents of the flask were aggitated by a magnetic stirrer. The top opening was used to acco-modate a buret for adding solutions. In general, 50 ml of one solution was placed in a flask and titrated with a second, an increment at a time while rapidly stirring, to obtain the data of interest.

To meet the *first* requirement, H_2O–ethanol solutions containing a small but fixed (10^{-3} M) concentration of HCl were measured using the pH meter. The dissociation of 10^{-3} M HCl is greater than 95% and the mean molar activity coefficient is greater than 0.85 over the entire solvent range.[6] Further, small differences in activity are of negligible importance when one is dealing with order of magnitude changes. The uncorrected meter reading for the solvent mixture is subtracted from the value measured for the H_2O solution containing the same concentration of HCl to obtain $C_{\gamma j}$. This term is the correction to be added to the meter reading to obtain p(H), which is the
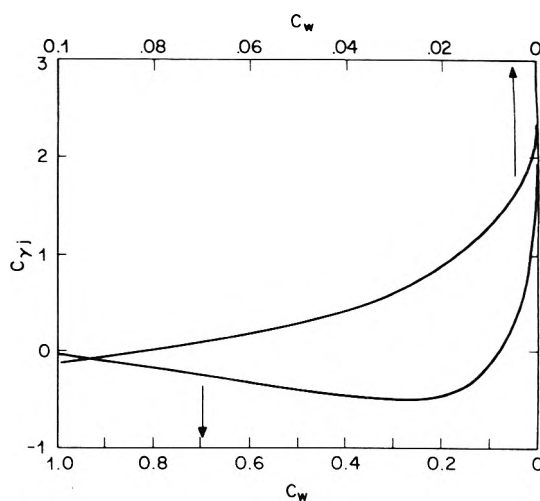

Figure 1. The combined correction ($C_{\gamma j}$) for HCl activity (C_γ) and liquid junction potential for the calomel electrode (C_j) vs. C_w. The addition of $C_{\gamma j}$ to the pH meter reading yields p(H), the negative logarithm of the hydrogen ion *concentration*.
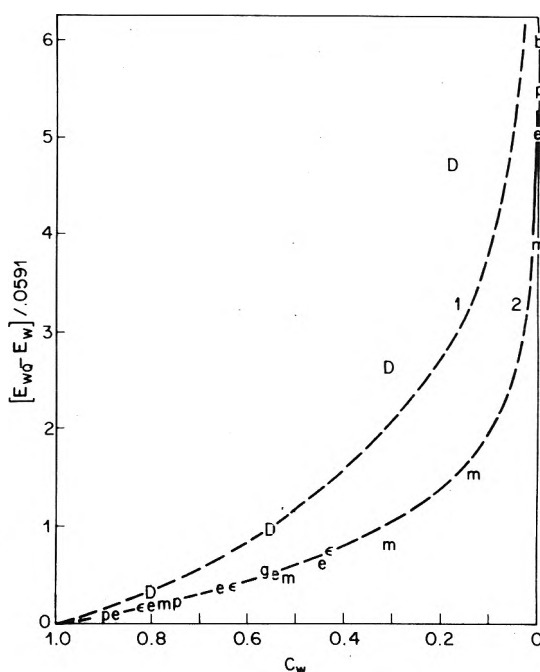
Figure 2. Logarithm of HCl activity vs. the volume fraction of H_2O in various H_2O–solvent Q mixtures: (D) *p*-dioxane, (b) butanol (and isopentanol), (e) ethanol, (ϵ) ethylene glycol, (g) glycerol, (m) methanol, (p) propanol. Curve 1 = -4 log C_w and curve 2 = -2 log C_w.

negative logarithm of the total *concentration* of H^+ species. The correction, $C_{\gamma j}$, is plotted vs. C_w, the volume fraction of H_2O, in Figure 1 (see caption). Symbols that are used throughout the text are defined in Appendix 1.

To meet the *second* requirement, data for the standard reduction potential of the cell

$$Pt:H_2|HCl, H_2O\text{–solvent } Q|AgCl:Ag \qquad (1)$$

was examined.[6,7] $(E_{wQ} - E_w)/0.0591$ is plottd vs. C_w in Figure 2. Here, E_w is the standard reduction potential for the cell using H_2O only as the solvent and E_{wQ} is the comparable value in the mixed solvent. The voltage difference equals the logarithm of the activity of HCl in the mixed solvent relative to unity for $C_w = 1.0$ (the square root of this activity value is termed the primary medium effect, γ_0, in ref 6).

To meet the *third* and *fourth* requirements, chelation titrations were carried out in water and in ethanol to

Figure 3. p(H) vs. log C_w for hydration titrations involving the first chelation of Ni^{2+} (lower curve) and the subsequent chelation of Ni^+Ch (upper curve) in the H_2O-ethanol system.
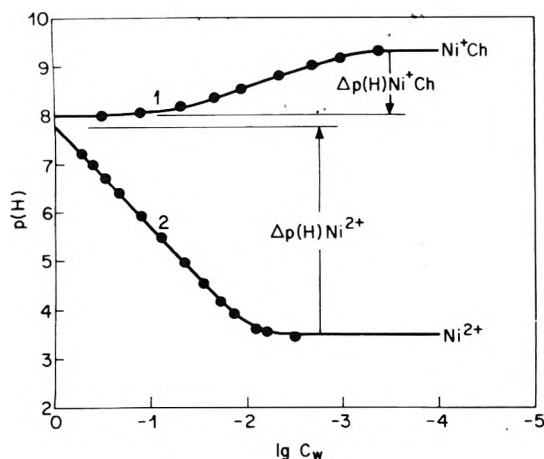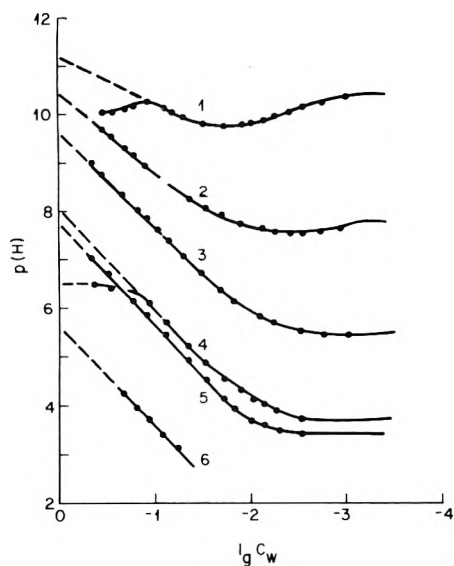

Figure 4. p(H) vs. log C_w for the hydration titrations involving the first chelation of (1) Ba^{2+}, (2) Ca^{2+}, (3) Mg^{2+}, (4) Zn^{2+}, (5) Ni^{2+}, and (6) Cu^{2+}.

Figure 5. p(H) vs. log C_w for the hydration titrations involving the chelation of (1) Ba^+Ch, (2) Ca^+Ch, (3) Mg^+Ch, (4) Zn^+Ch, and (5) Ni^+Ch.
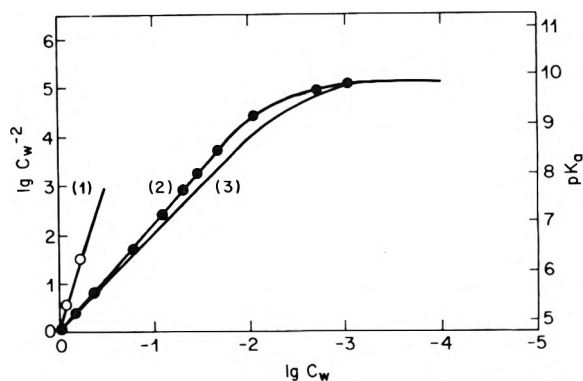
Figure 6. (Curve 1) pK_a for acetic acid in H_2O–dioxane vs. log C_w; (curve 2) pK_a for acetic acid in H_2O–ethanol vs. log C_w; (curve 3) the log C_w^{-2} representation of HCl activity in the H_2O–ethanol system, from curve 3 of Figure 2, vs. log C_w.

establish the characteristics of the interactions of interest. Details are not given here, but the information was used to design the *hydration titration* experiments discussed in Appendix 2 (supplementary material; see paragraph at end of text regarding supplementary material). The measurements were carried out in dilute solutions to keep the molar activity coefficients close to unity.[6] Typically, *hydration titration* solutions contained 10^{-4} mol of M-$(ClO_4)_2 \cdot xH_2O$ and 5×10^{-4} mol of ethyl acetoacetate (HCh) plus 5×10^{-5} mol of sodium ethoxide for the first chelation or 5 ml (270×10^{-4} mol) of HCh plus 15×10^{-5} mol of sodium ethoxide for the second and were titrated with H_2O. A large excess of HCh was used for the second chelation to avoid the formation of hydroxides. The data derived for p(H) vs. log C_w for the hydration titrations involving the first and second chelations of divalent nickel by HCh are plotted in Figure 3. Similar data for the whole set of divalent ions of Ba, Ca, Mg, Zn, Ni, and Cu, involving the first chelation, are shown in Figure 4 and, involving the second chelation, in Figure 5.

The pK_a of ethyl acetoacetate is 10.7 in H_2O and rises to (H^+) levels that are too low for accurate measurement by the glass electrode in ethanol. Since it was not feasible to determine the dependence of pK_a for this chelating agent upon C_w by direct means, acetic acid which has a
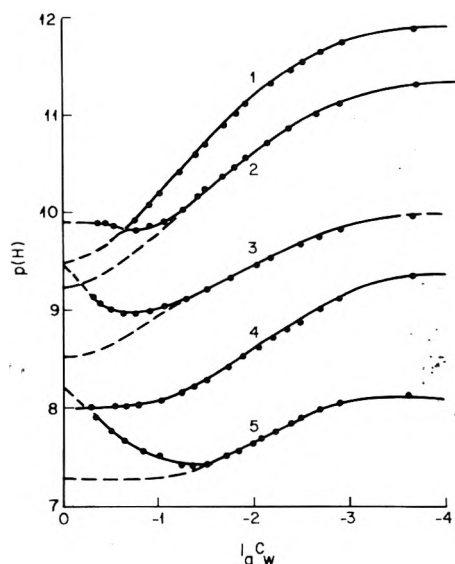
much lower pK_a was studied in its place. Data for solutions that contain equal amounts of sodium acetate (0.005 M) and acetic acid (0.005 M) in H_2O–ethanol mixtures are plotted in Figure 6. The meter readings were corrected by $C_{\gamma j}$ and for dilution to obtain p(H) $\simeq pK_a$ for this experiment.

Theoretical

For a fixed solvent, the molar activity coefficients are unity at infinite dilution. However, there can be a change in cell potential (i.e., activity) with an alteration of solvent composition. This medium effect, C_γ, may be attributed to changes in ion mobility or active ion concentration. The data herein indicate that the latter is the controlling factor.

Consider the hydronium ion; it is well established that, in H_2O at 25 °C, it is largely the tetrahydrate of the proton, $H_9^+O_4$.[8-10] Hence, one can write the equilibrium

$$H^* + 4H_2O \rightleftharpoons H_9^+O_4 \tag{2}$$

and a dissociation constant

$$K_p = (H^*)C_w^4/(H_9^+O_4) \tag{3}$$

This is to say, the concentration of free protons, in a solvent system wherein only H_2O solvates H^* and (H^+) is fixed, should vary as C_w^{-4}. Curves 1 and 2 of Figure 2 represent $-4 \log C_w$ and $-2 \log C_w$ vs. C_w, respectively. The data points for the activity of HCl in the H_2O–dioxane

Figure 7. The vector addition of $\Delta p(H)$ terms to $_{\phi\Sigma}(H^*)/(H^*)_1$ to derive $_{\phi\Sigma}(P^*)/(P^*)_1$ for Ni^{2*} or $(P^*)/(P^*)_1$ for Ni^*Ch. The logarithms of the concentration ratios are plotted vs. log C_w (H_2O–ethanol system).
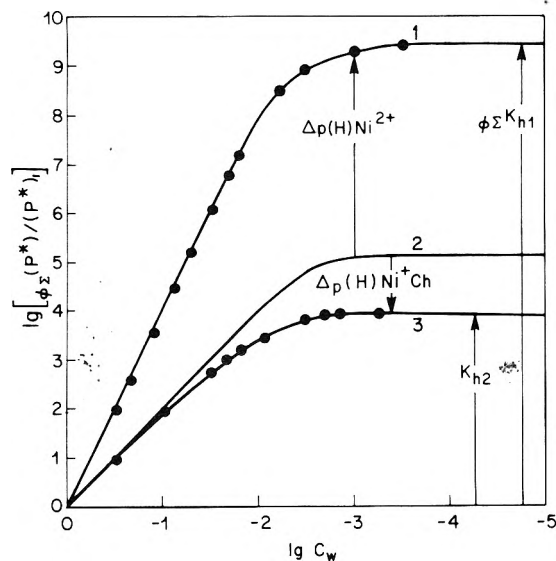
system fit the former curve from $C_w = 1.0$ to $C_w = 0.5$ in agreement with the expectation that the dominant hydrogen ion species in solution over that range is the tetrahydrate. The positive deviation of the data from curve 1 for lower values of C_w may be attributed to a disproportionate rise in the number of free protons due to the interference with H_2O movement by the relatively large dioxane molecules.

Wells has demonstrated that alcohol, ROH, can penetrate the hydronium complex and postulates the structure $ROH_2^+(H_2O)_3$.[9,10] Curve 2 of Figure 2 (representing $-2 \log C_w$ vs. C_w) is a good fit to the data for ethanol, propanol, and ethylene glycol and is a reasonable fit to the data for methanol and glycerol. It is consistent with the equilibrium

$$H^* + 2\Sigma + 2H_2O \rightleftharpoons H^*\Sigma_2(H_2O)_2 \tag{4}$$
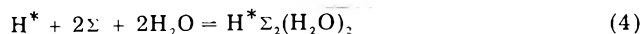
where Σ designates solvent molecules (H_2O and/or ROH) that coordinate exceptionally strong with the cation, e.g., to form $H^*\Sigma_2$. This implies that two ROH can interchange with two H_2O in the hydronium complex without greatly affecting its stability with the result that the term $(\Sigma)^2$ in the dissociation constant

$$K_p = (H^*)(\Sigma)^2 C_w^2/(H^*\Sigma_2(H_2O)_2) \tag{5}$$

does not change significantly in value as C_w changes.

In general, a subscript Σ is prefixed, $_\Sigma K$, to signify a dissociation constant that is larger or a formation constant that is smaller than the corresponding constant involving the unsolvated cation. The ratio is $(1 + K_\Sigma)$, where K_Σ is the constant for strong solvation of the cation in ROH. Similarly, a subscript ϕ is prefixed $(_\phi \Sigma K)$ to signify a further deviation by a factor $(1 + K_\phi)$, where K_ϕ is the constant for additional, but much weaker solvation of the cation by ROH, i.e., to form $H^*\Sigma_2\phi_x$; e.g.

$$_{\phi\Sigma}K_a^* = K_a^*(1 + K_\Sigma)(1 + K_\phi) \tag{6}$$

Curve 3 of Figure 6 or curve 2 of Figure 7 is obtained by plotting $-2 \log C_w$ vs. log C_w. The slope is obviously 2. However, the curve is drawn to cut off in accordance with a limit established by ROH solvation (the value for $C_w = 0$ in Figure 2). For ethanol, this value is

$$(E_Q - E_w)/0.0591 = \log 10^{5.1} \tag{7}$$

where E_Q is the standard reduction potential for (1) using pure ethanol as the solvent. This equation indicates an increase in (H^*) by a factor of $10^{5.1}$ for a fixed (H^+) upon going from water to ethanol.

The pK_a curve for acetic acid in the same solvent system (curve 2 of Figure 6) follows this modified $-2 \log C_w$ curve, indicating that the fall in (H^+) for the former tends to be reciprocally related to the rise in (H^*) for the latter. That is, as the ratio $(H^*)/(H^+)$ increases with decreasing C_w, less (H^+) is required to preserve (H^*) at a fixed value. This result indicates that (H^*) in the acetate buffer (where HA $= A^-$) does not change markedly with changes in solvent composition. Further, since $pK_a^* \simeq (H^*)$ in this experiment, the values for pK_a^*, and probably for all *particle* constants, are essentially independent of the solvent composition. Where deviations occur, they are small and may be traced to changes in anion solvation number. Nonetheless, in general, pK_w and pK_a can be directly compared to HCl activity in analyzing solvation effects.

The following relations are of interest: the dissociation constant of the chelating agent, the formation constant for the monochelate of the divalent metal ion, and the formation constant for the dichelate, as normally measured in aqueous solution, are respectively

$$K_a = (H^+)(Ch^-)/(HCh) \tag{8}$$

$$K_{f1} = (M^+Ch)/(M^{2+})(Ch^-) \tag{9}$$

$$K_{f2} = (MCh_2)/(M^+Ch)(Ch^-) \tag{10}$$

The comparable, fully solution independent constants, plus those for the hydration of the divalent and monochelated metal ions, are respectively

$$K_a^* = (H^*)(Ch^-)/(HCh) \tag{11}$$

$$K_{f1}^* = (M^*Ch)/(M^{2*})(Ch^-) \tag{12}$$

$$K_{f2}^* = (MCh_2)/(M^*Ch)(Ch^-) \tag{13}$$

$$K_{h1} = (M^{2+})/(M^{2*})C_w^T \tag{14}$$

$$K_{h2} = (M^+Ch)/(M^*Ch)C_w^{n'} \tag{15}$$

Except for K_{h2} and K_{f2}^*, these constants cannot be measured in a solvent where strong (Σ) solvation occurs (that is, in a Σ system). However, constants limited by Σ solvation but independent of the solution within the bounds of the Σ systems can be measured. These are

$$_\Sigma K_a^* = _\Sigma(H^*)(Ch^-)/(HCh) \tag{16}$$

$$_\Sigma K_{f1}^* = (M^+Ch)/_\Sigma(M^{2*}\Sigma_{T-n})(Ch^-) \tag{17}$$

$$_\Sigma K_{h1} = (M^{2+})/_\Sigma(M^{2*}\Sigma_{T-n})C_w^n \tag{18}$$

and those limited by ϕ solvation as well are

$$_{\phi\Sigma}K_a^* = _{\phi\Sigma}(H^*)(Ch^-)/(HCh) \tag{19}$$

$$_{\phi\Sigma}K_{f1}^* = (M^+Ch)/_{\phi\Sigma}(M^{2*}\Sigma_{T-n})(Ch^-) \tag{20}$$

$$_{\phi\Sigma}K_{h1} = (M^{2+})/_{\phi\Sigma}(M^{2*}\Sigma_{T-n})C_w^n \tag{21}$$

The Σ and ϕ solvation constants are

$$E_\Sigma = (M^{2*}\Sigma_2)/(M^2)(\Sigma)^2 \tag{22}$$

$$K_\phi = (M^2\Sigma_2\phi_x)/(M^{2*}\Sigma_2)(\phi)^x \tag{23}$$

In principal, constants (11), (12), and (14) could be measured in the H_2O–dioxane system. However, this was not possible with the equipment employed.

From (19), (20), and (21) and noting from Appendix 2 that $(M^+Ch) = (M^{2*}\Sigma_{T-n})$ for $C_w = 0$ one obtains

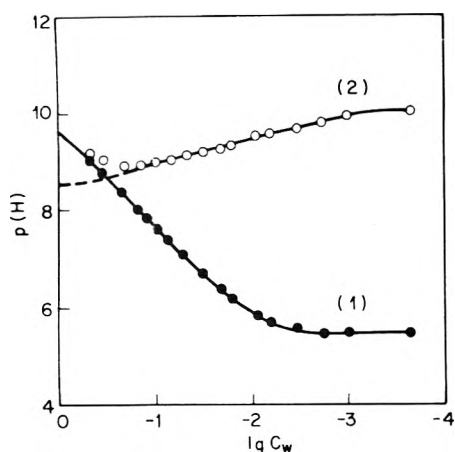$$_{\phi\Sigma}K_{h1} = _{\phi\Sigma}(H^*)_0/(H^*)_1 \tag{24}$$

Figure 8. p(H) vs. log C_w for hydration titrations involving the first chelation of Mg^{2+} (curve 2) and the subsequent chelation of Mg^+Ch (curve 1).

Further, from (7) one deduces that for the H_2O-ethanol system

$$_{\phi\Sigma}(H^*)_0/(H^*)_1 = 10^{5.1} \, _{\phi\Sigma}(H^+)_0(H^+)_1 \tag{25}$$

and therefore

$$\log \, _{\phi\Sigma}K_{h1} = p(H)_1 + 5.1 - \, _{\phi\Sigma}p(H)_0 \tag{26}$$

Similarly, starting with (19), (13), and (15)

$$\log K_{h2} = p(H)_1 + 5.1 - p(H)_0 \tag{27}$$

The constant $_{\phi\Sigma}K_h$ is smaller than $_{\Sigma}K_{h1}$; generally by a factor equal to K_ϕ, the constant for weak solvation by ethanol. However, K_{h2} is essentially independent of the solvent system. From (19) and (20)

$$_{\phi\Sigma}K_{f1} \, ^*_{\phi\Sigma}K_a^* \sim (H^*)/(M^{2*}\Sigma_{T-n}) \tag{28}$$

for any value of C_w as for each run (M^+Ch) and (HCh) are fixed. This is to say the affinity of Ch^- for H^* and for $M^{2*}\Sigma_{T-n}$ remain in a fixed ratio as the medium properties change. However, the ratio of these species to their hydrates can change. Since the hydrogen ion sensitive electrode only measures the free protons and not the hydrated species, it will show an emf change as proton hydration, as well as combination with Ch^-, proceeds. If $M^{2*}\Sigma_{T-n}$ hydrates more than H^*, the slackened competition by the former for Ch^- will cause more of the latter to combine with Ch and p(H) will rise (right to left for curve 2 of Figure 3). In the opposite event, more $M^{2*}\Sigma_{T-n}$ will combine with Ch, leading to further dissociation of HCh, and p(H) will fall (right to left for curve 1 in Figure 3). In either case, changes in p(H) merely reflect the change in (H^+) required to restore the $(H^*)/(M^{2*}\Sigma_{T-n})$ ratio. Therefore, the $\Delta p(H)$ values in Figure 3 should be added vectorily to curve 2 of Figure 7 to measure $_{\phi\Sigma}(Ni^{2+})/(Ni^{2+})_1$, curve 1 and $(Ni^*Ch)/(Ni^*Ch)_1$, curve 3, of Figure 7.

The dependence of p(H) upon log C_w is shown for the full set of hydration titrations involving the first chelation in Figure 4 and for those involving the second chelation in Figure 5. The downward deviation of the data for Zn^{2+} (curve 4 of Figure 4) at high values of C_w is due to hydroxide formation. This was avoided for the second chelation by using a much larger excess of chelating agent. The downward deviation for Ba^{2+} (curve 1 of Figure 4) is due to the overriding dissociation of HCh in the indicated p(H) range, near log $C_w = 0$. The correct value for the pK_a of ethyl acetoacetate at log $C_w = 0$ is 10.7; however, since
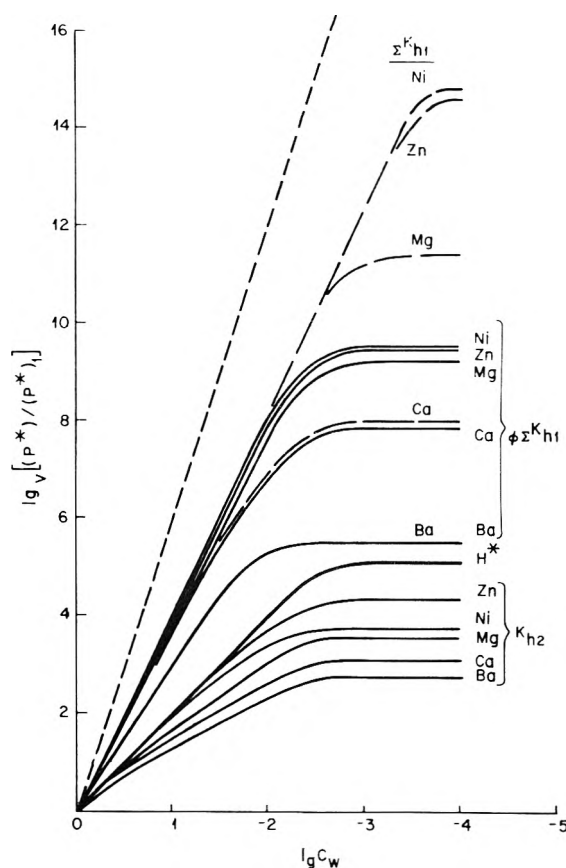

Figure 9. The composite sets of hydration curves for the set of M^{2+} ions of Ba, Ca, Mg, Zn, and Ni. These curves depict the relative availability of $M^{2*}\Sigma_{T-n}$ or M^*Ch vs. log C_w for the $_{\phi\Sigma}K_{h1}$ set, the $_{\Sigma}K_{h1}$ set, and the K_{h2} set. The broken line represents the slope of six expected for the K_{h1} set and the subscript v on the ordinate indicates a choice of sets.

the ratio $(HCh)/(Ch^-)$ tends toward 9/1, an effective value near 9.7 is obtained. The upswing deviations indicated for Ca^+Ch, Mg^+Ch, and Zn^+Ch in the same C_w range (curves 2, 3, and 5 of Figure 5) are due to the effect of the first chelation on the second. Figure 8 provides a clearer illustration of this interaction. Curves 1 and 2 represent the p(H) data for the hydration titrations of magnesium involving the second and first chelations respectively and are to be compared to the related curves for nickel in Figure 3. The data for nickel exhibit a relationship wherein there is relatively little tendency for M^{2+} to take on a second Ch^- prior to all M^{2+} ions chelating the first time. However, as indicated by the extrapolation (at high C_w) of curve 1 of Figure 8, there is a greater propensity for Mg^+Ch to take on a second Ch^- than for Mg^{2+} to chelate the first time in high C_w solutions. The latter circumstance relates to a much larger availability of the M^*Ch than of the $M^{2*}\Sigma_{T-n}$ species. The situation changes rapidly as the H_2O content of the solution decreases since K_{h2} varies as C_w^{-2} while $_{\Sigma}K_{h1}$ varies as C_w^{-4} and K_{h1} as C_w^{-6}. In general, when C_w is reduced by an order of magnitude the chelation steps no longer overlap.

Figure 9 depicts the relative availability of $M^{2*}\Sigma_{T-n}$ or M^*Ch vs. log C_w for the cations studied and is a more extensive assembly of data organized as for nickel alone in Figure 7. The curves involving the second chelation (K_{h2} set) do not require any further adjustment as the dichelate, in effect, is not solvated. However, the curves involving the first chelation in the H_2O-ethanol system ($_{\phi\Sigma}K_{h1}$ set) terminate at cutoff levels dictated by weak solvation (ϕ) with ethanol and therefore require further correction to get solvent independent values. To correct for ϕ, one must
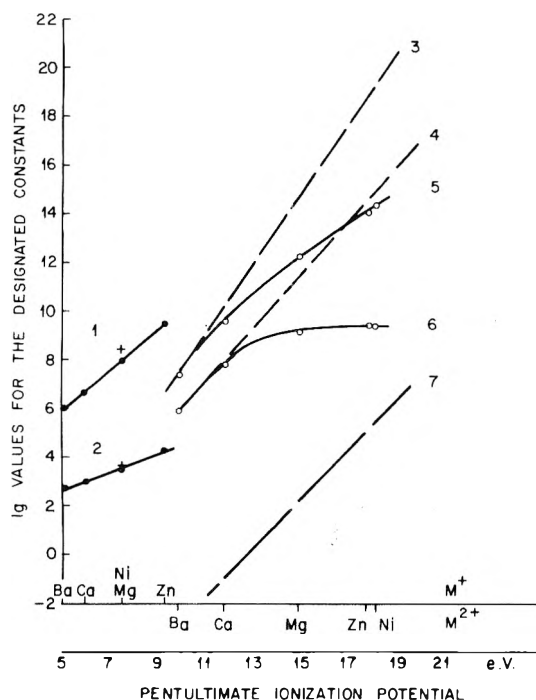
Figure 10. (1) log K_{f2} and (2) log K_{h2} vs. the first ionization potential of the metal, (+) indicates Ni; (3) log ΣK_{f1}, (4) log ΣK_{h1}, (5) log $_\phi\Sigma K_{f1}$, (6) log $_\phi\Sigma K_{h1}$, and (7) log K_ϕ vs. the second ionization potential of the metal.

estimate the value of K_ϕ. This is done with the aid of Figure 10. The curves obtained upon applying these corrections are designated as the $_\Sigma K_{h1}$ set represented by the broken lines in Figure 9. The initial slope for the K_{h1} set should be 6 as indicated by the dashed line in Figure 9. The cutoff levels for this set have not been determined.

Figure 10 depicts the values of the cutoff levels for the K_{h2} set and the $_\phi\Sigma K_{h1}$ set vs. the pentultimate ionization potential for the monovalent and divalent metal ions, respectively. The comparable values for $_\phi\Sigma K_{f1}$, K_{f2}, K_ϕ, and $_\Sigma K_{f1}$ are also shown.

Discussion

Marshall et al. have stressed the importance of treating the complete equilibrium constant in the thermodynamic analysis of solution properties.[4] Following this line, Woolley et al. examined the dependence of the dissociation constant of water, K_w, on C_w in the high H_2O region of the H_2O-dioxane, H_2O-ethanol, and other systems. They found up to seventh order relations from a consideration of initial slopes.[5] That is, up to seven H_2O molecules appear to be involved in the combined formation of the hydronium and hydroxyl complexes. From more exact data (ref 6) for water and propionic, acetic, and formic acid in the H_2O-dioxane system, initial slopes of 6.7, 6.4, 6.0, and 4.6, respectively, are estimated for plots of pK_w or pK_a vs. log C_w. The slopes represent the combined number of H_2O molecules bonding to H^+ and the anion. Since the solvation number for H^+ in this system is 4, the value for the anion is 2.7, 2.4, 2.0, and 0.6, respectively. These values decrease in the order of increasing acidity of the molecule (i.e., pK_w or pK_a in H_2O equals 14.00, 4.87, 4.76, and 3.75, respectively). From this trend, it is to be expected that the anion of a strong acid, such as HCl, will have little tendency to hydrate.

The initial slope for K_w is near 5 (see ref 5) while that for HCl activity (Figure 2) is 2, over the high C_w part of the H_2O-ethanol system. This indicates that the hydroxyl ion tends to be a trihydrate in this range of H_2O-ethanol solutions. However, for $C_w < 0.8$, the slope changes to 2,

paralleling the curve for HCl activity. This shows that ROH can replace H_2O bonded to the anion in the low C_w region.

As discussed above and depicted in Figure 6, the curve for pK_a of acetic acid vs. log C_w in the H_2O-dioxane system has an initial slope of 6, indicating that the anion is a bihydrate. However, in H_2O-ethanol the slope is reduced to 2.2 (see curve 2). Allowing for a reduction of 2 for the formation of $H^+(ROH)_2(H_2O)_2$, this indicates that the loss of two H_2O from the acetate ion complex is compensated by the attachment of 1.8 ROH on the average. Fortunately, in determining the hydration constants of the metal ions, one is concerned only with the ratio of the affinities of the chelate anion for H^* and $M^{2*}\Sigma_{T-n}$ or M*Ch and therefore it is not necessary to know the degree of solvation of the anion. However, it is important to know the extent of solvation of the chelating agent anion as well as that of the cation to determine the stability constants in which they are involved.

From (7), see (27), one deduces $_\phi\Sigma(H^*)_0/_\phi\Sigma(H^+)_0$ in ethanol is $10^{5.1}(H^*)_1/(H^+)_1$. This number could be larger but is limited by solvation of the hydrogen ion by two ROH. Mukherjee found an HCl activity in glacial acetic acid that was $10^{14.5}$ times the value in H_2O.[11] This higher cutoff may represent the value for the essentially non-solvated proton. The position of the cutoff level indicates the relative concentration of the species, H^*, for a fixed (H^+). Where the subscripts indicate (g) glacial acetic acid, (e) ethanol, and (w) water, respectively

$$_g(H^*) = 10^{9.4}{}_e(H^*) = 10^{14.5}{}_w(H^*) \qquad (29)$$

Further, as HCl activity scales with pK_a for weak acids

$$_g pK_a = 10^{9.4}{}_e pK_a = 10^{14.5}{}_w pK_a \qquad (30)$$

where $_g pK_a \simeq pK_a^*$

In Figure 3, the slope of curve 2, representing p(H) vs. log C_w for Ni^{2+}, is -2. This indicates that $M^{2*}\Sigma_{T-n}$ hydrates by a factor of C_w^{-2} more than H^*. However, as H^* hydrates in proportion to C_w^{-2} as well, the full hydration effect is proportional to C_w^{-4}. This result is obtained graphically by adding $\Delta p(H)Ni^{2+}$, from Figure 3, to curve 2 of Figure 7. The sum, curve 1 of Figure 7, is the absolute dependence of $(P^*)/(P^*)_1$ on log C_w where P^* may be H^* or $M^{2*}\Sigma_{T-n}$, see (28). The slope is $n = 4$ with the cutoff at $_\phi\Sigma K_{h1} = 10^{9.4}$. The slope of curve 1 of Figure 3 is variable. Adding the associated $\Delta p(H)Ni^+Ch$ correction vectorily to curve 2 of Figure 7, one obtains curve 3 which has an initial slope of $n' = 2$ and a cutoff at $K_{h2} = 10^{3.9}$. The two slopes add up to $n + n' = 6$ in good agreement with the expectation that six H_2O molecules should be removed upon forming $NiCh_2$.

As shown in Figure 9, an initial slope of 4 is typical of the $_\phi\Sigma K_{h1}$ set, save for Ba^{2+}. The $_\phi\Sigma K_{h1}$ plus K_{h2} data for the latter ion indicates a maximum solvation of 4 or 5. The smaller coordination number may be attributed, at least in part, to the low stability of the hydrated complex. The general shapes of the curves in Figure 9, the $_\phi\Sigma K_{h1}$ set for example, are derived from

$$(M^{2*})/(M^{2*})_1 = (_\phi\Sigma K_{h1}C_w^4 + K_\phi C_e^2)^{-1} \qquad (31)$$

where C_e is the volume fraction of ethanol.

The data for log K_{h2} in Figure 10 show a straight line relation to the first ionization potential of the metals. The data for log K_{f2} show a similar relation except for Ni^+Ch (a cation with available d orbitals). Similar results are obtained for the monochelates Ba^+Ch, Ca^+Ch, Mg^+Ch, and Zn^+Ch when plotted against the second ionization po-

TABLE I: Stability Constants Based on the H_2O-Ethanol System

log units	Ba²⁺	Ca²⁺	Mg²⁺	Zn²⁺	Ni²⁺	(pK)	H⁺
K_{f_1}	1.5	1.8	3.1	4.6	4.9	K_a	10.7
$_{\phi\Sigma}K_{h_1}$	5.9	7.8	9.2	9.5	9.5		5.1
$_{\phi\Sigma}K_{f_1}*$	7.4	9.6	12.3	14.1	14.4	$_{\phi\Sigma}K_a*$	15.8
K_ϕ	~-3	~-1	2.3	5.0	5.4		
$_{\Sigma}K_{h_1}$	5.9	7.9	11.4	14.5	14.9		
$_{\Sigma}K_{f_1}*$	7.4	10.0	14.6	19.1	19.8	$_{\Sigma}K_a*$	

Limit Due to Solvation by ROH

K_{Σ}							
$K_{f_1}*$						K_a*	~25

Dioxane or Glacial Acetic Acid Limit

	Ba⁺Ch	Ca⁺Ch	Mg⁺Ch	Zn⁺Ch	Ni⁺Ch	
K_{f_2}	3.4	3.7	4.4	5.3	4.9	
K_{h_2}	2.7	3.0	3.6	4.3	3.7	
$K_{f_2}*$	6.1	6.7	8.0	9.6	8.6	

Ionization potential of M° in eV

First	5.21	6.11	7.64	9.39	7.63		13.6
Second	10.00	11.87	15.03	17.96	18.15		

tential. However, the value for Ni⁺Ch is then quite low. The better fit to the first ionization potentials of the metals can be taken as evidence that the charge on the metal ion is reduced by exchange with the chelate anion.

The failure to obtain a linear relation for log $_{\phi\Sigma}K_{h1}$ or log $_{\phi\Sigma}K_{f1}$ vs. the second ionization potential is attributed to changes in effective solvation by ethanol. If $K_\phi \gg 1$ applied for all of the M^{2+} ions, one would find little difference in the values of log $_{\phi\Sigma}K_{h1}$ for this term then only measures the ratio of $_{\Sigma}K_{h1}$ to K_ϕ. Here, a fixed value for $_{\phi\Sigma}K_{h1}$ would only imply that the lines for log $_{\Sigma}K_{h1}$ and log K_ϕ are parallel as shown in Figure 10. The rapid drop in log $_{\phi\Sigma}K_{h1}$ actually seen as one moves toward Ba²⁺ is due to ineffectual solvation by ethanol as log K_ϕ drops below zero. Taking advantage of this situation, one can estimate the correct position of the log $_{\Sigma}K_{h1}$ line based on the positions for Ba²⁺ and Ca²⁺. The difference between positions on the log $_{\Sigma}K_{h1}$ and log $_{\phi\Sigma}K_{h1}$ lines were plotted to indicate the values for log K_ϕ and were also used to correct the log $_{\phi\Sigma}K_{f1}$ points to obtain the values for log $_{\Sigma}K_{f1}$. The values found for log $_{\Sigma}K_{h1}$ using Figure 10 were used as the cutoff values for the $_{\Sigma}K_{h1}$ set in Figure 9.

From (8), (20), and (21) for $C_w = 1$ and using Figure 3 to select p(H)₁, one finds for the first chelation of Ni²⁺Σ₂ by ethyl acetoacetate to form Ni⁺Ch

$$\log {}_{\phi\Sigma}K_{f1}* = {}_wpK_a + \log {}_{\phi\Sigma}K_{h1} - \log(HCh)$$
$$- p(H)_1 = 10.7 + 9.4 + 2.05 - 7.8 = 14.4 \quad (32)$$

and can be corrected to log $_{\Sigma}K_{f1}$ by replacing log $_{\phi\Sigma}K_{h1}$ by log $_{\Sigma}K_{h1}$.

$${}_{\Sigma}K_{h1} = {}_{\phi\Sigma}K_{h1}(1 + K_\phi) \quad (33)$$

Similarly, for the second chelation

$$\log K_{f2}* = pK_a + \log K_{h2} - \log(HCh) - p(H)_1$$
$$= 10.7 + 3.9 + 2.16 - 8.0 = 8.76 \quad (34)$$

The constants K_{h2} and $K_{f2}*$ should be independent of the solvent system. The values for $_{\phi\Sigma}K_{h1}$, $_{\phi\Sigma}K_{f1}*$, and $_{\phi\Sigma}K_a*$ will vary with the choice of solvent Q, largely due to changes in K_ϕ for Σ systems. However, the values of $_{\Sigma}K_{h1}$ and $_{\Sigma}K_{f1}*$ should be essentially independent of the Σ system as the ϕ contribution of solvent Q is discounted. The fully solvent independent constants K_{h1} and $K_{f1}*$ are undoubtedly several orders of magnitude larger than $_{\Sigma}K_{h1}$ and $_{\Sigma}K_{f1}*$.

It should be possible to correct chelate formation data for aqueous solutions in the literature to derive the solution independent constants for Σ systems. In general

$${}_{\Sigma}K_f* = K_f(1 + {}_{\Sigma}K_h) \quad (35)$$

Further, constants that were measured in mixed solvents can be corrected by taking C_w into account as well as $_{\Sigma}K_h$. Table I summarizes the constants deduced for the H_2O-ethanol system.

Conclusions

A simple view of ion activity, based on equilibria between free protons and hydronium(-like) complexes, free metal ions and their solvates, and anions and their solvates leads to a ready correlation of stability measurements in the H_2O-ethanol and related Σ systems. Deductions from these results include the following:

The hydronium ion is confirmed to be a tetrahydrate.

Two molecules of ROH can enter the hydronium complex to form the stable species $R_2H_7{}^+O_4$.

The hydroxyl ion tends to form a trihydrate in H_2O and, along with the organic acid anions, bisolvates in ethanol.

Two molecules of ROH can bond to divalent metal cations with strengths comparable to that for H_2O to form $M^{2+}\Sigma_2(H_2O)_4$.

For very low values of C_w, additional ROH can coordinate with the divalent metal ion to form $M^{2+}\Sigma_2\phi_x$, but the ϕ bonding is many orders of magnitude weaker.

In general, a net four molecules of solvation, corresponding to the ϕ group, are dropped in the first chelation and two, corresponding to the Σ group, are dropped for the second chelation.

The electron affinity of the cation is greatly decreased as a result of the first chelation. This greatly reduces the strength of hydration and essentially eliminates the possibility of M⁺Ch bonding with ROH.

Values found for particle constants in Σ systems are essentially independent of solvent composition in these systems. The constants involving the monochelate, K_{h2} and $K_{f2}*$, should be nearly independent of solvent composition in non Σ systems as well.

Appendix 1. Broadly Used Symbols

*	Denotes a *particle* species or its related constant. The particle is an immediate product of dissociation. The asterisk may replace the charge sign on the cation
C_w	the volume fraction of H_2O
C_e	the volume fraction of ethanol
Ch⁻	the chelating agent anion
H⁺	the combination of all hydrogen ion species

(H^+)	the total concentration of H^+ species
H*	The "free" proton or the hydrogen ion species read by the electrode. Changes in concentration of this species are measured not absolute values
$(H*)$	the concentration of H*
$H_9^+O_4$	the hydronium ion $H^+(H_2O)_4$
HCh	the chelating agent, ethyl acetoacetate
K	the constants are defined in connection with relations (8) through (23).
M^{2+}	the fully hydrated, $M^{2+}(H_2O)_6$, species
$M^{2\bullet}$	the fully desolvated M^{2+} ion
$M^{2\bullet}\Sigma_{T-n}$	the $M^{2\bullet}\Sigma_{\sim 2}$ ion
M^+Ch	the fully hydrated $M^+Ch(H_2O)_{T-n}$ ion
$M*Ch$	the M^+Ch species less $n'\,H_2O$
MCh_2	the metal dichelate
n	the number of solvate molecules dropped in the first chelation
n'	the number of H_2O molecules dropped in the second chelation
$p(H)$	the negative log of (H^+)
P*	the general symbol for a particle
Q	the nonaqueous component of the solvent system
T	the maximum coordination number for the divalent cation
Σ	the term represents H_2O and/or alcohol that is strongly coordinated to the cation
ϕ	represents nonaqueous solvent molecules that bond weakly to $M^{2\bullet}$
$()_0$	concentration at $C_w = 0$
$()_1$	concentration at $C_w = 1$
$_\Sigma()$	a constant reduced by the effects of Σ bonding
$_{\phi\Sigma}()$	a constant that is reduced by the effects of ϕ as well as Σ bonding

Supplementary Material Available: Calculations necessary to the derivation of the p(H) vs. log C_w data plotted in Figures 3–5 are given for the first chelation of Ni^{2+} and the subsequent chelation of Ni^+Ch in the microfilm edition (3 pages). Ordering information is available on any current masthead page.

References and Notes

(1) J. Bjerrum, "Metal Ammine Formation in Aqueous Solutions", P. Haase and Sons, Copenhagen, 1941.
(2) M. Calvin and E. Martell, "Chemistry of the Metal Chelate Compounds", Prentice-Hall, New York, N.Y., 1952.
(3) J. J. Christensen and R. M. Izatt, "Handbook of Metal Ligand Heats and Related Thermodynamic Quantities", Marcel Dekker, New York, N.Y., 1970.
(4) W. L. Marshall, *J. Phys. Chem.*, **74**, 346 (1970).
(5) E. A. Woolley, D. G. Hurkot, and L. G. Hepler, *J. Phys. Chem.*, **74**, 3908 (1970).
(6) H. S. Harned and B. B. Owen, "Physical Chemistry of Electrolytic Solutions", 3d, ed, Reinhold, New York, N.Y., 1958.
(7) R. A. Robinson and R. H. Stokes, "Electrolyte Solutions", 2d ed, Academic Press, New York, N.Y., 1959.
(8) E. Wicke, M. Eigen, and Th. Ackermann, *Z. Phys. Chem. (Frankfurt am Main)*, **1**, 340 (1954).
(9) C. F. Wells, *Trans. Faraday Soc.*, **61**, 2194 (1965); **62**, 2815 (1966); **63**, 147 (1967).
(10) C. F. Wells, *J. Phys. Chem.*, **77**, 1994, 1997 (1973).
(11) L. M. Mukherjee, *J. Am. Chem. Soc.*, **79**, 4040 (1957).

Micellar Formation under Pressure

Silvio Rodriguez and Henry Offen*

Department of Chemistry, University of California, Santa Barbara, California 93106 (Received March 26, 1976; Revised Manuscript Received October 12, 1976)

Micellar formation of sodium dodecyl sulfate has been measured using naphthalene as a probe up to 5500 bars. A value of $\Delta V = 15$ cm^3/mol is obtained from differential absorbance measurements. The critical micelle concentration (cmc) increases with pressure and, contrary to electrical conductance measurements, does not reverse its behavior above $\sim$1500 bars.

I. Introduction

There is a sudden change in the solution properties of amphiphilic molecules,[1] called the critical micelle concentration (cmc), at which the surface-active molecules aggregate into clusters of 40 to 100 molecules.[2] The thermodynamics of micellar formation is best described in terms of the law of mass action. Assuming monodispersed micelles and a reversible equilibrium, we have

$$nS^- + (n - z)X^+ \rightleftharpoons M^{z-} \qquad (1)$$

where S^-, X^+, and M^{z-} represent monomer, counterion, and anionic micelle, respectively. In eq 1, the aggregation number and net charge of the micelle are indicated by n and z. If we assume activity coefficients of unity,[3-5] the standard free energy change of micellization per mole of monomer is

$$\Delta G_m^\circ = 2.303RT \left\{ \log [S^-] + \frac{n - z}{n} \log [X^+] \right.$$
$$\left. - \frac{1}{n} \log [M^{z-}] \right\} \qquad (2)$$

In the absence of added electrolyte, and at surfactant concentrations above cmc, we can assume that $[S^-] = [X^+]$ = cmc and the term $(1/n) \log [M^{z-}]$ is negligible. For example, in the present case this term is less than 2% for $[M^{z-}] > 10^{-5}$ m. With this approximation, eq 2 reduces to

$$\Delta G_m^\circ = 2.303RT \left\{ \left(1 + \frac{n - z}{n} \right) \log \text{cmc} \right\} \qquad (3)$$

It is customary to define the fraction of charge on the micelle or the degree of dissociation of counterions α as equal to z/n.

In this work we are interested in the effect of high pressure on micelle formation. Since

$$\left(\frac{\partial}{\partial P}\Delta G^{\circ}\right)_T = \Delta V^{\circ} \qquad (4)$$

we find for the volume change per mole of monomer, expressed in terms of α

$$\Delta V_m{}^{\circ} = 2.303RT\left\{\frac{\partial}{\partial P}(2-\alpha)\log \text{cmc}\right\}_T \qquad (5)$$

Partial molar (or molal) volumes of surfactants in aqueous solutions, measured at 1 atm by a variety of techniques, range in magnitude from 1.2 cm^3/mol for nonionic dimethylnonylamine oxide[6] to 16 cm^3/mol for the ionic surfactant sodium tetradecyl sulfate.[7a] The volume change upon micellization is positive and generally increases with the length of the alkyl chain of the amphiphilic molecule.[8]

As a consequence of the greater volume of amphiphiles in the micellar state compared to the unassociated state, compression of these solutions through an externally applied pressure inhibits micelle formation, i.e., higher concentrations of monomers are required at high pressures to achieve micellization. With two exceptions[9,10] the pressure studies of surfactants have used conductivity measurements to follow the cmc as a function of pressure.[11-17] From the first experiments of Hamann[11,18] the measured pressure response of cmc has been most unusual. The initial slope d log cmc/dP is positive and of the correct order of magnitude, but above 1-2 kbars, the slope reverses sign. This inversion in the pressure response has been observed in all amphiphiles measured by conductivity and been the object of considerable speculation, invoking such factors as solidification of the micellar interior,[11,19] the greater compressibility of micelles vs. monomers,[12] the pressure-induced increase in dielectric constant of water,[12] or other aspects related to the structure of water.[16,17]

Since the electrical conductance method has led to the observed cmc(P) behavior, it appeared important to monitor the pressure response of ionic micelles by another technique. The present work on micellar formation under pressure employs differential absorption spectroscopy applied to aqueous solutions of sodium dodecyl sulfate. Significantly, the measurements of cmc(P) are at variance from those obtained by Hamann using conductivity as the indicator of micellar behavior.

II. Experimental Section

This work uses two high pressure cells, modeled after a design reported by Fichten,[20] to fit into the sample and reference compartment of the Cary 14 spectrophotometer. Both cells could be pressurized simultaneously up to 5500 atm with hexane as a pressure-transmitting fluid. The experimental technique permits differential spectral measurements in the ultraviolet-visible region of aqueous solutions at different pressures.

The surfactant chosen for this work, anionic sodium dodecyl sulfate (SDS), has been well characterized at 1 atm. The compound (Sigma Chemical Co.) was recrystallized several times from ethanol-water solutions. The optical probe for micellar formation is zone-refined naphthalene (James Hinton). A stock solution of 10^{-2} m surfactant was used to prepare samples. Excess naphthalene was added to the detergent solution and its solubilization monitored by the 275-nm absorption peak.
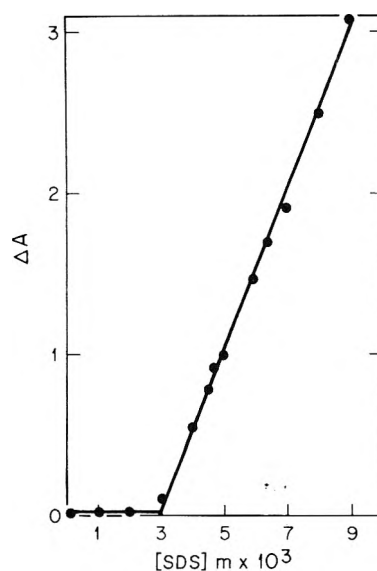

Figure 1. Solubilization of naphthalene in sodium dodecyl sulfate at 1 atm. ΔA represents the differential absorbance of the L_a band (λ_{max} ≈275 nm) of the aromatic molecule.

Typically, stabilization was achieved after 2 weeks. The solutions of SDS plus naphthalene, and naphthalene alone in water, are then centrifuged to remove traces of suspended material and placed in the sample capsules of the high pressure optical cell. The cell in the reference beam contains the saturated solution of naphthalene in water.

Differential absorption spectra are measured at a temperature of 25 °C for a series of pressures. The absorbance measurements at high pressure are corrected for solvent compression.[21]

III. Results

Naphthalene was the optical probe in the present study. A Beer's law plot indicates that the solubility of naphthalene in water is 2.7×10^{-4} m, in good agreement with previous determinations.[22-24] The solubility s decreases linearly with increasing pressure to a value of 1.3×10^{-4} m at 4100 bars; the slope d log s/dP is found to be smaller than reported previously.[24] The direction of the pressure response is advantageous for the present study, its magnitude is unimportant because the pressure dependence of the solubility in water will cancel in the differential experiments executed here.

Many cmc values of surfactants have been measured via optical detection of organic compounds incorporated in the micellar aggregates above cmc.[2,25,26] In the present work naphthalene is solubilized by SDS, as shown in Figure 1. The change in slope extrapolates to cmc = 3×10^{-3} m. The accepted value for cmc is 8×10^{-3} M[26] in the absence of additives, while impurities are known to decrease this value, e.g., cmc = 6×10^{-3} M in the presence of benzene.[27] The depression of cmc is expected to be proportional to the size of the hydrophobic group of the solubilizate,[5] therefore the observed value for cmc in the presence of naphthalene is not unreasonable.

The differential absorption spectrum of naphthalene in micellar solutions is identical with that observed in dodecane, which suggests that the aromatic molecule is located in the interior (hydrocarbon-like) environment of the micelle. The differential absorbance (ΔA) as a function of pressure was measured for a series of SDS solutions with different initial concentrations. Figure 2 shows that ΔA decreases with pressure, as expected from a pressure-induced disruption of micelles, thereby releasing naphthalene to the saturated aqueous environment. The compression
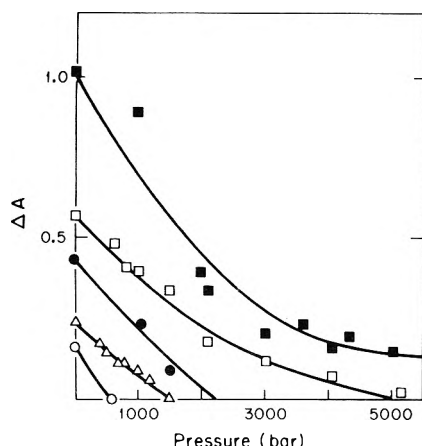
Figure 2. Differential absorbance of the L_a band of naphthalene in aqueous surfactant solution as a function of pressure. Concentrations of sodium dodecyl sulfate are: 4×10^{-3} m (O); 4.5×10^{-3} m ($\triangle$); 6×10^{-3} m (●); 7×10^{-3} m (□), and 9×10^{-3} m (▢).
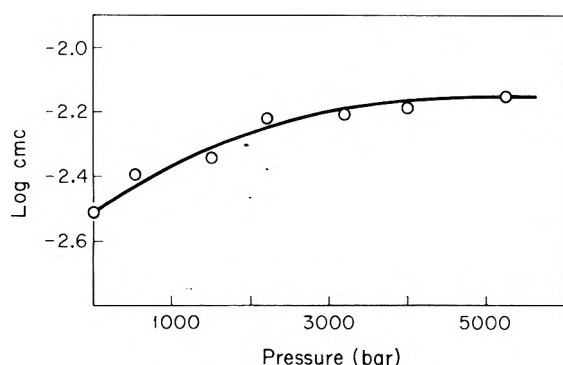

Figure 3. Pressure dependence of the critical micellar concentration of sodium dodecyl sulfate.

required to attain $\Delta A = 0$ is identified with the surfactant cmc at that particular pressure. The error in estimating the intercept with the pressure axis in Figure 2 is small below 2 kbars and $\sim 10\%$ for the 2–5-kbar range. The solution with SDS at 9×10^{-3} m (Figure 2) extrapolates to a pressure of 13 ± 3 kbars, which is outside of our experimental pressure range (and probably represents the frozen state at $\Delta A = 0$). The results are consistent with the postulate that the more concentrated SDS solutions (above cmc) require a higher pressure to reverse micellization. The data suggest that this trend does not reverse below ~ 13 kbars.

The information obtained from ΔA vs. P plots is displayed in Figure 3 as the desired result of cmc(P). The experimental points can be fitted to the quadratic log cmc $= A + BP + CP^2$, with $A = -2.511$, $B = 1.43 \times 10^{-4}$ bar^{-1}, and $C = -1.49 \times 10^{-8}$ bar^{-2}. A volume change can be calculated from eq 5 if we assume α to be independent of pressure. Hence

$$\Delta V = 2.3RT(2 - \alpha)(\text{d log cmc}/\text{d}P)_{P = 1\,\text{bar}} \qquad (6)$$

Since the reported values of α for SDS range from 0.13 to 0.21,[2] the ΔV values range from 15.0 ± 2.0 to 14.4 ± 1.9 cm^3/mol, respectively. The partial molar volumes $\Delta V_m{}^\circ$ reported from density measurements at 1 atm are 12.1,[6] 11,[7a] 10,[7b] and 12 cm^3/mol.[8] Hamann[11] obtained $\Delta V = 11$ cm^3/mol ($\alpha = 0.20$) and Kaneshina et al.[16] report $\Delta V = 10.0$ cm^3/mol ($\alpha = 0.270$) from the initial slope (eq 6) of the cmc(P) plot.

The higher ΔV value obtained in the present work is primarily attributed to the presence of the naphthalene additive which decreases the cmc and increases the ag-

gregation number n at 1 atm.[5] This would raise the volume change, although the additional increment observed in the presence of naphthalene has not been independently verified.

IV. Discussion

The salient feature of this work is the absence of a maximum in the cmc(P) plot (Figure 3), which is always observed by monitoring the conductance.[11–17] The results from the present work lend themselves to a more satisfactory explanation than those derived from conductivity under pressure and parallel those of many other pressure-dependent properties. It is unclear what factors are responsible for the measured maximum, but the optical probe is independent of the electrical and hydrodynamic characteristics of micellar solutions, i.e., the possible pressure effects on micellar shape, aggregation number, counterion binding, and transport numbers. The presence of the naphthalene probe in the micellar interior is a disadvantage of this study, but the depression of the cmc should not distract from the general characteristics of micellar solutions under pressure.

The ΔV of micellar formation under pressure has been calculated from eq 6 which ignores the pressure dependence of α. The use of $\alpha = 0.2$ at 1 atm in the presence of naphthalene is reasonable (in eq 6) because another study has found that the degree of counterion binding is not significantly altered by the addition of organic solutes.[28] What happens to α under pressure is unclear, but Kaneshina et al.[16] deduce from their conductance measurements an increase in α to yield $\text{d}(2 - \alpha)/\text{d}P = -8.9 \times 10^{-5}$ bar^{-1}. Such a term would make a very significant contribution to ΔV values obtained from eq 6. Further experiments may determine whether the approximations leading to eq 6 are indeed justified to calculate ΔV values which can be compared with 1 atm density measurements.

In conclusion, the meaning of ΔV for micellar formation under pressure calculated from eq 6 has not been ascertained, but the positive sign and the absence of a sign reversal at high pressures are expected from disruption of hydrophobic interactions in compressed aqueous solutions. As Hamann[18] stated in his recent review, "the inversion of behavior is most unusual". Since the present optical study does not confirm the presence of the inversion detected by electrical measurements, additional studies are required to identify the factors responsible for the discrepancy in these complex aqueous systems.

References and Notes

(1) C. Tanford, "The Hydrophobic Effect: Formation of Micelles and Biological Membranes", Wiley, New York, N.Y., 1973.
(2) J. H. Fendler and E. J. Fendler, "Catalysis in Micellar and Macromolecular Systems", Academic Press, New York, N.Y., 1975.
(3) J. N. Phillips, Trans. Faraday Soc., 51, 561 (1955).
(4) P. Mukerjee, Adv. Colloid. Interface Sci., 1, 241 (1967).
(5) G. C. Kresheck, "Water: A Comprehensive Treatise", F. Franks, Ed., Vol. 4, Plenum Press, New York, N.Y., 1975, Chapter 2.
(6) L. Benjamin, J. Phys. Chem., 70, 3790 (1966).
(7) (a) K. Shinoda and T. Soda J. Phys. Chem., 67, 2072 (1963); (b) L. M. Kushner, B. C. Duncan, and J. I. Hoffman, J. Res. Natl. Bur. Stand., 49, 85 (1952).
(8) J. M. Corkill, J. F. Goodman, and J. R. Tate, "Hydrogen Bonded Solvent Systems", A. K. Covington and P. Jones, Ed., Taylor and Francis, London, 1968, p 181; J. M. Corkill, J. F. Goodman, and T. Walker, Trans. Faraday Soc., 63, 768 (1967).
(9) T. Sugano, M. Tsuchiya, and K. Suzuki, "The 21st Symposium of Colloid and Surface Chemistry", Japan Chemical Society, Kyoto, 1968, p 147.
(10) S. D. Hamann, Rev. Phys. Chem. Jpn., 35, 109 (1965).
(11) S. D. Hamann, J. Phys. Chem., 66, 1359 (1962).
(12) R. F. Tuddenham and A. E. Alexander, J. Phys. Chem., 66, 1839 (1962).
(13) J. Osugi, M. Sato, and N. Ifuku, Rev. Phys. Chem. Jpn., 35, 32 (1965).
(14) J. Osugi, M. Sato, and N. Ifuku, Rev. Phys. Chem. Jpn., 38, 58 (1968).

(15) M. Tanaka, S. Kaneshina, K. Shin-No, T. Okajima, and T. Tomida, J. Colloid Interface Sci., 46, 132 (1974).

(16) S. Kaneshina, M. Tanaka, T. Tomida, and R. Matuura, J. Colloid Interface Sci., 48, 450 (1974).

(17) M. Tanaka, S. Kaneshina, S. Kuramoto, and R. Matuura, Bull. Chem. Soc. Jpn., 48, 432 (1975).

(18) S. D. Hamann, "Modern Aspects of Electrochemistry No. 9", B. E. Conway and J. O'M. Bockris, Ed., Plenum Press, New York, N.Y., 1974, p 47.

(19) K. Suzuki and Y. Taniguchi, "The Effects of Pressure on Organisms", Symposia of the Society for Experimental Biology XXVI, Academic Press, New York, N.Y., 1972, p 103.

(20) D. B. Fitchen, Rev. Sci. Instrum., 34, 673 (1963).

(21) P. W. Bridgman, Proc. Am. Acad. Arts Sci., 66, 185 (1931).

(22) J. E. Gordon and R. L. Thorne, J. Phys. Chem., 71, 4390 (1967).

(23) R. L. Bohon and W. F. Claussen, J. Am. Chem. Soc., 73, 1571 (1951).

(24) K. Suzuki, Y. Taniguchi, T. Ishigami, and M. Tsuchiya, "Proceedings of the 4th International Conference on High Pressure", Physical Chemists Society of Japan, Kyoto, 1974, p 615.

(25) K. Shinoda, Ed., "Solvent Properties of Surfactant Solutions", Marcel Dekker, New York, N.Y., 1967.

(26) P. Mukerjee and K. J. Mysels, Natl. Stand. Ref. Data Ser., Natl. Bur. Stand., No. 36 (1971).

(27) S. J. Rehfeld, J. Phys. Chem., 74, 117 (1970).

(28) W. K. Mathews, J. W. Larsen, and M. J. Pikal, Tetrahedron Lett., 6. 513 (1972).

Intramolecular Donor–Acceptor Systems. 2. Substituent Effects on the Fluorescence Probes: 6-(N-Arylamino)-2-naphthalenesulfonamides

Hanna Dodiuk[1a] and Edward M. Kosower*[1a,b]

Department of Chemistry, Tel-Aviv University, Ramat-Aviv, Tel-Aviv, Israel and the Department of Chemistry, State University of New York, Stony Brook, New York, 11794 (Received July 14, 1976)

The fluorescent probes, 6-(N-arylamino)-2-naphthalenesulfonamides (1a–c, 2a–c), all exhibit charge-transfer fluorescence behavior consistent with the general scheme previously proposed. No special solvent effects are required to explain the data for the corresponding sulfonates.

Fluorescent molecules which are added to various systems for the purpose of revealing characteristics of the system to which they are added are called probes. In general, some fluorescence parameter of the probe molecule is altered within the system. Among the parameters which might be examined are emission maximum, fluorescence lifetime, and excitation spectrum. In order to interpret changes in the parameter used, a precise understanding of the origin of the fluorescence emission is necessary. In cases for which only the presence or absence of the probe is evaluated (localization within cells or within cell organelles, motion of labeled system, etc.), knowledge about the mechanism is still important so that quenching or promoting conditions will not cause the results to be misinterpreted.

Among the fluorescent probes which have been often used for biochemical and biological systems (see the review by Azzi[2]) are 6-(N-arylamino)-2-naphthalenesulfonates (ANS, e.g., 2a). The key to understanding the fluorescence of ANS lay in use of solvent polarity parameters (such as, $E_T(30)$ and Z values[3]) which revealed the existence of two rather different fluorescence emissions from a number of ANS derivatives.[4] An earlier and somewhat similar study by Turner and Brand[5] combined data from so many different solvents that the change in emission type was obscured. Many further investigations on ANS derivatives using solvent polarity effects, solvent viscosity effects, fluorescence lifetimes, and excited state spectra (using laser pulse excitation) have led to considerable clarification in the radiative and nonradiative processes which ensue after light absorption by ANS derivatives.[6] ANS derivatives may be viewed as intramolecular donor–acceptor systems in which, for all cases of interest in this article, the N-phenyl group is a donor and the naphthalenesulfonate moiety is an acceptor. The appearance of two emissions can be explained in terms of two excited states, $S_{1,np}$ (phenyl group perpendicular to the naphthalene ring) and $S_{1,ct}$ (phenyl group radical cation perpendicular to a naphthalene radical anion) which respond differently to

intramolecular changes (substituent polarity and size, heavy atom effects)[7] and extramolecular changes (solvent polarity and viscosity). A slightly condensed version of the scheme for ANS derivatives is shown in Figure 1.

Greene[8] has recently reported the interesting result that conversion of the sulfonate group of the usual ANS derivative to a sulfonamide (i.e., 2a → 2b or 2c) led to compounds for which the emission maxima were "much more sensitive to solvent polarity" than those of the sulfonate. It was suggested that the sulfonate was anomalous in response due to some unspecified combination of general and specific solvent polarity effects. In order to find out if the sulfonamide emissions fit the scheme shown in Figure 1, we have reexamined the compounds of Greene together with a number of new ANS derivatives. Our results show quite clearly that the sulfonamide fluorescences are charge transfer (emissions from an $S_{1,ct}$ state) and are completely consistent with our general scheme for ANS excited state processes.
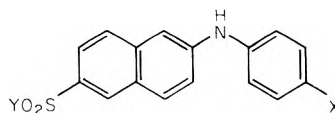
1a: Y = N(CH₃)₂, X = H
  b: Y = N(CH₃)₂, X = CH₃
  c: Y = N(CH₃)₂, X = OCH₃
2a: Y = O⁻Na⁺, X = CH₃
  b: Y = NH₂, X = CH₃
  c: Y = NHCH₂CH₂⁺NH₃, Cl⁻, X = CH₃
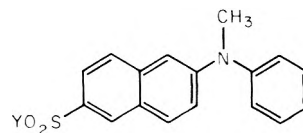
3a: Y = N(CH₃)₂
  b: Y = Cl

Experimental Section

Syntheses of ANS derivatives (1a–c, 3a,b) were carried

TABLE I: Emission Data for 1a,b and 2b,c in Dioxane–Water Mixtures[a,b]

Solvent % dioxane–water[c]	$E_T(30)$ value[c]	$\lambda_{max}(\Phi_F)$[f]			
		1a	1b	2b	2c
100	36.1	420(0.57)	438(0.50)	433(0.60)	438(0.40)
99.60	37.1	423(0.62)	440(0.50)	436(0.58)	441(0.35)
99.0	38.6	426(0.66)	443(0.45)	440(0.60)	445(0.38)
98.1	41.2	429(0.66)	450(0.44)	445(0.64)	450(0.34)
96.1	42.9	434(0.57)	458(0.36)	451(0.51)	460(0.27)
95.2	43.5	437(0.56)	465(0.33)	456(0.43)	466(0.24)
94.2	44.4	440(0.55)	470(0.27)	461(0.42)	471(0.20)
92.3	45.7	444(0.49)	474(0.18)	466(0.33)	476(0.14)
90.3	46.6	450(0.39)	479(0.10)	471(0.15)	480(0.10)
85.5	47.9	455(0.34)	485(0.09)	476(0.11)	485(0.05)
80.6	48.9	460(0.27)[f]	490(0.08)	480(0.09)	490(0.03)
75.8	49.8	465(0.19)	g	485(0.05)	494(0.02)
71.0	50.7	469(0.14)		488(0.04)	g
66.1	51.5	473(0.10)		491(0.03)	
61.3	52.1	476(0.07)		494(0.02)	
56.5	52.8	480(0.07)		g	
51.0	53.4	g			

[a] Temperature 25 ± 2 °C. Temperature effects on the position of the fluorescence maximum or the intensity of the emission over this temperature range are small. [b] For details of the measurements and instrumentation refer to the Experimental Section. [c] Percentage of dioxane by volume mixed with water. [d] Values were either taken from Table 2, p 28 in Ch. Reichardt and K. Dimroth, *Fortschr. Chem. Forsch.*, 11, 1 (1968) or derived from values in that table by linear interpolation. [e] In nanometers ± 10% or less, according to reproducibility. Quinine sulfate in 0.1 N H_2SO_4, Φ_F = 0.55. [g] Solutions of this polarity or greater exhibited the fluorescence of a protonated form (Dodiuk and Kosower, ref 19).
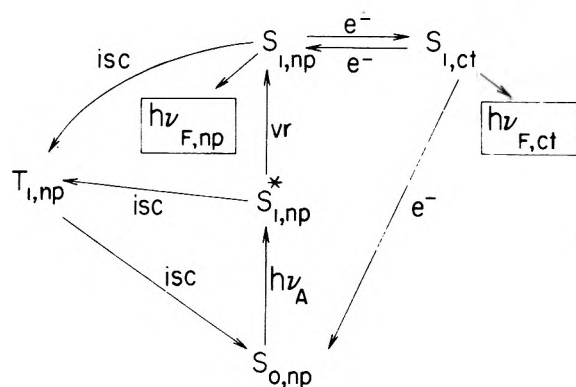

Figure 1. A scheme illustrating some of the excited states which participate in the radiative and nonradiative processes which follow absorption of light by a 6-(N-arylamino)-2-naphthalenesulfonate. The symbols are as follows: $S_{0,np}$, ground state with nonplanar (np) relationship between the planes of the N-aryl group and the naphthalene ring; $S_{1,np}^*$, vibrationally excited lowest excited singlet state; $S_{1,np}$, relaxed lowest excited singlet state; $S_{1,ct}$, charge-transfer state, in which an electron has been transferred from the aryl group to the naphthalene ring (the nitrogen p orbitals are conjugated with the phenyl radical cation); $T_{1,np}$, triplet state; isc, intersystem crossing; vr, vibrational relaxation; e⁻, electron-transfer process; $h\nu_F$, fluorescence emission; $h\nu_A$, light absorption. (For a more complete version of the scheme, see Kosower et al.[6,19])

out according to Greene[8] by a modification of the method of Cory et al.,[10] using 40% aqueous dimethylamine as the amine. Chromatography on silica gel and/or crystallization were used to obtain pure products (single spot on TLC with CH_3OH:benzene 40:60) for which NMR and UV were used to establish structures.

1a: mp 115–116 °C; NMR, $CDCl_3$ arom H, δ 7–8.3, m; NH δ 6.1–6.2, 1 H, broad s, removed with D_2O; $N(CH_3)_2$, δ 2.75, s, 6 H; UV, 278 (29 000), 329 (26 300), 359 (7300)[18] maxima in dioxane.

1b: mp 136–137 °C, crystallized from Me_2CO–H_2O; NMR, 1a + CH_3, δ 2.34, 3 H, s; UV, 278 (22 600), 329 (20 700), 360 (7300)[18] maxima in dioxane.

1c: mp 125–127 °C; NMR, 1a + CH_3O, δ 3.8, 3 H, s; UV 269 (26 700), 324 (22 300), 362 (6700)[18] in dioxane.

3a: mp 117–118 °C, crystallized from hexane–EtOAc;

Figure 2. A plot of emission energies, E_F, and emission quantum yields for **2b** and **2c** vs. the solvent polarity parameter, $E_T(30)$, using fluorescence maxima obtained for a series of dioxane–water solutions. All units are in kilocalories per mole.

H NMR, 1a + N–CH_3, δ 3.45, 3 H, s; UV identical with that of the amide (Cory et al.[10]).

3b: sulfonyl chloride was chromatographed on silical gel in CCl_4. UV as reported by Cory et al.[10] Structure of the water-sensitive compound confirmed by conversion to 3a.

Absorption spectra were recorded on a Cary 17 spectrophotometer. Emission spectra were recorded on a
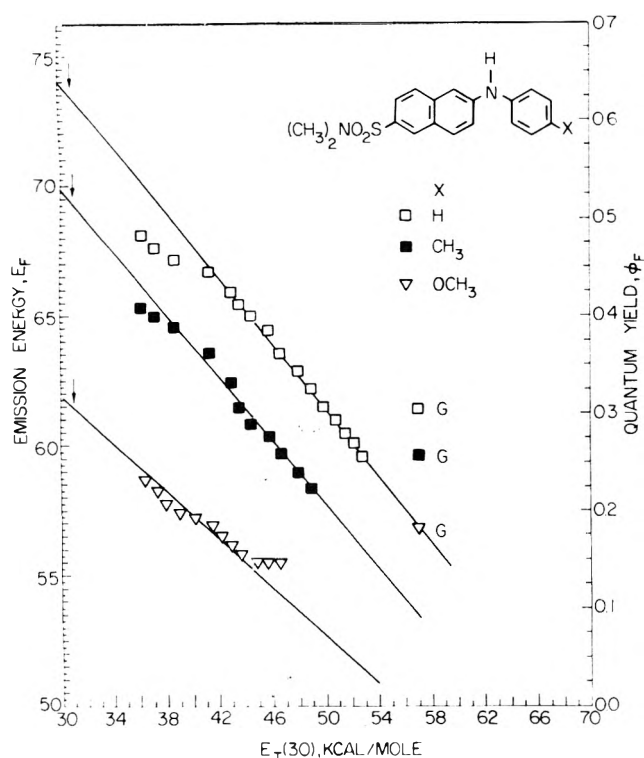
Figure 3. A plot of emission energies, E_F, for **1a**, **1b**, and **1c** vs. the solvent polarity parameter, $E_T(30)$, using fluorescence maxima obtained for a series of dioxane–water solutions. The emission energy for each substance in glycerol solution (point marked G) is also shown. All units are in kilocalories per mole. Arrows indicate values of extrapolated charge-transfer emission energy.

Perkin-Elmer-Hitachi Model MPF-4 spectrofluorimeter with corrected spectra attachment and a digital integrator was used, with quinine sulfate in 0.1 N H_2SO_4 as reference ($\phi_F = 0.55$). Preparations of solutions and plotting of data were carried out as previously described (Kosower et al.).[6] Solutions of **1a–c** in glycerol contained 0.01% ethanol.

Results

Emission data, both maximum and quantum yield, were obtained in a series of dioxane–water solutions for the amides obtained from Greene[8] (**2b,c**). These data are listed in Table I and are plotted against the solvent polarity parameter $E_T(30)$ in Figure 2. It is worth reiterating that an intramolecular transition which involves considerable loss of charge separation is best compared to an *intra*molecular reference. Z values represent an *inter*molecular charge-transfer transition. In most solvents there is a proportionality between $E_T(30)$ and Z, the latter being appreciably more sensitive to solvent than the former. The use of solvent polarity parameters is discussed in depth by Kosower.[3]

The dimethylamide derivatives of 6-N-arylamino-2-naphthalenesulfonates were chosen as likely to be soluble in a suitable range of nonpolar solvents. Since they are easy to prepare, purify, and characterize, such derivatives might well be of interest in many cases. Data for three dimethylsulfonamides (**1a–c**) are also listed in Tables I and II, and are plotted against $E_T(30)$ in Figure 3.

The use of N-methyl ANS derivatives[9,10] as fluorescent probes in the form of amide derivatives[11,12] made a brief comparison of interest, and data for the dimethylamide **3a** are also given in Table III. The closely related chloride (**3b**) (of interest because of the strong electron-withdrawing power of the SO_2Cl group) could only be examined in CCl_4 (emission maximum 476 nm, $\phi_F = 4 \times 10^{-4}$) and was extremely sensitive to traces of water in most other solvents,

TABLE II: Emission Data for **1c** in Dioxane–Water Mixtures[a]

Solvent % dioxane–water	$E_T(30)$ value	$\lambda_{max}(\phi_F)$
99.9	36.3	487(0.10)
99.6	37.2	491(0.08)
99.3	37.9	495(0.07)
98.9	39.0	498(0.06)
98.0	41.4	502(0.05)
97.1	42.1	506(0.03)
96.1	42.8	509(0.02)
95.2	43.5	512(0.02)
93.6	44.8	515(0.01)
92.5	45.6	515(0.01)
90.5	46.5	515(0.01)
85.0	47.9	b

[a] See footnotes to Table I.   [b] See footnote g of Table I.

TABLE III: Emission Data for **3a** in Dioxane–Water Mixtures[a]

Solvent % dioxane–water	$E_T(30)$ value	$\lambda_{max}(\phi_F)$
99.9	36.3	445(0.47)
99.6	37.0	450(0.45)
99.1	38.5	455(0.44)
98.1	41.4	460(0.44)
97.2	42.0	465(0.39)
95.3	43.2	470(0.37)
92.5	45.6	475(0.33)
90.6	46.5	480(0.30)
85.9	47.8	485(0.28)
81.3	48.7	494(0.19)
71.9	50.5	505(0.09)
62.5	52.0	510(0.06)
53.1	53.2	515(0.04)
43.2	54.9	520(0.02)
39.1	55.8	b

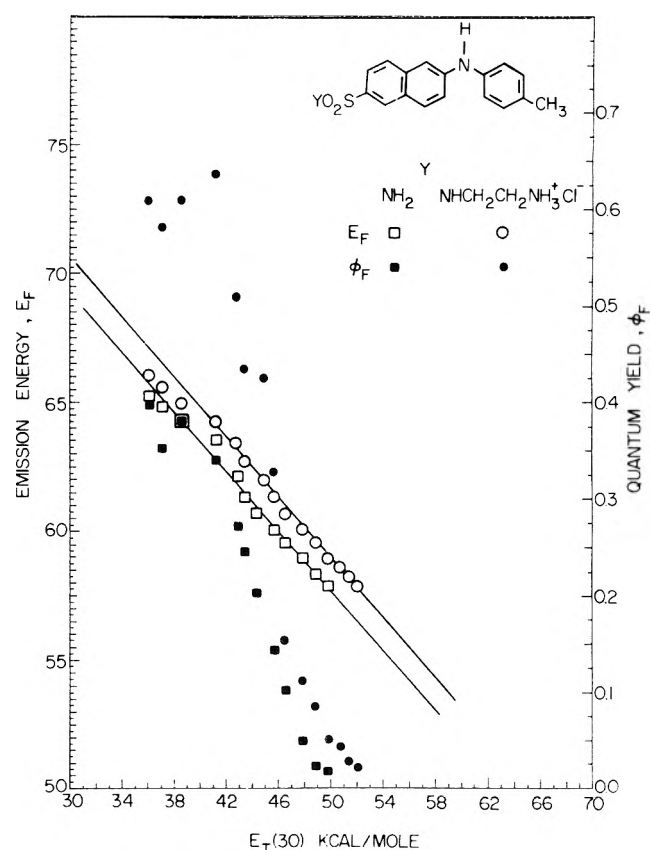[a] See footnotes to Table I.   [b] See footnote g of Table I.

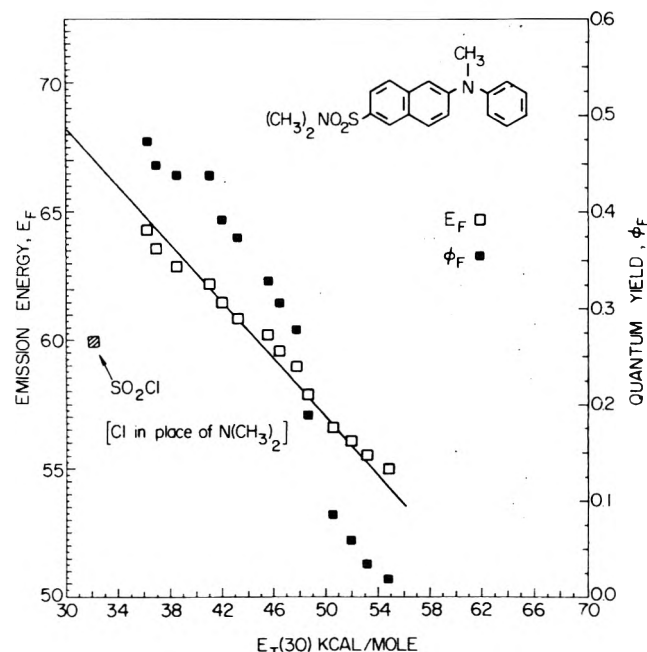
Figure 4. A plot of emission energies, E_F, and emission quantum yields for **3a** vs. the solvent polarity parameter, $E_T(30)$, using fluorescence maxima obtained for a series of dioxane–water solutions. The point for the sulfonyl chloride (**3b**, Y = Cl) in CCl_4 is also shown. All units are in kilocalories per mole.

yielding the sulfonate. Data for **3a** are plotted in Figure 4.

TABLE IV: Emission Data for 1a-c in Glycerol

	λ_{max}, nm	$\emptyset_F{}^a$
1a	465	0.074
1b	480	0.056
1c	502	0.015

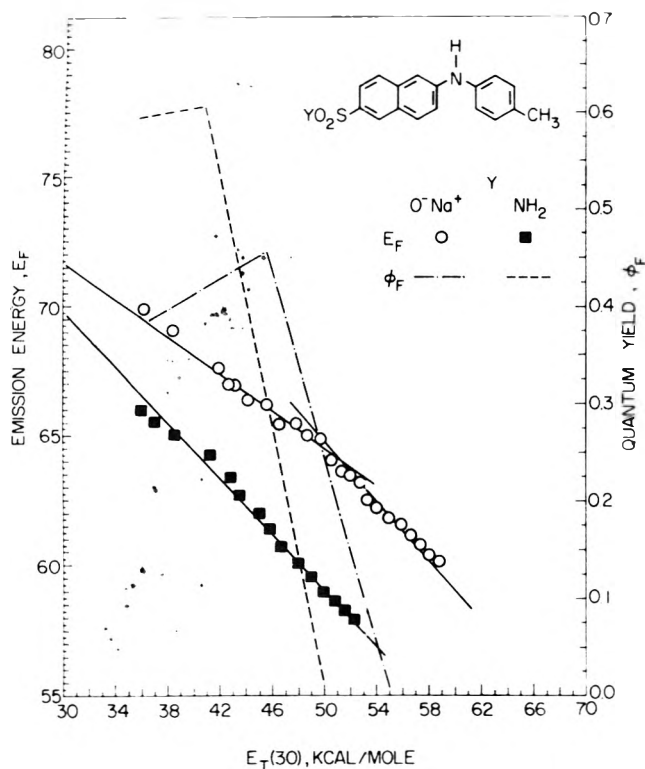^{a} Corrected for refractive index of glycerol.

Figure 5. A plot of emission energies, E_F, and emission quantum yields for 2a and the corresponding amide 2b vs. the solvent polarity parameter, $E_T(30)$. Data for 2a is taken from Kosower et al.[6] and that for 2b from Figure 2. All units are in kilocalories per mole.

The dioxane-water results for all amide derivatives (1a-c,2b,c) may be summarized as follows. The emission energies uniformly yield almost parallel straight lines when plotted against $E_T(30)$, permitting extrapolation to hydrocarbon solvent ($E_T(30) = 31$) and allowing a reasonably accurate estimate of emission energies under nonsolvating conditions. The quantum yields of fluorescence for all derivatives fall off rapidly as solvent polarity is increased.

The points for the amides 1a,b and 2b,c in two or three of the least polar solvents fall somewhat below the correlation lines. The corresponding quantum yields show some deviation from a linear relation with solvent polarity, but do not rise as seen for 2a in the same solvent polarity range.

Emission data for the amides 1a-c in glycerol are listed in Table IV. The emissions are clearly different from those in dioxane-water solution.

Discussion

The effect on fluorescence emission which is produced by the change from a sulfonate to an amide group is best illustrated by a comparison plot for data on 2a and 2b (Figure 5). As previously demonstrated, the low slope region of the plot for the sulfonate represents emission from the $S_{1,np}$ state. The high slope portion of the plot correlates emissions from the $S_{1,ct}$ state. In particular, only a charge-transfer emission could exhibit so great a sensitivity to solvent polarity, with the slope of the plot against $E_T(30)$ being between 0.6 and 0.7. The fluorescence
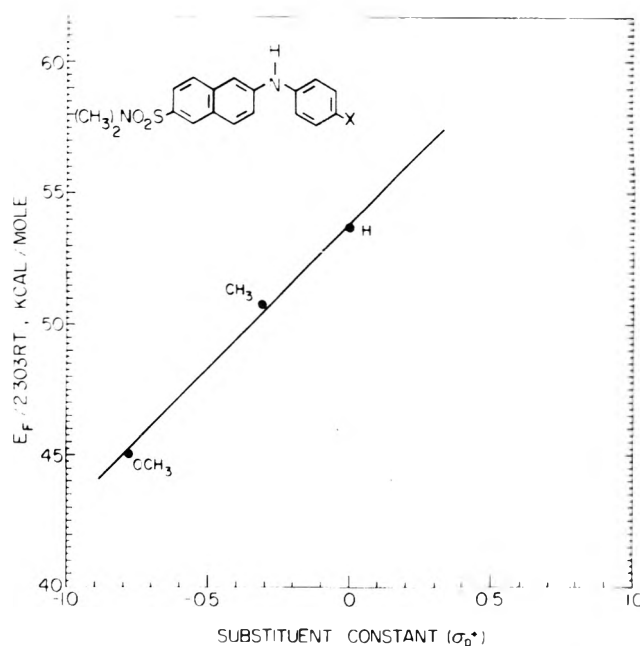

Figure 6. A plot of extrapolated emission energies (assigned as $S_{1,ct}$ emissions) divided by $2.3RT$ vs. the Hammett-Brown-Okamoto $\sigma_p{}^+$ parameter, using values for 1a-c

TABLE V: Extrapolated Values for $S_{1,ct}$ Emissions in Hydrocarbon Solvent^{a,b} for ANS Derivatives

	Y = N(CH$_3$)$_2$		Y = O$^-$	
X = (in 1)	$E_{F,ct}$, kcal/ mol	$\sigma_p{}^+$	$E_{F,ct}$, kcal/ mol	ΔE_F, kcal/ mol
H(1a)	73.3	0	78.0	4.7
CH$_3$(1b)	69.3	-0.31	75.6	6.3
OCH$_3$(1c)	61.5	-0.78	69.2	7.7

^{a} $F_T(30) = 31.0$. ^{b} See Figure 2 and Kosower et al.[6] for illustrations of the extrapolation lines.

quantum yield from the charge-transfer state ($S_{1,ct}$) is also very sensitive to solvent polarity, because the quenching reaction is an electron-transfer reaction.[6]

All of the amide derivatives (1a-c, 2b,c) exhibit emisions for which the energies and the quantum yields vary with solvent polarity in a way very much like that of the charge-transfer emission of the sulfonate. The slopes for the emission energy-solvent polarity correlations are between 0.6 and 0.7. We regard this similarity as strong evidence for the identification of the emitting states of the amides as $S_{1,ct}$.

The conclusions that the amide emitting states are charge transfer is confirmed through a correlation of the extrapolated emission energies with the Hammett-Brown-Okamoto substituent constant $\sigma_p{}^+$. The extrapolated emission energies are listed together with the substituent constants in Table II. The plot of the emission energies against substituent constants is shown in Figure 6. The slope, or ρ value, for the correlation is about -11, a value so high as to provide very clear evidence for the assignment of the emitting state as $S_{1,ct}$.

We may then ask why conversion of the sulfonate to sulfonamide has such a strong effect on the nature of the fluorescence emission observed. The answer is simply that the sulfonamide is a much stronger electron-withdrawing group than the sulfonate. The σ_p for the SO$_2$NH$_2$ group is 0.94 whereas for $\sigma_p{}^-$ for SO$_3{}^-$ group is 0.09 (we here assume that σ_p for SO$_3{}^- = \sigma_p$).[13] The extrapolated charge-transfer energies for the amides may be compared with the corresponding extrapolated values for $S_{1,ct}$

emissions for the sulfonates. The latter have been included in Table V and lead to an approximate ρ value for the naphthalene ring as an acceptor of 5.4, according to the relation, average $\Delta F_F/2.3RT = \rho(\Delta\sigma)$ in which $\Delta\sigma = \sigma_p (SO_2NH_2) - \sigma_p (SO_3^-)$. We would expect the ρ value for naphthalene charge-transfer processes to be much lower than that for benzene derivatives since the greater number of sites available for delocalizing charge diminishes the effect of the substituent. Thus, the change in the energy of the naphthalene–tropylium ion charge-transfer band for the substitution of a 2-methyl group is a little less than half of that for the substitution of a methyl group into benzene.[14]

In order to confirm that the scheme shown in Figure 1 applied in all of its details to the ANS amides, we also measured the emissions for 1a–c in glycerol. Our previous work had shown that the high viscosity of glycerol lowered the rate for conversion of $S_{1,np}$ to $S_{1,ct}$, extending the lifetime of the $S_{1,np}$ state in the highly polar environment of glycerol so much that only emission from the $S_{1,np}$ state can be observed. The points included in Figure 2 show clearly how different the emission in glycerol is from that in dioxane–water mixtures.[15]

Our approach to the analysis of fluorescence emissions of ANS compounds (and, by implication, many other probe molecules) is to identify specific excited states and apply stringent tests to confirm our assignments. For biochemical and biological applications, it seems likely that this precise understanding of probe behavior will be more helpful than nonspecific references to "general solvent polarity" or uninterpretable correlations with the quasi-macroscopic Lippert–Mataga equation.[16]

Knowledge of the fluorescence mechanisms along with the ρ value which allow us to evaluate substituent effects

should make it possible to design ANS derivatives with properties appropriate for many needs.

References and Notes

(1) (a) Tel-Aviv University; (b) State University of New York, Stony Brook, N.Y.
(2) A. Azzi, *Q. Rev. Biophys.*, **8**, 237–316 (1975).
(3) E. M. Kosower, "An Introduction to Physical Organic Chemistry", Wiley, New York, N.Y., 1968.
(4) E. M. Kosower and K. Tanizawa, *Chem. Phys. Lett.*, **16**, 419 (1972).
(5) D. C. Turner and L. Brand, *Biochemistry*, **7**, 3381 (1973).
(6) E. M. Kosower, H. Dodiuk, K. Tanizawa, M. Ottolenghi, and N. Orbach, *J. Am. Chem. Soc.*, **97**, 2167 (1975).
(7) E. M. Kosower and H. Dodiuk, *Chem. Phys. Lett.*, **26**, 545 (1974).
(8) F. C. Greene, *Biochemistry*, **14**, 747 (1975).
(9) H. Dodiuk and E. M. Kosower, *Chem. Phys. Lett.*, **34**, 253 (1975).
(10) R. P. Cory, R. R. Becker, R. Rosenbluth, and I. Isenberg, *J. Am. Chem. Soc.*, **90**, 1643 (1968).
(11) R. B. Freedman, D. J. Hancock, and G. Radda in "Probes of Structure and Function of Macromolecules and Membranes", Vol. 1, B. Chance, C-p. Lee, and J. K. Blasie, Ed., Academic Press, New York, N.Y., 1971.
(12) G. P. Sachdev, A. D. Brownstein, and J. S. Fruton, *J. Biol. Chem.*, **250**, 501 (1975).
(13) J. Shorter, "Correlation Analysis in Organic Chemistry: An Introduction to Linear Free Energy Relationships", Clarendon Press, Oxford, 1973, p 14.
(14) R. Foster, "Organic Charge-Transfer Complexes", Academic Press, New York, N.Y., 1969, p 294.
(15) E. M. Kosower and H. Dodiuk, *J. Am. Chem. Soc.*, **96**, 6195 (1974).
(16) E. Lippert, *Z. Naturforsch. A*, **10**, 541 (1955).
(17) N. Mataga, Y. Kaifu, and M. Koizumi, *Bull. Chem. Soc. Jpn.*, **28**, 690 (1955).
(18) Maximum was resolved from a shoulder.
(19) H. Dodiuk and E. M. Kosower, *J. Am. Chem. Soc.*, in press.

Infrared Spectra of N-Aryl Imines of o-Hydroxybenzaldehyde between 2000 and 1500 cm⁻¹

John W. Ledbetter, Jr.

Department of Biochemistry, Medical University of South Carolina, Charleston, South Carolina 29401 (Received July 1, 1976)

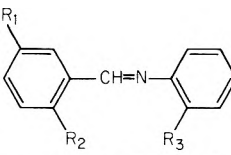*Publication costs assisted by the Medical University of South Carolina*

A thorough study of various protonic equilibria involving 2-[(phenylimino)methyl]phenol and other substituted aryl imines has been possible through the assignment of new infrared bands. In KBr, dimethyl sulfoxide, and fluorinated alcohols, $\nu_{C=O}$ and $\nu_{C=C}$ frequencies at 1640 and 1525–1547 cm⁻¹, respectively, were found, the result of an enol–keto tautomerism. In addition, in KBr and in 1,1,1,3,3,3-hexafluoro-2-propanol a $\nu_{C=NH^+}$ band was observed at 1627 cm⁻¹. Addition of the proton to the imine nitrogen in KBr is apparently intramolecular and precursory to keto formation. The effects of electron-withdrawing and -releasing groups on the equilibria were studied.

Introduction

The structure of N-aryl imines of benzaldehydes, viz., N-(phenylmethylene)benzenamine (I) and 2-[(phenylimino)methyl]phenol (II), has been widely studied. From studies in solution by optical[1-4] and ¹H NMR[5] spectroscopic techniques it has been clearly established that for II an enol imine–keto enamine tautomerism exists.

II
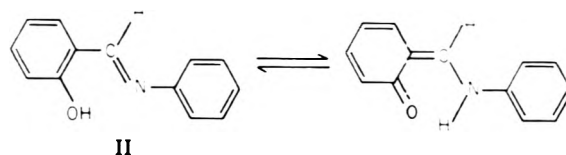
This tautomerism has been found to lie far on the enol

TABLE I: Vibrational Assignments of the Infrared Bands[a]

		R₁	R₂	R₃
	I	H	H	H
	II	H	OH	H
	III	H	OH	OH
	IV	H	OCH₃	H
	V	NO₂	OH	OH
	VI	OH	OH	OH

Compd	Solvent[b]	$\nu_{C=O}$	$\nu_{C=NH^+}$	$\nu_{C=N}$	ν_{Ph}	ν_{Ph}	$\nu_{Ph+C=N}$	$\nu_{C=C}$
I	CHCl₃			1625		1591	1578	
II				1620		1593	1573	
III	CH₂Cl₂			1620	1598	1590	1573	
IV	CHCl₃			1620	1598	1590	1577	
V	p-Dioxane			1620		1594	1573	
VI				1611			1580	
I	KBr			1625		1589	1577	
II				1615		1589	1570	
III		1638	1627	1615		1592		1525
IV				1618	1597	1587	1576	
V		1640		1615		1593		1545
VI			1640		1602	1596		1547
I	HFP		1652	1620		1592	1570	
II		1638	1627			1593		1544
III		1638	1627	1615	1600			1542
IV			1647		1610	1591	1575	
II	HFP-d₂		1619			1593		1527
III		1640	1621		~1600			1532
II	TFE			1616		1590	1572	
III		1640		1622		1592		1535
V	Me₂SO	1640		1615		1593		1545
VI				1609		1590	1575	

[a] Wavenumbers.   [b] See text for abbreviations.

side. Estimates made from the ¹H NMR data and from data obtained in this laboratory show that ΔH is about -1 kcal/mol. Dipole moment[6] and LCAO-MO[7] calculations also show that the benzenoid structure is strongly favored. Inasmuch as no quinoid structure was observed, infrared work on II and the N-alkyl analogues[9,10] demonstrates that the benzenoid structure is favored. However, substitution of the oxygen in II and in its para analogue with sulfur results in almost exclusively the keto tautomer in dimethyl sulfoxide.[11] In the study of the infrared spectrum of the Schiff base formed from salicylaldehyde and the amino acid valine,[12] strong absorption was observed at 1634 cm⁻¹ in KBr and was assigned to an amide I carbonyl stretching vibration. Another band was observed at 1513 cm⁻¹ and was assigned to either a C═C or a C═N stretching vibration of the conjugated amide. The authors have cited this as evidence of a tautomeric form in which the phenolic proton has transferred to the imine nitrogen. The enol tautomer is present in a smaller fraction.

It would appear, therefore, that the quinoid tautomer of N-aryl and N-alkyl imines of salicylaldehyde has not been observed in the infrared region. This investigation was initiated to determine the carbonyl stretching frequency of the quinoid tautomer of II and to study further the band assignment at ca. 1513 cm⁻¹ as noted above.

Experimental Section

The imines were prepared by the condensation of the appropriate aldehyde and amine in 95% ethanol.[13] After several recrystallizations, the compounds were dried and analyzed for C, H, and N content. The analyses proved to be in agreement with theory.

Solvents used in the experiments were used without further purification. Since water has its bending vibration in the 1650-cm⁻¹ region, a region in which the carbonyl stretching frequency is expected, careful attention was given to water present in the solvents. The presence of water was determined by observing the $\nu_2 + \nu_3$ combination band of H₂O in the manner described by Bonner.[4] In the case of 2,2,2-trifluoroethanol (TFE) and 1,1,1,3,3,3-hexafluoro-2-propanol (HFP) no water was observed. In CH₂Cl₂ and CHCl₃ only traces of water were observed. In the case of dimethyl sulfoxide (Me₂SO) a water content of 0.01% was observed. These determinations and other ultraviolet and visible spectra were made with a Cary Model 14 recording spectrophotometer. The above solvents were purchased from Matheson Coleman and Bell and with the exception of the fluorinated alcohols they were Spectroquality solvents. 1,1,1,3,3,3-Hexafluoro-2-propanol-d₂ (HFP-d₂) was purchased from Merck and Co., Inc. The imine solutions were prepared in a dry N₂ atmosphere.

The infrared spectra were determined with a Perkin-Elmer Model 421 recording spectrophotometer. Wavelength calibration with water vapor was within one wavenumber. For the fluorinated alcohols Irtrans-2 cells were used. In order to improve the solubility of certain of the imines a Barnes Engineering variable temperature chamber was used.

For correlation studies ultraviolet and visible spectra of the imines were determined in KBr pellets. This presented no particular difficulty, except that the accuracy of the concentrations is limited. The imines were weighed on a Cahn electrobalance and combined with a known quantity of KBr to produce a pellet of known volume. The imine concentrations were known to two significant figures and were in the neighborhood of 10⁻³ M. The pellets were run in dry N₂ in the spectrophotometer.

Results and Discussion

Spectra in Aprotic Solvents. The spectra of II, 2-[(2-hydroxyphenylimino)methyl]phenol (III), and N-[(2-methoxyphenyl)methylene]benzenamine (IV) between 2000 and 1500 cm⁻¹ in chloroform or methylene chloride are shown in Figure 1. Table I lists the molecular structures and wavenumbers of the bands. Inasmuch as
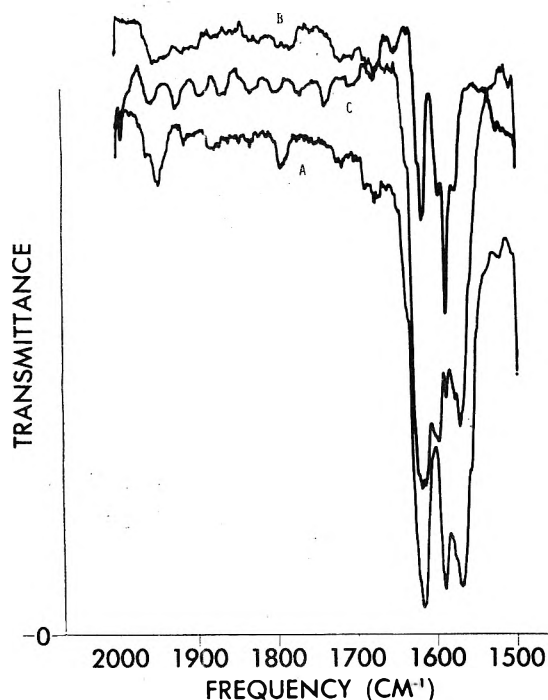
Figure 1. Infrared spectra of imines in aprotic solvents between 2000 and 1500 cm^{-1}. A is 0.5 M II in CHCl$_3$ in 0.1-mm cells. B is 0.04 M III in CH$_2$Cl$_2$ in 1.0-mm cells. C is 0.1 M IV in CHCl$_3$ in 0.1-mm cells.
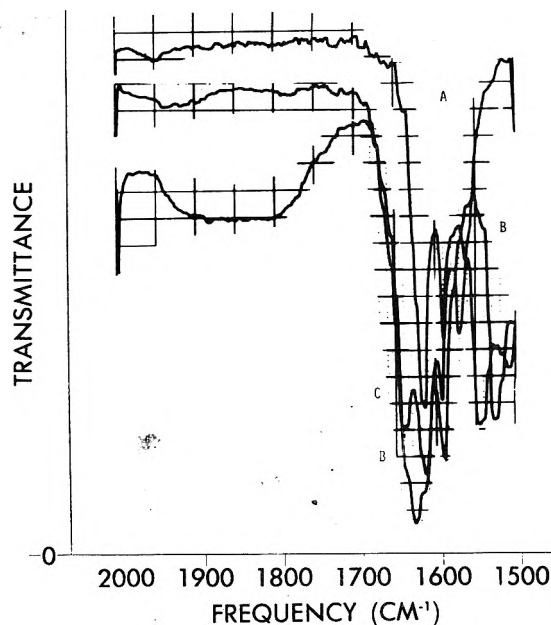

Figure 2. Infrared spectra of imines in KBr between 2000 and 1500 cm^{-1}. A, B, and C are II, III, and IV, respectively, at a 1% by weight concentration.

all the compounds exhibit a $\nu_{C=N}$ at 1620 cm^{-1} and two other bands, one near 1590 cm^{-1} and one near 1575 cm^{-1}, it is established that clearly the molecules exist in the imine structure. The latter two of these bands have been assigned[15] to quadrant stretching vibrations which are said to be resolved in substituted benzenes when the substituents are conjugated. Through a study of ^{15}N-labeled compounds, the lower frequency of the quadrant doublet has been found to be vibrationally coupled to $\nu_{C=N}$.[10] Since the two bands usually appear with a conjugated substituent it does appear possible. Data given below will support this conclusion. In III and IV another band occurs at 1598 cm^{-1} and it is interesting to note the change in the relative intensities of the bands. If a relation exists between the 1598- and 1590-cm^{-1} frequencies, at the moment it is not understood. Both are thought to be associated with the aromatic stretching vibrations.

Spectra in Potassium Bromide. The spectra of the compounds in KBr pellets are also recorded. The frequencies are shown in Table I. For compounds II and IV the frequencies are essentially unchanged. Due to the change in medium there is a slight shift of 3–5 cm^{-1} to lower frequencies. In the spectrum of III there is a considerable difference which can be seen in Figure 2. Instead of a slight shift to lower frequencies as noted above there occurs a broad band with a maximum at 1627 cm^{-1} and with shoulders at 1615 and 1638 cm^{-1}. There is still a band at 1592 cm^{-1} which is very probably a quadrant stretching vibration. The second of these bands near 1575 cm^{-1} is now missing and, a new band occurs at 1525 cm^{-1}.

It is known from earlier studies[3] that compounds such as III exhibit more keto structure in solution than those such as II. In other words, the o-hydroxyl in the aniline ring has a stabilizing influence on the keto structure. In order to investigate the possibility of keto structure being observed for III in KBr, the spectra of several type III compounds in which substituents were placed in the 4 position of the phenylmethylene ring were recorded in the 2000–1500-cm^{-1} region and in the 400-nm region. Shown in Figure 2 is the spectrum of 4-nitro-2-[(2-hydroxy-

phenylimino)methyl]phenol (V) in KBr. This compound has been found to exhibit a large degree of keto structure because of the electron-withdrawing nature of the nitro group.[13] This spectrum is very revealing. A band occurs at 1615 cm^{-1} which is readily assigned to $\nu_{C=N}$. This undoubtedly accounts for the shoulder in III. Another strong band occurs at 1640 cm^{-1}. This band is suspected of being the $\nu_{C=O}$ of the keto isomer of III because there are several examples of conjugated hydrogen bonded ketones which absorb in the low 1600-cm^{-1} region. The quadrant stretching band occurs at 1592 cm^{-1}. Again, a new band occurs, this time at 1545 cm^{-1}, and another weaker one also appears at 1509 cm^{-1}. Another compound to give a strong band at 1640 cm^{-1} in KBr was 4-hydroxy-2-[(2-hydroxyphenylimino)methyl]phenol (VI). Other bands were observed at 1602, 1596, and 1547 cm^{-1}. There is essentially no absorption at the $\nu_{C=N}$ frequency. This frequency, shown in Table I, is obtained from the spectrum taken in p-dioxane. This makes the situation unique in that OH is strongly electron releasing and, as shown earlier in solution studies[13] and here in Me$_2$SO, does not facilitate the incursion of keto structure as readily as other substituents. Evidently, in this case the molecule exists entirely in a structure other than the imine structure. The band at 1547 cm^{-1} is very similar to that obtained in V.

Regarding the 1640-cm^{-1} band, if it is due to $\nu_{C=O}$ then there must be a correlation between its intensity and the intensity of the visible band at 440 nm. Compounds which had been prepared earlier and whose substituents at the 4 position represented a wide range in electron-donating and -withdrawing ability were used for the correlation. Both visible and infrared spectra were obtained in KBr disks. It was clear from the ultraviolet and visible absorption spectra that the tautomerism was occurring. A correlation plot for those compounds which clearly showed an absorption band or shoulder near 1640 cm^{-1} is shown in Figure 3. This plot is very similar to one obtained earlier[13] and does show a positive correlation of the intensity of the infrared band with that of the visible band. Since most of the 1640-cm^{-1} bands are not resolved from nearby bands it is not possible to obtain a better correlation. This is probably the reason why the points rep-

TABLE II: Variation of Band Frequencies with Substituents[a]

Substituent, R_1	KBr				HFP			
	$\nu_{C=O}$	$\nu_{C=NH^+}$	$\nu_{C=N}$	$\nu_{C=C}$	$\nu_{C=O}$	$\nu_{C=NH^+}$	$\nu_{C=N}$	$\nu_{C=C}$
NO_2 (V)	1640	Missing	1615	1545	(1650–1570 broad)			1548
CN	1638	1627	1618	1525				
$COOCH_2CH_3$	1640	b	1615	1525	1638	b	1618	1525
Br	b	1625			1637	1625	1615	1525
Cl	1638	1627		1525	1638	b	1618	1525
I	1638	1625		1525				
F	1637	1628		1528	1639	b		1538
H (III)	1638	1627	1615	1525	1638	1627	1615	1542
C_6H_5	1638	b	1620	1525	1637	1628	b	1540
CH_3	b	1623		1520	1637	1628		1535
OCH_3	1638	1625		1527	1636	b		1531
OH (VI)	1640	Missing		1547				

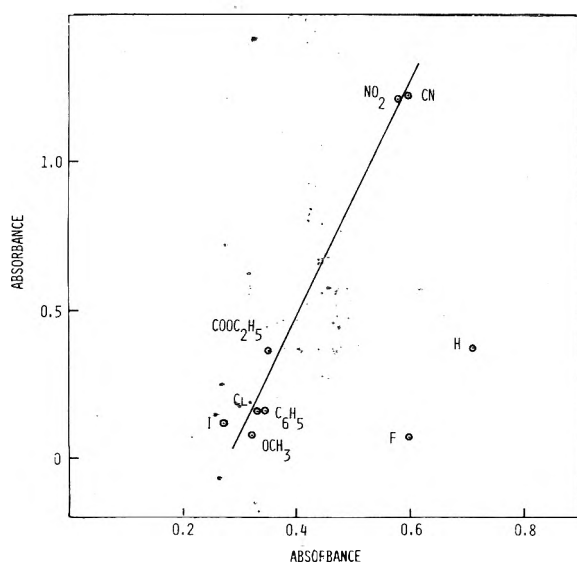[a] Wavenumber units. [b] Present but indeterminate because of overlapping bands.

Figure 3. Correlation plot of intensity of the quinoid absorption band near 440 nm with intensity of the $\nu_{C=O}$ absorption band at 1640 cm^{-1}. The visible data, plotted on the ordinate, are corrected for a 1.0×10^{-3} M concentration in the 1-mm pellet pathlength. The infrared data are for a 1% by weight concentration.
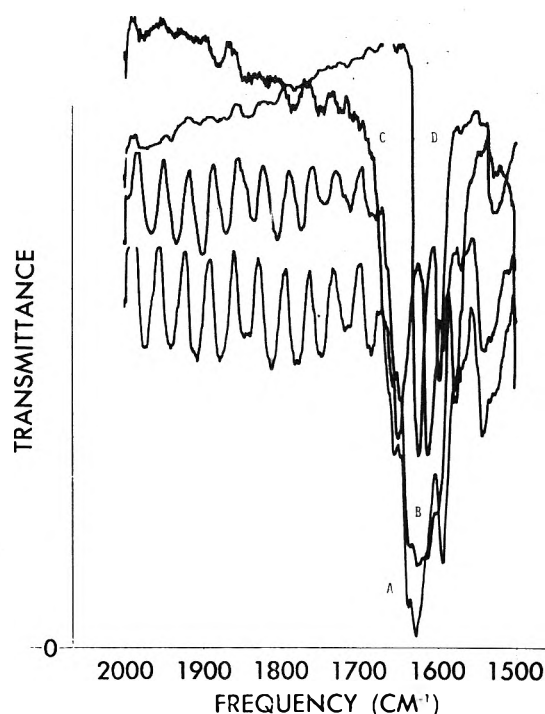

Figure 4. Infrared spectra of imines in 1,1,1,3,3,3-hexafluoro-2-propanol between 2000 and 1500 cm^{-1}. A, B, and C are II, III, and IV, respectively. D is II in the deuterated solvent. Solutions were 0.1 M in 0.1-mm cells.

resented by H and F substituents lie too far to the right on the plot. See the spectra of III in KBr. It is also assumed that the molar absorptivities of the bands used in the correlation study are roughly the same. This has been discussed earlier[13] regarding the visible bands.

The study of these various substituted imines in KBr has established that along with the appearance of a band at 1640 cm^{-1} the band near 1575 cm^{-1} disappears and a new band appears between 1550 and 1520 cm^{-1}. This became evident when the infrared spectra of the substituted imines were determined in apolar solvents. For example, V and VI exhibited bands at 1620, 1594, and 1573 cm^{-1} and at 1611 and 1580 cm^{-1}, respectively, in p-dioxane; the 4-C_6H_5-substituted compound exhibited bands only at 1621, 1598, and 1578 cm^{-1} in methylene chloride. The frequencies of the new band between 1550 and 1520 cm^{-1} for several compounds are listed in Table II. They will be discussed more later.

The strong absorption at 1627 cm^{-1} could be the result of the overlap of the two bands at 1638 and 1615 cm^{-1}. Considering the spectrum of V with these two bands in the same position and the absence of the strong absorption at 1627 cm^{-1}, it is apparent that three bands are present. Considering the possibilities, the band at 1627 cm^{-1} is thought to be due to a protonated imine nitrogen and is assigned to $\nu_{C=NH^+}$. Heyde[16] has assigned the $\nu_{C=NH^+}$ frequency to 1650 cm^{-1} in aniline derivatives of retinal. As

will be shown below for N-(phenylmethylene)benzenamine (I) in acidic solvents, this band occurs at 1652 cm^{-1}. This frequency would surely be less in the case of III because of resonance contributions to the structure. Additional supportive evidence will be given below.

Spectra in Acidic Solvents. It has been demonstrated that the keto structure is more favored in protonic solvents and with increasing dielectric constant. To produce larger amounts of keto structure in order to observe $\nu_{C=O}$, the imines were studied in HFP. The study in this solvent proved complex but revealing. It is of interest to note from Figure 4 that II and III in HFP have spectra very similar to III in KBr. The $\nu_{C=O}$ frequency occurs at 1638 cm^{-1} and the band at 1570 cm^{-1} is notably missing. Again a new band appears around 1544 cm^{-1}.

HFP is a very strong alcohol having acidlike properties. Not only can it facilitate the keto structure but also protonate the imine nitrogen. Additional evidence for this is provided by the electronic absorption spectra shown in Figure 5. For II and III in HFP a shoulder is observed at about 440 nm which must be due to quinoid structure. In addition the strong bands observed at 380 and 325 nm represent a very large bathochromic shift of 30–50 nm from
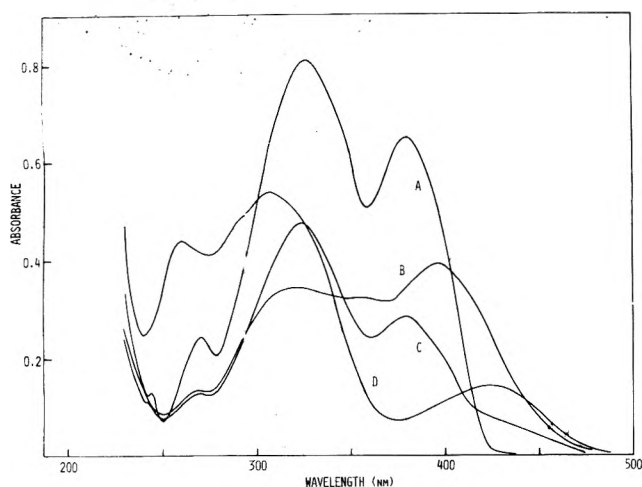
Figure 5. Electronic absorption spectra of the imines in fluorinated alcohols. A, B, and C are IV, III, II, respectively, in 1,1,1,3,3,3-hexafluoro-2-propanol at 5.0, 2.8, and 1.6 × 10^{-5} M concentrations in 1.0-cm cells. D is 4.0 × 10^{-5} M II in 2,2,2-trifluoroethanol.

the spectra in methanol. These latter bands are observed also for IV and were observed for III in H$_3$CCOOH, HCOOH, and H$_2$SO$_4$.[3] Since the quinoid concentration does not appear to be very high, and since hydrolysis is not occurring, the reasonable conclusion is that the larger fraction of molecules is protonated at the imine nitrogen. It is revealing to point out in Figure 5 that the spectrum of II in TFE better demonstrates the equilibrium between the benzenoid and quinoid tautomers, both unprotonated.

The infrared spectra of I and IV in HFP show a band at 1652 and at 1647 cm^{-1}, respectively. This band is well displaced toward higher frequencies from the $\nu_{C=N}$. Since it is almost certain that the larger fraction of molecules are protonated, this band is assigned to $\nu_{C=NH}^+$. It does agree well with Heyde's observation. If now the o-hydroxyl were allowed to interact with this band, due to resonance effects the frequency would lower. The frequency at 1627 cm^{-1} in II and III is assigned, therefore, to $\nu_{C=NH}^+$. It is of interest to note that for I and IV in HFP the quadrant stretching bands occur, including the one at about 1570 cm^{-1}, and that no band occurs between 1550 and 1500 cm^{-1}.

To provide additional evidence on the origin of the 1544-cm^{-1} band, the spectra of II and III were determined in HFP-d_2. A strong band occurred around 1620 cm^{-1}. Since electronic absorption spectra show that the molecules are protonated, the band was assigned to $\nu_{C=ND}^+$. From the infrared and electronic spectra it is determined also that the keto structure of II is not present. This is not too surprising since deuteration of the o-hydroxyl would make it less acidic and, thereupon, less apt to enter into tautomerization. The $\nu_{C=O}$ band for III is observed, however. In going from CHCl$_3$ to HFP the $\nu_{C=N}$ band shifts by 5 cm^{-1} to lower frequencies. Therefore, the band in HFP-d_2 at 1620 cm^{-1} must represent not the free C=N bond but the deuterated bond. The shift of the $\nu_{C=NH}^+$ band on deuteration is, therefore, about 7 cm^{-1}. The quadrant stretching bands for II and III occur at 1593 and about 1600 cm^{-1}, respectively; the 1570-cm^{-1} band is absent for both. The new band does appear at 1527 cm^{-1} for II and at 1532 cm^{-1} for III.

In view of the position of the new band, it might possibly be an amide II type band. This is ruled out because the band does not shift some 90 cm^{-1} on deuteration as does the band in polypeptides and because it may appear when the keto structure is not indicated, as in the case of II in HFP-d_2. It is also revealing to note that the band does not occur for I or IV in HFP. This is interpreted to mean that

when the molecule is incapable of strongly resonating contributions from an o-hydroxyl group the band will not occur. There also must occur strong hydrogen bonding or protonation of the imine nitrogen. Furthermore, for those structures and situations which tend to form the keto structure, the band occurs around 1545 cm^{-1}; while for those structures which exist mainly as the protonated imine nitrogen, the band occurs around 1525 cm^{-1}. (See Table I and Table II.) In some cases such as II and III in HFP the band is broad and probably reflects contributions from both frequencies. In the case of III in HFP-d_2, wherein there is less keto formation than in HFP because of deuteration, the band occurs at 1532 cm^{-1}. This position represents a 5-cm^{-1} shift to higher frequencies over II and is apparently because of a more keto-like structure; but, it still represents an intermediate case. All this evidence supports the conclusion that the origin of the band is the vibration of the vinyl C$\equiv$C bond between the azomethine group and the phenylmethylene ring. When it is normally singly bonded it occurs at lower frequencies; but, when it contains some double bond character it absorbs between 1550 and 1500 cm^{-1}. The more double bond character (the more nearly a keto structure) the higher the frequency. It may also be possible that the C$\equiv$N bond may be vibrationally coupled but this is difficult to determine without ^{15}N-substituted spectral data. It is observed, however, that the 1570-cm^{-1} band which does exhibit vibrational coupling with the C=N bond is missing when the C=N is protonated in the case of the o-hydroxyl derivatives or when the keto tautomer is present. The 1570-cm^{-1} band and the 1545–1525-cm^{-1} band appear to be mutually exclusive. The coupling between the quadrant stretching vibration and $\nu_{C=N}$ is apparently lost when the character of the C=N bond is reduced from that of the bond in II in aprotic solvents.

In the study[12] of the infrared spectra of Schiff bases formed from amino acids and pyridoxal analogues, N-salicylidenevaline was investigated in KBr. A band of medium intensity at 1513 cm^{-1} was found and was assigned to the C=C stretching vibration similarly observed in amide vinylogs. This assignment was based on earlier work[17] which found in acetylacetoneimines in Nujol mulls a band around 1540 cm^{-1}. This band was assigned by the authors to either a "lowered" C=C or an "enhanced" C–N frequency and probably to the former. As you can see, this is essentially the same conclusion reached in this study.

Spectra in Other Solvents and Conclusions. As demonstrated by electronic absorption spectra, TFE facilitates keto formation through strong hydrogen bonding while not protonating the imine nitrogen. It should give, therefore, an equilibrium mixture of only the enol and the keto tautomers. The infrared spectrum bears this out. For III the $\nu_{C=O}$ band is observed at 1640 cm^{-1} and the $\nu_{C=N}$ band at 1622 cm^{-1}. This latter frequency being slightly higher than that of II probably represents the strong hydrogen bonding by the solvent. The 1570-cm^{-1} band of III is missing and the $\nu_{C=C}$ occurs at 1525 cm^{-1}. This band like that of II in HFP-d_2 represents an intermediate case of keto-like structure. Compound V in Me$_2$SO represents an example of the equilibrium without strong hydrogen bonding from the solvent. See also that the 1570-cm^{-1} band is missing and that the band at 1545 cm^{-1} is present, indicative of strong keto formation. As pointed out earlier, it was unexpected that VI in KBr existed exclusively as the keto tautomer. In Me$_2$SO, however, as expected there was little evidence of the keto tautomer.

Briefly, in conclusion the aryl imines may be found to be involved in various equilibria which are determined by

the solvent. In KBr identification of the $\nu_{C=N}$, $\nu_{C=C}$, $\nu_{C=NH^+}$, and $\nu_{C=O}$ frequencies leads one to conclude that equilibria 1, 2, and 3 are involved. In protonic solvents
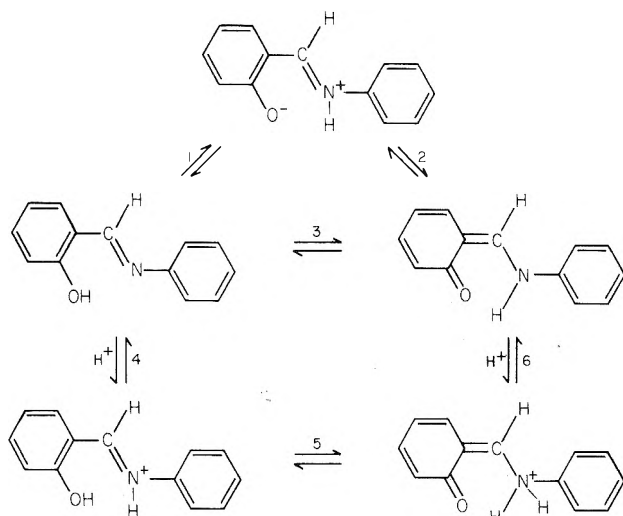
which are not too acidic (TFE inclusive) and for aprotic solvents having a high dielectric constant, equilibrium 3 is solely involved. In these solvents except for $\nu_{C=NH^+}$ all the frequencies found above in KBr were present. There are apparently no stabilizing forces as there must be in KBr to maintain the zwitterionic form. In strongly acidic

solvents, including HFP, equilibria involving the protonated species do occur. The $\nu_{C=NH^+}$ band in addition to the other bands is observed. Also, the ultraviolet spectrum indicates protonated species present. Equilibria 3–6 with 4 predominating, therefore, must be involved. The extent to which any species may be present in any equilibrium also depends on the substitutions in the rings.

References and Notes

(1) J. D. Margerum and J. A. Sousa, *Appl. Spectrosc.*, **19**, 91 (1965).
(2) R. S. Becker and W. F. Richey, *J. Am. Chem. Soc.*, **89**, 1298 (1967).
(3) J. W. Ledbetter, *J. Phys. Chem.*, **70**, 2245 (1966).
(4) J. W. Ledbetter, *J. Phys. Chem.*, **71**, 2351 (1967).
(5) G. O. Dudek and E. P. Dudek, *J. Am. Chem. Soc.*, **88**, 2407 (1966).
(6) V. I. Minkin et al., *Dokl. Akad. Nauk SSSR*, **145**, 336 (1962).
(7) V. I. Minkin et al., *Zh. Fiz. Khim.*, **38**, 938 (1964).
(8) L. A. Kazitsyna and V. V. Mishchenko, *Dokl. Acad. Nauk SSSR*, **150**, 555 (1963).
(9) J. J. Charette, *Spectrochim. Acta*, **19**, 1275 (1963).
(10) G. C. Percy and D. A. Thornton, *J. Inorg. Nucl. Chem.*, **34**, 3357, 3369 (1972).
(11) V. I. Minkin et al., *Dokl. Akad. Nauk SSSR*, **184**, 605 (1969).
(12) D. Heinert and A. E. Martell, *J. Am. Chem. Soc.*, **84**, 3257 (1962).
(13) J. W. Ledbetter, *J. Phys. Chem.*, **72**, 4111 (1968).
(14) O. D. Bonner and Y. S. Choi, *J. Phys. Chem.*, **78**, 1723 (1974).
(15) A. R. Katritzky, *Quart. Rev.*, **13**, 353 (1959).
(16) M. E. Heyde et al., *J. Am. Chem. Soc.*, **93**, 6776 (1971).
(17) N. H. Cromwell et al., *J. Am. Chem. Soc.*, **71**, 3337 (1949).

Singlet–Triplet Absorption and Emission Spectra of Substituted Cyanocobaltate(III) Complexes

Barbara Loeb and Fernando Zuloaga*

Instituto de Ciencias Químicas, Universidad Católica de Chile, Santiago, Chile (Received February 3, 1976)

Singlet–triplet transitions in monosubstituted cyanocobaltate(III) complexes are studied by absorption and emission spectroscopy. The measurements reveal anomalous results when the spectral behavior of $Co(CN)_5NO_2^{3-}$ and $Co(CN)_5SO_3^{4-}$ are compared among themselves and with the parent $Co(CN)_6^{3-}$ compound. A further analysis shows that the spectral parameters of the parent compound can be used to find the energies of the emission bands in terms of the axial field created by the substituting ligand. The emission has been assigned to the $^3A_2 \rightarrow {}^1A_1$ transition whereas the lowest excited state in the absorption process is shown to be the ^3E_a component of the $^3T_{1g}$ state of the parent compound.

Introduction

Experimental studies of luminescences of transition metal ion complexes have rapidly expanded during the last few years so that it has become increasingly important to record luminescence as well as absorption spectra. However, in spite of their great spectroscopic and photochemical interest, cobalt(III) complexes have received very little attention with regard to their emissions. In fact, only two cobalt(III) complexes have been reported to luminesce[1,2] under direct UV excitation of the crystals: $Co(CN)_6^{3-}$ and *trans*-$Co(CN)_4(SO_3)_2^{5-}$. Moreover, considerable effort has recently been focused on the photophysical properties of the hexacyanocobaltate(III) ion.

Thus, the emission spectrum of $K_3[Co(CN)_6]$ down to 4.2 K and its natural lifetime dependence with temperature has recently been published.[3] At the same time, evidence

for intermolecular energy transfer from $Co(CN)_6^{3-}$ to $Cr(CN)_6^{3-}$ in powders has been reported.[4] Finally, it is known that the emitting level is the $^3T_{1g}$ state of the cobalt(III) complex which corresponds to the metal localized interconfigurational $t_{2g}^5 e_g \rightarrow t_{2g}^6$ process under O_h microsymmetry.[5]

The luminescent behavior of the two above-mentioned cobalt(III) complexes is really anomalous. For example, their emission maxima lie at $14\,030$ cm^{-1} for the $Co(CN)_6^{3-}$ ion and at $14\,300$ cm^{-1} for its disulfito derivative. In fact, this 270 cm^{-1} difference does not correlate with absorption data for both compounds even if one takes into account the splitting of the $^3T_{1g}$ excited state into $^3A_{2g}$ and ^3E_g for the $Co(CN)_4(SO_3)_2^{5-}$ ion. It has also been pointed out[6] that the close similarity observed between the absorption spectra of d^3 and d^6 complexes does not extend to the emission

spectra. The reason lies in the fact that, although both atomic systems show spin-forbidden levels lying below the first excited spin-allowed state, the ground state nuclear equilibrium position is reached in the lowest spin-forbidden excited state for a d^3 system whereas this is not true for a d^6 system. This means that the ground state and lowest excited spin-forbidden state potential surfaces are parallel for d^3 complexes and rather well displaced for d^6 complexes thus making possible the existence of overlapping or crossing regions among them[7] and creating good conditions for radiationless decay to the ground state. In summary, all the circumstances favoring phosphorescence from d^3 emitters appear to be unfavorable ones for d^6 emitters and force one to choose rather carefully the ligands for cobalt(III) complexes.

It is the aim of this paper to present the results obtained for the low temperature (77 K) singlet–triplet absorption and emission data of two monosubstituted cyanocobaltate(III) complexes together with a discussion of the experiments within the context of ligand field theory. We also report here a consistent assignment scheme for their singlet–triplet transitions.

Experimental Section

Preparation of Compounds. The starting materials for the preparation of monosubstituted cyanocobaltate(III) complexes were $K_3[Co(CN)_6]$ prepared by a well-known procedure[8] and $[Co(NH_3)_5Cl]Cl_2$ from Fluka A-G. A 0.1 M solution of the $Co(CN)_5OH_2^{2-}$ complex was prepared by exhaustive photolysis of a 0.08 M solution of $Co(CN)_6^{3-}$ in a 0.2 M acetic acid solution. We have found that this is an excellent method to obtain rather concentrated solutions of $Co(CN)_5OH_2^{2-}$ without problems of polymerization or other interfering reactions.[9] The irradiation was accomplished with a ACE UV equipment filtered with a pyrex sleeve. The course of the reaction was monitored by observing the growth of the 380-nm absorption band of the aquo-substituted cyanocobaltate(III) complex. Finally, the resulting solution was evaporated under vaccum at room temperature to adjust the concentration to 0.1 M of $Co(CN)_5OH_2^{2-}$.

The synthesis of $K_4[Co(CN)_5SO_3]\cdot H_2O$ was accomplished by dissolving 0.4 g of $K_2S_2O_5$ in 18 ml of the 0.1 M solution of $Co(CN)_5OH_2^{2-}$ and then adjusting the pH to a value of ~9 and keeping it at 50 °C for 2 h. The substitution reaction was controlled by measuring the 335-nm absorption band of the sulfito derivative complex and the potassium salt was obtained by adding methanol. Finally, the sulfitocyanocobaltate(III) complex was fractionally recrystallized from an aqueous solution by adding methanol to it and dryed under vacuum to obtain the monohydrated crystals. The same compound was also obtained by using an already published procedure[10] to compare their emission spectra. They were exactly the same. The preparation of $K_3[Co(CN)_5NO_2]$ was accomplished by the method of Wilmarth et al.,[11] that is, by using the acidopentaamminecobalt(III) salt as the starting material. All of the compounds were analyzed for C, N, and H and the results were satisfactory.

Measurements. UV, visible, and near-infrared absorption spectra were measured with a PE 450 absorption spectrophotometer and also with a 1800 Pye Unicam spectrophotometer. Low temperature spectra were obtained by using a variable temperature cryostat (Janis Research) and a quartz microdewar with the samples completely immersed in liquid nitrogen.

The glassy solutions for the low temperature absorption measurements were made in situ by using a saturated aqueous solution of the corresponding complex and mixing

in ethylene glycol to a 2.5/1 volume ratio for the Co-$(CN)_5SO_3^{4-}$ ion and to a 5/1 ratio for the $Co(CN)_5NO_2^{3-}$ ion. Absorption spectra of $Co(CN)_6^{3-}$ were also run under the same conditions. Spectra were corrected for base line shift.

Luminescence measurements were performed by irradiating directly the crystals immersed in liquid nitrogen with a 500-W Hg arc (Oriel Co) filtered with a 2-cm $CuSO_4$ solution, a 5-cm $CoCl_2$ solution,[12] and a Corning 7-54 color filter for the $K_4[Co(CN)_5SO_3]\cdot H_2O$ case. For the nitrito derivative solutions of $NiSO_4$ (2 cm) and $Ni(NH_3)_6^{2+}$ (10 cm) were used. The detecting system was composed of a 0.5-m Jarrell Ash Mark V monochromator equipped with a Corning 3-66 color filter and a 400-Hz tuning fork chopper (Bulova time products) on its entrance slit and a 540 grooves/mm grating blazed at 750 nm. The light signal was measured by a S-1 response cooled (-56 °C) photomultiplier tube and amplified through a 103 Keithley nanovolt meter and a 840 Keithley lock-in amplifier. Finally, luminescences were corrected for the sensitivity of the measuring system by using a standard lamp of known color temperature.

Lifetime measurements were done by means of an extremely fast two slots variable speed rotating shutter. The excitation of the crystals was done by a 500-W Hg arc whose light was filtered as already described. The emitted light intensity was followed by an EMI 9558 CQ photomultiplier tube with a 1 kΩ load resistor. The electrical signal was fed into a calibrated 5103 N Tektronix storage oscilloscope and several decay curves were taken from each sample.

The lifetime for each compound was calculated by fitting the decay curve to a single exponential function.

Results and Discussion

Cobalt(III) complexes in the strong field limit are expected to show low lying spin-allowed and spin-forbidden transitions, both of them parity forbidden. The resulting molecular states can be classified according to O_h or C_{4v} symmetries for the unsubstituted or monosubstituted[13] cyano complexes, respectively. In this manner, the spin allowed ${}^1A_{1g} \rightarrow {}^1T_{1g}$ and ${}^1T_{2g}$ transitions under O_h are split into ${}^1A_1 \rightarrow {}^1E_a$ and ${}^1A_2$ for the first case and ${}^1A_1 \rightarrow {}^1E_b$ and ${}^1B_2$ for the second in C_{4v}. The spin-forbidden transitions also obey the same splitting pattern so that we can make the following general statements. (a) The ${}^1A_1 \rightarrow {}^1A_2$ transition in monosubstituted cyano complexes appears at the same energy position as the ${}^1A_{1g} \rightarrow {}^1T_{1g}$ transition for the parent octahedral compound.[14] Its value can then be given in terms of Δ and C for the $Co(CN)_6^{3-}$ complex and it is orbitally forbidden in C_{4v}. It appears only through coupling with equatorial metal–cyanide vibrational modes and its energy is

$$E({}^1A_2) = \Delta - C \tag{1}$$

(b) The ${}^1A_1 \rightarrow {}^1E_a$ transition will almost always be the lowest energy spin-allowed transition for the $[Co(CN)_5X]^{n-}$ complexes.

Its energy position is displaced to lower values in reference to the ${}^1A_1 \rightarrow {}^1T_{1g}$ transition of the parent compound because of the substituting ligand and it can also be expressed in terms of Δ and C of $Co(CN)_6^{3-}$ plus the contribution from the axial substituent X (see Appendix).

$$E({}^1E_a) = \frac{3}{4}\Delta + \frac{5}{12}\frac{Z_x\langle r^4\rangle}{R_x^5} - C \tag{2}$$

where R_x and Z_x represent the metal–ligand distance and the new charge of the substituting ligand. (c) The ${}^1A_1 \rightarrow$
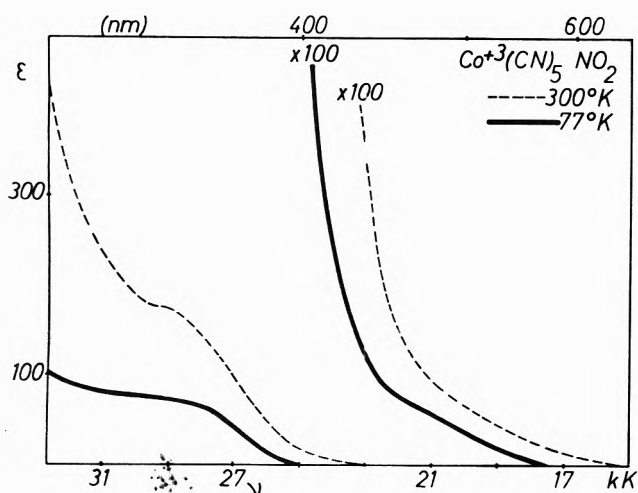
Figure 1. Absorption spectra of Co(CN)₅NO₂³⁻ in aqueous (300 K) and aqueous glassy (77 K) solutions.
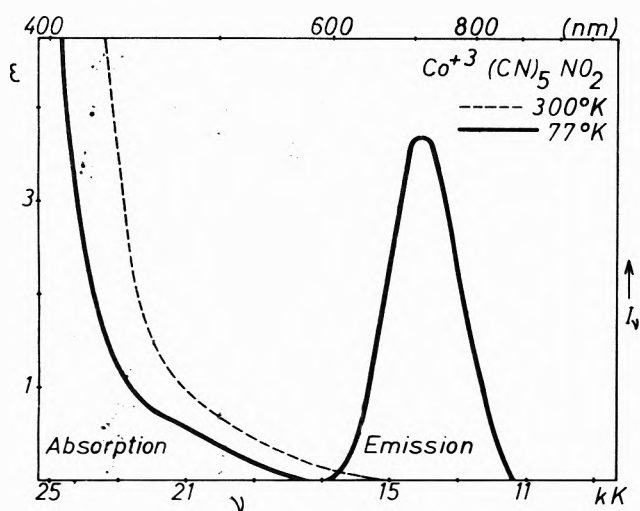
Figure 2. Singlet–triplet transitions of Co(CN)₅NO₂³⁻. The emission intensity was measured directly from the crystals.

Figure 3. Absorption spectra of Co(CN)₅SO₃⁴⁻ in aqueous (300 K) and aqueous glassy (77 K) solutions.
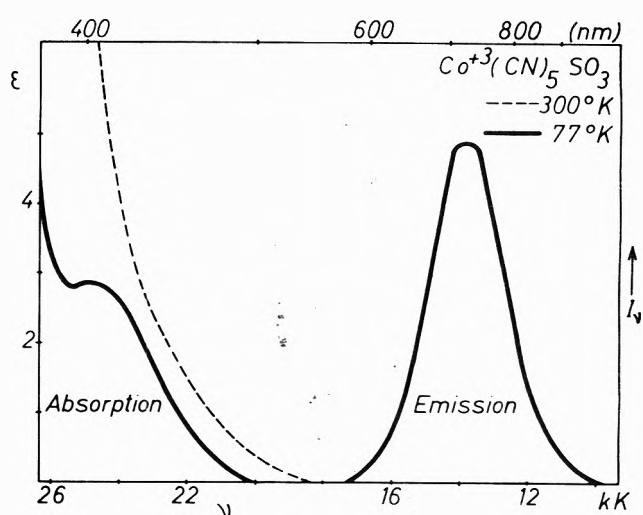
Figure 4. Singlet–triplet transitions of Co(CN)₅SO₃⁴⁻. The emission intensity was measured directly from the crystals.

^3E_a and $^1A_1 \rightarrow {}^3A_2$ transitions obey the same rules as the corresponding spin-allowed transitions though their energy positions change. They can also be related to the spin-forbidden transition of the parent compound in terms of Δ and C of Co(CN)₆³⁻ and we find that

$$E(^3A_2) = \Delta - 3C \qquad (3)$$

and

$$E(^3E_a) = \frac{3}{4}\Delta + \frac{5}{12}\frac{Z_x \langle r^4 \rangle}{R_x{}^5} - 3C \qquad (4)$$

so that both lowest excited states are no longer parallel in monosubstituted cyano complexes.

Figure 1 shows the absorption spectra of Co(CN)₅NO₂³⁻ where we can easily distinguish the $^1A_1 \rightarrow {}^1E_a$ transition at 29 200 cm⁻¹ in the low temperature spectrum. Moreover, the tail of the low temperature spectrum resolves in a shoulder at ∼22 200 cm⁻¹ with an $\epsilon \simeq 0.6$ which undoubtedly corresponds to the $^1A_1 \rightarrow {}^3E_a$ absorption band.

Figure 2 shows the measured spin-forbidden absorption and emission bands for this nitrito derivative complex. The emission band is centered at 14 100 cm⁻¹ with a half-band width of 2 600 cm⁻¹. It can also be seen that there is a ν shift of ∼8 100 cm⁻¹ between the absorption and the emission maxima for this complex. The emission band appears as a structureless broad band characteristic for the cobalt(III) complexes at 77 K and there is no doubt
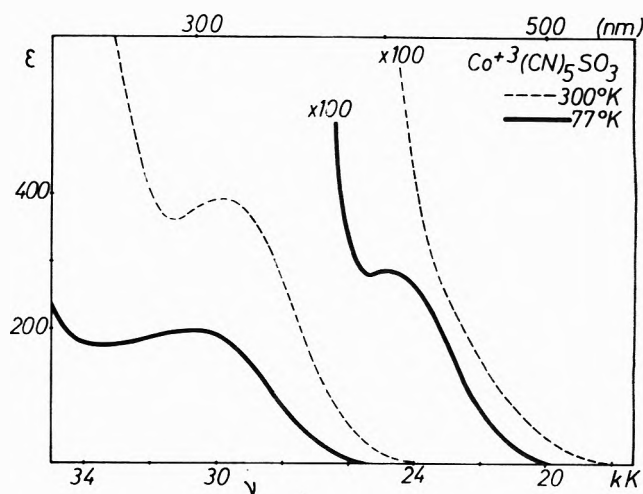
that it possesses the normal features of a broad interconfigurational metal localized vibronic transition.

In Figure 3 we present the absorption measurements for the Co(CN)₅SO₃⁴⁻ ion complex. The low temperature singlet–triplet absorption band at 24 390 cm⁻¹ is better resolved than the corresponding one for the nitrito derivative complex. This last result is a clear indication of the heavy atom effect of the S bonding to the Co³⁺ metal ion.

Figure 4 shows the emission band for this sulfito derivative complex together with the spin-forbidden absorption band. The emission maxima at 13 830 cm⁻¹ displays a half-band width of 2600 cm⁻¹ that coincides rather well with the measured value for the nitrito derivative and with the value of 2670 cm⁻¹ for the parent Co(CN)₆³⁻ ion.

Finally, Table I summarizes the main features for all the known chelated cobalt(III) emitters where the measured lifetime for each of them is also included. The absorption and emission maxima shown in Table I for these complexes do not follow the same pattern. To begin with, the emissions are located at ∼14 000 cm⁻¹ without any relation at all with the ligand field strength for each complex. It can be seen that the strongest ligand field is due to the six CN⁻ ions for a complex in the ground state M–L equilibrium distance. Moreover, the substitution of a CN⁻ ion in the parent octahedral compound by a NO₂⁻ ion shifts

TABLE I: Absorption and Emission[a] Spectral Data for Cobalt(III) Complexes at 77 K

Complex	$^1E(T_1)$,[b] cm^{-1}	$^3E(T_1)$,[b] cm^{-1}	$^3A_2 \rightarrow$ $^1A_1$, cm^{-1}	Life-time, μs
Co(CN)$_6$$^{3-}$	31 850 (180)	25 400 (0.92)	14 030	660
Co(CN)$_5$-SO$_3$$^{4-}$	30 300 (197)	24 390 (3.87)	13 830	290
Co(CN)$_5$-NO$_2$$^{3-}$	29 200 (95)	22 200 (0.58)	14 100	340
Co(CN)$_4$-(SO$_3$)$_2$$^{5-}$	27 300 (630)	18 180	14 300	470

[a] Measured from crystals.   [b] ϵ values shown in brackets.

the lowest singlet–triplet absorption maxima 3200 cm^{-1} to the red. However, this trend does not hold for the excited state M–L equilibrium distance since the same substitution shifts the triplet–singlet emission 70 cm^{-1} to the blue. Similar results are obtained by comparing absorption and emission data for the other cobalt(III) compounds against the Co(CN)$_6$$^{3-}$ complex ion. Finally, it can also be seen that the huge Stokes shift between the lowest absorption and the emission maxima for the parent octahedral compound decreases when one of its CN$^-$ ions is replaced by another anion.

Let us analyze first the meaning of the Stokes shift for the Co(CN)$_6$$^{3-}$ octahedral complex and find its dependence with the ligand field change due to the excitation. We will assume that the expression for the crystal field parameter Δ in terms of the M–L distance R is valid and write

$$d\Delta = -\frac{5}{R_0}\Delta_0 \, dR \tag{5}$$

where $d\Delta = (\Delta_{ex} - \Delta_0)$ is the difference between the ligand field parameter in the excited state and in the ground state. Since the Stokes shift has the same meaning as $d\Delta$, we can certainly obtain the increase (dR) of the M–L distance upon excitation (this result is valid only for a perfect octahedral compound). The experimental data shown in Table I for Co(CN)$_6$$^{3-}$ allow us to obtain $\Delta_0 = 35070$ cm^{-1} and $\Delta_{ex} = 23700$ cm^{-1} for this complex. By using these values in eq 5 we estimate an increase for the M–L distance of 0.12 Å over the 1.89-Å ground state value. This result agrees rather well with the value obtained by Crosby et al.[3] using other methods of calculation.

We can continue this analysis by assuming that the potential surface for the $^3T_{1g}$ state is mainly controlled by the potential energy term due to the vibrational mode of a$_{1g}$ symmetry. On the other hand, the rate of change $d\Delta$ in terms of the normal vibration Q_α of type a$_{1g}$ symmetry can also be written in a closed form as[15]

$$d\Delta = \frac{\partial \Delta}{\partial R}\frac{\partial R}{\partial Q_\alpha}dQ_\alpha = \left(-5\frac{\Delta_0}{R_0}\right)\frac{1}{\sqrt{6}}dQ_\alpha \tag{6}$$

By applying this equation to Co(CN)$_6$$^{3-}$ with $\nu_{a_{1g}} = 414$ cm^{-1} and the force constant $k = (0.65)^{1/2}$ (2.62 mdyn/Å) for this upper level[3,14] we deduce that the potential energy $^1/_2$ $k|\delta Q_\alpha|^2$ represents an harmonic oscillator in a vibrational quantum number of $n \approx 11$. Thus, the vertical electronic excitation process leaves the complex in a high vibrational level of the excited state potential surface. Now, if we consider an absorption bandwidth of ~ 2670 cm^{-1} (as found for its emission spectrum), we see that the interconfigurational transition starts at $n \approx 8$ and ends at $n \approx 14$. Therefore, one normally does not observe vibrational fine structure in this type of experiments unless the temperature is extremely low.[3]

TABLE II: Axial and Equatorial Parameters[a] for Cobalt(III) Complexes at 77 K from Absorption and Emission Measurements

Complex	$(Z\langle r^4\rangle/R^5)_{abs}$, cm^{-1}	$(Z\langle r^4\rangle/R^5)_{em}$, cm^{-1}
Co(CN)$_6$$^{3-}$	21 052[b]	14 220[b]
Co(CN)$_5$SO$_3$$^{4-}$	17 332[c]	13 741[d]
Co(CN)$_5$NO$_2$$^{3-}$	14 690[c]	14 389[d]

[a] The Racah parameters for the Co(CN)$_6$$^{3-}$ ion are $C = 3224$ cm^{-1} and $B = 441$ cm^{-1}. The octahedral parameters are $\Delta_0 = 35070$ cm^{-1} and $\Delta = 23700$ cm^{-1}. [b] Axial or equatorial contributions. [c] Axial contribution. [d] Equatorial contribution.

Now we want to know more about the states involved in the absorption and emission processes. To begin with, let us write eq 1 and 3 in the alternate form

$$E(^1A_2) = \frac{3}{4}\Delta + \frac{5}{12}\frac{Z_{cn}\langle r^4\rangle}{R_{cn}^5} - C \tag{1a}$$

$$E(^3A_2) = \frac{3}{4}\Delta + \frac{5}{12}\frac{Z_{cn}\langle r^4\rangle}{R_{cn}^5} - 3C \tag{3a}$$

where the term $Z_{cn}\langle r^4\rangle/R_{cn}^5$ plays the role of an "equatorial" contribution to the energy of the given excited state whereas $Z_x\langle r^4\rangle/R_x^5$ of eq 2 and 4 represents an "axial" (z axes) contribution to the ^3E_a and ^1E_a excited states. As it is evident, the "axial" and "equatorial" contributions are exactly the same for the parent compound of O_h symmetry giving rise to a triply degenerate level. However, this is not the case in C_{4v} symmetry. Let us calculate now the axial or equatorial term $Z\langle r^4\rangle/R^5$ for CN$^-$ by introducing the absorption maxima of Co(CN)$_6$$^{3-}$ from Table I in eq 1a or 2. The calculated value is 21 052 cm^{-1} as shown in Table II where we also tabulate the axial term for [Co(CN)$_5$X]^n obtained from eq 2 and the corresponding absorption data (Δ_0 and C are taken from the parent compound). It is important to notice that these results are all different and they obey satisfactorily the ordering of the spectrochemical series.

Surprising results appear when one calculates the axial and equatorial contributions of the ligand ions from emission data together with the values of Δ_{ex} and C for the parent compound. First, the $^3T_{1g} \rightarrow {}^1A_{1g}$ emission of Co(CN)$_6$$^{3-}$ appears at ~ 14030 cm^{-1} yielding a value of 14 220 cm^{-1} for the CN$^-$ ions in the axial or equatorial positions. Second, the corresponding values for the $Z\langle r^4\rangle/R^5$ term obtained from eq 3a or 4 for Co(CN)$_5$SO$_3$$^{4-}$ and Co(CN)$_5$NO$_2$$^{3-}$ are also shown in Table II and they are remarkably similar to the value for Co(CN)$_6$$^{3-}$. We need to find out if these numbers represent axial or equatorial contributions to the excited state energies since eq 3a and 4 are of the same nature but with a different meaning.

We know from absorption measurements that the axial contribution of CN$^-$, SO$_3$$^{2-}$, and NO$_2$$^-$ are different and a similar difference should also appear from emission measurements. Since this behavior does not agree with the results shown in Table II we conclude that the emitting state of [Co(CN)$_5$X]^n contains only equatorial contributions to its energy and therefore the observed emissions correspond to the $^3A_2 \rightarrow {}^1A_1$ transition. This is an interesting conclusion since the $^1A_1 \rightarrow {}^3E_a$ transition gives rise to the lowest absorption band whereas the observed emission does not arise from the ^3E_a state as would be expected.

A qualitative description of the electronic absorption and emission processes for the [Co(CN)$_5$X]^n complexes is suggested in Figure 5. We observe there a crossing between the excited states of the same multiplicity in going
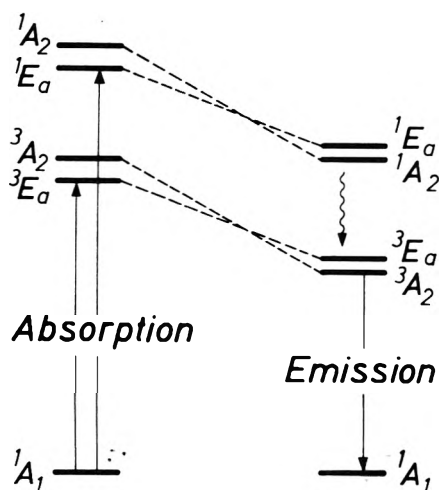
Figure 5. Absorption and emission processes for the $[Co(CN)_5X]^{n-}$ complexes.

from absorption to emission. The reason for this is the difference in mass and geometry between the X ligand and the CN^- ion and, unless the axial X ligand relaxes its M–L distance to the same extent as the equatorial CN^- ions, the emitting level will be the $^3A_2$ state.

This analysis explains why the emission maxima shown in Table I appear in the vicinity of the $14\,030$ cm^{-1} value for the $Co(CN)_6^{3-}$ parent ion. It is also remarkable how constant the $^3A_2 \rightarrow {}^1A_1$ emission energy is kept in relation to the parent compound and it makes valid the assumption of taking C as a constant throughout these complexes. Finally, the *trans*-disulfito derivative shown in Table I has also a similar ligand field effect and its emission corresponds to the $^3A_{2g} \rightarrow {}^1A_{1g}$ transition in D_{4h} symmetry.

Appendix

Let us assume that in the octahedral $Co(CN)_6^{3-}$ ion we substitute along the z axes a CN^- ligand by a X ligand. In this case, the new C_{4v} symmetry gives rise to a ligand field potential of the form[16]

$$V(C_{4v}) = A_{20}Y_{20}r^2 + [A_{40}Y_{40} + A_{44}Y_{44}$$
$$+ A_{4-4}Y_{4-4}]r^4 \tag{a}$$

where

$$A_{nm} = \frac{4\pi}{2n+1}(-1)^m \sum_i Z_i R_i^{-n-1} Y_{n-m}(\theta_i, \phi_i) \tag{b}$$

and $Y_{nm}(\theta, \phi)$ is a spherical harmonics in the usual sense. The sum in eq b must be performed over the ligand positions and, in our case, the X ion occupies the $(R_X, \theta = 0°, \phi = 0°)$ position coordinates in reference to the central metal ion. On the other hand, the five CN^- ions are located at the same R distance from the metal ion but with different (θ, ϕ) orientations to occupy the octahedral positions. Thus, A_{40}, A_{44} and A_{4-4} can be written

$$A_{40} = \sqrt{\frac{4\pi}{9}}\frac{1}{8}\left[8\frac{Z_x}{R_x^5} + 20\frac{Z_{cn}}{R_{cn}^5}\right] \tag{c}$$

$$A_{44} = A_{4-4} = \sqrt{\frac{7}{10}}\left[A_{40} - \sqrt{\frac{4\pi}{9}}\frac{Z_x}{R_x^5}\right] \tag{d}$$

Now we have to specify the $^3A_2$ and the ^3E_a state function components of the $^3T_{1g}$ state of the parent compound. The equivalence between electrons and holes for the d^6 electron system allow us to write[16]

$$|^3A_2\rangle = |\theta^2 \epsilon^+ \zeta^+\rangle$$

$$|^3E_a\rangle = -\frac{1}{2}|\theta^2 \epsilon^+ \eta^+\rangle + \frac{\sqrt{3}}{2}|\theta^+ \epsilon^2 \eta^+\rangle \tag{e}$$

and for the ground state

$$|^1A_1\rangle = |\theta^2 \epsilon^2\rangle \tag{f}$$

The expectation values of $V(C_{4v})$ over the wave functions given in eq e and f yield the ligand field contributions E' to the energies of the triplet states (referred to the $^1A_1$ ground state) as

$$E'(^3E_a) = \frac{1}{2}\sqrt{\frac{9}{4\pi}}A_{40}\langle r^4\rangle - \frac{1}{12}\frac{Z_x}{R_x^5}\langle r^4\rangle$$

and

$$E'(^3A_2) = \frac{2}{3}\sqrt{\frac{9}{4\pi}}A_{40}\langle r^4\rangle - \frac{2}{3}\frac{Z_x}{R_x^5}\langle r^4\rangle \tag{g}$$

The substitution of A_{40} by eq c and $\Delta = 5Z_{cn}\langle r^4\rangle/3R_{cn}^5$ for the parent compound yield

$$E'(^3E_a) = \frac{3}{4}\Delta + \frac{5}{12}\frac{Z_x}{R_x^5}\langle r^4\rangle \tag{h}$$

and

$$E'(^3A_2) = \Delta$$

which, together with the interelectronic repulsion parameter C, are written in eq 4 and 3, respectively. Finally, eq 1 and 2 for the singlet excited states are obtained in a similar manner.

References and Notes

(1) M. Mingardi and G. B. Porter, *J. Chem. Phys.*, **44**, 4354 (1966).
(2) F. Zuloaga and M. Kasha, *Photochem. Photobiol.*, **7**, 549 (1968).
(3) K. W. Hipps and G. A. Crosby, *Inorg. Chem.*, **13**, 1543 (1974).
(4) F. Castelli and L. S. Forster, *J. Phys. Chem.*, **78**, 2122 (1974).
(5) Y. Tanabe and S. Sugano, *J. Phys. Soc. Jpn.*, **9**, 753 (1954).
(6) C. Furlani, *Coord. Chem. Rev.*, **1**, 51 (1966).
(7) D. W. Clack and W. Smith, *J. Chem. Soc., Dalton Trans.*, 2015 (1974).
(8) J. H. Bigelow, *Inorg. Syn.*, **2**, 225 (1946).
(9) A. W. Adamson, A. Chiang, and E. Zinato, *J. Am. Chem. Soc.*, **91**, 5467 (1969).
(10) J. Fujita and Y. Shimura, *Bull. Chem. Soc. Jpn.*, **36**, 1281 (1963).
(11) R. Grassi, A. Haim, and W. K. Wilmarth, *Inorg. Chem.*, **6**, 237 (1967).
(12) S. F. Pellicori, *Appl. Opt.*, **3**, 361 (1964).
(13) V. M. Miskowski and H. B. Gray, *Inorg. Chem.*, **14**, 401 (1975).
(14) R. A. D. Wentworth and T. S. Piper, *Inorg. Chem.*, **4**, 709 (1965).
(15) E. I. Solomon and C. J. Ballhausen, *Mol. Phys.*, **29**, 279 (1975).
(16) H. Watanabe, "Operator Methods in Ligand Field Theory", Prentice-Hall Englewood Cliffs, N.J., 1966.

Electronic Spectra and Solvatochromism of the p-Polyphenylyltropylium Ions and a Comparative Study of the Cyclopropyltropylium Ion

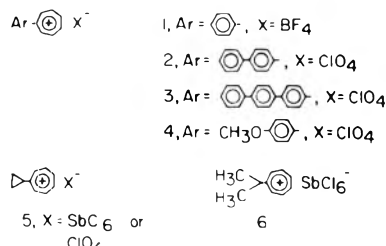## M. A. Battiste, M. W. Couch,* and R. Rehberg

Departments of Chemistry and Radiology, University of Florida, Gainesville, Florida 32610 (Received June 21, 1976)

Publication costs assisted by the Department of Radiology, University of Florida

Three p-polyphenylyltropylium salts (phenyltropylium fluoroborate (1), p-biphenylyltropylium perchlorate (2), and p-terphenylyltropylium (3)) were prepared and their electronic spectra examined in several solvents. A bathochromic shift of the long wavelength maximum arose in this series upon successive addition of p-phenyl groups to the tropylium cation residue. This shift, which was markedly solvatochromic, was attributed to an aryl substituent-to-tropylium ion ring intramolecular charge-transfer transition. The tropylium ion was shown to be a superior probe of the electron donor properties of the cyclopropyl ring in cyclopropyltropylium hexachloroantimonate (5).

Introduction

In connection with earlier attempts to determine the efficacy of the tropylium ion as a sensitive intramolecular probe of electronic donor properties of an attached substituent in monosubstituted tropylium ions we prepared and examined the electronic spectra of the p-polyphenylyltropylium ion salts phenyltropylium tetrafluoroborate (1), p-biphenylyltropylium perchlorate (2),

$$Ar \text{-} \textcircled{\oplus}\ X^-$$

1, Ar = phenyl, X = BF_4
2, Ar = biphenylyl, X = ClO_4
3, Ar = terphenylyl, X = ClO_4
4, Ar = CH_3O-phenyl, X = ClO_4

$$\triangleright \text{-} \textcircled{\oplus}\ X^-$$

5, X = SbCl$_6$ or ClO$_4$

$$\begin{array}{c} H_3C \\ H_3C \end{array}\text{>-}\textcircled{\oplus}\ SbCl_6^-$$

6

and p-terphenylyltropylium perchlorate (3). In this series the successive addition of p-phenyl groups to the tropylium residue produced the expected bathochromic shift of the long-wavelength maximum, this band extending into the visible region of the spectrum in 2 and 3. On the basis of theoretical considerations[1,2] and the effect of substituents on the position and intensity of the long-wavelength band, this band has been attributed to an aryl substituent-to-tropylium ring intramolecular charge-transfer transition by us[3] and others.[4] Both Harmon's recent disclosure of previously unpublished data from Dauben's laboratory[4] and our observations on the isoelectronic relationship of the p-polyphenylyltropylium series to the classic p-polyphenyl series prompted us to describe in full our spectral results for the series 1-3 including a study of their solvatochromic behavior. In addition we provide an illustration of the utility of the tropylium cation as a superior probe of the electron donor properties of the cyclopropyl ring in the cyclopropyltropylium ion (5).

Experimental Section

Synthesis of the p-polyphenylyltropylium ions involves the preparation of the 7-monoaryltropilidene from the corresponding aryllithium reagent and tropylium fluoroborate, thermal isomerization to the 3 isomer, and finally hydride abstraction from the 3-monoaryltropilidene by means of trityl fluoroborate (to give 1) or perchlorate (to give 2, 3, and 4).[5-10] Salts 1, 2, and 4 have been previously synthesized.[5] p-Terphenylyltropylium, prepared in three steps from p-terphenyl-4-yllithium[11] and tropylium

TABLE I: Proton Chemical Shifts for Some Tropylium Cations

Cation (solvent)	Ring protons[a] Tropylium	Ring protons[a] Aryl	Alkyl protons[a]
Tropylium[e]	9.2		
1[b](CH$_3$CN)	9.15	7.86	
		7.68	
2[c](CF$_3$COOH)	9.02	7.79	
		7.43	
3[c,d](CF$_3$COOH)	~8.6	7.69	
		7.53	
		7.31	
5, X = SbCl$_6^-$ (CD$_3$CN)	8.89		2.55 (αCH)
			1.87 (βCH)
			1.55 (βCH)
6, X = SbCl$_6^-$ (CD$_3$CN)	9.2		3.65 (CH)
			1.56 (CH$_3$)

[a] In ppm downfield from TMS. [b] Tetramethylsilane as external standard. [c] Tetramethylammonium fluoroborate as internal standard. [d] Tropylium proton signal partially masked by solvent. [e] Reference 16.

fluoroborate, was obtained in approximately 80% overall yield, mp 279-282 °C (dec). Anal. Calcd. for $C_{25}H_{19}ClO_4$: C, 71.68; H, 4.57; Cl, 8.46. Found: C, 71.47; H, 4.77; Cl, 8.25.

Additional proof of structures 1-3 was afforded by the reaction of the monoaryltropylium ions with hydrogen peroxide to give the corresponding monoarylbenzenes.[5,7] Thus 1, 2, and 3 gave biphenyl, p-terphenyl, and p-quarterphenyl, respectively.

Cyclopropyltropylium hexachloroantimonate (5, X = SbCl$_6^-$) (mp 123 °C. Anal. Calcd. for $C_{10}H_{11}SbCl_6$: C, 25.79; H, 2.38. Found: C, 25.68; H, 2.40.) and the less stable perchlorate (5, X = ClO$_4^-$), mp 82 °C, were prepared by treatment of 7-cyclopropyltropilidene[12] (synthesized by the reaction of cyclopropyl magnesium bromide[13] with 7-tropyl ethyl ether[14]) with trityl hexachloroantimonate[15] and trityl perchlorate,[6] respectively. The corresponding isopropyltropylium hexachloroantimonate (5), mp 112 °C, was prepared in a similar manner.

Results and Discussion

In the NMR spectra of 1, 2, and 3 (Table I), the tropylium protons appeared in the same region as the unsubstituted ion. The 1.90-ppm downfield shift for the unsubstituted tropylium ion with respect to benzene has been attributed to decreased electron density at the in-

TABLE II: Ultraviolet Absorption Maxima (nm) of Monoaryl and Monoalkyl Tropylium Ions in Various Solvents[a]

R-⊕

Tropylium salt	CH₃CN	CH₂Cl₂	CHCl₃	CF₃COOH
1	367(17 600)	387(18 100)	384[b]	386(15 800)
	269(15 700)	274(13 100)		270(9500)
	231[c]	232[c]	237[b]	
2	414(14 200)	449(14 800)[d]	442[b]	448(21 100)
	275(sh 7950)			
	247(16 000)	257(14 800)[d]	260[b]	258(29 700)
3	432(17 400)	~483-490[b,c]	473[b]	480[b]
	273(28 100)	282[b]	283[b]	275[b]
4	432.5(24 500)	463(18 700)		
	274(8700)	279(sh 3780)	457(21 800)	456(19 600)
	232[c]	238(15 700)	271(4860)	271(7400)
5	327(12 300)	335(16 600)		
	247(29 800)	254(30 900)		
6	274(14 400)	277(13 900)		
	225(32 200)	234.5(35 850)		

[a] ε values in parentheses. [b] Solute incompletely soluble in this solvent. [c] Was not accurately determined. [d] 10-cm cells used.
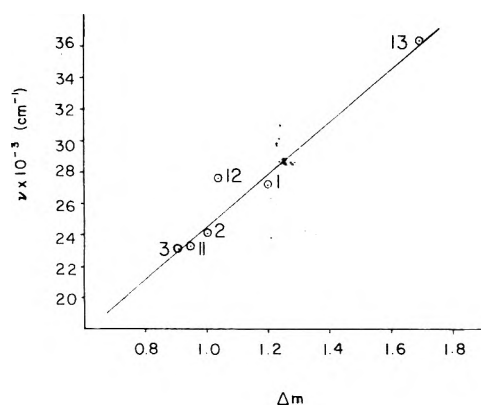

Figure 1. Observed frequencies (ν_{max}) of monoaryl tropylium ions and HMO energy differences (Δm).

dividual carbon atoms and a subsequent deshielding of the protons in the positively charged seven-membered ring.[6] Hence the slight but steady upfield shift of the tropylium protons with each additional p-phenyl group must correspond to some reduction of the positive charge in the seven-membered ring. In other words, delocalization of charge into the phenyl rings in the ground state does occur, if only to a slight extent. Similar arguments hold for cation 5 although it is clear that cyclopropyl electron release is superior to phenyl in the ground state for this cationic system. The downfield shift for the α and β protons of the cyclopropyl ring in 5 is consistent with the modest electron demands of the tropylium ring.

Electronic Spectra. The electronic spectra of the p-polyphenyltropylium carbonium ions in four solvents are summarized in Table II. As in the p-polyphenyl series,[17] the successive addition of p-phenyl groups to the tropylium system produces a bathochromic shift of the longest wavelength absorption band. A straight-line correlation is noted between the observed frequencies for the long-wavelength maxima of several tropylium salts obtained by us and other investigators,[5] and Δm (the HMO calculated energy difference (in units of β) between the highest occupied and lowest unoccupied molecular orbital).[1,18] (See Table III and Figure 1.) Similar good correlations have been observed in other homologous conjugated systems.[19] These bathochromic shifts can be attributed to an extension of the π-electron delocalization and the resultant decrease in the transition energy.

Most importantly the long wavelength charge-transfer bands for 1, 2, and 3 show marked solvatochromic be-

TABLE III: Observed Frequencies (ν), Calculated Transition Energies (Δm) of Monoaryl Tropylium Cations, and Ionization Potentials of the Donor Hydrocarbons (I_p)

Ar-⊕

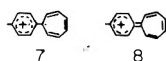| No.	Ar	ν,[a,g] cm⁻¹	Δm	I_p of ArH,[f] eV
1	C₆H₅	27 250	1.2004[b,c]	9.245
2	p-C₆H₅-C₆H₄-	24 150	1.0042[b,c]	8.27[h]
3	p-C₆H₅-C₆H₄-C₆H₄-	23 150	0.9100[c]	
4	p-CH₃O-C₆H₄-	22 990		8.20
5	Cyclopropyl	31 200		10.53[i]
6	Isopropyl	36 500		
11	2-Naphthyl	23 300	0.9464[b]	8.12
12	m-C₆H₅-C₆H₄-	27 600	1.0560[b]	8.27[h]
13	H	36 400	1.6920	
14	p-CH₃-C₆H₄-	25 450		8.82
15	p-HOC₆H₄-	22 990		8.50
16	p-FC₆H₄-	26 850		9.19
17	p-ClC₆H₄-	26 740		9.07
18	p-BrC₆H₄-	26 420		8.98

[a] Sovent: acetonitrile. [b] Reference 18. [c] Reference 1. [d] Reference 5. [e] W. von E. Doering and L. H. Knox, *J. Am. Chem. Soc.*, **76**, 3203 (1954). [f] K. Watanabe, *J. Chem. Phys.*, **26**, 542 (1957). [g] Compounds 4-11, ref 5. [h] K. Watanabe and T. Nakayamo, ASTIA Report AD-152934. [i] H. Basch, M. B. Robin, N. A. Keubler, C. Baker, and D. W. Turner, *J. Chem. Phys.*, **51**, 52 (1969).

havior, the magnitude of the bathochromic shift increasing with decreasing solvent polarity. Although a plot of Kosower's Z values,[20] a measure of solvent polarity, vs. transition energy of these maxima in three solvents shows some deviation from a straight line relationship, this plot does indicate a correlation between the magnitude of shift and solvent polarity. The solvatochromic behavior of the p-polyphenylyltropylium ions can be interpreted in the same manner as other systems such as the pyridinium cyclopentadienylium[21,22] and pyridinium phenolates[23] which also exhibit intramolecular charge-transfer transitions. The magnitude of this solvent shift is also a function of the electron donor capabilities of the substituent. Thus the shift in the long wavelength absorption bands of 1, 2, and 3 when solvent is changed from CH₃CN to CH₂Cl₂ is 20, 35, and 51 nm, respectively, the extent of electron delocalization in aryl substituents increasing in the same direction. The presence of electron-donating heteroatomic substituents also cause increased shift between solvents. For example, the p-methoxyphenyl-

tropylium cation (4) (see Table III) exhibits a shift (31 nm) which is comparable to that observed for 2.

A comparison of solvent effects of the p-polyphenylyltropylium salts with the p-polyphenyl series indicates little similarity. The solvent effects in the latter system are small and hypsochromic as contrasted with the large, bathochromic shifts in the tropylium ions, a fact consistent with the typical $\pi \rightarrow \pi^*$ transition characteristics for p-polyphenyls.

Although we have so far discussed the electronic spectra of the monoaryltropylium ions in terms of molecular orbital theory, these spectra can also be described either in terms of an electron transfer from the phenyl ring, a π-electron donor, to the seven-membered tropylium ring, a π-electron acceptor (7), or in terms of valence bond structure 8. The former viewpoint is more formalized;

7 **8**

however, either description clearly depicts the essential charge-transfer nature of the transition. We can, in fact, consider 1, 2, and 3 to be typical type III tropylium ions, their long wavelength absorption bands being attributed to substituent-to-ring charge-transfer excitation.[4] The breadth of the long-wavelength absorption bands of 1–3 also suggests a charge-transfer transition since such bands are characteristically broad.[23]

The concept of the tropylium cation acting as a π-electron acceptor is not without precedent. For example, intermolecular charge-transfer complexes have been shown to arise from interactions between the tropylium ion and various aromatic hydrocarbons.[24-27] Charge-transfer complexation between the seven-membered ring and the halide ion also occurs in solid tropylium halides and their methylene chloride solutions to give dark colors.[28] Similar interactions are also postulated to occur in the hexa- and heptaphenyltropylium halides.[29,30]

Mathematically, the energy of a charge-transfer transition can be given to the first approximation by the expression

$$E_{CT} = h\nu = I_P - E_a - C$$

where I_p is the ionization potential of the donor, E_a is the electron affinity of the acceptor, and C is the Coulombic electrostatic energy.[31] Since, in the monoaryltropylium salts, E_a remains constant and C can also be considered invariant, the frequency of the charge-transfer band (ν) should be proportional to the ionization potential of the donor. A plot of the frequency of the long-wavelength maxima observed for a variety of monoaryl tropylium salts vs. the ionization potential of the corresponding aromatic hydrocarbons gave a linear correlation. (See Table III and Figure 2.)

The deviations from this straight-line relationship can be readily explained. In the m-biphenylyltropylium salts, delocalization of the positive charge into the remote phenyl ring gives rise to a high energy structure and, as a result, the m-biphenyl group has, effectively, a lower ionization potential than does p-biphenyl and behaves more like an unsubstituted phenyl group. Phenol, as has been demonstrated in other studies, acts as a better electron donor than is indicated by its ionization potential.[32]

The results analyzed above for the monoaryltropylium ions clearly establish the tropylium ion as an effective and sensitive probe of the electron donor properties of substituents in direct conjugation with the seven-membered ring. Since the cyclopropyl ring is known to be an efficient electron donor in the ground state, it was reasoned that the tropylium ion might prove to be superior to either a
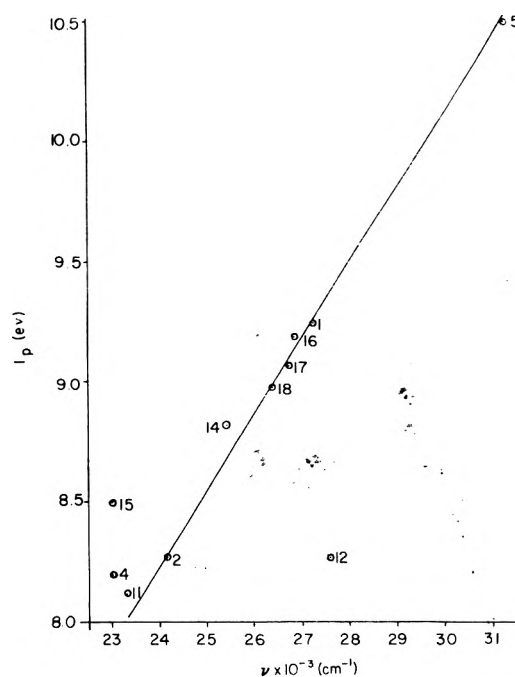

Figure 2. Observed frequencies (ν_{max}) and ionization potentials (I_p) for monoaryl tropylium ions.

benzenoid or another carbonium ion probe of the electron-donating ability of the cyclopropyl group in the excited state. Although a cation, the tropylium ion should behave more like a phenyl group than a typical carbonium ion.

Previous spectroscopic studies of phenylcyclopropanes and some related rigid model systems have established conjugative interaction between the phenyl and cyclopropyl rings,[33,34] however, the steric relationship between the two rings was originally considered to have little spectroscopic importance.[34]

More recent ultraviolet spectral studies of cyclopropyl nitroaromatics by Hahn and his co-workers[35] have shown that the latter conclusion is erroneous and probably reflects the minimal conjugative response of a cyclopropane ring to the weak electron demand of aromatic hydrocarbons.

The electronic spectral characteristics of neutral aromatic systems and the generally small (5–10 nm) bathochromic shifts induced by cyclopropyl substitution greatly hampers the further detailed study of geometric and substituent influences on cyclopropyl conjugation in the first excited state. This problem could be partly overcome by use of a positively charged chromophore, such as a carbonium ion, which elicits a much greater electronic response from the cyclopropyl ring. Thus, as previously reported by Deno and co-workers,[36] cyclopropyl substitution at the terminal carbon of an allylic cation such as 9 results in a significant bathochromic shift of λ_{max} when compared to the methyl substituted ion 10. There are, however, major disadvantages in performing spectroscopic studies on such reactive cationic species as 9 which are largely negated in stable tropylium ion salts such as 5 and 6.

9 **10**

λ_{max} 309 nm (ϵ 28,000) λ_{max} 275 nm (ϵ 11,000)

$\Delta\lambda$ (nm) 34
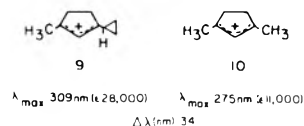
As revealed by the comparison of ions 5 and 6, in Table III, cyclopropyl substitutions of the tropylium ion produced a significantly greater bathochromic shift of the long-wavelength maxima ($\Delta\lambda^{MeCN}$ 53 nm) than did the

identical substitutions in allylic ion 9. Furthermore the shift in λ_{max} for 5 is essentially an order of magnitude greater than that observed for cyclopropyl aromatic hydrocarbons. By Harmon's designation cation 5 would be classified as a type II substituted tropylium cation displaying moderate intramolecular charge-transfer character. The somewhat greater sensitivity of λ_{max} of 5 to a change in solvent polarity (CH_3CN to CH_2Cl_2) than the isopropyl ion 6 is consistent with this interpretation.

Given the above results it would now appear that the tropylium cation should be the preferred chromophoric probe of geometric and substituent influences on cyclopropyl conjugations in the excited state. Photochemical reactions of these ions should also be of interest for future exploration.

References and Notes

(1) J. B. Williams, Ph.D. Dissertation, University of Florida, 1967.
(2) G. Hohlneicher, R. Kiessling, H. C. Jutz, and P. A. Straub, *Ber. Bensenges. Phys. Chem.*, **70**, 60 (1966).
(3) M. W. Couch, M.S. Thesis, University of Florida, 1966.
(4) K. M. Harmon, "Carbonium Ions", Vol. 4, G. A. Olah and P. von R. Schleyer, Ed., Wiley-Interscience, New York, N.Y., 1973, and references therein.
(5) C. Jutz and F. Voithenleitner, *Chem. Ber.*, **97**, 29 (1964).
(6) H. J. Dauben, L. R. Honnen, and K. M. Harmon, *J. Org. Chem.*, **25**, 1442 (1960).
(7) A. Cairncross, Ph.D. Dissertation, Yale University, 1963.
(8) A. P. terBorg and H. Kloosterziel, *Recl. Trav. Chim., Pays-Bas*, **82**, 741 (1963).
(9) A. P. terBorg, H. Kloosterziel, and N. Van Meurs, *Recl. Trav. Chim., Pays-Bas*, **82**, 717 (1963).

(10) A. P. terBorg and H. Kloosterziel, *Recl. Trav. Chim., Pays-Bas*, **84**, 241 (1965).
(11) H. Gilman and E. A. Weipert, *J. Org. Chem.*, **22**, 446 (1957).
(12) N. L. Bauld, J. D. McDermed, C. E. Hudson, Y. S. Rim, J. Zoeller, Jr., R. D. Gordon, and J. S. Hyde, *J. Am. Chem. Soc.*, **91**, 6666 (1969); these authors also report the preparation of cyclopropyltropylium fluoroborate (5, X = BF_4^-) and NMR spectrum (D_2O) but do not comment further on the spectral properties of the cation.
(13) M. Hanack and H. Eggensperger, *Annales*, **663**, 31 (1963).
(14) K. Conrow, *J. Am. Chem. Soc.*, **83**, 2343 (1961).
(15) D. W. A. Sharp and N. Sheppard, *J. Chem. Soc.*, 674 (1957).
(16) G. Fraenkel, R. E. Carter, A. McLachlan, and J. H. Richards, *J. Am. Chem. Soc.*, **82**, 5846 (1960).
(17) A. E. Gillam and D. H. Hey, *J. Chem. Soc.*, 1170 (1939).
(18) G. V. Boyd and N. Singer, *Tetrahedron*, **22**, 547 (1966).
(19) A. Streitweiser, Jr., "Molecular Orbital Theory for Organic Chemists", Wiley, New York, N.Y., 1961.
(20) E. M. Kosower, *J. Am. Chem. Soc.*, **80**, 3253 (1958).
(21) D. Lloyd and J. S. Sneezum, *Tetrahedron*, **3**, 334 (1958).
(22) E. M. Kosower and P. E. Klinedenst, Jr., *J. Am. Chem. Soc.*, **78**, 3493 (1956).
(23) G. Briegleb, "Elektronen-Donator-Acceptor-Komplexe", Springer-Verlag, Berlin, 1961.
(24) M. Feldman and S. Winstein, *J. Am. Chem. Soc.*, **83**, 3338 (1961).
(25) M. Feldman and S. Winstein, *Tetrahedron Lett.*, 853 (1962).
(26) M. Feldman and S. Winstein, *Theor. Chem. Acta*, **10**, 86 (1968).
(27) H. J. Dauben, Jr., and J. D. Wilson, *Chem. Commun.*, 1629 (1968).
(28) K. Harmon, F. E. Cummings, D. A. Davis, and D. J. Diestler, *J. Am. Chem. Soc.*, **84**, 3349 (1962).
(29) M. A. Battiste, *J. Am. Chem. Soc.*, **83**, 4101 (1961).
(30) T. Barton, Ph.D. Dissertation, University of Florida, 1967.
(31) J. N. Murrell, *Quart. R. Chem. Soc. (London)*, **15**, 191 (1961).
(32) H. H. Jaffee and N. Orchen, "Theories and Applications of Ultraviolet Spectroscopy", Wiley, New York, N.Y., 1962.
(33) M. T. Rogers, *J. Am. Chem. Soc.*, **69**, 2544 (1947).
(34) A. L. Goodman and R. H. Eastman, *J. Am. Chem. Soc.*, **86**, 908 (1964).
(35) R. C. Hahn, P. H. Howard, S. M. Kong, G. A. Lorenzo, and N. L. Miller, *J. Am. Chem. Soc.*, **91**, 3558 (1969); R. C. Hahn, P. H. Howard, and G. A. Lorenzo, *J. Am. Chem. Soc.*, **93**, 5816 (1971).
(36) N. C. Deno, H. G. Richey, Jr., J. S. Liu, D. N. Lincoln, and J. O. Turner, *J. Am. Chem. Soc.*, **87**, 4533 (1965).

Infrared Spectra of Tl⁺NO₃⁻ Ion Pairs Variably Hydrated or Ammoniated in an Argon Matrix

G. Ritzhaupt and J. P. Devlin*

Department of Chemistry, Oklahoma State University, Stillwater, Oklahoma 74074 (Received May 20, 1976; Revised Manuscript Received November 8, 1976)

The vapor phase ion pairs, $Tl^+NO_3^-$, have been isolated in argon matrices containing varying amounts of water or ammonia. The infrared spectra for these systems show quite clearly the effect of stepwise coordination of the Tl^+ ion by the solvent molecules. In particular, the splitting of the degenerate $\nu_3(e)$ nitrate mode, which is 275 cm⁻¹ for a pure argon matrix, is reduced in rather obvious steps to the limiting values of 53 and 18 cm⁻¹ for the contact ion pairs in pure glassy H_2O and NH_3, respectively. The manner in which this splitting collapses is markedly different from the smooth reduction reported previously for $Li^+NO_3^-$ and this contrasting behavior is analyzed in terms of the more covalent character of the bonding of Tl^+ to NO_3^-, together with an apparent tendency for the Tl^+ to move to the "roll on" position as it becomes solvated.

Introduction

Several recent papers have emphasized that the volatility of polyatomic anion salts of the alkali metals, in particular the nitrates, chlorates, and perchlorates, makes it possible to position the corresponding ion pairs in a great range of environments for spectroscopic study.[1] In particular data have been reported for ion pairs isolated in argon matrices and variably solvated in argon matrices containing water or ammonia.[1c] Like the alkali metal nitrates, thallium nitrate is known to volatilize associatively

so the vapor phase ion pairs, $Tl^+NO_3^-$, are readily condensed for matrix isolation spectroscopic measurements.[1a,d] Thus, the ion pair vibrational spectrum has been reported for pure argon matrices with the most notable feature being the unusually strong distortion of the NO_3^- ion as reflected in the magnitude of the $\nu_3(e)$ doublet splitting.[1a] This splitting (275 cm⁻¹) indicated that, although Tl^+ resembles the K^+ ion in size, the thallium cation is as effective as the much smaller Li^+ ion in distorting the nitrate anion and, further, that the Tl^+--NO_3^- interaction

must be through the oxygen atom(s).

The large $\nu_3(e)$ splitting led to the suggestion that the $Tl^+NO_3^-$ bonding includes a sizeable ($\sim 50\%$) covalent component between the ions. However, Brooker and Bredig subsequently argued that, provided the Tl^+ polarizing power is properly evaluated, the splitting can be understood in terms of cation polarization of the anion.[2]

Though $TlNO_3$ has been the subject of several molten phase Raman studies,[3-5] solution phase data are quite limited. However, Gardiner et al. have recently concluded from a Raman investigation that Tl^+ in an NH_3 solution associates with NO_3^- via interaction with the $NO_3^- \pi$-electron cloud.[6] The contact ion pair is believed to maintain a basically C_{3v} symmetry so that, though the interaction may be strong, the nitrate degenerate modes are not split substantially. This argument reopens questions regarding the general importance of covalent contributions to the cation–anion interaction. Since $TlNO_3$ is readily volatilized and information about cation–anion interaction for different stages of ion solvation can be obtained from the vibrational spectra of contact ion pairs isolated in either pure glassy solvents or mixtures of the solvents with argon, the spectra for $Tl^+NO_3^-$ variably solvated with H_2O or NH_3 in argon matrices have been measured with the particular objectives of (a) noting any evidence of covalency in the ion-pair interaction and (b) determining whether or not the matrix data support the specific idea of a C_{3v} complex with π bonding of the Tl^+ with the NO_3^-, particularly for matrices rich in NH_3.

Experimental Section

Thallium nitrate was vaporized from the melt in resistance heated pyrex glass Knudsen cells at temperatures in the 250 °C range. The matrix gases, argon containing a range of NH_3 and H_2O mole percentages, were metered through a Fisher-Porter 1/16 in. glass flowmeter and cocondensed with the $TlNO_3$ molecular beam within a standard low-temperature infrared cell adapted to an Air Products CS-202, closed-cycle helium refrigerator. Matrix to sample ratios necessary for complete isolation of the ion pairs were established for the pure argon matrix. The same cell temperature and matrix gas flow rates were then employed throughout this study. The infrared spectra were recorded in the 600–4000 cm^{-1} range using a Beckman IR-7 infrared spectrometer.

Results and Discussion

Variation of $\Delta\nu_3$. Though absorption bands for each of the nitrate ion fundamentals have been observed for many of the samples only the intense $\nu_3(e)$ doublet has been apparent in all cases, since strong H_2O and NH_3 absorptions otherwise interfere. Fortunately it is this doublet that is most sensitive to anion distortion so the interference from solvent bands has not been a serious problem. The emphasis here will be on the appearance of this ν_3 doublet as a function of matrix composition. Thus, Figure 1 shows how the $\nu_3(e)$ band system changes from the 275-cm^{-1} doublet splitting ($\Delta\nu_3$) to a doublet spacing of 53 cm^{-1} as the matrix composition is varied from pure argon to pure H_2O. The series of bands shows quite clearly the stepwise hydration of the Tl^+ ion, which proceeds rapidly in the 3–12% H_2O range. As in the case of the alkali metal nitrate ion pairs, the extent of cation solvation is markedly greater for a given H_2O percentage than predicted statistically, apparently because the surface mobility of the matrix, as it forms, permits the water and ion pairs to move about and preferentially associate with one another. Since the H_2O is the more mobile species, the extent of ion pair hydration, for a given matrix composition, is assumed to
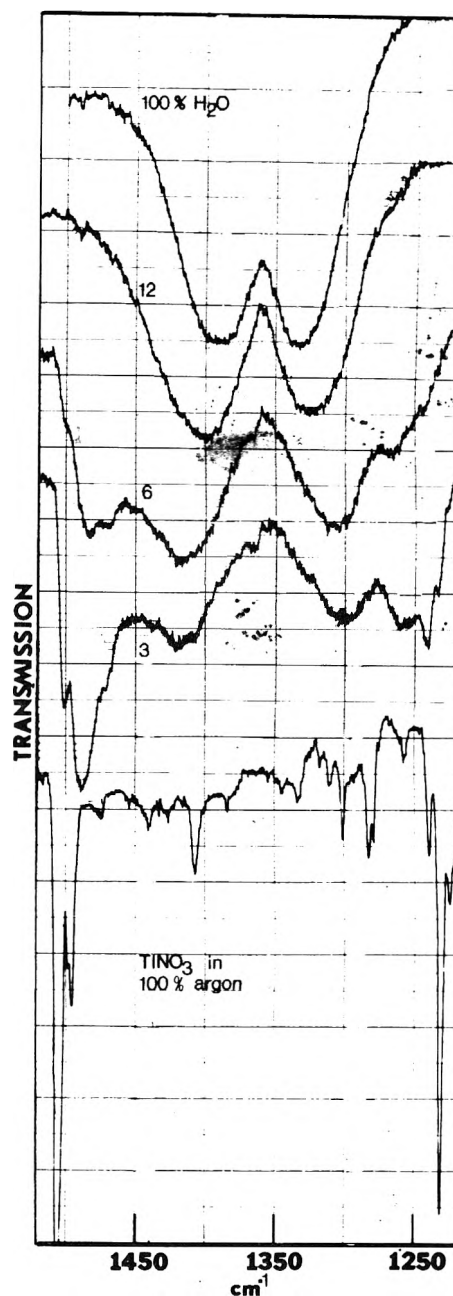

Figure 1. Infrared bands for the ν_3 nitrate mode for $Tl^+NO_3^-$ ion pairs isolated in matrices with composition varying from pure argon to pure H_2O. The numbers indicate the percent H_2O in the matrices.

be the same for all ion pairs regardless of the cation involved.

It is clear from Figure 1 that one water, coordinated to Tl^+, reduces the splitting from 275 to 233 cm^{-1}, as broad dominant bands appear at 1255 and 1488 cm^{-1} in the 3% sample. In the 6% sample a new species, most probably the ion pair with the Tl^+ doubly hydrated, is dominant with a $\Delta\nu_3$ value of 110 cm^{-1} and band positions at 1307 and 1417 cm^{-1}. Shoulders at 1325 and 1400 cm^{-1} in the 6% sample become the major bands in the 12% case with $\Delta\nu_3$ only 75 cm^{-1}, apparently corresponding to the triply hydrated Tl^+ ion pair. There can be little doubt about the assignment for the singly hydrated pair, since the sharp features of the completely argon isolated ion pair are also apparent in the 3% sample spectrum, but the precise degree of solvation becomes less certain at higher H_2O concentrations.

The remarkable feature in the stepwise hydration of the $Tl^+NO_3^-$ pair is the very small effect of the first H_2O
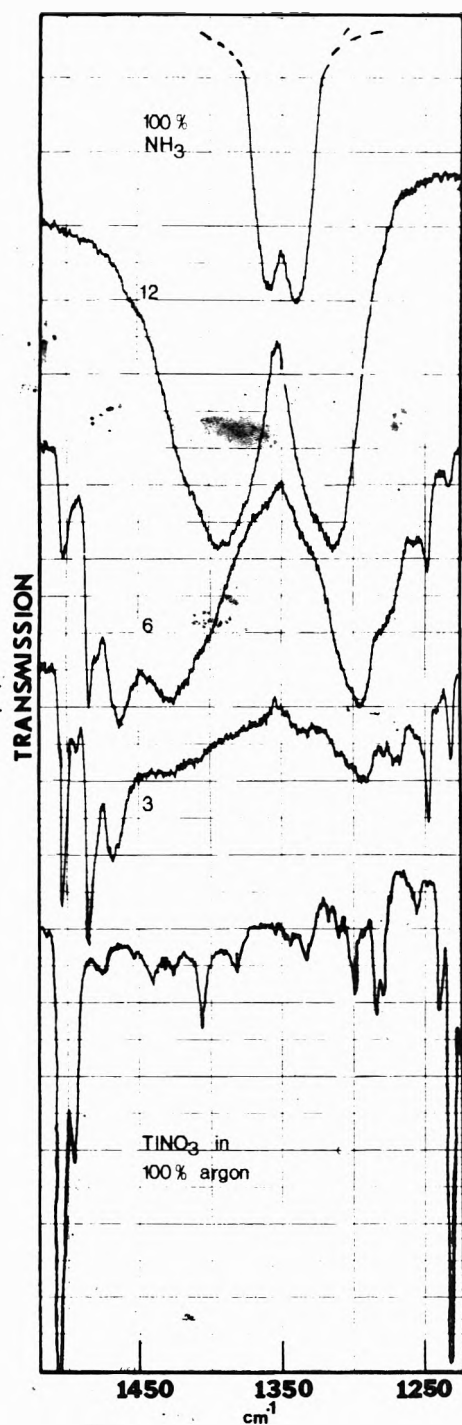
Figure 2. Infrared bands for the ν_3 nitrate mode for Tl⁺NO₃⁻ ion pairs isolated in matrices with composition varying from pure argon to pure NH₃. The numbers indicate the percent NH₃ in the matrices.

TABLE I: Peak Maxima in cm⁻¹ for the Dominant Fundamental Band Components, as well as $\Delta \nu_3$ Values, for Tl·NO₃⁻ Ion Pairs in Mixed Argon–Water Matrices

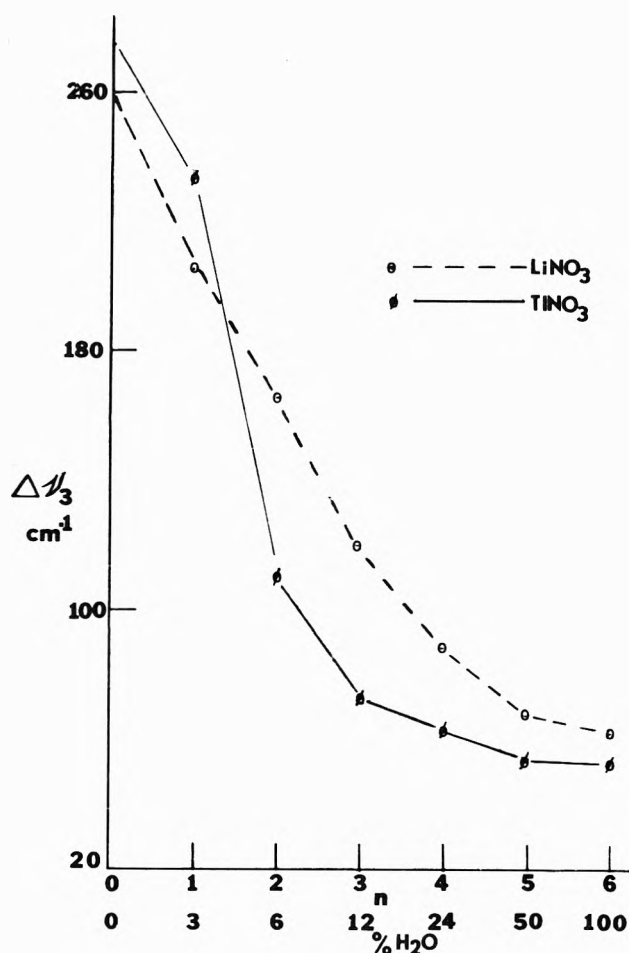|	Argon	3% H₂O	6% H₂O	12% H₂O	25% H₂O	50% H₂O	H₂O
ν_{3a}	1232	1255	1307	1325	1330	1333	1335
ν_{3b}	1507	1488	1417	1400	1396	1386	1388
$\Delta \nu_3$	275	233	110	75	66	53	53
ν_1	1012	1014	1025	1032	1033	1038	1038
ν_2	808	815	817	820			
ν_{4a}	720	718	720				
ν_{4b}	727						

Figure 3. Variation in the value of $\Delta \nu_3$, the splitting of the ν_3 doublet, for the dominant infrared features of Tl⁺NO₃⁻ and Li⁺NO₃⁻ as a function of matrix composition.

coordinated to Tl⁺ and the dramatic effect of the second water of hydration. These features will be related to the corresponding behavior of alkali metal nitrate ion pairs during stepwise hydration after we first examine the ammoniation of the Tl⁺NO₃⁻. Figure 2 displays the progressive reduction of the $\Delta \nu_3$ value as NH₃ is coordinated in a stepwise manner to the Tl⁺ ion. Since the nitrate ion is little distorted through solvation by NH₃,[1c,7-9] the ultimate reduction in $\Delta \nu_3$ is to 18 cm⁻¹ rather than the 53-cm⁻¹ value for the pure H₂O matrix. It is likely that both the 18-cm⁻¹ splitting for pure NH₃ and the 53 cm⁻¹ for pure glassy H₂O reflect strictly solvent distortion of the nitrate ion but, as has been established for other ion pairs,[1c] the Tl⁺ remains in contact with the nitrate as is clear from the absolute frequencies of the ν_{3a} and ν_{3b} bands. These

average considerably (>10 cm⁻¹) lower than for Li⁺NO₃⁻ or K⁺NO₃⁻ in a manner reminiscent of the pure crystalline and liquid phases of TlNO₃.

The manner in which $\Delta \nu_3$ varies with Tl⁺ ammoniation is clear from Table I which also includes the measured values for the nitrate fundamentals for all cases considered in this paper. A remarkable difference between the H₂O and NH₃ effect is revealed. After two NH₃ molecules have coordinated to Tl⁺, the splitting ($\Delta \nu_3$) is still very large (200 cm⁻¹), but the third and fourth NH₃ molecules have an amplified effect as the splitting drops to 77 cm⁻¹.

There are some interesting and undoubtedly significant differences between the response of the Tl⁺NO₃⁻ $\Delta \nu_3$ value to solvation by NH₃ and H₂O compared to what has been reported for the alkali metal nitrate ion pairs. It has been shown that there is relatively steady decrease in $\Delta \nu_3$ for Li⁺NO₃⁻ during stepwise hydration (Figure 3) with the effect of water of coordination slowly attenuated by the

presence of other coordinated H_2O molecules. By comparison, the influence of successive H_2O coordination on the $\Delta\nu_3$ value for $Tl^+NO_3^-$, the stepwise character of which is perhaps even more apparent than for Li^+NO_3, is much less regular. The plot of $\Delta\nu_3$ vs. the extent of Tl^+ hydration (Figure 3) shows that most of the reduction occurs in a single step apparently associated with coordination of the second water by the Tl^+ while the first water of hydration has a smaller influence in the thallium case than for $Li^+NO_3^-$. On the other hand, the effect of additional water molecules on the $\Delta\nu_3$ value is sufficient to indicate that the Tl^+ retains contact with the NO_3^-. As mentioned this is also indicated by the lower than usual absolute frequencies of the ν_{3a} and ν_{3b} components in the pure H_2O matrix. The completely hydrated NO_3^- ion, with no contacting cation, has component values of 1347 and 1395 cm^{-1} [10] compared to the hydrated $Tl^+NO_3^-$ ion pair values of 1335 and 1388 cm^{-1} (Table I).

A tentative explanation of the hydration (ammoniation) effect on the $\Delta\nu_3$ value of $Tl^+NO_3^-$ can be given in terms of the two previously published suggestions: (1) the ion pair association has a strong covalent component[1c] and (2) at some point in the solvation of the Tl^+ ion the NO_3^- ion moves into the roll-on position for which the $\Delta\nu_3$ value for anion distortion by the cation, because of the approach of the structure to a C_{3v} symmetry, is markedly reduced.[6] Because the covalent component of the Tl^+--NO_3^- interaction is relatively insensitive to reduction of the effective cation charge that results from hydration, the first H_2O of hydration (and the first two NH_3 molecules coordinated) has only a minor effect on $\Delta\nu_3$, the association being reflected primarily by the broadening of the ν_{3a} and ν_{3b} components, an effect characteristic of hydration of ion pairs. As the NO_3^- ion moves into the roll-on position, simultaneously with the coordination of a second H_2O molecule, the $\Delta\nu_3$ value drops from a magnitude greater than the corresponding value for $Li^+NO_3^-$ to a value (110 cm^{-1}) much lower than the corresponding 168 cm^{-1} reported for $Li^+NO_3^-$ (Figure 3). At this point, because of the new geometry, the $\Delta\nu_3$ value loses its usual significance as a measure of the cation–anion interaction strength. An extension of this analysis would suggest that, though the geometry of the Tl^+--NO_3^- pair is altered, the covalent interaction may remain relatively strong even as additional H_2O molecules are bound to the Tl^+ but $\Delta\nu_3$ only weakly reflects the more symmetric distortion of the NO_3^- ion.

The same viewpoint can apparently be applied to understanding the variation of $\Delta\nu_3$ of $Tl^+NO_3^-$ during ammoniation (Figure 2), except that neither the first nor second NH_3 of solvation has a great impact on the nature of the Tl^+--NO_3^- interaction. Again, because of the large covalent component, this interaction is relatively insensitive to diffusion of the Tl^+ charge density that accompanies ammoniation. However, the third NH_3 of solvation apparently promotes movement of the NO_3^- ion into the roll-on position. The sizeable drop in $\Delta\nu_3$ with subsequent ammoniation steps would then reflect both further diffusion of the Tl^+ charge, an effect that dominates the alkali metal solvation process, and further movement of the Tl^+--NO_3^- interaction toward the "C_{3v}" structure proposed by Gardiner et al.[6] In the limit of a pure NH_3 matrix, the NO_3^- $\Delta\nu_3$ splitting is much less than for $Li^+NO_3^-$ despite the fact that for isolation in pure argon the $Tl^+NO_3^-$ splitting exceeds that for $Li^+NO_3^-$ by 15 cm^{-1}. Some quite different effect of solvation is apparent and the foregoing is merely one reasonable explanation that is consistent with the data as well as previous thoughts on $Tl^+NO_3^-$ ion pairing.
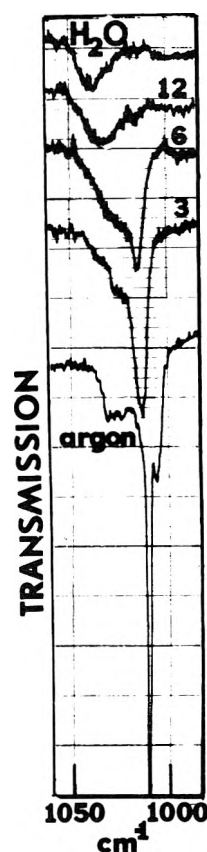
Figure 4. Variation in the ν_1 nitrate infrared band as a function of matrix composition. The numbers represent the percent H_2O in the matrices.

It should be noted that the plot of the $Li^+NO_3^-$ data (Figure 3) is somewhat different than presented in the original paper[1c] but reflects the current judgement that the first significant reduction in $\Delta\nu_3$ when H_2O is added to the argon matrix, and which is apparent in Figure 5 of ref 1c, is the result of the first water of hydration on the Li^+, rather than outer-shell water molecules as was previously speculated. This judgement reflects the fact that at the corresponding NH_3 and H_2O percentage composition (3%) the Tl^+ ion apparently has one coordinated solvent molecule, judging from the broad character of the ν_3 components, particularly for the H_2O case. Also, the results of an unpublished GAUSSIAN 70 molecular orbital calculation for $Li^+NO_3^-$ indicate that the reduction in the NO_3^- ion distortion which accompanies the first hydration step is considerably less than the earlier assignment would require.[11] Since Li^+ is supposedly limited to five coordination, the significance of n greater than four in Figure 3 is not clear.

Nitrate ν_1, ν_2, and ν_4 Bands. In principle the behavior of the ν_4(e) nitrate bending mode as a function of extent of cation solvation is as interesting as the response of $\Delta\nu_3$ considered above. Unfortunately, despite the apparently strong distortion of the NO_3^- ion by a Tl^+ cation it is not possible to firmly identify more than one ν_4 component for most environments of the $Tl^+NO_3^-$ ion pair. From Tables I and II which include the frequencies for the NO_3^- fundamentals, it is clear that is some cases more than a single feature appears in the ν_4 region, but the spacing is invariably small and the multiple features may arise from the different degrees of cation solvation within the same sample. Even $Tl^+NO_3^-$ isolated in pure argon has only a single intense ν_4 component (727 cm^{-1}) though a very weak feature at 720 cm^{-1} has been tentatively assigned as ν_{4a}.

Briefly stated, ν_1 and ν_2 increase in frequency as the Tl^+ cation is solvated while ν_4 decreases but less markedly. The

TABLE II: Peak Maxima in cm^{-1} for the Dominant Fundamental Band Components, as well as $\Delta\nu_3$ Values, for Tl$^+$NO$_3^-$ Ion Pairs in Mixed Argon-Ammonia Matrices

	Ar-gon	3% NH$_3$	6%^{a} NH$_3$	12% NH$_3$	25% NH$_3$	50% NH$_3$	NH$_3$
ν_{3a}	1232	1247	1268	1295	1315	1332	1337	1340
ν_{3b}	1507	1485	1468	1428	1392	1377	1370	1358
$\Delta\nu_3$	275	238	200	133	77	45	33	18
ν_2	808	816	821		823	823	825	827
ν_{4a}	720	718	717		717	715	715	
ν_{4b}	727	721	721					

^{a} 6% NH$_3$ sample shows $n = 2$ and $n = 3$ cases with comparable intensities.

behavior of ν_1 as depicted in Figure 4 seems most compatible with the variation in $\Delta\nu_3$ discussed in the previous section. That is, the first H$_2$O of hydration has little effect (2 cm^{-1} shift) but the ν_1 band shifts 11 cm^{-1} from 1014 to 1025 cm^{-1} with the second H$_2$O of hydration, and eventually moves to 1038 cm^{-1} for the pure glassy H$_2$O matrix. By contrast, but for no obvious reason, much of the ν_2 shift occurs for single hydration. The behavior of ν_1 during ammoniation is obscured by the ν_2 NH$_3$ band, but the ν_2 nitrate band behaves very similarly as during the hydration of Tl$^+$NO$_3^-$. A review of the new data and that from previous H$_2$O and NH$_3$ matrix work suggests that, with the

exception of ν_{3a} and ν_{3b}, the nitrate fundamental frequencies for the different ion pairs M$^+$NO$_3^-$ all converge on nearly the same values as the cation coordination is saturated with NH$_3$ or H$_2$O. These values are ν_1, 1038; ν_2, 828; ν_4, 715 cm^{-1}.

References and Notes

(1) See, for example, (a) D. Smith, D. W. James, and J. P. Devlin, *J. Chem. Phys.*, **54**, 4437 (1971); (b) N. Smyrl and J. P. Devlin, *J. Phys. Chem.*, **77**, 3067 (1973); (c) G. Ritzhaupt and J. P. Devlin, *ibid.*, **79**, 2265 (1975); (d) A. A. Ishchenko, V. P. Spiridonov, and E. Z. Zasorin, *Zh. Strukt. Khim.*, **15**, 300 (1974).
(2) M. H. Brooker and M. A. Bredig, *J. Chem. Phys.*, **58**, 5319 (1973).
(3) D. W. James and W. H. Leong, *Trans. Faraday Soc.*, **66**, 1948 (1970).
(4) D. W. James, R. D. Carlisle, and W. H. Leong, *Aust. J. Chem.*, **23**, 1779 (1970).
(5) D. W. James and J. P. Devlin, *Aust. J. Chem.*, **24**, 743 (1971).
(6) D. J. Gardiner, A. H. Haji, and B. P. Straughan, *J. Chem. Soc., Faraday Trans.*, **72**, 93 (1976).
(7) D. J. Gardiner, R. E. Hester, and W. E. L. Grossman, *J. Chem. Phys.*, **59**, 175 (1973).
(8) J. W. Lundeen and R. S. Tobias, *J. Chem. Phys.*, **63**, 924 (1975).
(9) A. T. Lemley and J. J. Lagowski, *J. Phys. Chem.*, **78**, 708 (1974).
(10) (a) D. E. Irish and A. R. Davis, *Can. J. Chem.*, **46**, 943 (1968); (b) D. J. Lockwood, *J. Chem. Soc., Faraday Trans. 2*, **71**, 1440 (1975).
(11) J. C. Moore, private communication.
(12) E. J. Sutter, D. M. Updegrove, and J. F. Harmon, *Chem. Phys. Lett.*, **36**, 49 (1975).

Rotational Barriers in the Cation Radicals of 4,4′-Dimethoxybiphenyl and 4,4′-Dihydroxybiphenyl

Paul D. Sullivan* and Joseph Y. Fong

Department of Chemistry, Ohio University, Athens, Ohio 45701 (Received July 8, 1976)

The temperature dependent ESR spectra of 4,4′-dimethoxybiphenyl (DMBP) and 4,4′-dihydroxybiphenyl (DHBP) cation radicals have been interpreted in terms of a four-jump exchange model due to restricted rotation of the alkoxyl groups. Activation barriers of 8.46 ± 0.50 kcal/mol for DMBP$^+$ and 7.31 ± 0.35 kcal/mol for DHBP$^+$ have been obtained. The INDO calculated barrier to rotation about the C–O bond for DHBP$^+$ is 7.6 kcal/mol. The existence of cis-trans isomers for 3,3′-dimethyl-4,4′-dihydroxybiphenyl cation radical provides further evidence that the rotational barrier about the 1–1′ bond in these biphenyl cation radicals is certainly >10 kcal/mol. These results support the general conclusion that the 1–1′ rotational barrier in biphenyl radical ions is generally much larger than that in their neutral counterparts.

Introduction

The cation radical of 4,4′-dimethoxybiphenyl (DMBP) has been the topic of several previous ESR investigations. The spectrum was first observed by Buck, Bloemhoff, and Oosterhoff[1] and later by Allara, Gilbert, and Norman.[2] The occurrence of cis-trans isomers at low temperatures was first reported by Forbes and Sullivan[3] in AlCl$_3$–CH$_3$NO$_2$, however, it was not clear whether the cis-trans isomerization was caused by restricted rotation about the C–O bond or the 1–1′ bond. Tylli[4] reinvestigated DMBP$^+$ in concentrated H$_2$SO$_4$ and showed that rapid rotations occur about either the C–O or 1–1′ bond in this medium at temperatures above room temperature. A temperature dependence of the ortho proton splitting constant was also detected which was further analyzed[5] in terms of a torsional oscillation about the 1–1′ bond with a barrier of ca. 1 kcal/mol.

As part of a general study on the influence of the addition or removal of an electron on barriers to rotation we

recently carried out some INDO calculations on the barriers in the biphenyl and 4,4′-dihydroxybiphenyl anion and cation radicals.[6] The results of these calculations suggested that the addition or removal of an electron from a neutral biphenyl should result in a large increase in the rotational barrier about the 1–1′ bond. Specifically the calculated barriers to rotation in 4,4′-dihydroxybiphenyl are 15.8 kcal/mol for the 1–1′ bond and 7.6 kcal/mol for rotation around the C–O bond. This calculation suggests that the line width effects due to restricted rotation which are observed for 4,4′-dimethoxybiphenyl disappear at high temperatures owing to an increased rate of rotation about the C–O rather than the 1–1′ bond. Any rotational barrier extracted from the ESR spectra should therefore correspond to restricted rotation about the C–O bond.

In order to further substantiate the INDO calculations the cation radicals of 4,4′-dimethoxybiphenyl and 4,4′-dihydroxybiphenyl have been reinvestigated in an effort to extract the rotational barriers. The 3,3′-dimethyl-
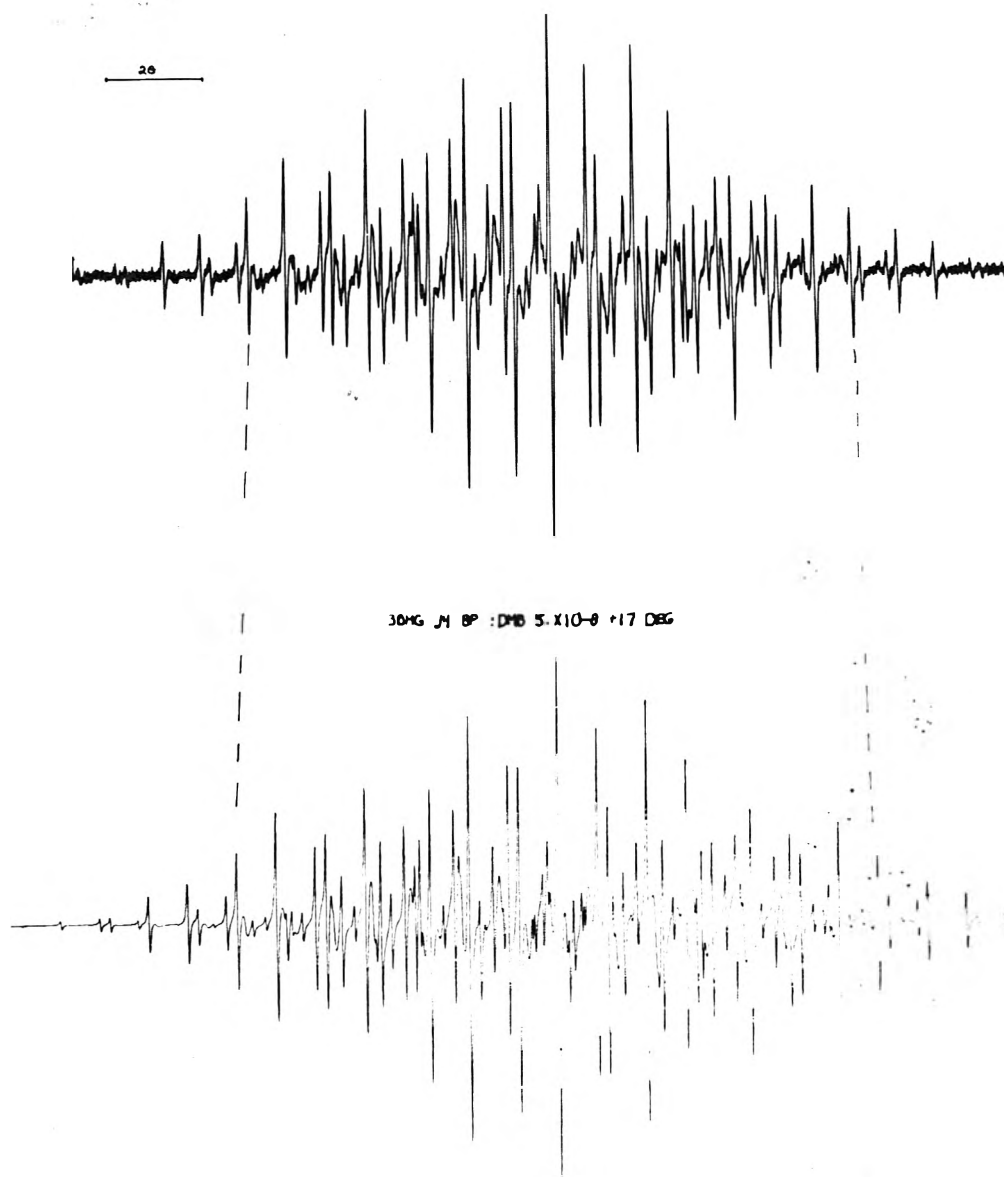
Figure 1. The upper spectrum is the ESR spectrum of DMBP in TFA–TFAn–CH₃NO₂ at +17 °C. The lower spectrum is the matched computer simulation with a conformational lifetime of 5×10^{-8} s; the splitting constants used are those given in the text.

4,4'-dihydroxybiphenyl cation radical has also been investigated. It can be predicted that the presence of the methyl groups should lock the hydroxyl groups in this compound but that the restricted rotation about the 1–1' bond should still lead to cis–trans isomers if the barrier is sufficiently large.

Experimental Section

The cation radicals of 4,4'-dihydroxybiphenyl and 3,-3'-dimethyl-4,4'-dihydroxybiphenyl were prepared in $AlCl_3$–CH_3NO_2 mixtures. Due to the tendency of these compounds to oxidize further than the one electron step several trials were required before spectra with good resolution and high intensity were obtained. The 4,4'-dimethoxybiphenyl cation radical was prepared by dissolving the parent compound in a mixture of 10 parts by volume trifluoroacetic acid (TFA), 1 part trifluoroacetic acid anhydride (TFAn), and 10 parts nitromethane. The mixture was degassed and the radical slowly formed over a period of 10–15 min. The ESR spectra were measured on a Varian E-15 spectrometer using a modulation frequency of 10 MHz. The temperature of the sample was continuously monitored with a microprobe thermocouple directly in the ESR cavity. The simulations were carried out using a slightly modified version of the density matrix program described by Heinzer.[7] Least-squares analysis of splitting constants were carried out using previously described methods.[8]

Results

4,4'-Dimethoxybiphenyl (DMBP). The ESR spectra of DMBP⁺ which were obtained in TFA–TFAn–CH₃NO₂ were considerably better resolved than any previously reported (see Figure 1). The line width was ca. 30 mG between –30 and +40 °C increasing somewhat at higher and lower temperatures. Spectra were obtained from +58 to –57 °C. At the highest temperatures rapid rotation occurs and the analysis was straightforward in terms of three splitting constants of 1.913 ± 0.0010, 1.763 ± 0.0012, and 0.776 ± 0.0016 G for 4, 6, and 4 protons, respectively. As the temperature is lowered one observes that the lines from the largest splitting exhibit the well-known effects of modulated splitting constants. That is, the $\bar{M}_1 = \pm 1$ lines of the original five-line pattern broaden out and other lines reappear to give a triplet of triplets pattern. In the intermediate limit it is possible to distinguish between two- and four-jump mechanisms since the unbroadened lines should give a 1:4:1 pattern in the former case and a 1:2:1

TABLE I: Summary of Experimental ESR Results

Compound	Splitting constants[a]				
	a_2	a_3	a_5	a_6	a_{OR}
DMBP⁺ (+55 °C)	1.9136 ± 0.0010	0.7759 ± 0.0016	0.7759 ± 0.0016	1.9136 ± 0.0010	1.7629 ± 0.0012
Temp coeff[b]	(−0.23 ± 0.02)	(−0.03 ± 0.02)	(−0.03 ± 0.02)	(−0.23 ± 0.02)	(−0.14 ± 0.03)
DMBP⁺ (−57 °C)	2.3008 ± 0.0029	0.729 ± 0.0036	0.838 ± 0.004	1.568 ± 0.003	1.7768 ± 0.0022
DHBP⁺ (−16 °C)	1.951 ± 0.005	0.752 ± 0.005	0.752 ± 0.005	1.951 ± 0.005	1.682 ± 0.005
DHBP⁺ (−57 °C)	1.874 ± 0.005	0.752 ± 0.005	0.752 ± 0.005	2.029 ± 0.005	1.722 ± 0.005
DMDHBP⁺ᶜ (−8 °C)	1.454	0.820ᵈ	0.566	2.342	1.641
	1.454	0.751ᵈ	0.631	2.342	1.641

[a] Splitting constants in Gauss.   [b] Temperature coefficients in mG/deg.   [c] Cis and trans isomers not assigned, all splittings ±0.005 G.   [d] Methyl proton splittings.

TABLE II: Summary of Activation Parameters for DMBP and DHBP

	DMBP	DHBP
E_a, kcal/mol	8.46 ± 0.50	7.31 ± 0.35
log A	13.66 ± 0.38	12.85 ± 0.32
$\Delta H^{\ddagger}$, kcal/mol	7.93 ± 0.44	6.87 ± 0.34
$\Delta S^{\ddagger}$, eu	−2.20 ± 1.70	1.22 ± 1.50
$\Delta G^{\ddagger}_{273}$, kcal/mol	8.53 ± 0.49	6.54 ± 0.36

pattern in the latter. Experimentally the 1:2:1 pattern is observed indicating that a four-jump process is responsible for the modulation. If the temperature is lowered still further after the larger set (ortho protons) has reached it's slow exchange limit the lines from the other set of four protons (meta) are observed to exhibit the same modulation phenomena. When the temperature is lowered to −57 °C both the ortho and meta protons are observed to fall into two groups of two equivalent protons (see Table I). The low temperature spectrum can however be fully interpreted in terms of only one species which in view of the need for a four-jump process to explain the line intensities at intermediate exchange rates suggests that the spectra of the cis and trans forms must be identical (see later discussion). Simulations of the exchange process were carried out using density matrix methods[7] for both two- and four-jump models. The simulations convincingly showed that the four-jump model is correct. Because of the different dependence of the ortho and meta protons on temperature it was possible to accurately fit the spectra over a wide temperature range (+50 to −50 °C). From the rate vs. temperature data the activation parameters shown in Table II were obtained.

The splitting constants of DMBP were also accurately fitted with a least-squares program in order to obtain the temperature coefficients. The values obtained are shown in Table I; the ortho and methoxyl protons both have significant negative temperature coefficients, whereas that of the meta proton is almost negligible.

4,4′-Dihydroxybiphenyl (DHBP). The ESR spectrum of DHBP⁺ in AlCl₃–CH₃NO₂ at −30 °C is consistent with the fast exchange limit; splittings are observed from groups of 4, 4, and 2 equivalent protons (see Table I). Between −30 and −50 °C the larger group of four protons (assigned to the ortho protons) pass from the fast to the slow exchange limit of two groups of two protons. No effects were observed on the meta protons although spectra could not be taken below −57 °C. Simulations were made assuming that a four-jump cis–trans isomerization occurs and that the splittings of the cis and trans isomers are identical. Spectra were measured at 3 °C intervals between −30 and −57 °C and the simulations were fitted to the experimental spectra as shown in Figure 2. The activation parameters derived from this data are shown in Table II.

3,3′-Dimethyl-4,4′-dihydroxybiphenyl (DMDHBP). The spectrum of this compound at −8 °C in AlCl₃–CH₃NO₂ is

shown in Figure 3. The spectrum which has a large central line and shows no evidence of a 1:6:15:20:15:6:1 pattern from the methyl protons is typical of that expected for cis–trans isomers of equal g value in which the methyl splitting is different in the two isomers. A careful study of the wings under high gain enabled us to propose the analysis given in Table I. A simulated spectrum using these parameters and using a 65/35 trans–cis ratio shows a good agreement with the experimental spectrum (see Figure 3). As the parameters in Table I indicate the meta proton and methyl group splittings are different in the two isomers whereas the ortho splittings are similar. Other simulations in which the ortho splittings were different in the two isomers did not give such good agreement with the experimental spectra.

The spectra were examined from +15 to −20 °C; the cis–trans isomers were still present at +15 °C and all changes in the spectra over this limited temperature range were explained in terms of a slight temperature dependence of the splitting constants.

Discussion

Rotational Barriers. The existence of cis–trans isomers in DMDHBP⁺ at +15 °C compared to the fast exchange of the cis–trans isomers in DHBP⁺ at the same temperature indicates that the barrier to rotation around the C–O bond is less than that about the 1–1′ bond in DHBP⁺. Thus the activation energy obtained from DHBP⁺ can be attributed to the rotational barrier of the C–O bond. The experimental value of 7.31 ± 0.35 kcal/mol is in excellent agreement with the value calculated using the INDO method of 7.6 kcal/mol.[6] This certainly increases our confidence in the calculated value for rotation about the 1–1′ bond (i.e., 15.8 kcal/mol).

The results for DMBP⁺ should be similarly interpreted and the value of 8.46 ± 0.5 kcal/mol can be attributed to the restricted rotation about the C–O bond.[9]

An alternative check on the rotational barriers can be obtained from the temperature coefficients of the hydroxyl and methoxyl splitting constants. For DHBP⁺, da_{OH}^H/dT is estimated to be ca. −1 mG/deg which is of the same magnitude as that in duroquinol[10] where the rotational barrier is 7 ± 1 kcal/mol. The methoxyl coefficient in DMBP⁺ has been measured more accurately as −0.14 ± 0.03 mG/deg. This value falls between those measured for dimethoxybenzene (−0.09 mG/deg) and 1,4-dimethoxynaphthalene (−0.41 mG/deg) for which the rotational barriers have been estimated as >15 and 4.9 ± 0.5 kcal/mol, respectively.[8]

Our measured temperature coefficient of −0.23 mG/deg for the ortho protons of DMBP⁺ is in contrast to the suggested positive value for this temperature coefficient.[5] Since our measurements have been more accurately analyzed we must suggest that the previously reported barrier to rotation about the 1–1′ bond of 1 kcal/mol was based
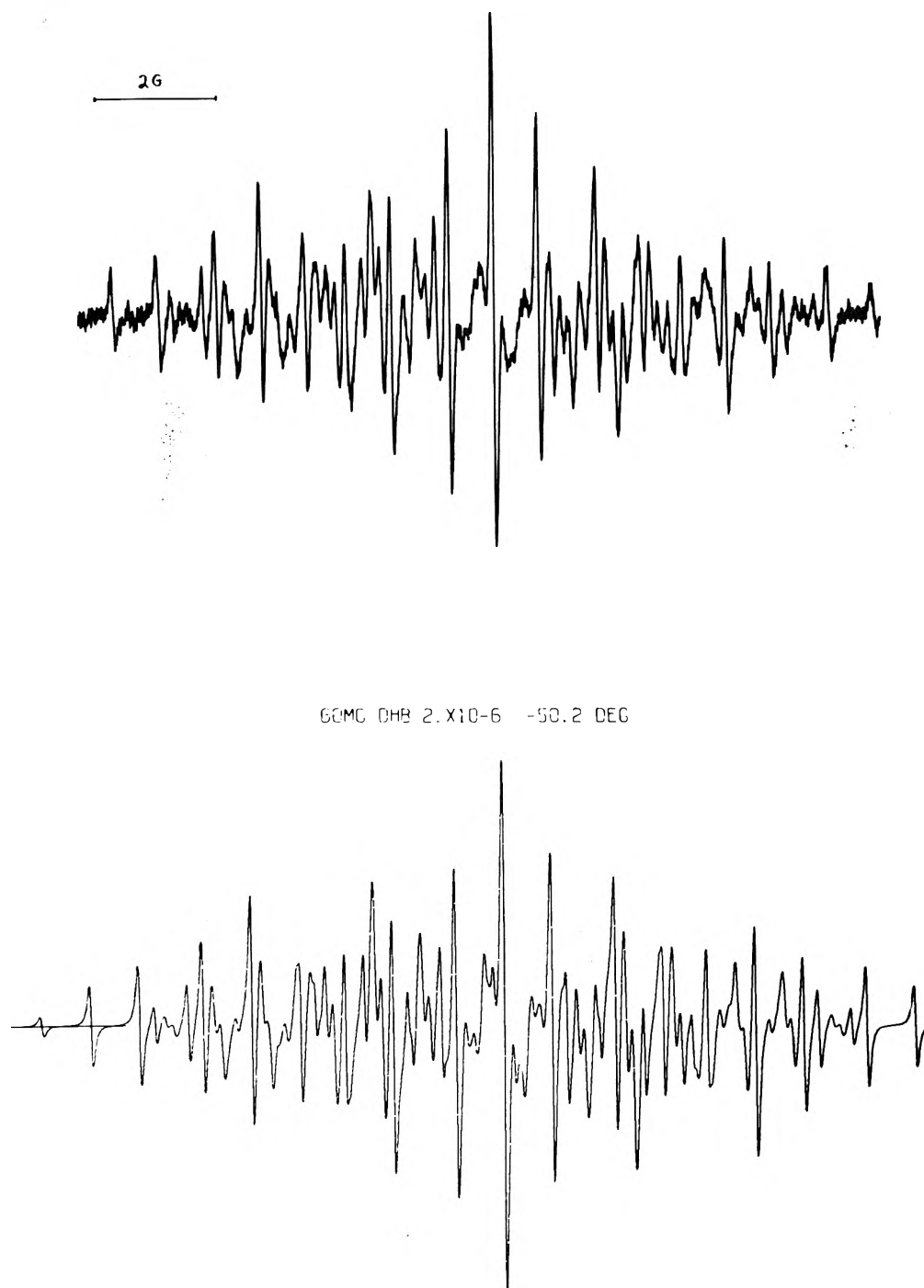
Figure 2. The upper spectrum is the ESR spectrum of DHBP in $AlCl_3$-CH_3NO_2 at -50 °C. The lower spectrum is the matched computer simulation with a conformational lifetime of 2 X 10^{-6} s; the splitting constants used are those given in the text.

upon inaccurate data and should be reevaluated.

Molecular Orbital Calculations of Splitting Constants. It was indicated in the results section that the exchange process occurring in $DMBP^+$ and $DHBP^+$ can be confidently analyzed as a four-jump process but that the spectra of the cis and trans isomers are required to have essentially identical splitting constants. Thus it is apparent that one ring is unaffected by the orientation of the alkoxyl group in the other ring. To substantiate this observation the splitting constants calculated for the minimum energy configuration of $DHBP^+$ in the INDO approximation were compared with the experimental values. Although the absolute magnitudes of the splitting constants (Table III) are not in good agreement with experiment the splittings of the two isomers are found to be almost identical with a very low energy difference of ca. 7 cal/mol. Only the

ortho protons are calculated to be nonequivalent whereas the meta protons are completely equivalent, as was experimentally observed. The calculation also predicts that the large ortho proton is cis to the hydroxyl group. Tylli has published some INDO calculations on $DMBP^{+5}$ which also indicate the equivalence of the splittings in the cis and trans isomers of this compound. The calculated ring splitting constants in this case were in even poorer agreement with experiment (see Table III) probably due to the large value used for the 1-1' bond length. The results do, however, indicate that both the ortho and meta protons are inequivalent in this molecule.

In order to rationalize the splittings from $DMDHBP^+$ it was necessary to utilize some McLachlan modified HMO calculations since this molecule proved too large for the INDO program. The basic parameters used were $h_O =$
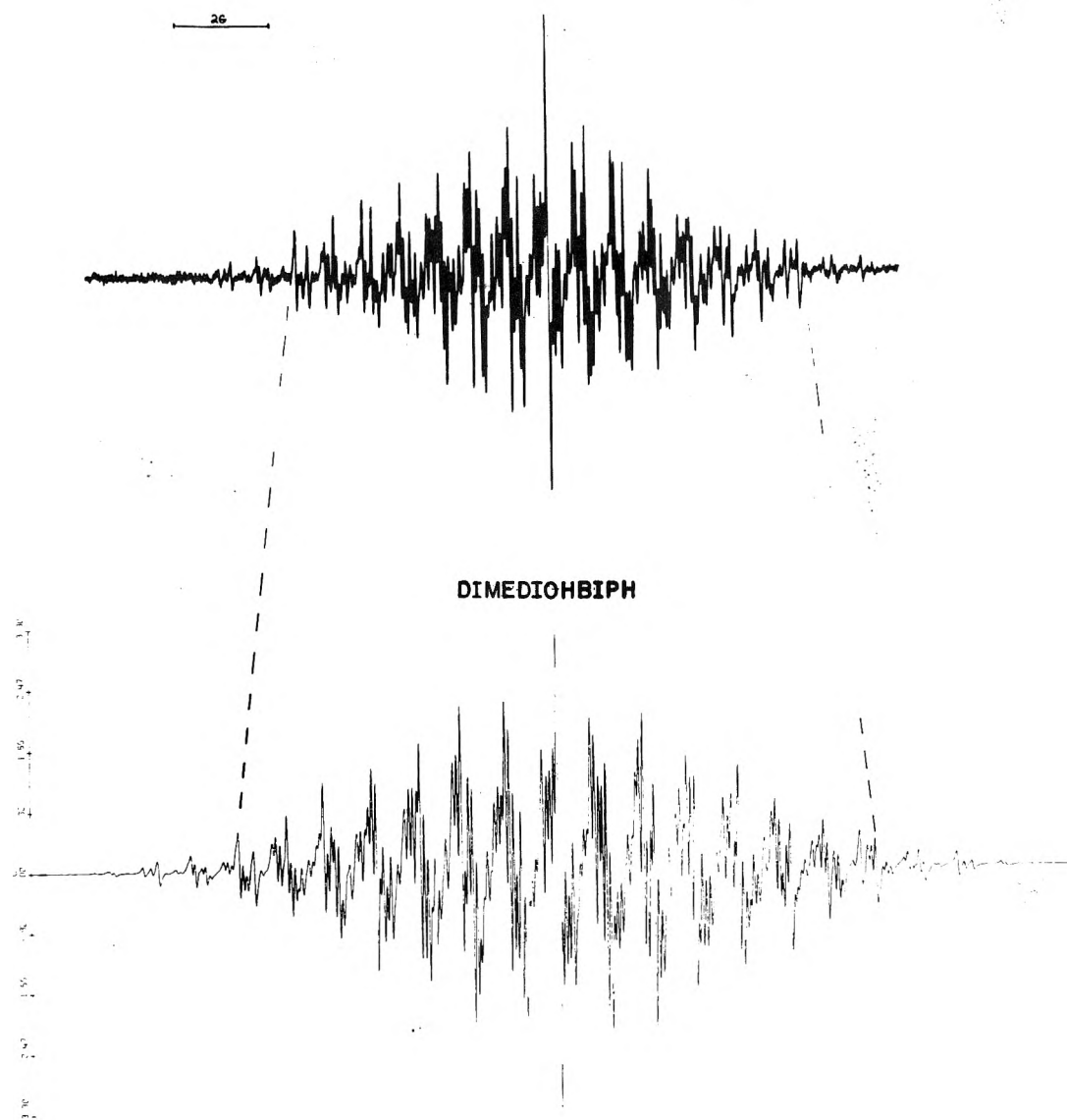
Figure 3. The upper spectrum is the ESR spectrum of DMDHBP in $AlCl_3-CH_3NO_2$ at -8 °C. The lower spectrum is a computer simulation in terms of cis and trans isomers using the parameters given in the text.

TABLE III: Summary of Molecular Orbital Calculations of Splitting Constants

Compd	$a_{2,2}'$	$a_{3,3}'$	$a_{5,5}'$	$a_{6,6}'$	a_{OR}	Calcd method
DHBP (trans)	-2.030	0.187	0.187	-1.984	-2.516	INDO[a]
DHBP (cis)	-2.027	0.186	0.187	-1.986	-2.516	INDO[a]
DMBP (trans)	-0.79	0.07	0.03	-0.71	1.53	INDO[b]
DMBP (cis)	-0.80	0.07	0.03	-0.71	1.53	INDO[b]
DHBP	1.98^c	0.744	0.744	1.98	1.698^d	HMO
DHBP[e]	2.142	0.688	0.794	1.894	1.680	HMO
DMDHBP[f]	1.33	1.06^g	0.49	2.466	1.734	HMO

[a] Using parameters given in ref 6. [b] Taken from ref 5. [c] Calculated assuming $Q_{CH}^H = |271|$ G, $h_O = 1.93$, $k_{OC} = 1.12$, $k_{CC'} = 1.25$. [d] Calculated assuming $Q_{OH}^H = |301|$ G. [e] $h_O = 1.93$, $k_{OC} = 1.12$, $k_{CC'} = 1.25$, $h_{C_5} = h_{C_5'} = 0.04$. [f] As above plus $h_{C_3} = h_{C_3'} = -0.14$. [g] Methyl splitting calculated assuming $Q_{CCH}^H = |271|$ G.

1.93, $k_{OC} = 1.12$, $k_{CC'} = 1.25$ which give good agreement for the fast exchange state of DHBP$^+$ (see Table III). The effect of the restricted rotation of the hydroxyl group was taken into account by the addition of an auxiliary parameter $h_{C_6} = h_{C_6'} = 0.04$. This results in a nonequivalence of both the ortho and meta splittings in contrast to the observed nonequivalence of only the ortho protons. The larger ortho splitting is cis to the hydroxyl group in agreement with the INDO calculations. The addition of the methyl groups in DMDHBP$^+$ can be modeled by the further addition of $h_{C_3} = h_{C_3'} = -0.14$. This gives the results shown in Table III and is in reasonable agreement with experiment if the splittings are assigned as shown in Table

I. The difference between the cis and trans isomers of DMDHBP$^+$ is not, however, accounted for in this manner.

The Structure of Biphenyl Radical Ions. Both qualitative and quantitative[6,11] theory has indicated that the bond order of the $1-1'$ bond in biphenyl should increase on radical ion formation with concomitant increase in the rotational barrier. Many studies on biphenyl radical anions have substantiated this conclusion. Particular attention should be paid to 3,3'-disubstituted biphenyl radical anions which should exist as cis-trans isomers. Only one case has definitely been analyzed in these terms, namely, the 3,-3'-dimethoxybiphenyl radical anion.[12] However, Allred and Bush also mentioned the possibility that 3,3'-difluorobi-

phenyl radical anion exists as cis and trans isomers and their published spectra[13] support this hypothesis. Similarly the published spectrum of 3,3'-dicyanobiphenyl is suggestive of the presence of cis-trans isomers.[14] Somewhat surprisingly the 3,3'-dimethylbiphenyl anion radical which has been studied by ESR,[15] ENDOR,[16] and NMR line broadening[17] techniques does not show any signs of restricted rotation. Perhaps in this case the methyl group acts as such a small perturbation that the splittings of the cis and trans isomers are identical.

In this paper 3,3'-dimethyl-4,4'-dihydroxybiphenyl cation radical has been analyzed in terms of cis and trans isomers. Both 3,3'-dimethyl-4,4'-dimethoxybiphenyl and 3,3',4,4'-tetramethoxybiphenyl cation radicals also exhibit spectra which are thought to be due to cis and trans isomers.[18] The rotational barriers in DMBP[+] and DHBP[+] are attributed to restricted rotation about the C–O bond indicating that the barrier to rotation about the 1–1' bond should be larger than these barriers (i.e., >10 kcal/mol). A previous study by Ishizu et al.[19] has compared the twist angle in 2,2',4,4',6,6'-hexamethylbiphenyl cation radical with that in 2,2',6,6'-tetramethylbiphenyl anion radical. The evaluation of the twist angle in these molecules was based on comparisons with HMO calculated spin densities and required a constant Q factor for the methyl splittings. The results which indicate a greater angle of twist for the cation radical may be open to question since qualitatively one would not predict a great difference for these two compounds.

In conclusion the evidence strongly supports the theoretical conclusion that the barrier to rotation about the 1–1' bond in biphenyl radical ions is much larger than that in the neutral molecule. No reliable experimental mea-surements of this barrier have yet been reported. From the results in this paper one can say that the barrier is probably >10 kcal/mol in DMBP[+] and DHBP[+]. It may prove feasible to estimate the 1–1' rotational barrier from the temperature dependence of the ring proton splittings and this possibility is currently under investigation.

References and Notes

(1) H. M. Buck, W. Bloemhoff, and L. J. Oosterhoff, *Tetrahedron Lett.*, 5 (1960).
(2) D. L. Allara, B. C. Gilbert, and R. O. C. Norman, *Chem. Commun.*, 1, 319 (1965).
(3) W. F. Forbes and P. D. Sullivan, *Can. J. Chem.*, 46, 325 (1968).
(4) H. Tylli, *Fin. Kemistsamf. Medd.*, 81, 24 (1972).
(5) H. Tylli, *Fin. Kemistsamf. Medd.*, 82, 60 (1973).
(6) P. D. Sullivan and J. Y. Fong, *Chem. Phys. Lett.*, 38, 555 (1976).
(7) J. Heinzer, *Mol. Phys.*, 22, 167 (1971).
(8) P. D. Sullivan, *J. Phys. Chem.*, 74, 2563 (1970).
(9) The spectrum of 3,3'-dimethyl-4,4'-dimethoxybiphenyl cation radical has been observed and also appears to consist of cis and trans isomers. The spectrum has not, however, been fully interpreted.
(10) P. D. Sullivan, *J. Phys. Chem.*, 75, 2195 (1971).
(11) A. Golebiewski and A. Parczewski, *Z. Naturforsch. A*, 25, 1710 (1970).
(12) H. Tylli, *Fin. Kemistamf. Medd.*, 81, 113 (1972).
(13) A. L. Allred and L. W. Bush, *Tetrahedron*, 24, 6883 (1964).
(14) H. Sikata, K. Ishizu, Y. Deguchi, and H. Takaki, *Bull. Chem. Soc. Jpn.*, 43, 3274 (1970).
(15) K. Ishizu, *Bull. Chem. Soc. Jpn.*, 37, 1093 (1964).
(16) T. C. Christidis and F. W. Heineken, *Chem. Phys.*, 2, 239 (1973).
(17) J. W. M. de Boer, M. R. Arick, and E. de Boer, *J. Chem. Phys.*, 59, 638 (1973).
(18) P. D. Sullivan, unpublished information.
(19) K. Ishizu, M. Ohuchi, F. Nemoto, and M. Suga, *Bull. Chem. Soc. Jpn.*, 46, 2932 (1973).

Nitrogen-14 Nuclear Magnetic Relaxation in Aqueous Micellar Solutions of n-Hexadecyltrimethylammonium Bromide and Chloride

Ulf Henriksson,* Lars Ödberg, Jan Christer Eriksson, and Lennart Westman[†]

Department of Physical Chemistry, The Royal Institute of Technology, S-100 44 Stockholm 70, Sweden (Received May 28, 1976)

[14]N spin–lattice (T_1) and spin–spin (T_2) relaxation times have been measured in aqueous solutions of n-hexadecyltrimethylammonium bromide (CTAB) and chloride (CTAC) as functions of the concentration. It is confirmed that CTAC forms spherical micelles at all concentrations above the cmc while CTAB at higher concentration forms larger aggregates. The thermal motions of the surfactant molecules can be described by a local rapid anisotropic motion and a slower motion over distances of the order of the dimension of the aggregates. The fast motion is characterized by a correlation time $\tau_c^f \approx 5.6 \times 10^{-10}$ s in CTAB micelles and it is approximately twice as fast in CTAC micelles. The correlation time for the slow motion in CTAB micelles increases rapidly with concentration. From comparison with models for the motion of rodlike aggregates it is concluded that the large micelles probably are flexible.

Introduction

Nuclear magnetic relaxation can be used to obtain information about the molecular dynamics in micellar solutions. Sofar, the most detailed dynamic information has

† Present address: The Swedish Forest Products Research Laboratory, S-114 86 Stockholm, Sweden.

been obtained from ^{13}C relaxation[1-4] since the chemical shift separation of the different alkyl carbons permits relaxation time measurements for individual carbon atoms. Furthermore, for alkyl carbons the relaxation is dominated by [1]H–[13]C magnetic dipole interaction, the magnitude of which is known, and the calculation of effective correlation times from experimental data is straightforward. In

aqueous solutions of sodium n-hexanoate, the effective correlation times for the different alkyl carbons are longer and differ more in the micelles than in the monomers, indicating that slower molecular motions are of significance in micelles. However, the effective correlation times depend on the overall motion of the surfactant molecule and the internal rotation about each carbon–carbon bond and a detailed interpretation is difficult.[4] In this work we have used ^{14}N nuclear magnetic relaxation to study the motions of the surfactant molecules in micelles of n-hexadecyltrimethylammonium bromide (CTAB) and chloride (CTAC).

Experimental Section

Materials. CTAB (Merck, p.a.) was recrystallized from ethanol. CTAC (Eastman Kodak Co) was recrystallized several times from acetone–ether mixtures. n-Hexyltrimethylammonium bromide (HTAB) and n-hexylpyridinium bromide (HPyB) were prepared by allowing vacuum distilled n-hexylbromide (Merck, zur Synthese) to react with trimethylamine (Fluka, purum) and pyridine (Mallincrodt, analytical reagent) respectively in ethanol solution.[5] The salts were recrystallized repeatedly from acetone–ether mixtures. The water was doubly distilled, the second time from a quartz glass apparatus, and deoxygenated by bubbling with oxygen-free nitrogen. Deuterium oxide (Merck, 99.7% D) was used without further purification.

Methods. The ^{14}N relaxation times were measured at 6.50 MHz using a Bruker B-KR 322s pulsed NMR spectrometer equipped with a Bruker BNC 12 computer. The longitudinal relaxation times T_1 were measured using the inversion-recovery method.[6] To obtain a better signal-to-noise ratio, a modification of this method which allows the use of shorter waiting times between the pulse sequences was used.[7,8] The ^{14}N transverse relaxation times T_2 were calculated from the half-width of the absorption signal in the Fourier transform spectrum using the relation $(\pi T_2)^{-1} = \Delta\nu - \Delta\nu_{inhom}$ where $\Delta\nu$ is the experimental line width and $\Delta\nu_{inhom}$ is the contribution to the line width from magnetic field inhomogeneities. $\Delta\nu_{inhom}$ was determined from the spectrum of an aqueous solution of ammonium nitrate, which has a negligible contribution to the line width from relaxation. The temperature of the samples was kept at 28.5 ± 0.5 °C with the use of a temperature controlled nitrogen stream. The ^{13}C spin–lattice relaxation times were measured with a Varian CFT 20 spectrometer using the progressive saturation method.

Theory

The ^{14}N nucleus has a spin quantum number $I = 1$ and thus an electric quadrupole moment eQ which interacts with the electric field gradient at the nucleus. This interaction can affect both the spin energy levels and the relaxation of a ^{14}N nucleus. The Hamiltonian for quadrupole interaction can be written[9]

$$H_Q = \frac{eQ}{2I(2I-1)} \sum_{q=-2}^{2} V_{-q} A_q \qquad (1)$$

where V_q is a component of the electric field gradient tensor and A_q is a component of an irreducible tensor operator working on the nuclear spin functions. The electric field gradient at the nitrogen nucleus in n-alkyltrimethylammonium ions is assumed to be of intramolecular origin (vide infra) and the principal axis system of the field gradient tensor is fixed in the molecule. The field gradient tensor is diagonal in this system and, according to the Laplace equation, traceless. It can thus be

characterized by two quantities

$$eq = V_{zz}^{p} \qquad (2)$$

$$\eta = (V_{xx}^{p} - V_{yy}^{p})/V_{zz}^{p} \qquad (3)$$

where the superscript p represents the principal axis system, eq is the largest component of the electric field gradient in this system, and η is the asymmetry parameter. The strength of the quadrupole interaction in frequency units is often expressed by the quantity ν_Q given by

$$\nu_Q = \frac{3}{4} \frac{e^2qQ}{I(2I-1)h} \qquad (4)$$

where e^2qQ/h is the quadrupole coupling constant.

The nuclear spins are quantized along the direction of the static magnetic field $\vec{B}_0$ and it is natural to express the A_q's in a laboratory fixed coordinate system. If H_Q is evaluated in the laboratory system, the V_q's must be transformed to this system. H_Q thus depends on the orientation of the principal axis system relative to the laboratory system. When molecular motions are present H_Q is time dependent and can be divided into a time independent part H_Q^0 and a time dependent part $H_1(t)$.

$$H_Q(t) = H_Q^0 + H_1(t) \equiv H_Q^0 + [H_Q(t) - H_Q^0] \qquad (5)$$

H_Q^0 is the time average of H_Q taken over times longer than $1/\nu_Q$. This is the static Hamiltonian that gives rise to quadrupole splittings in the spectrum from solids and liquid crystals, while $H_1(t)$ is responsible for relaxation. In liquids, H_Q is averaged to zero and the relaxation times are determined by the strength of the quadrupole interaction ν_Q and the frequency distribution in the molecular motions that modulate H_Q. This frequency distribution is described by a spectral density function $\tilde{J}(\omega)$ which measures the Fourier component of the molecular motions at the angular frequency ω. For $I = 1$ the spin–lattice relaxation rate $1/T_1$ and the spin–spin relaxation rate $1/T_2$ are given by[9]

$$\frac{1}{T_1} = \frac{8}{15}\pi^2 \nu_Q^2 \left(1 + \frac{\eta^2}{3}\right) [\tilde{J}(\omega_0) + 4\tilde{J}(2\omega_0)] \qquad (6)$$

$$\frac{1}{T_2} = \frac{8}{15}\pi^2 \nu_Q^2 \left(1 + \frac{\eta^2}{3}\right) \left[\frac{3}{2}\tilde{J}(0) + \frac{5}{2}\tilde{J}(\omega_0) + \tilde{J}(2\omega_0)\right] \qquad (7)$$

where ω_0 is the Larmor frequency. It is seen that T_1 and T_2 can give information about the intensity of the molecular motions at zero frequency and at frequencies around the Larmor frequency.

The time scale of the molecular motions is usually characterized by a parameter τ_c, the correlation time.[9] The rotational motion of isotropically reorienting molecules can be described by a single correlation time related to the rotational diffusion constant R. In this case $\tilde{J}(\omega)$ is given by

$$\tilde{J}(\omega) = \frac{\tau_c}{1 + \omega^2\tau_c^2} \qquad (8)$$

$$\tau_c = 1/6R \qquad (9)$$

In general, separate correlation times for the rotation about the different axes must be used.[10,11] An effective correlation time which is a weighted average of the different correlation times that characterize the motion can, however, be introduced in this case. The power available in the molecular motions is according to eq 8 rather evenly distributed in the frequency range 0 to $1/\tau_c$. Short τ_c

means rapid molecular motions and if $\tau_c \ll \omega_0^{-1}$ (the "extreme narrowing" condition), $\tilde{J}(0) = \tilde{J}(\omega_0) = \tilde{J}(2\omega_0)$ which according to eq 6 and 7 implies that $T_1 = T_2$.

Results and Discussion

Determination of ν_Q. As is seen in eq 6 and 7, ν_Q and η have to be known in order to obtain correlation times from the experimental relaxation times. As a consequence of the cylindrical symmetry of the electric field gradient around the N–C$_\alpha$ bond, the asymmetry parameter $\eta = 0$ in n-alkyltrimethylammonium ions. To our knowledge, ν_Q for the ^{14}N nucleus in n-alkyltrimethylammonium ions has not been reported in the literature. For a given compound ν_Q can in principle be obtained from the spectrum of a single crystal or of a powder sample.[12] For CTAB and CTAC we have, however, not been able to grow large enough single crystals for the observation of a ^{14}N spectrum and the spectrum from a powder sample is too broad to be observed. ν_Q can also be determined by nuclear quadrupole resonance (NQR) where the transitions between the nuclear spin energy levels are observed in the absence of a magnetic field. Sensitivity limits this method to $\nu_Q \gtrsim 1$ MHz. Since there is an almost tetrahedral symmetry around the nitrogen in n-alkyltrimethylammonium ions the above condition is not fulfilled. ν_Q can also be determined from measured relaxation times by the use of eq 6–8 if the correlation time can be determined in an independent way. This last approach will be used here to get an approximate value for ν_Q in CTAB.

The symmetry axis of the electric field gradient is along the N–C$_\alpha$ bond. It is not possible to determine the correlation time for the motion of this bond from relaxation time measurements for other nuclei in the CTAB molecule due to the internal motions in the molecule. Another molecule must therefore be found in which there is a correlation time that can be assumed to be the same as the correlation time for the N–C$_\alpha$ bond in CTAB and that can easily be measured. The correlation time for the motion of the p-C–H bond in hexadecylpyridinium bromide (CPyB) can be determined from ^{13}C relaxation times. This C–H bond makes the same angle with the main axis of the molecule as does the N–C$_\alpha$ bond in CTAB. To assume that the correlation times in CTAB and CPyB are equal is, however, uncertain since the motions depend strongly on the details of micellar structure (vide infra). Measurements were therefore made on the corresponding hexyl compounds in aqueous solution below the cmc where the motions can be assumed to be approximately the same. T_1 for the para carbon in HPyB was found to be 2.1 s (0.55 M in D$_2$O). In extreme narrowing τ_c can be calculated from the relation

$$1/T_1 = \hbar^2 \gamma_H^2 \gamma_C^2 r_{CH}^{-6} \tau_c \tag{10}$$

where γ_H and γ_C are the magnetogyric ratios for ^{1}H and ^{13}C, respectively, and r_{CH} is the carbon–hydrogen distance. A value $\tau_c = 2.1 \times 10^{-11}$ s is obtained. The ^{14}N relaxation time in HTAB is 0.26 s (0.55 M in D$_2$O). Using the above τ_c value and eq 6 and 8 a value $\nu_Q = 83.5$ kHz is obtained for HTAB. This is also assumed to be the value of ν_Q in CTAB and CTAC. This last assumption is supported by a ^{14}N line width study of aqueous solutions of Et$_3$N$^+$ (CH$_2$)$_n^+$NEt$_3$,2Br$^-$ with $n = 2$–4[14] from which it can be concluded that for small n values there are considerable differences in ν_Q between the different compounds, but for $n \geq 5$ the length of the alkyl chain does not seem to have much influence on the electric field gradient at the nitrogen nucleus.

From ^{14}N and ^{2}H relaxation times in aqueous solution of the compound Et$_3$N$^+$CD$_2$CH$_2$CH$_2$CD$_2^+$NEt$_3$, 2Br$^-$, ν_Q
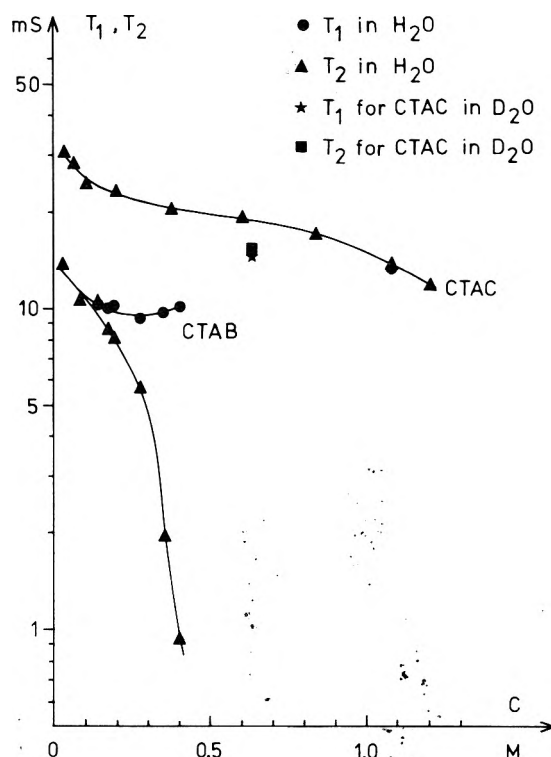

Figure 1. ^{14}N relaxation times in aqueous solutions of CTAB and CTAC at 28.5 °C.

= 110 kHz for the ^{14}N nucleus has been obtained assuming that the correlation times are equal for the motion of the nitrogen and deuterium nuclei.[13] The value $\nu_Q = 83.5$ kHz in HTAB obtained in this work thus seems reasonable.

The quadrupole moment for the ^{14}N nucleus has not been determined directly, but it can be estimated from the measured quadrupole coupling constant in the N$_2$ molecule and electronic wave functions from MO calculations. The value $Q = 1.55 \times 10^{-30}$ m^2 is a mean value from several such calculations which probably does not deviate from the correct value by more than 10%.[13] This gives $eq \approx 3.0 \times 10^{20}$ V/m^2 for the electric field gradient at the nitrogen nucleus in HTAB.

The intermolecular contribution to the electric field gradient at the nitrogen in the n-alkyltrimethylammonium ions is composed of contributions from the charges of counterions and neighboring cations and the electric dipoles of the surrounding water molecules. These contributions are added vectorially and they partially cancel. To get an estimate of the order of magnitude of the intermolecular electric field gradients we calculate the contribution from a point charge Ze at a distance r from the nitrogen nucleus. This contribution is given by[12]

$$eq = \frac{1}{4\pi\epsilon_0}(1 + \gamma_\infty)\frac{2\epsilon + 3}{5\epsilon}\frac{2Ze}{r^3} \tag{11}$$

where ϵ is the dielectric constant of the medium and γ_∞ is the Sternheimer antishielding factor which accounts for the polarization of the electrons of the molecule in the electric field from the point charge. γ_∞ is not known for tetraalkylammonium ions but it is probably small since the electrons are involved in chemical bonds and consequently not so easily polarizable as, for instance, in alkali or halide ions. Using $(1 + \gamma_\infty) = 1$ eq 11 gives $eq \approx 10^{19}$ V/m^2 for $Z = 1$ and $r = 5$ Å which is only 3% of the experimental field gradient in HTAB.

The conclusion that the electric field gradient mainly is of intramolecular origin and independent of the length of the alkyl chain in n-alkyltrimethylammonium ions with
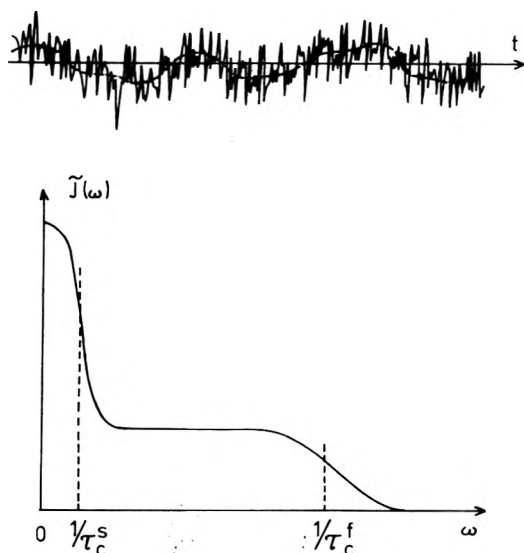
Figure 2. A schematic picture of the fluctuation of the quadrupole interaction due to rapid and slow motions. The resulting spectral density function J(ω) is also shown (after Berendsen and Edzes[18]).

Figure 3. Definition of the angle θ_{DP}. For details see the text.

not too short chain lengths has also been reached by Larsen, who studied the effects of added electrolyte on the ^{14}N relaxation.[15]

Results for Aqueous Solutions of CTAB and CTAC. In Figure 1 the measured ^{14}N relaxation times are plotted as functions of the concentration for aqueous solutions of CTAB and CTAC. The cmc for CTAB and CTAC is close to 1 mM.[16] All measurements reported here have been performed at concentrations well above the cmc. CTAB solutions could not be studied at concentrations above 0.4 M since broadening of the signal reduces the signal-to-noise ratio. It is seen that the relaxation behavior is quite different for the two surfactants. For concentrations lower than about 0.1 M, $T_1 = T_2$ for both CTAB and CTAC solutions and the extreme narrowing condition is thus fulfilled. The relaxation times are, however, about twice as long for the CTAC solutions as for the CTAB solutions. When the concentration of CTAC is increased there is only a slight decrease in the relaxation time and $T_1 = T_2$ also at these concentrations. For the CTAB solutions, T_2 decreases rapidly with increasing concentration while T_1 decreases more slowly and passes through a broad minimum at $c \approx 0.28$ M. From small-angle X-ray scattering measurements, it has been shown that CTAC forms spherical micelles in the whole concentration range from the cmc up to its solubility limit, while CTAB forms spherical micelles at concentrations between the cmc and $c \approx 0.15$ M and rod-shaped micelles at higher concentrations.[17] As will be shown below, these differences in micellar size and shape give rise to the widely different relaxation behavior of CTAB and CTAC solutions.

Fast and Slow Molecular Motions. The molecular motion of a *n*-hexadecyltrimethylammonium ion in a micelle is too complex to be described by eq 8 and 9 which predict that when T_2 decreases due to a longer correlation time, T_1 will increase just as rapidly. As is seen in Figure 1 this is not the case for the concentration dependence of T_1 and T_2 in aqueous CTAB solutions. To get a more detailed description, we start by considering the quadrupole Hamiltonian and the different motions that modulate it. Figure 2 shows a schematic picture of how H_Q fluctuates due to molecular motions.[18] The rapid fluctuations are caused by a local anisotropic motion of the molecule. The time scale of this motion is short. Averaging $H_Q(t)$ over these short times gives rise to a nonzero quadrupole Hamiltonian $\bar{H}_Q$. Due to slower
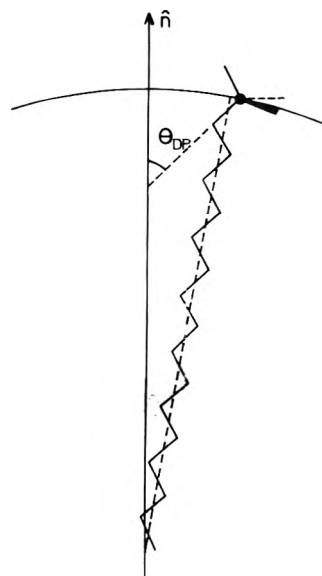
motions by which a molecule moves over a distance of the order of micellar dimensions, $\bar{H}_Q$ will fluctuate on a longer time scale as is shown in Figure 2 and the average of $\bar{H}_Q$ taken over a time of the order $1/\nu_0$ is zero.[18,19] The presence of both rapid and slow motions, which modulate different parts of H_Q, gives rise to a spectral density function with the general appearance as shown in Figure 2. The enhancement at the lower frequencies is due to the slow motion.

In order to separate the contributions from the fast and the slow motions to the spectral density function, $\bar{H}_Q$ must be evaluated. We therefore introduce a local director which is normal to the surface of the micelle.[19] Due to the fast local motion of a surfactant molecule the direction of the principal axis system of the electric field gradient in the molecule relative to this local director fluctuates (see Figure 3). This leads to a partial averaging of H_Q. The resulting average quadrupole interaction is $|\nu_Q S|$ where S is a local order parameter given by the time average

$$S = \frac{1}{2} \overline{(3 \cos^2 \theta_{DP} - 1)} \tag{12}$$

and θ_{DP} is the angle between the director and the direction of the largest component of the electric field gradient tensor in the principal axis system. The slow motions are treated as fluctuations of the orientation of the director relative to the laboratory axis system (defined by the static magnetic field $\bar{B}_0$). The spectral density functions $\tilde{J}(\omega)$ to be used in eq 6 and 7 can now be written[19]

$$\tilde{J}(\omega) = S^2 \tilde{J}^s(\omega) + (1 - S^2) \overline{\tilde{J}^f(\omega)} \tag{13}$$

where $\tilde{J}^s(\omega)$ is the spectral density function for the slow motions and $\overline{\tilde{J}^f(\omega)}$ for the fast motions averaged over all directions.

To proceed, we assume that the fast and the slow motions can each be described by a single effective correlation time τ_c^f and τ_c^s, respectively, and that the spectral density functions $\tilde{J}^f(\omega)$ and $\tilde{J}^s(\omega)$ can be evaluated from eq 9. The equations for the relaxation rates obtained contain three unknown quantities τ_c^f, τ_c^s, and S. Thus, it is only for the case when $T_1 \neq T_2$ that more detailed dynamic information can be obtained from the experimental data.

With the assumption $\tau_c^f \ll \omega_0^{-1}$ (extreme narrowing for the fast motion) the following explicit expressions for the

TABLE I: Calculated $\tau_c{}^s$ and T_1 from Experimental T_2 Data at Different Concentrations in Aqueous CTAB Solutions[a]

C, M	T_2, ms	$\tau_c{}^s$, ns	$(T_1)_{calcd}$, ms
0.15	9.4	1.1	9.4
0.20	7.9	3.6	7.8
0.25	6.4	7.9	6.8
0.30	4.4	34	7.2
0.35	2.1	160	9.4
0.40	1.1	340	9.7

[a] $\tau_c{}^f = 5.6 \times 10^{-10}$ s and $|S| = 0.21$ have been used at all concentrations.

relaxation rates are obtained from eq 6, 7, 8, and 13:

$$\frac{1}{T_1} = \frac{8}{15}\pi^2 \nu_Q{}^2 [S^2 \, f(\tau_c{}^s) + (1 - S^2)5\tau_c{}^f] \qquad (14)$$

$$\frac{1}{T_2} = \frac{8}{15}\pi^2 \nu_Q{}^2 [S^2 \, g(\tau_c{}^s) + (1 - S^2)5\tau_c{}^f] \qquad (15)$$

where

$$f(\tau_c) = \frac{\tau_c}{1 + \omega_0{}^2 \tau_c{}^2} + \frac{4\tau_c}{1 + 4\omega_0{}^2\tau_c{}^2} \qquad (16)$$

and

$$g(\tau_c) = \frac{3}{2}\tau_c + \frac{5}{2}\frac{\tau_c}{1 + \omega_0{}^2\tau_c{}^2} + \frac{\tau_c}{1 + 4\omega_0{}^2\tau_c{}^2} \qquad (17)$$

Evaluation of $\tau_c{}^f$, $\tau_c{}^s$, and $|S|$ in CTAB Solutions. As is seen from Figure 1, $1/T_1$ has only a weak dependence on concentration. The only reasonable explanation for this behavior is that the fast motion makes a predominant, approximately constant contribution to the relaxation rate. Thus we assume that $\tau_c{}^f$ is independent of concentration. To interpret the relaxation data for aqueous solutions of CTAB we further assume that S is independent of concentration. It has been found that the local order parameter is almost the same in hexagonal and lamellar lyotropic liquid crystalline phases.[20,21] It is thus reasonable to assume a constant order parameter S in our system. At high concentrations where the micelles are rod shaped $\tau_c{}^s$ is long and its contribution to $1/T_1$ is negligible. Hence $(1 - S^2)\tau_c{}^f$ can be evaluated from eq 14 using the measured T_1 at high concentrations. This gives $(1 - S^2)\tau_c{}^f = 5.3 \times 10^{-10}$ s. According to eq 14, the T_1 minimum occurs where $f(\tau_c)$ has its maximum value. At 6.50 MHz this occurs for $\tau_c = 1.5 \times 10^{-8}$ s, which thus is the value of $\tau_c{}^s$ at $c \approx 0.28$ M where T_1 has a minimum. $g(\tau_c{}^s)$ at this concentration can now be evaluated from eq 17 and from the measured T_2, the order parameter S can be obtained using eq 15. This gives $|S| = 0.21$ and $\tau_c{}^f = 5.6 \times 10^{-10}$ s. From the T_2 values, $\tau_c{}^s$ can be calculated at different concentrations. The results are given in Table I, where T_1 calculated from eq 14 using these $\tau_c{}^s$ values is also given. The experimental T_1 values are longer and have a broader minimum. This can be accounted for assuming a distribution of correlation times for the slow motion[22] that is tied to the distribution of aggregation numbers of the micelles. A distribution of correlations times does not affect T_2 to the same extent.

The approximations introduced affect the parameters determined as follows. An incorrect value of ν_Q influences $\tau_c{}^f$ and S according to eq 14 and 15. In the evaluation scheme used it does not affect $\tau_c{}^s$. The concentration for which T_1 has a minimum, 0.28 M, cannot be determined very accurately. This introduces uncertainties in S and $\tau_c{}^s$. However, the value of $|S|$ agrees rather well with the

order parameter for the α-methylene group in the hydrocarbon chain obtained in lyotropic liquid crystalline phases.[21,23,24] To get an idea of the influence of the location of the T_1 minimum on $\tau_c{}^s$ for the most concentrated solution (0.4 M) we assume that the T_1 minimum is located in the range 0.28 ± 0.05 M. This gives $\tau_c{}^s$ in the range $2-7 \times 10^{-7}$ s.

The increase in the relaxation times at low concentrations in both CTAB and CTAC solutions seen in Figure 1 can be due to contributions from the monomers to the observed relaxation rate or it could also be due to a shorter $\tau_c{}^f$ at these concentrations.

Discussion of the Molecular Dynamics in CTAB Solutions. Due to the mainly radial arrangement of the surfactant molecules within the micelles, each molecule will move in an approximately conical volume for times shorter than $\tau_c{}^f$. The angle θ_{DR} in eq 12 is the angle between the N–C_α bond and the axis of the cone (see Figure 3). From the value of the local order parameter $|S| = 0.21$ the time average $|\theta_{DP}| \approx 47°$ is obtained from eq 12. This value is quite reasonable since a surfactant molecule with its alkyl chain in the trans configuration and its long axis coinciding with the director has $\theta_{DP} = 35°$. The local motion characterized by $\tau_c{}^f = 5.6 \times 10^{-10}$ s is thus likely to be mainly a rotational diffusion of the surfactant molecule around its axis.

The correlation time for the rotational motion of a CTAB monomer in aqueous solution is not known since ^{14}N relaxation time measurements at these low concentrations can not be carried out. However, in the homologue n-nonyltrimethylammonium bromide, $\tau_c = 2 \times 10^{-11}$ s below the cmc.[25] For a CTAB monomer, τ_c should be somewhat longer but still the rotational motion of a n-hexadecyltrimethylammonium ion within the micelle is approximately an order of magnitude slower than for the monomer in aqueous solution.

It is seen in Table I that the correlation time for the slow motion increases rapidly with concentration. This is most likely due to formation of rod-shaped aggregates, the length of which increases with concentration. The length of CTAB micelles at different concentrations has been studied by Götz and Heckmann[26] using the anisotropy of the electrical conductivity in flowing solutions. The lowest concentration studied by Götz and Heckmann was 15% by weight which is slightly higher than the highest concentration used in this work (0.4 M). At this concentration, the length of a CTAB micelle was found to be 2000 Å. We now consider which type of slow motion in aggregates with this geometry that are compatible with the correlation time $\tau_c{}^s = 3.4 \times 10^{-7}$ s.

Relaxation caused by a reorientational motion that can be described as rotational diffusion has been treated by Woessner.[10] In general three rotational diffusion constants R_1, R_2, and R_3 have to be used. When $R_2 = R_3$ the effective correlation time for the reorientational motion is given by

$$\tau_c = \frac{A}{6R_2} + \frac{B}{R_1 + 5R_2} + \frac{C}{4R_1 + 2R_2} \qquad (18)$$

where the constants A, B, and C depend on an angle ϑ which in our case is the angle between the local director and the rotational axis 1.

$$A = \frac{1}{4}(3\cos^2\vartheta - 1)^2 \qquad (19)$$

$$B = 3\cos^2\vartheta(1 - \cos^2\vartheta) \qquad (20)$$

$$C = \frac{3}{4}(\cos^2\vartheta - 1)^2 \qquad (21)$$

The rotational Brownian motion of the whole micelle is one possible reorientational motion. Hydrodynamic equations giving the rotational diffusion constants of an ellipsoid moving in a viscous medium has been derived by Perrin.[27,28] If the rod-shaped micelle is treated as an ellipsoid with long axis 2a and both short axes 2b, the rotational diffusion constants are given by

$$\frac{1}{R_1} = \frac{32\pi\eta}{3kT}b^3\frac{x^3}{2x^2 - 2\ln x} \tag{22}$$

$$\frac{1}{R_2} = \frac{32\pi\eta}{3kT}b^3\frac{x^3}{4\ln 2x - 2} \tag{23}$$

where η is the viscosity of the medium and $x = a/b$ is assumed to be $\gg 1$. With the values $a = 1000$ Å and $b = 40$ Å, the hydrodynamic radius of a spherical micelle,[29] we obtain $R_1 = 1.8 \times 10^5$ s^{-1} and $R_2 = 2.0 \times 10^3$ s^{-1} and from eq 18-21 with $\vartheta = 90°$, $\tau_c = 2.3 \times 10^{-5}$ s is obtained.

The lateral translation diffusion of surfactant molecules on the curved surface of the micelle is also a possible mechanism for the slow motion. In this case the rate of the diffusional motion is determined by a translational diffusion constant D. The value of D is estimated from the measured self-diffusion constant in the cubic phase in the system potassium laurate-water to $D = 6 \times 10^{-7}$ cm^2/s.[20]

The rotational diffusion constants to be used in eq 18 can be estimated as $R_1 = D/b^2 = 3.8 \times 10^6$ s^{-1} and $R_2 = D/a^2 = 6.0 \times 10^3$ s^{-1} which gives $\tau_c = 7.0 \times 10^{-6}$ s.

The effective correlation times calculated from these two models are seen to be more than one order of magnitude longer than τ_c^s evaluated from the experimental relaxation data. Even if correlation times calculated from hydrodynamic equations often are too long,[30] the discrepancy is likely to be significant in this case. That too long correlation times are obtained from the calculations can be due to the fact that the rod-shaped micelles have been assumed to be stiff. Actually, rod-shaped micelles are probably quite flexible and exist in the solution in coiled "wormlike" configurations as has been suggested earlier by Stigter[31] from studies of the intrinsic viscosity in dodecylammonium chloride solutions. When part of such a micelle reorientates, there is not the same hydrodynamic resistance to the motion as for a stiff rod and τ_c^s will be shortened. Likewise, for the translational diffusion model, a molecule does not have to diffuse the same distance in a coiled micelle to change its direction.

CTAC Solutions. For the CTAC micelles, the relaxation times are approximately constant except for a slight decrease at the highest concentrations and the relaxation times are about twice as long as for the CTAB micelles at low concentration. Since the local rapid motion dominates the relaxation in extreme narrowing this implies that τ_c^f is about a factor of 2 shorter for CTAC micelles.

It is known that, due to its higher polarizability, bromide ions are located closer to a phase boundary than chloride ions.[32] The bromide ions can in this way lower the electrostatic repulsion between the cationic head groups in the CTAB micelles and make a closer packing and tighter binding of the surfactant molecules on the micellar surface possible which would explain the longer τ_c^f in CTAB. This might also be the reason why CTAB but not CTAC forms large micelles.

The molecular motions are slower in D_2O than in H_2O[33] due to higher mass of the D_2O molecule and stronger hydrogen bonds in D_2O. The correlation time τ_c^f in 0.65 M CTAC solution is increased by 25% when H_2O is replaced by D_2O as solvent (see Figure 1). This indicates

that the trimethylammonium group is coupled to the surrounding water.

Comparison with ^{14}N T_1 from Proton Line Shapes. ^{14}N spin-lattice relaxation times for 0.05 M aqueous solutions of alkyltrimethylammonium iodides have been measured by Larsen[15] using the influence of the ^{14}N relaxation on the line shape of the proton signal of the $-N-(CH_3)_3$ group. For the lower homologues, the proton line is split due to spin-spin coupling to the ^{14}N nucleus and there is little reason to doubt the values obtained for these compounds. However, for the longer micelle-forming homologues, there is only a very slight broadening of the proton line and the ^{14}N relaxation times obtained differ by more than an order of magnitude from those reported here. The change of bromide to iodide as counterion should not affect T_1 that much. Our results should be reliable since they are obtained by direct studies of the ^{14}N nucleus. The proton line shape method can be very susceptible to errors. An increase in the natural line width of the protons, occurring at the cmc[34,35] will in this method be attributed to ^{14}N relaxation and erroneous results are obtained.

Conclusions

Correlation times for the fast local motion and the slow motion over micellar distances of the surfactant molecules in CTAB micelles have been obtained from ^{14}N nuclear magnetic relaxation. The correlation time for the slow motion increases rapidly with concentration due to the formation of rod-shaped micelles. From model calculations and experimentally determined lengths of the aggregates it appears that the rod-shaped micelles have considerable flexibility. It is also confirmed that CTAC does not form rod-shaped micelles.

References and Notes

(1) E. Williams, B. Sears, A. Allerhand, and E. H. Cordes, *J. Am. Chem. Soc.*, **95**. 4871 (1973).
(2) R. T. Roberts, and C. Chachaty, *Chem. Phys. Lett.*, **22**, 348 (1973).
(3) M. Alexandre, C. Fouchet, and P. Rigny, *J. Chim. Phys.*, **70**, 1073 (1973).
(4) U. Henriksson, and L. Odberg, *Colloid Polym. Sci.*, **254**, 35 (1976).
(5) A. B. Scott and H. V. Tartar, *J. Am. Chem. Soc.*, **65**, 692 (1943).
(6) R. L. Vold, J. S. Waugh, M. P. Klein, and D. E. Phelps, *J. Chem. Phys.*, **48**, 3831 (1965).
(7) U. Henriksson, Thesis, Stockholm, 1975.
(8) D. Canet. G. C. Levy, and I. R. Peat, *J. Magn. Reson.*, **18**, 199 (1975).
(9) A. Abragam, "The Principles of Nuclear Magnetism", Oxford University Press, Oxford, 1961, Chapter 8.
(10) D. E. Woessner, *J. Chem. Phys.*, **37**, 647 (1962).
(11) W. T. Huntress, *Adv. Magn. Reson.*, **4**, 1 (1970).
(12) H. M. Cohen and F. Reif, *Solid State Phys.*, **5**, 321 (1957).
(13) J. M. Lehn and J. P. Kintzinger in "Nitrogen NMR", M. Witanowski, and G. A. Webb, Ed., Plenum Press, London, 1973.
(14) J. M. Lehn and M. Franck-Neumann, *J. Chem. Phys.*, **43**, 1421 (1965).
(15) D. W. Larsen, *J. Phys. Chem.*, **75**, 509 (1971).
(16) P. Mukerjee and K. J. Mysels, *Natl. Stand. Ref. Data Ser.*, *Natl. Bur. Stand.*, **No 36** (1971).
(17) F. Reiss-Husson and V. Luzzati, *J. Phys. Chem.*, **68**, 3504 (1964).
(18) H. J. C. Berendsen and H. T. Edzes, *Ann. N. Y. Acad. Sci.*, **204**, 459 (1973).
(19) H. Wennerstrom, G. Lindblom, and B. Lindman, *Chem. Scripta*, **6**, 97 (1974).
(20) J. Charvolin and P. Rigny, *J. Chem. Phys.*, **58**, 3999 (1973).
(21) U. Henriksson, L. Odberg, and J. C. Eriksson, *Mol. Cryst. Liquid Cryst.*, **30**, 73 (1975).
(22) J. Schaefer in "Carbon-13 NMR Spectroscopy", G. C. Levy, Ed., Wiley, New York, N.Y., 1974.
(23) J. Charvolin, P. Manneville, and B. Deloche, *Chem. Phys. Lett.*, **23**, 345 (1973).
(24) J. Seelig and W. Niederberger, *Biochemistry*, **13**, 1585 (1974).

(25) U. Henriksson, unpublished results.
(26) K. G. Gotz and K. Heckmann, Z. Phys. Chem., 20, 42 (1959).
(27) F. Perrin, J. Phys. Radium, 5, 497 (1934).
(28) F. Perrin, J. Phys. Radium, 7, 1 (1936).
(29) P. Ekwall, L. Mandell, and P. Solyom, J. Colloid Interface Sci., 35, 519 (1971).
(30) R. W. Mitchell and M. Eisner, J. Chem. Phys., 33, 86 (1960).
(31) D. Stigter, J. Phys. Chem., 70, 1323 (1966).

(32) K. Johansson and J. C. Eriksson, J. Colloid Interface Sci., 49, 469 (1974).
(33) See, e.g., J. Jarzynski and C. M. Davis in "Water and Aqueous Solutions", R. A. Horne, Ed., Wiley-Interscience, New York, N.Y., 1972.
(34) J. Clifford, Trans. Faraday Soc., 61, 1276 (1965).
(35) L. Odberg, B. Svens, and I. Danielsson, J. Colloid Interface Sci., 41, 298 (1972).

Vinyl Cyanide, Vinyl Isocyanide, and the Isomerization Reaction. A Theoretical Study

J. B. Moffat

Department of Chemistry, University of Waterloo, Waterloo, Ontario, Canada N2L 3G1 (Received July 9, 1976)

Ab initio calculations with a STO-3G and a 6-31G basis set have been performed on vinyl cyanide and isocyanide to establish optimized geometries and the associated electronic structures and energies. The energy of conversion of the cyanide to the isocyanide is calculated as 17.66 kcal mol^{-1}. The ionic character of the isocyanide appears to be a factor of 2 larger than that for the cyanide. Calculations with a two-parameter transition model for the conversion of cyanide to isocyanide produced an approximately isosceles triangular configuration at the barrier peak corresponding to 87.5 and 69.9 kcal mol^{-1} for conversion from the cyanide and isocyanide, respectively. The ionic character of the transition state is much smaller than that of the cyanide. No evidence for the existence of a metastable transition state was obtained.

Introduction

Unimolecular reactions are of interest from both the theoretical and experimental point of view, and the isomerization of isocyanides to cyanides is of particular appeal since it would appear to involve both bond scission and formation. The isomerization of methyl isocyanide is a reaction which lends itself to experimental study and for this reason, among others, a substantial amount of both experimental and theoretical information on this reaction is available. A portion of such work and that on the isocyanide–cyanide rearrangement in general has been reviewed recently[1] at which time the results of a semi-empirical calculation on methyl cyanide, isocyanide, and the isomerization reaction, involving the CNDO/2 method, were reported. A MINDO/2 calculation has also been performed by Dewar and co-workers.[2] The activation barrier for methyl isocyanide isomerization was calculated as 32.9 kcal mol^{-1} (experimental,[3] 38.4 kcal mol^{-1}), and the total electronic energy of methyl cyanide was found to be approximately 0.12 hartree (75.2 kcal mol^{-1}) lower than that of the isocyanide.

In contrast to the isomerization of methyl isocyanide, that of vinyl isocyanide has been relatively little studied, either experimentally or theoretically. Vinyl cyanide and its isomeric form are interesting molecules in their own right, from a theoretical point of view, and the versatility of vinyl cyanide from a practical point of view is well known to all chemists. It seems both valuable and interesting to examine these two molecules and their isomerization reaction from a theoretical point of view and to compare the results with those obtained for methyl cyanide.

Apparently the first synthesis of vinyl isocyanide was achieved as recently as 1967[4] and the results of simple Huckel-type molecular orbital calculations on both the cyanide and isocyanide were also reported at that time.

No other more recent theoretical work on this isocyanide appears to have been reported. In the case of vinyl cyanide or acrylonitrile a number of theoretical studies are available. An ab initio, all-electron wave function was obtained with two relatively small basis sets in this laboratory[5] using the experimental geometry of Costain and Stoicheff.[6] Neither exponent nor geometry optimization was attempted at that time. The larger of the two basis sets (35GTF) produced a total electronic energy of −160.6908 hartree and an ionization energy of 0.4252 hartree (experimental 0.3951 hartree[7]). More recently Leibovici[8] has applied CNDO, INDO, and modified CNDO-CI methods to vinyl cyanide. Other semiempirical methods have been applied by Mullen and Orloff[9] and Radeglis and Gey.[10]

The present calculations were performed with a number of aims: the calculation and comparison of the total electronic energies, orbital energies, and electron populations for the geometry-optimized molecules, vinyl cyanide and isocyanide, and, subsequently, an examination of the potential energy surface associated with the isomerization to provide similar information to that obtained in the case of methyl isocyanide. In the present work ab initio calculations with the GAUSSIAN 70 program of Hehre, Lathan, Ditchfield, Newton, and Pople[11] have been performed. Both STO-3G and extended 6-31G basis sets were employed. The bond lengths and bond angles of the cyanide and isocyanide were energy-optimized cyclicly and independently to ±0.001 Å and ±0.1°, respectively, with both the STO-3G and 6-31 G basis sets. Examination of the potential surface for the transition was done with the STO-3G basis and partly with the 6-31G basis set.

Results and Discussion

The energy-optimized nuclear configurations for vinyl cyanide and isocyanide, as obtained with both STO-3G and

TABLE I: Energy-Optimized Nuclear Configuration for Vinyl Cyanide and Isocyanide

Bond	Vinyl cyanide			Vinyl isocyanide			Transition model	
	STO-3G	6-31G	Expt[a]	STO-3G	6-31G	Expt[b]	STO-3G	6-31G
Bond Length, Å								
C^1-C^6	1.461	1.432	1.426				1.647	1.901
C^1-N^6				1.416	1.385	1.376	1.825	1.844
C^1-C^2	1.316	1.329	1.339	1.315	1.323	1.339	1.318	1.314
C^6-N^7	1.157	1.148	1.164	1.175	1.167	1.165	1.226	1.164
C^1-H^5	1.083	1.072[c]	1.086	1.088	1.071[c]	1.086	1.085	1.069
C^2-H^3	1.083[c]	1.072[c]	1.086	1.081[c]	1.071[c]	1.086	1.083[c]	1.069
C^2-H^4	1.083[c]	1.072[c]	1.086	1.081[c]	1.071[c]	1.086	1.083[c]	1.069
Bond angles, deg								
$\angle C^1C^2H^3$	121.2	120.7	121.2	120.8	120.7	121.7	120.9	120.0
$\angle C^1C^2H^4$	122.3	122.1	121.2	122.0	121.6	121.7	122.5	120.0
$\angle C^2C^1H^5$	121.7	121.2	121.7	122.8	122.6	120.8	122.2	120.0
$\angle C^6C^1C^2$	122.9	123.2	122.6				122.3	127.4[d]
$\angle N^6C^1C^2$				123.0	123.2	123.6	1.631	178(r)
							80.1(θ)	93.0(θ)
							97.1(ϕ)	

[a] Reference 6. [b] Reference 13. [c] Parameters optimized together. [d] Angle between arm of length r and C_1C_2 (Figure 1).

TABLE II: Total Electronic Energy, Orbital Energies, Nuclear Repulsion Energy, and Dipole Moment of Vinyl Cyanide, Vinyl Isocyanide, and the Transition Model in Their Optimized Configurations[a]

	Vinyl cyanide	Vinyl isocyanide	Transition model
Total energy	-169.693 924	-169.665 795	-169.554 492
Nuclear repulsion energy	90.552 904	92.830 324	90.820 522
Orbital energies	-15.599 85	-15.611 01	-15.626 63
	-11.296 66	-11.317 15	-11.342 92
	-11.294 22	-11.303 15	-11.298 13
	-11.281 59	-11.258 51	-11.275 31
	-1.256 799	-1.298 164	-1.321 340
	-1.105 361	-1.092 803	-1.085 308
	-0.885 952 1	-0.906 017 7	-0.823 486
	-0.729 501 3	-0.742 963 3	-0.704 060
	-0.663 084 4	-0.667 215 9	-0.637 271
	-0.581 949 6	-0.575 917 3	-0.603 070
	-0.548 501 3	-0.562 492 5 (π)	-0.533 572 (π)
	-0.524 881 5 (π)	-0.491 325 5	-0.527 015
	-0.475 438 8	-0.471 601 3	-0.464 917
	-0.395 166 2 (π)	-0.379 272 0 (π)	-0.410 881 (π)
	+0.095 028 55 (π*)	+0.115 408 6 (π*)	+0.133 037 (π*)
Ionization energy	+0.395 2 (0.3951)[b]	+0.379 3	+0.410 9
Dipole moment, D	4.301 7 (3.89)[c]	3.138 4 (3.56)[d]	

[a] Energies are reported in hartrees (6-31G basis). [b] Reference 7. [c] Reference 12. [d] Reference 13.
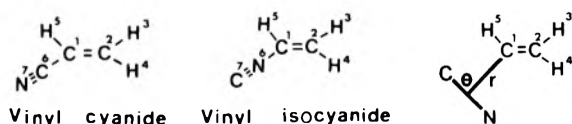

Figure 1. Vinyl cyanide, vinyl isocyanide, and transition model.

6-31G bases, are given in Table I, using the atom labeling of Figure 1. For comparison purposes the experimental values of the geometrical parameters for vinyl cyanide are also shown in Table I. It should be noted that the "experimental" values for vinyl isocyanide have been obtained from related structures.[13] With the 6-31G basis, the C–H bond distances in the particular molecule were assumed to be identical and optimization was carried out under this constraint. With the STO-3G basis, the two ethylenic hydrogen atoms situated on the same carbon were optimized together.

Table II contains the total electronic energy, nuclear repulsion energy, orbital energies, ionization energy, and dipole moment for each molecule. As in our previous work on vinyl cyanide,[5] the highest occupied orbital is a π type. Interestly the same is predicted for the isocyanide. In the present work, however, the total energy for the cyanide is some 9 hartrees lower than obtained previously.[5] The experimental and theoretical values of the ionization

energy for the cyanide agree quite well but it is difficult to say how fortuitous this is. The calculated dipole moments in both molecules agree with experimental values to approximately 10%. It is interesting to note the reasonable similarity between the orbital energies for the cyanide and isocyanide. This is, at least on qualitative grounds, not surprising. The nuclear configurations of the two molecules, aside from the interchange of the N and C atoms, are essentially the same. Hence, one might anticipate that relatively little change in the orbital energies should occur. However, as expected, the interchange of the carbon and nitrogen atoms produces some difference in the electron populations (Table III); the carbon to which either the cyanide or isocyanide group is attached being reduced in electron population when it finds itself adjacent to a nitrogen atom.

Table II also shows that vinyl cyanide would, not unexpectedly, be the more stable of the two molecules, the energy required for the conversion of the cyanide to the isocyanide being calculated as 17.66 kcal mol⁻¹. This is quite similar to the value of 17.4 kcal mol⁻¹ calculated recently for the conversion of methyl cyanide to isocyanide by ab initio methods.[14] The energy for the hydrogen cyanide–isocyanide isomerization has been calculated as 8.41 kcal mol⁻¹ by Booth and Murrell[15] using a minimum basis of Slater orbitals, and as 9.5 and 14.6 kcal mol⁻¹ by

TABLE III: Atomic Charges[a]

	Vinyl cyanide	Vinyl isocyanide	Transition model
C^1	-0.089	+0.231	-0.222
C^2	-0.297	-0.345	-0.311
H^3	+0.195	+0.187	+0.206
H^4	+0.209	+0.199	+0.224
H^5	+0.240	+0.231	+0.274
C^6	+0.042	+0.169	+0.177
N^7	-0.500	-0.673	-0.346

[a] 6-31G basis.

TABLE IV: Electron Distributions[a]

		Vinyl cyanide	Vinyl isocyanide	Transition model
N	2S	1.834	1.548	1.872
	2PX	1.244	1.250	1.048
	2PY	1.083	1.462	1.304
	2PZ	1.141	1.415	1.123
C_1	2S	1.118	1.061	1.245
	2PX	0.961	0.786	0.879
	2PY	1.066	1.030	1.094
	2PZ	0.946	0.895	1.006
C_2	2S	1.284	1.277	1.284
	2PX	1.144	1.138	1.136
	2PY	0.905	0.980	0.934
	2PZ	0.967	0.953	0.960
C_6	2S	1.059	1.794	1.726
	2PX	0.965	0.846	0.619
	2PY	0.947	0.529	0.669
	2PZ	0.990	0.664	0.811

[a] 6-31 G basis.

Figure 2. Total electronic energy (6-31 G basis) of transition model: (a) as a function of r, (∇) $\theta = 85°$, ($\square$) $\theta = 90°$, ($\bullet$) $\theta = 93°$, (C) $\theta = 95°$, ($\triangle$) $\theta = 100°$; (b) as a function of θ, ($\lozenge$) $r = 1.6$ Å, ($\blacktriangle$) $r = 1.7$ Å, ($\blacksquare$) $r = 1.8$ Å, ($\blacktriangledown$) $r = 1.9$ Å.

Pearson, Schaefer and Wahlgren[16] by means of an SCF calculation with a double ζ plus polarization quality of basis in the first case, and a configuration interaction calculation in the latter case.

It is of interest to consider the charge distribution of the two molecules. The present results suggest that the cyanide and isocyanide could be represented as $[C_2H_3^{0.258+}][CN^{0.258-}]$ and $[C_2H_3^{0.499+}][NC^{0.499-}]$, respectively, using the data from Table III. It is not surprising to find the ionic character of the isocyanide greater than that of the cyanide. However it is somewhat unexpected to find that the carbon atom of both cyanide and isocyanide groups has a positive net atomic charge. However the carbon atom attached to these two latter groups possesses a net negative and a net positive charge, respectively. Liskow, Bender, and Schaefer[14] found that methyl cyanide and isocyanide could be represented as $[CH_3^{0.12+}][CN^{0.12-}]$ and $[CH_3^{0.27+}][NC^{0.27-}]$, respectively, the same approximate doubling of ionic character in passing from the cyanide to the isocyanide as has been found in the present work with vinyl cyanide.

Table IV summarizes the electron distributions as obtained from a Mulliken population analysis. The electron distribution associated with the ethylenic carbon atom (C_2) distant from the nitrile or isonitrile group is, as expected, essentially identical in the cyanide and iso-cyanide molecules. The removal of electron density (Table III) from the other ethylenic carbon atom (C_1) in passage from the cyanide to the isocyanide is evidently (Table IV) associated primarily with the 2PX atomic orbital, and to a lesser extent the 2S and 2PZ orbitals. Presumably the loss of 0.32 in atomic charge which is sustained by C_1 when the isocyanide is formed can then be largely related to a transfer of σ electrons. However, in forming the isocyanide from the cyanide, the nitrile carbon loses 0.127 of atomic charge, while the nitrogen gains 0.373 of atomic charge
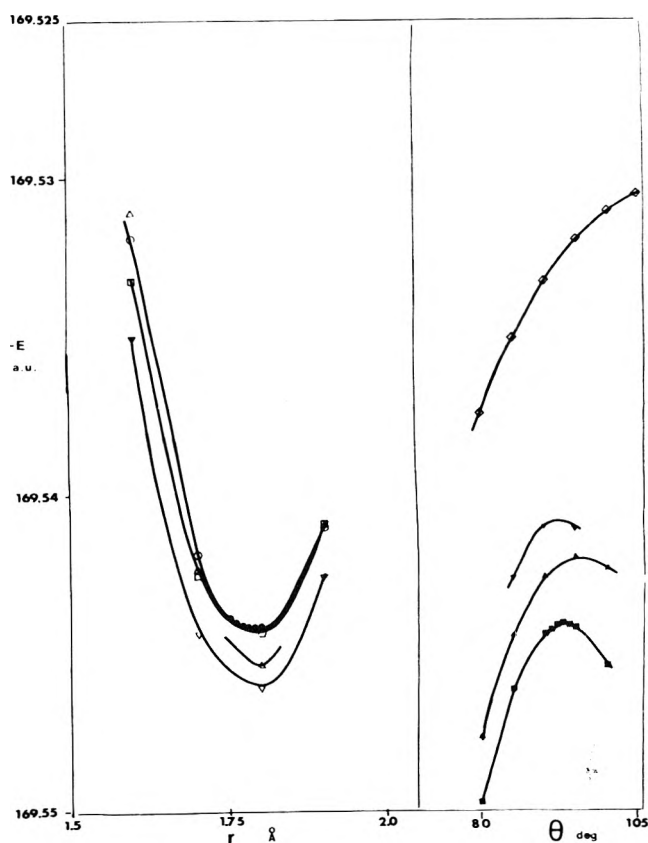
(Table III), that is, the nitrile carbon becomes more positive and the nitrogen more negative. In so doing the 2S density of the nitrile carbon increases by approximately 0.7 while all the 2P density decreases by approximately 0.8 (Table IV). In contrast, the 2S density of the nitrogen atom decreases by approximately 0.3 when the isocyanide forms and the 2P density increases by about 0.6. These alterations in atomic charge densities appear to be at least semiquantitatively consistent with the chemists's picture. Part of the substantial increase in 2S density on the nitrile carbon and the decrease in 2S density on the nitrogen atom in passing to the isocyanide is undoubtedly to be associated with the transfer of the lone pair from the nitrogen to the carbon atom. The decrease and increase in 2P density on the nitrile carbon and nitrogen atoms, respectively, can be related to the classical picture of the isocyanide in which the carbon is represented as contributing two electrons, the nitrogen four electrons to the isocyanide bonding. Table IV shows that the π density associated with the nitrogen atom increases by approximately the same amount as that of the nitrile carbon atom decreases, thus appearing as a "directed" π bond.

In order to study the isomerization process from the cyanide to the isocyanide, the transition model shown in Figure 1 was employed. This permitted the isomerization to be considered in terms of two variables, r, the separation of the center of the CN group from the nearest carbon of the vinyl group, and θ, the angle between the internuclear axis of the CN group and the line joining its center to the nearest carbon atom of the vinyl group. Calculations employing the 6-31G basis were carried out for values of θ varying in increments of 5° from 80 to 100° for each of 1.6, 1.7, 1.8, and 1.9 Å as values for r, without optimization of geometry. The results of these calculations are shown in Figure 2, where Figure 2a shows the variation of total
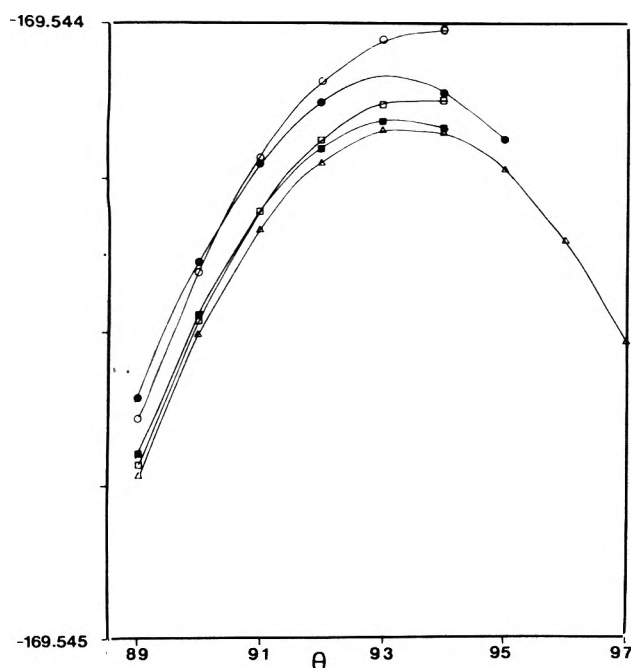
Figure 3. Total electronic energy (6-31 G basis) as a function of θ: (O) r = 1.76 Å, (□) r = 1.77 Å, (△) r = 1.78 Å, (■) r = 1.79 Å, (●) r = 1.80 Å.

energy as a function of r, for different values of the angle, θ, while Figure 2b illustrates the same data plotted as a function of the angle for various values of r.

From Figure 2 it can be seen that the lowest energy barrier on the potential surface is found in the region with r equal to 1.7–1.8 Å and θ equal to 90–95°. Calculations were then performed for values of θ from 90 to 95° in increments of 1° with each of the values of r from 1.7 to 1.8 Å in increments of 0.01 Å. The results of these calculations are shown in Figure 3. From these data the values of r and θ producing the lowest energy for the isomerization barrier are 1.78 Å and 93°, respectively. The energy associated with this barrier height is –169.544 17 hartree. A geometry-optimization of this structure (Tables I and II), with r and θ held at 1.78 Å and 93°, respectively, produced an energy of –169.554 49 hartree, which corresponds to barrier heights of 87.52 and 69.87 kcal mol^{-1} from the cyanide and isocyanide, respectively. The charge separation in the transition model corresponds to $[C_2H_3^{0.168+}CN^{0.168-}]$ which is much less ionic than that of the stable forms. Examination of Figure 2 shows no indication of the existence of a metastable intermediate, as evidenced by the absence of even a shallow well in the vicinity of the barrier peak. The transition model has π-orbital energies quite similar in value and position to those for the isocyanide (Table II). However in the transition model the carbon atom (C_1) has a net negative charge, apparently in large part as a result of transfer of electrons from the nitrogen atom in the isocyanide form.

It is interesting to compare the present results with those found previously for CH_3CN isomerization. The shape of the transition configuration is approximately the same in both cases, namely, that of an isosceles triangle. However the barrier height for the present molecule is approximately twice as large as in the methyl cyanide case. Unfortunately there does not appear to be any corresponding experimental data with which to compare. The energy of conversion of the cyanide to the isocyanide is, however, almost identical in both cases (17.5 kcal mol^{-1}). This is not particularly surprising since the net process may be viewed as the breaking of one bond and the forming of another, and it seems reasonable to believe that

any perturbation of the R–C bond in RCN as a result of variation in the R substituent would be approximately the same as the perturbation of the R–N bond in RNC. The ab initio calculations on CH_3CN isomerization showed that the methyl carbon possesses a negative charge in the cyanide, isocyanide, and transition state and that the ab initio transition state is even less ionic than CH_3NC. In the present case, there is agreement with the latter conclusion but the charge of the carbon atom attached to the nitrile or isonitrile group undergoes a transition from a negative to an even more negative and finally to an equally positive value as the transition from cyanide to isocyanide occurs.

In the transition model (see Table III) the charge on the nitrile carbon is nearly identical in both the isocyanide and transition model, while the cyanide and transition model have approximately similar atomic charges on the nitrogen. From Table IV it can be seen that the nitrile carbon in the transition model has taken up the 2S density of the isocyanide, while the nitrogen atom has similar 2S densities in both the cyanide and the transition model. This implies, as would be expected intuitively, that lone pairs have appeared on both the nitrile carbon and nitrogen in the transition model. Further the total 2P density on the nitrogen in the cyanide and transition model are similar, while that on the nitrile carbon in the isocyanide and transition model are similar. So in the transition model the nitrile carbon is like that in the isocyanide while the nitrogen is similar to that in the cyanide and the excess density has been pushed to the ethylenic carbon resulting in a less positively charged ethylenic group and hence a less ionic molecule than in either the cyanide or isocyanide molecules themselves.

Some further examinations of the transition model were performed with the STO-3G basis. Within the transition model the CN bond was allowed to rotate out-of-plane and about the arm of length r, and the out-of-plane angle was labeled ϕ. r, θ, and ϕ were varied one at a time to find the lowest barrier height as before, and values of 1.63 Å, 80.1°, and 97.1°, respectively, were so obtained. With these values fixed the remaining variables were energy-optimized and the results are reported in Table I. In this case the distances from the nitrile carbon and nitrogen to the point of joining to the arm of length r were also separately optimized and found to be 0.641 and 0.585, respectively. An energy of –167.508 647 hartrees was obtained compared to –167.593 144 and –167.627 292 hartrees for the STO-3G energy-optimized configurations of the isocyanide and cyanide, respectively. These values yield a isocyanide to cyanide isomerization energy of 21.43 kcal mol^{-1}, and transition barriers of 53.0 and 74.5 kcal mol^{-1} from the isocyanide and cyanide, respectively. The STO-3G isomerization energy is slightly higher than that calculated with the 6-31G basis, but the transition energies are considerably lower with the STO-3G basis. As would be expected the atomic charges calculated within the STO-3G basis do not agree quantitatively with those found with the 6-31G basis. The trends are, however, in semiquantitative agreement.

References and Notes

(1) J. B. Moffat and K. F. Tang, *Theor. Chim. Acta (Berl.)*, **32**, 171 (1973).
(2) M. J. S. Dewar and M. C. Kohn, *J. Am. Chem. Soc.*, **94**, 2704 (1972).
(3) S. C. Chan, B. S. Robinovitch, J. T. Bryant, L. D. Spicer, T. Fujimoto, Y. N. Lin, and S. P. Pavlou, *J. Phys. Chem.*, **74**, 3160 (1970).

(4) D. S. Matteson and R. A. Bailey, *Chem. Ind.*, 191 (1967); *J. Am. Chem. Soc.*, **90**, 3761 (1968).

(5) J. B. Moffat and R. J. Collens, *J. Mol. Spectrosc.*, **27**, 252 (1968).

(6) C. C. Costain and B. P. Stoicheff, *J. Chem. Phys.*, **30**, 777 (1959).

(7) J. D. Morrison and A. J. C. Nicholson, *J. Chem. Phys.*, **20**, 1021 (1952).

(8) C. Leibovici, *J. Mol. Struct.*, **9**, 177 (1971).

(9) P. A. Mullen and M. K. Orloff, *Theor. Chim. Acta (Berl.)*, **23**, 278 (1971).

(10) R. Radeglis and E. Gey, *J. Prakt. Chem.*, **314**, 43 (1972).

(11) W. J. Hehre, R. F. Stewart, and J. A. Pople, *J. Chem. Phys.*, **51**, 2657 (1969), and subsequent papers; QCPE program no. 236.

(12) W. S. Wilcox, J. M. Goldstein, and J. W. Simmons, *J. Chem. Phys.*, **22**, 516 (1954).

(13) K. Bolton, N. L. Owen, and J. Sheridan, *Spectrochim. Acta, Part A*, **26**, 909 (1970).

(14) D. H. Liskow, C. F. Bender, and H. F. Schaefer, III, *J. Am. Chem. Soc.*, **94**, 5178 (1972).

(15) D. Booth and J. N. Murrell, *Mol. Phys.*, **24**, 1117 (1972).

(16) P. K. Pearson, H. F. Schaefer, and V. Wahlgren, *J. Chem. Phys.*, **62**, 350 (1975).

COMMUNICATIONS TO THE EDITOR

Competitive Radiotracer Evaluation of Relative Rate Constants at Stratospheric Temperatures for Reactions of ^{38}Cl with CH_4 and C_2H_6 Vs. CH_2=$CHBr^1$

Sir: The rate constants and activation energy for the abstraction of H from CH_4 by atomic Cl, as in (1), have

$$Cl + CH_4 \rightarrow HCl + CH_3 \qquad (1)$$

been evaluated by several techniques over the past decade and especially during the last 2 years.[2,3] The rate constant is of special interest in the 210–270 K range because of its importance with respect to the stratospheric ClO_x chain reaction which results in ozone removal.[4-6] Since estimates of the ozone depletion corresponding to a given stratospheric chlorine concentration vary almost linearly with this rate constant (slower rate corresponding to more ozone depletion), an error of a factor of 1.5 at 225 K assumes considerable practical significance. We have now applied a radiotracer method to the study of the competitive reactions of ^{38}Cl with a hydrocarbon (methane, ethane) vs. reaction with vinyl bromide, using ^{38}Cl atoms formed in situ by irradiation of gaseous $CClF_3$ with thermal neutrons from a nuclear reactor.[7] Variation of the ambient temperature of the samples during irradiation between 243 and 361 K has permitted evaluation of the relative activation energies and relative rate constants for the reactions with the two gaseous hydrocarbons, and could be readily applied to other hydrogen-containing compounds.[8] Our measurements indicate a rate constant for k_1 at 243 K of 3.2 ± 0.6) × 10^{-14} cm^3 molecule^{-1} s^{-1}, in agreement with the lower limits of values considered in the past several years.

The fundamental measurement in each system is the percentage yield of CH_2=$CH^{38}Cl$ from ^{38}Cl reactions with CH_2=$CHBr$, following the sequence of reactions outlined in equations 1–4. The ^{38}Cl atoms, although formed with

$$^{38}Cl + CH_2=CHBr \rightarrow C_2H_3Br^{38}Cl^* \qquad (2)$$

$$C_2H_3Br^{38}Cl^* + M \rightarrow C_2H_3Br^{38}Cl + M \qquad (3)$$

$$C_2H_3Br^{38}Cl + HI \rightarrow C_2H_4Br^{38}Cl + I \qquad (4)$$

$$C_2H_3Br^{38}Cl^* \rightarrow CH_2=CH^{38}Cl + Br \qquad (5)$$
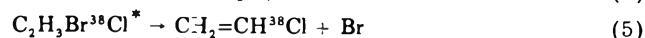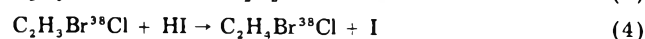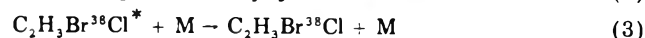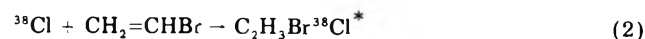
excess kinetic energy from the $^{37}Cl(n,\gamma)^{38}Cl$ nuclear reaction, are thermalized by multiple collisions with the excess of inert $CClF_3$.[7] The competitive deexcitation of $C_2H_3Br^{38}Cl^*$ by collision in (3), and subsequent reaction of the thermalized radical can be confirmed through the observation of $CH_2BrCH_2^{38}Cl$ in the presence of a hydrogen-donating scavenger molecule such as HI. In the present experiments molecular O_2 was used as a scavenger to remove the stabilized radicals of (3) without the release of CH_2=$CH^{38}Cl$.

At any particular temperature and pressure of $CClF_3$ a fixed fraction of the radicals formed in (2) will subsequently decompose to CH_2=$CH^{38}Cl$ by reaction 5. However, when hydrogen abstraction from a hydrocarbon is also available for removal of ^{38}Cl atoms, as in (1) or (6),

$$^{38}Cl + C_2H_6 \rightarrow H^{38}Cl + C_2H_5 \qquad (6)$$
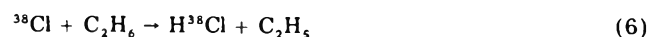
the yield of CH_2=$CH^{38}Cl$ will be correspondingly reduced to the extent that the thermal ^{38}Cl atoms have been prevented from reacting with CH_2=$CHBr$ through prior reaction with the hydrocarbon. This competition is expressed in eq 7 for CH_4 and CH_2=$CHBr$, in which

$$\frac{1}{Y_{(CH_2=CH^{38}Cl)}} = A + \left(\frac{k_1}{Bk_2}\right)\left(\frac{(CH_4)}{(CH_2=CHBr)}\right) \qquad (7)$$

$Y_{CH_2=CH^{38}Cl}$ is the fractional yield of ^{38}Cl as CH_2=$CH^{38}Cl$ and all of the ^{38}Cl is assumed to be available for reactions 1, 2, and 6. (If small corrections are made for "hot" reactions with $CClF_3$ the numerator on the left-hand side is about 0.95 instead of 1.00.)

The intercept parameter A and the slope parameter B both involve reactions 2–4, but are independent of the concentration of RH as long as (RH) ≪ ($CClF_3$). In these experiments the mole fraction of $CClF_3$ was always ≥0.9. The expected linear plots of $(Y_{CH_2=CH^{38}Cl})^{-1}$ vs. (RH)/(CH_2=$CHBr$) are observed for either added CH_4 or C_2H_6 at 243, 298, and 361 K, although C_2H_6 is very much more efficient in interfering with the vinyl bromide reaction. The measured values of A, (k_1/Bk_2), and (k_6/Bk_2) from these experiments are summarized in Table I. The value of A is dependent on both the pressure and temperature and is useful only for the evaluation of reactions with CH_2=$CHBr$, including (2) to (5) plus any others that

TABLE I

Temp, K	(% yield of $CH_2=CH^{38}Cl)^{-1}$			
	A^a	k_1/Bk_2	k_6/Bk_2	k_6/k_1
361	3.7	1.2×10^{-2}	1.8	150 ± 20
298	4.3	6.4×10^{-2}	2.3	360 ± 40
243	6.7	1.7×10^{-3}	2.7	1700 ± 300

a These samples contained approximately 5 atm total pressure at the temperature of irradiation. Since the time between collisions varied with temperature the values of A given in the table are not directly comparable.

occur, e.g., abstraction of H.

With both A and Bk_2 fixed for low mole fractions of $CH_2=CHBr$ and of RH in excess $CClF_3$ at each pressure and temperature, the relative values of k_1 for CH_4 and k_6 for C_2H_6 can be directly obtained at each temperature, as shown in the final column of Table I. These rate constant ratios can be directly compared at each temperature, while the variation of this ratio with temperature provides an estimate of the difference in activation energies for abstraction from CH_4 and C_2H_6, as shown in Figure 1. The rate constant for reaction 5 at 243 K as used in stratospheric calculations has varied from 3.2×10^{-14} to 5.1×10^{-14} cm^3 molecule^{-1} s^{-1}.[9,10] Two recent measurements of the rate constant for reaction 6 indicate very little variation with temperature and values of 5×10^{-11} and 6×10^{-11} cm^3 molecule^{-1} s^{-1} at 243 K.[12,13] At this temperature our measured ratio of (1700 ± 300) for k_6/k_1 corresponds to a value of $(3.2 \pm 0.6) \times 10^{-14}$ cm^3 molecule^{-1} s^{-1} for k_1 in reasonable agreement with the slower rate. Several other recent determinations have been reported, whose values are, respectively, at 243 K (in 10^{-14} cm^3 molecule^{-1} s^{-1}): 4.2,[13] 3.6,[14] 4.1,[15] 4.4,[16] and 3.4.[17] The agreement is now rather satisfactory on a value in the vicinity of (3.8 ± 0.5) $\times 10^{-14}$ cm^3 molecule^{-1} s^{-1} at 243 K.

The solid line in Figure 1 represents an activation energy difference between abstraction from CH_4 and from C_2H_6 of 3300 kcal/mol. This could be consistent, for example, with an activation energy of 3560 kcal/mol[2,9] for (1) and about 260 kcal/mol for (6), e.g., $k_6 = 7.6 \times 10^{-11}$ $exp(-130/T)$ cm^3 molecule^{-1} s^{-1}. Our data are not consistent with activation energies for (1) in the vicinity of 2500 kcal/mol. The dotted line in Figure 1 represents the rate equation for $k_1 = 7.4 \times 10^{-12}$ $exp(-1226/T)$.[16] Several recent experiments have given "curved Arrhenius plots" for k_1,[13-16] with deviations in the opposite direction from the apparent deviations of our results from the solid line of Figure 1. Our measurements, of course, are limited to relative rates and activation energies and provide no indication of either on an absolute basis.

Measurements of the rate of reaction of chlorine atoms with ethane indicate it to be very fast at room temperature, and the values of (k_6/Bk_2) indicate that the addition to vinyl bromide proceeds at a comparable rate. Since the value of B, the reciprocal of the fraction of ^{38}Cl additions to vinyl bromide which eventually lead to observable $CH_2=CH^{38}Cl$, lies in the range of 2–4 for these temperatures and pressures, the addition of chlorine atoms to vinyl bromide must have a rate constant of $\sim 1 \times 10^{-10}$ cm^3 molecule^{-1} s^{-1}, as well as a very low activation energy. Experiments with crossed molecular beams of chlorine atoms and vinyl bromide have shown large reaction cross sections (20–35 Å^2) together with forward–backward symmetry for the vinyl chloride product indicative of a long-lived C_2H_3BrCl complex ($\geq 5 \times 10^{-12}$ s).[18] Our observation of pressure-dependent yields of $CH_2=CH^{38}Cl$ indicates that such complexes have lifetimes of $\sim 10^{-10}$ s, and the only product found from reaction 3 is $CH_2BrCH_2^{38}Cl$. These observations are consistent with
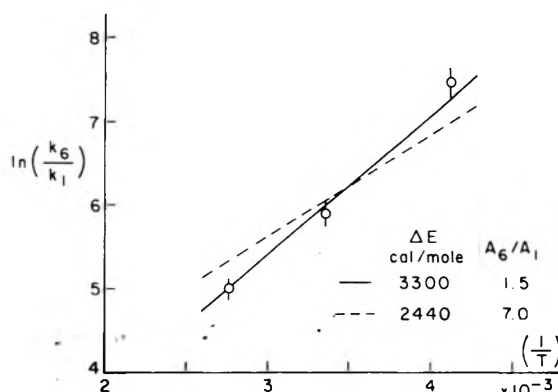

Figure 1. Temperature dependence of the ratio of reaction rates for abstraction from C_2H_6 and CH_4.

the postulate[18] that the rate-determining step in the loss of Br from $C_2H_3Br^{38}Cl$ is the 1,2 migration of H or ^{38}Cl, followed by extremely rapid loss of Br from the newly isomerized radical.

References and Notes

(1) This research was supported by ERDA Contract No. AT(04-3)-34, P.A. 126.
(2) (a) NBS Technical Note 866, June, 1975. (b) R. T. Watson, *J. Phys. Chem. Ref. Data Ser.*, in press.
(3) M. A. A. Clyne and R. F. Walker, *J. Chem. Soc., Faraday Trans. 1*, **69**, 1547 (1973).
(4) M. J. Molina and F. S. Rowland, *Nature (London)*, **249**, 810 (1974).
(5) F. S. Rowland and M. J. Molina, *Rev. Geophys. Space Phys.*, **13**, 1 (1975).
(6) Halocarbons: Effects on Stratospheric Ozone, Panel on Atmospheric Chemistry, National Academy of Sciences, Sept., 1976.
(7) F. S. C. Lee, Ph.D., Thesis, University of California, Irvine, 1975.
(8) A similar competitive procedure has been applied (without temperature variations) to the reactions of thermal ^{18}F with hydrocarbons vs. C_2H_2 and/or C_2H_4. R. L. Williams and F. S. Rowland, *J. Phys. Chem.*, **77**, 301 (1973).
(9) The Arrhenius rate equation for (1) and ref 2a is 5.1×10^{-11} $exp(-1790/T)$ for the temperature range 300–686 K. This equation was extrapolated to stratospheric temperatures in the first ozone depletion estimates (see ref 5). The value at 243 K is 3.2×10^{-14} cm^3 molecule^{-1} s^{-1}.
(10) The basic calculation of ozone depletion in the 1976 National Academy of Sciences report (ref 6) used the rate equation 5.4×10^{-12} $exp(-1133/T)$ for reaction 1. With this equation the rate constant for (1) at 243 K is 5.1×10^{-14} cm^3 molecule^{-1} s^{-1}. This equation was given as a preliminary value in ref 2a and 11.
(11) R. T. Watson, D. D. Davis, R. L. Schiff, S. Fischer, and E. Machado, results reported at 4th C.I.A.P. Conference in Boston, Feb. 4–7, 1975, and at the 169th National Meeting of the American Chemical Society, Philadelphia, Pa., April 6–11, 1975.
(12) R. T. Watson, D. D. Davis, E. S. Machado, B. Y. Conaway, and Y. Oh, presented at the 4th C.I.A.P. Conference, Boston, Mass., Feb., 1975.
(13) R. G. Manning and M. J. Kurylo, *J. Phys. Chem.*, in press, give for k_6 the rate equation 7.9×10^{-11} $exp(-61/T)$ cm^3 molecule^{-1} s^{-1} corresponding to 6.1×10^{-11} cm^3 molecule^{-1} s^{-1} at 243 K. The rate equation for k_1 is 7.93×10^{-12} $exp(-1272/T)$.
(14) M. Zahniser, J. Chang, and F. Kaufman, unpublished results. The rate equation is 8.44×10^{-12} $exp(-1328/T)$ between 200 and 300 K.
(15) J. H. Lee, J. V. Michael, W. A. Payne, L. J. Stief, and D. A. Whytock, International Conference on Stratosphere and Related Problems, Logan, Utah, Sept. 15–17, 1976. The rate equation is 6.78×10^{-12} $exp(-1242/T)$ below 300 K.
(16) Successive evaluations of the data first reported in ref 2a and 11 have given the rate equations 5.4×10^{-12} $exp(-1133/T)$; 7.4×10^{-12} $exp(-1226/T)$; and the current equation 7.94×10^{-12} $exp(-1260/T)$.
(17) M. T. Leu and W. B. DeMore, private communication. They have measured the equation for k_1 as 4.0×10^{-11} $exp(-1720/T)$ above 300 K with no indication of deviation from this Arrhenius expression at lower temperatures.
(18) J. T. Cheung, J. D. McDonald, and D. R. Herschbach, *J. Am. Chem. Soc.*, **95**, 7889 (1973).

Department of Chemistry
University of California
Irvine, California 92717

Frank S. C. Lee
F. S. Rowland[*]

Chemical Oscillations in the Absorbance of Rhodamine B in Solvents of Low Dielectric Constant

Sir: While monitoring the optical absorbance of rhodamine B at 5600 Å oscillatory fading was observed. This phenomena was noted in several solvents: 1,2-dichloroethane (DCE), dimethylformamide (DMF), and tetrahydrofuran (THF).

Approximately 10% of the DCE solutions ($\sim 10^{-5}$ M in a 2.0-cm cell closed to air) exhibited periodic behavior, Figure 1. Prior to the "spontaneous" fading, induction periods were noted (0->20 min); whereas, the remaining solutions showed little or no change in absorbance over extended periods of monitoring. Purging samples with N_2 gas prior to monitoring induced oscillations in a significantly greater number of solutions. Exposure to short periods of high intensity white light at any time during the reaction resulted in a rapid return of absorbance at 5600 Å. Similar oscillatory fading could then be observed in the "recycled" solutions, Figures 1a and 1b. Prolonged exposure to white light, however, produced an irreversible photobleaching. Trace amounts of ammonium hydroxide added to any of the DCE solutions produced immediate color fading and continuous monitoring of solutions containing NH_4OH, subsequent to periods of irradiation, showed an oscillatory absorbance/time growth curve at 5600 Å.

Dilute solutions of rhodamine B base (the lactone dye form) in DCE ($\sim 10^{-5}$ M) were colorless.[1] Irradiation of these solutions again resulted in oscillations in the absorbance/time growth curve at 5600 Å, Figure 2a. In this system, however, oscillations could also be induced when the solvent was irradiated prior to addition of the dye.

Dilute solutions of rhodamine B in DMF were colorless. Concentrations $\gtrsim 10^{-4}$ M were required in each case to obtain the desired absorbance at 5600 Å.[1] Again, only a small percentage of solutions exhibited the "spontaneous" fading in a closed or open cell. However, fading with fluctuations was induced in nearly all DMF solutions subsequent to irradiation, Figure 2b. Oscillations could also be generated when DMF was irradiated prior to addition of the dye. Each sample irradiated was periodically rotated to minimize possible diffusion effects resulting from highly absorbing species near the cell walls. Alternate periods of dark and monitoring produced no apparent changes in the resulting waveforms and similar results were generally obtained with solutions open to air or purged with N_2 and then closed. In one notable exception an open cell was necessary to induce fluctuations in a solution which otherwise exhibited an approximate logarithmic absorbance/time decay curve at 5600 Å. The logarithmic absorbance/time behavior was typical of the few irradiated DMF solutions in which oscillations were not observed. Prolonged exposure of DMF to high intensity light appeared only to accelerate fading of the dye.

"Spontaneous" oscillatory fading was observed in a number of closed THF solutions. This system was not studied further since large amplitude fluctuations, similar to those in DCE and DMF, could not be induced.

The lactone form of rhodamine B was identified in each sample initially colorless or induced to fade by absorption maxima in the UV at ~ 2400, 2700, and 3200 Å[1-3] (the photobleached DCE solutions yielded intense peaks at 2600 and 3100 Å, and a weak absorption at ~ 5000 Å). Although a suitable autocatalytic or feedback step cannot be proposed at this point which would lead to oscillatory behavior in these systems, any initiation step based on light
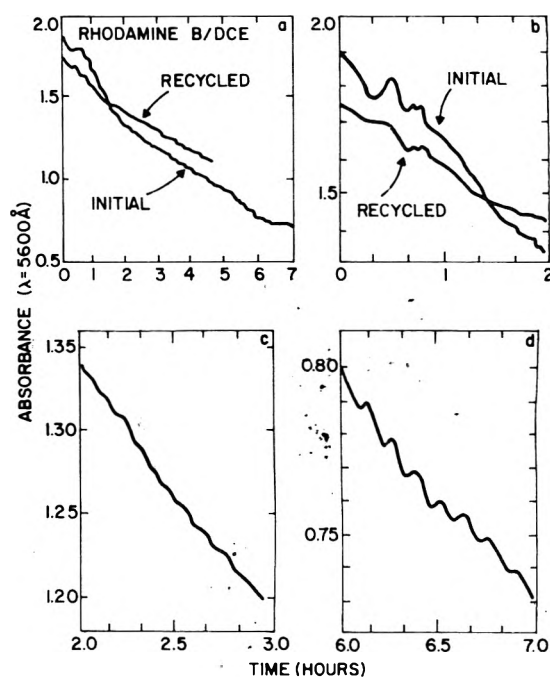

Figure 1. Absorbance (5600 Å) vs. time for the rhodamine B/DCE solutions which exhibited oscillatory fading. (a) Oscillations in the initial and "recycled" solutions for the full period of monitoring. (b-d) are expanded portions of (a) showing the detailed structure of the waveforms.
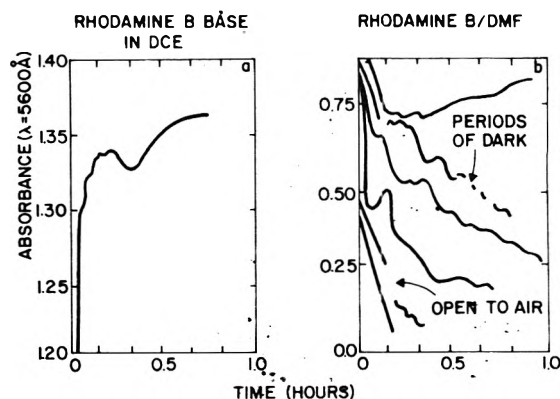

Figure 2. Absorbance (5600 Å) vs. time for the irradiated rhodamine B base/DCE and rhodamine B/DMF solutions. (a) The absolute absorbance subsequent to ~ 10-s irradiation of the colorless solution. (b) Typical fading behavior of the DMF solutions. The initial value for the absorbance in each solution has been arbitrarily displaced for ease in comparison.

absorption by the dye or energy transfer from some excited solvent species is eliminated by the fact that these relatively slow reactions proceed in the dark as well as in irradiated solvents. Also, there was no evidence of spatial phenomena in any of the solutions.[4] It was noted in several samples that fading was sensitive to exclusion of air, suggesting that a gaseous species is critical to the observed phenomena. Such observations in oscillating reactions are not unprecedented.[5] It has been reported that exclusion of oxygen from rhodamine B/acetone solutions leads directly to formation of the lactone and that acetone in acetonitrile, when properly deoxygenated and irradiated, can exhibit temporal fluctuations. Attempts to duplicate these results in acetone using only N_2 purging proved unsuccessful. Induction periods have been observed in other oscillating systems, as well as in solution photooxidation/reduction studies of similar xanthene dyes.[7,8] In the latter case this was interpreted as an oxygen consumption period. Distinctly different effects were induced

when the DMF and DCE systems were irradiated: a shift to the lactone occurred in DMF, while stabilization of the charged form resulted in DCE. It has been shown that DMF supports a lactone/dye equilibrium which is dependent on concentration and hydrogen bonding impurities.[1] In this study the species stabilizing the charged dye form may be actual organic additives, dissolved oxygen or ions inherent to the dye (H$^+$ or Cl$^-$). It is probable that photolysis of DMF yields a product which neutralizes the impurity. Photolysis of DCE, on the other hand, leads directly to ionic species which stabilize the charged dye form.[9] These differences in solvent properties may also explain why oscillations in DMF appear relatively insensitive to N$_2$ purging compared to DCE.

Further evidence that rhodamine B may not be the "source" of oscillations is contained in Figure 1. Close examination reveals that fading of rhodamine B in DCE was initially characterized by several large amplitude fluctuations. Distinctive periodic behavior was established during the third hour of reaction where a frequency of 12 cycles/h was obtained; while 4 h later a frequency of ~8 cycles/h was obtained. These oscillations appear superimposed on a larger and slower sinusoidal variation of ~0.25 cycles/h, decaying exponentially to some steady-state concentration. It has been shown in chemical systems that several species may simultaneously exhibit oscillating phenomena.[5] Also, it has been demonstrated that oscillations which contain both a rapid and a very slow variation may be the result of a beat frequency or projection phenomena derived from a bimolecular combination of intermediates oscillating at similar frequencies[10]

$$\phi_1(t) + \phi_2(t) \xrightarrow{k} C \xrightarrow{k'}$$
(1)

where $\phi_1(t) = A \sin \omega_1 t$ and $\phi_2(t) = B \cos \omega_2 t$. These forms represent excursions about the exponentially decaying quasi-steady-state concentration and, therefore, can exhibit negative values during part of the cycle. Solution of the kinetic equation for the time rate of change of C yields terms containing the sine and cosine of the sums and differences of the frequencies ω_1 and ω_2. Assuming, from Figure 1, that $\omega_1 + \omega_2 \simeq 8$ cycles/h and $\omega_1 - \omega_2 \simeq 0.25$ cycles/h gives ω_1 and ω_2 equal to 4.0 and 3.85 cycles/h, respectively. Assuming appropriate values for the constants,[10] the expression for C contains the main features of the oscillations observed for rhodamine B in DCE. This model, however, does not indicate the nature of the proposed intermediates and fails to describe either the apparent irregular large amplitude fluctuations observed in both DMF and DCE or the time dependent frequency of the established oscillations in the DCE solutions.

Further work is thus required to identify the various chemical species involved in these reactions which will lead to the mechanism responsible for the oscillatory phenomena.

References and Notes

(1) H. P. Lundgen and C. H. Binkley, *J. Polym. Sci.*, **14**, 139 (1954).
(2) B. Stevens and W. S. W. Bingham, *J. Soc. Dyers Colour.*, **79**, 632 (1963).
(3) M. Ikeda and S. Taguchi, *J. Photogr. Sci.*, **23**, 6 (1975).
(4) J. A. DeSimone, D. L. Beil, and L. E. Scriven, *Science*, **186**, 946 (1973).
(5) H. Degn, *Nature (London)*, **213**, 589 (1967).
(6) T. L. Nemzek and J. E. Guillet, *J. Am. Chem. Soc.*, **98**, 1032 (1976).
(7) M. Imamura and M. Koizumi, *Bull. Chem. Soc. Jpn.*, **29**, 899 (1956).
(8) Y. Usui, K. Itoh, and M. Koizumi, *Bull. Chem. Soc. Jpn.*, **38**, 1015 (1965).
(9) J. G. Calvert and J. N. Pitts, Jr., "Photochemistry", Wiley, New York, N.Y., 1966.
(10) J. Higgins, *Ind. Eng. Chem.*, **59**, 19 (1967).

Xerox Corporation   R. W. Bigelow
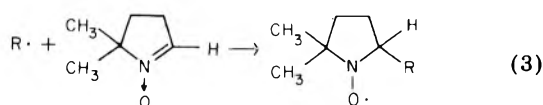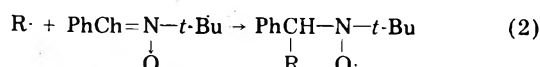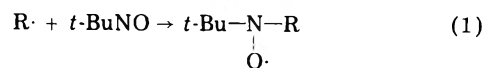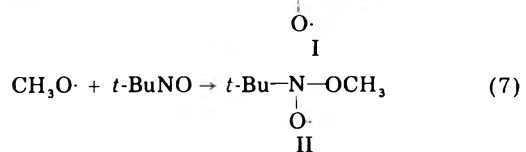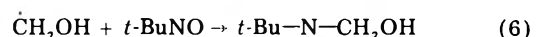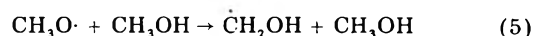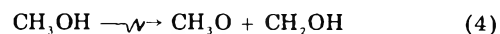Webster Research Center
Webster, New York   14580

An Estimate of the Rate of Spin Trapping of Methoxy Radicals by 2-Methyl-2-nitrosopropane (tert-Nitrosobutane)

Sir: The technique of spin trapping has been extensively used to determine reaction mechanisms involving free radicals.[1,2] The method involves the addition of the free radical to a nitrone or nitroso compound as in reactions 1–3 to produce a stable nitroxide, the electron spin resonance

$$R\cdot + t\text{-BuNO} \rightarrow t\text{-Bu}-\underset{\underset{O\cdot}{|}}{N}-R \qquad (1)$$

$$R\cdot + PhCh{=}N{-}t\text{-Bu} \rightarrow PhCH{-}\underset{\underset{O\cdot}{|}}{N}{-}t\text{-Bu} \qquad (2)$$

(3)

onance spectrum of which is characteristic of the radical trapped. The most commonly used trapping agents are 2-methyl-2-nitrosopropane, N-(tert-butyl)-α-phenyl nitrone, and 5,5-dimethylpyrroline 1-oxide (DMPO). The rates of addition to these compounds are not well established but have been estimated to be in the range of 10^3 to 5×10^8 M^{-1} s^{-1}. To place spin trapping on a more quantitative basis these rate constants must be determined for various radicals. In this communication, we estimate the rate of addition of methoxy radicals to t-BuNO by combining pulse radiolysis and spin trapping data. Recently we have used t-BuNO to trap, identify, and measure the yields of radicals produced in the radiolysis of alcohols.[3-5] In methanol, both $\dot{C}H_2OH$ and $CH_3O\cdot$ were trapped and the relative yields of the nitroxides I and II resulting from reactions 4–7 were measured[5] during radiolysis

$$CH_3OH \xrightarrow{\sim\hspace{-2pt}\sim} CH_3O + CH_2OH \qquad (4)$$

$$CH_3O\cdot + CH_3OH \rightarrow \dot{C}H_2OH + CH_3OH \qquad (5)$$

$$\dot{C}H_2OH + t\text{-BuNO} \rightarrow t\text{-Bu}-\underset{\underset{O\cdot}{|}}{N}-CH_2OH \qquad (6)$$
$$I$$

$$CH_3O\cdot + t\text{-BuNO} \rightarrow t\text{-Bu}-\underset{\underset{O\cdot}{|}}{N}-OCH_3 \qquad (7)$$
$$II$$

diolysis with 3-MeV electrons at ~45 °C. The plot of [I]/[II] vs. [t-BuNO]$^{-1}$ was a straight line (Figure 1) consistent with the reaction scheme 4–7. This simple competition for CH$_3$O· leads to the following expression where G_0 refers to the initial radiation chemical yields:

$$\frac{[I]}{[II]} = \frac{k_5[CH_3OH]}{k_7[t\text{-BuNO}]}\left[1 + \frac{G_0(\dot{C}H_2OH)}{G_0(CH_3O\cdot)}\right] + \frac{G_0(\dot{C}H_2OH)}{G_0(CH_3O\cdot)} \qquad (8)$$
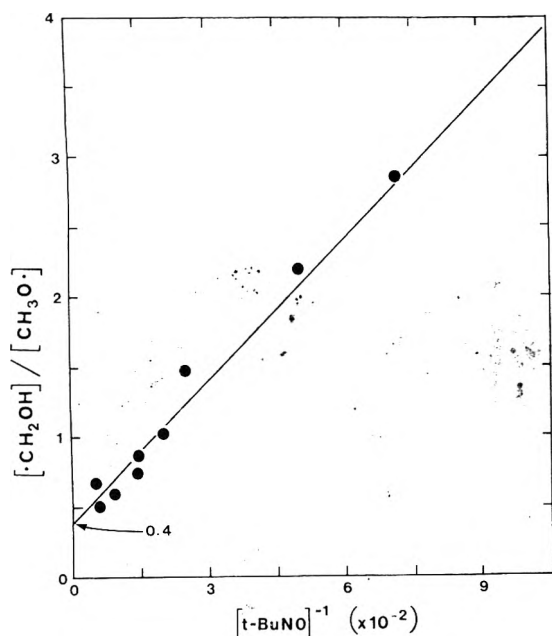
Figure 1. The ratio of yields of CH_2OH and $CH_3O\cdot$ trapped by t-BuNO for in situ irradiated methanol solutions at -45 °C.

Substituting the slope, 3.3×10^{-3}, of the line in Figure 1 and the intercept of 0.4 in the above expression gives

$$k_7 = 424 k_5 [CH_3OH] \qquad (9)$$

To obtain the rate constant for spin trapping of methoxy radicals we need to know k_5. We have determined[6] the rate of reaction 5 at -45 °C by a pulse radiolysis method using the competitive reaction 10 and by monitoring the buildup

$$CH_3O\cdot + TMPD \rightarrow TMPD^+ + CH_3O^- \qquad (10)$$

of the N,N,N',N'-tetramethylphenylenediamine cation, $TMPD^+$, absorption at 565 nm.[7,8] Deaerated solutions of TMPD in methanol were pulse irradiated at -45 °C and the buildup of $TMPD^+$ observed following the 50-ns pulse of 3-MeV electrons. The buildup was exponential and the rate constant, k_{obsd}, was a linear function of the TMPD concentration:

$$k_{obsd} = k_5[CH_3OH] + k_{10}[TMPD] \qquad (11)$$

Plots of k_{obsd} vs. [TMPD] gave an intercept of 3×10^5 corresponding to $k_5[CH_3OH]$. Substituting this in eq 9 leads to a value of 1.3×10^8 M^{-1} s^{-1} for k_7. This is much greater than the rate constant found by Janzen and Evans[9] for the trapping of $tert$-butoxy radicals. However, their value of 1.5×10^6 M^{-1} s^{-1} can be regarded only as a lower limit since it was deduced from the rate of buildup of nitroxides from t-BuNO and DMPO and the $tert$-butoxy adduct of t-BuNO is known to be unstable at ambient temperatures.[1,10] It is also most probable that the rate of addition of methoxy radicals will be higher than that for butoxy due to steric considerations.

Pulse radiolysis experiments using both spectrophotometric and ESR detection are in progress which will compare the rate of spin trapping of radicals with reactions having well-established rate constants.

References and Notes

(1) E. G. Janzen, Acc. Chem. Res., **4**, 31 (1971).
(2) C. Lagercrantz, J. Phys. Chem., **75**, 3466 (1971).
(3) F. P. Sargent, E. M. Gardy, and H. R. Falle, Chem. Phys. Lett., **24**, 120 (1974).
(4) F. P. Sargent and E. M. Gardy, Can. J. Chem., **52**, 3645 (1974).
(5) F. P. Sargent and E. M. Gardy, J. Phys. Chem., **80**, 854 (1976).

(6) Unpublished results presented in part at the 58th Canadian Chemical Conference (CIC) May 1975 Toronto, "The Energy of Activation for the Reaction of Methoxy Radicals with Methanol in Solution". A pulse radiolysis method by F. P. Sargent, R. S Dixon, E. M. Gardy, and V. J. Lopata.
(7) F. S. Dainton, I. Janovsky, and G. A. Salmon, Proc. R. Soc. London, Ser. A, **327**, 305 (1972).
(8) D. H. Ellison, G. A. Salmon, and F. Wilkinson, Proc. R. Soc. London, Ser. A, **328**, 23 (1972).
(9) E. G. Janzen and C. A. Evans, J. Am. Chem. Soc., **95**, 8205 (1973).
(10) M. J. Perkins and B. P. Roberts, J. Chem. Soc., Perkin Trans. 2, 297 (1974).

Research Chemistry Branch Whiteshell   **Frederick Peter Sargent**
   Nuclear Research Establishment
Atomic Energy of Canada Limited
Pinawa, Manitoba, ROE 1L0, Canada

Intermediates of the Hydrogenation of α-Olefins on a MoS$_2$ Catalyst

Sir: So far, the structure of the intermediates of the hydrogenation reaction of olefins has been deduced from the hydrogen exchange reaction between D_2 and olefins assuming that the hydrogenation and the hydrogen exchange reactions occur via a common intermediate. The intermediate of the hydrogenation of olefins, however, is not always identical with that of the exchange reaction even if the exchange reaction proceeds by the associative mechanism.

The authors have confirmed that hydrogenation of olefins and hydrogen mixing of olefins proceed independently on the MoS$_2$ catalyst, which contains different kinds of active sites, and have inferred that the hydrogenation reaction takes place on the sites (C) having three degrees of coordinative unsaturation, while the hydrogen mixing of olefins, as well as the isomerization reaction, proceed on sites having two degrees of coordinative unsaturation to which one hydrogen atom is coordinated (BH sites).[2-4] The α-olefins such as propene and but-1-ene undergo especially rapid mutual hydrogen exchange of the vinylic hydrogens on BH sites, and microwave spectroscopic analysis of the propene-d_1 and the but-1-ene-d_1 formed in the exchange reaction between d_0 and perdeuterio olefins strongly suggests an associative mechanism via the half-hydrogenated intermediate. The ratio of olefin-2-d_1, $C=C(D)$—R, to olefin-1-d_1, $DC=C$—R, suggests that the n-alkyl intermediate is formed preferentially over the isoalkyl intermediate in the vinylic hydrogen exchange on BH sites; the amount of n-alkyl is about 70% and the isoalkyl intermediate is 30% for both propene and but-1-ene.[5]

Under such circumstances, it is difficult to deduce the structure of the intermediate of the hydrogenation reaction of the α-olefins from the results of the exchange reaction. A new method, based upon the determination of the orientation of HD addition,[6] appears promising. It has been established that the molecular identity of hydrogen is conserved to about 85% in the hydrogenation of olefins on the MoS$_2$ catalyst,[7] and that the slow step of the hydrogenation reaction seems to be the addition of the first hydrogen to form the σ-alkyl intermediate. Accordingly, the ratio of alkane-2-d_1 to alkane-1-d_1 will be determined by the σ-alkyl intermediate formed as illustrated in the following scheme for the formation of the isoalkyl intermediate:
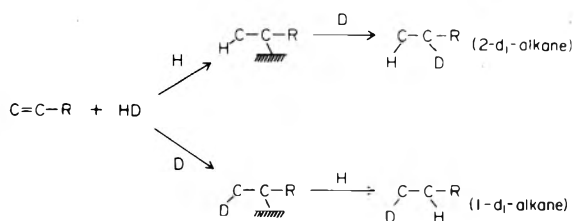
If the hydrogenation reaction proceeds through the isoalkyl intermediate, the value of the ratio of alkane-2-d_1/alkane-1-d_1 will become larger than unity due to the kinetic isotope effect. On the contrary, the ratio will be smaller than unity for hydrogenation through the n-alkyl intermediate. Furthermore, if the orientation of HD addition is caused by the above mechanism, the alkane-2-d_1/alkane-1-d_1 ratio should agree with the isotope effect observed in the reaction with H_2 and D_2, alkane-d_0/alkane-d_2.

The hydrogenations of propene and but-1-ene with HD (H_2; 2%, HD; 98%, D_2; 0%) were carried out on the MoS_2 catalyst at room temperature. The pretreatment and the physical properties of the catalyst were described in a previous paper.[3] The results obtained in the separate experiments are summarized in Figure 1, where the correction of 85% conservation in the HD addition was made. In these experiments, the analysis of the geometrical isomers of the propane-d_1, that is, propane-1-d_1 and -2-d_1, was carried out by microwave spectroscopy, and the analysis of butane-2-d_1 and -1-d_1 was performed with a mass spectrometer by combining the deuterium distribution of butane and that of the fragment ion formed by splitting off the methyl group. In the isotope effect calculation of the H_2 and D_2 addition reaction, the correction was made for the alkane-d_2 formed from the reaction of the olefin-d_1 with HD. The corrected values of alkane-d_0/alkane-d_2 ratio were divided by the H_2/D_2 ratio during reaction to give the isotope effect, since the reaction showed first-order dependence on the hydrogen pressure. As shown in Figure 1, the isotope effects obtained by this procedure agree reasonably well with the ratios of the two isomers, alkane-2-d_1/alkane-1-d_1, and the values are apparently larger than unity for both propene and but-1-ene. As propane has very a small dipole moment (0.08 D), the accuracy of the analysis is not as high as for propene, however, the results of this paper clearly indicate that the hydrogenation of the α-olefins taking place on the C sites proceeds
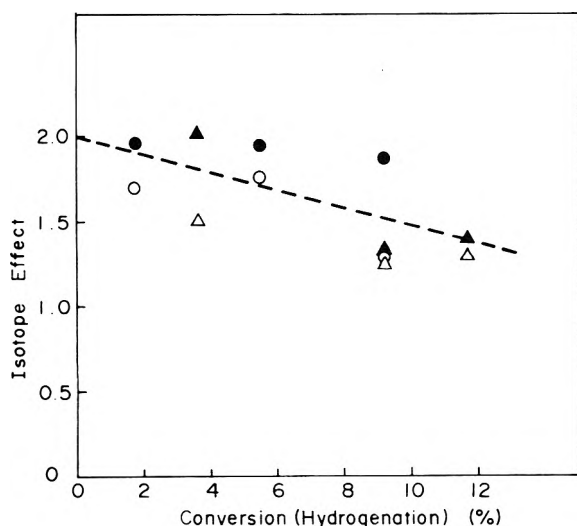

Figure 1. Isotope effects in the hydrogenation of α-olefins with H_2 and D_2, (d_0/d_2), and the orientation of HD addition, (2-d_1)/(1-d_1): (O) propane-d_0/propane-d_2; (●) propane-2-d_1/propane-1-d_1; (△) butane-d_0/butane-d_2; (▲) butane-2-d_1/butane-1-d_1.

through the isoalkyl intermediates, while the hydrogen exchange reaction on the BH sites prefer the n-alkyl intermediates. These differences in the intermediates may be due to differences in the structural environment of the active sites at which they are formed. These results call to mind the findings that show the size of the ligands in nickel complexes determines the proportion of n-propyl to isopropyl nickel complex in the dimerization of propylene.[8]

References and Notes

(1) Sagami Chemical Research Center, Nishi Ohnuma, Sagamihara-shi, Kanagawa, Japan.
(2) A. Takeuchi, K. Tanaka, and K. Miyahara, *Chem. Lett.*, 171, 411 (1974); *J. Catal.*, 40, 101 (1975); A. Takeuchi, K. Tanaka, I. Toyoshima, and K. Miyahara, *ibid.*, 40, 94 (1975).
(3) T. Okuhara. S. Sato, K. Tanaka, and K. Miyahara, *J. Catal.*, 43, 360 (1976).
(4) S. Siegel, *J. Catal.*, 30, 139 (1973).
(5) T. Okuhara and K. Tanaka, *J. Am. Chem. Soc.*, in press.
(6) T. Okuhara, T. Kondo, and K. Tanaka, *Chem. Lett.*, 717 (1976); T. Okuhara and K. Tanaka, *J. Chem. Soc., Chem. Commun.*, 199 (1976).
(7) T. Okuhara, K. Tanaka, and K. Miyahara, *J. Chem. Soc., Chem. Commun.*, 42 (1976).
(8) B. Bogdanovic, B. Henc, H-G. Karmann, H-G. Nussel, D. Walter, and G. Wilke, *Ind. Eng. Chem.*, 62, No. 12, 34 (1970).

Research Institute for Catalysis   Toshio Okuhara
Hokkaido University   Toshihiko Kondo[1]
Sapporo, Japan   Ken-ichi Tanaka*
                         Koshiro Miyahara

The Analogy between Temperature Dependent Radiation Effects in Alkali Halide Crystals and Crystalline Ammonia

Sir: Pikaev, Ershov, and Makarov recently reported in this journal[1] the characteristic shape of Arrhenius-type dependence for F-centers slow part (milisecond) decay in alkali halide crystals irradiated at different temperatures (Figure 1 insert). The decay rate is constant when the temperature is below the limiting value (T_{lim}) and exhibits constant activation energy (E_A) at temperatures above T_{lim} up to the melting point.

We have observed a similar dependence for crystalline ammonia radiolysis yields (H_2 and N_2) in the temperature range from 77 to 195 K (ammonia melting point) with a limiting value of 105 K for N_2 and 119 K for H_2 (Figure 1). The coincidence between Pikaev and our data does not seem to be formal and there are indications showing a closer analogy between these two cases.

(1) Both solid ammonia and alkali halides are typical face-centered cubic crystals with movement of extended defects (dislocations, glide planes) governed by temperature increase.[2]

(2) The Frenkel type excitons |e$^-$–h$^+$| are most probably the primary species formed by irradiation in both cases.

(3) The F-centers slow part decay in alkali halides occurs due to their recombination with hole centers (perhaps in form of aggregated centers). A postulated mechanism for the observed crystalline ammonia high radiolysis yields involves electron–hole pair recombination with formation of an excited ammonia molecule yielding H_2 and N_2 via a diimide (N_2H_2) precursor.[3,4]

(4) Both solids heavily irradiated produce gas-filled microbubbles due to vacancy aggregation inside the crystal.[5,6]

TABLE I

	T_M, K	E_{lat}, kcal mol^{-1}	T_{lim}, K	E_A, kcal mol^{-1}	E_A/E_{lat}	T_{lim}/T_M
NaCl	1081	183.5[a]	623[c]	20.9[c]	0.114	0.58
KCl	1045	167.9[a]	523[c]	15.9[c]	0.095	0.50
KBr	1021	161.3[a]	473[c]	19.2[c]	0.119	0.46
CsI	894	142.5[a]	443[c]	25.6[c]	0.180	0.50
NH$_3$ (H$_2$ yield)	195.4	7.0[b]	119[d]	0.9[d]	0.129	0.61
NH$_3$ (N$_2$ yield)	195.4	7.0[b]	105[d]	1.2[d]	0.171	0.54

[a] Reference 7. [b] Reference 8. [c] Reference 1. [d] Value calculated from data in Figure 1.
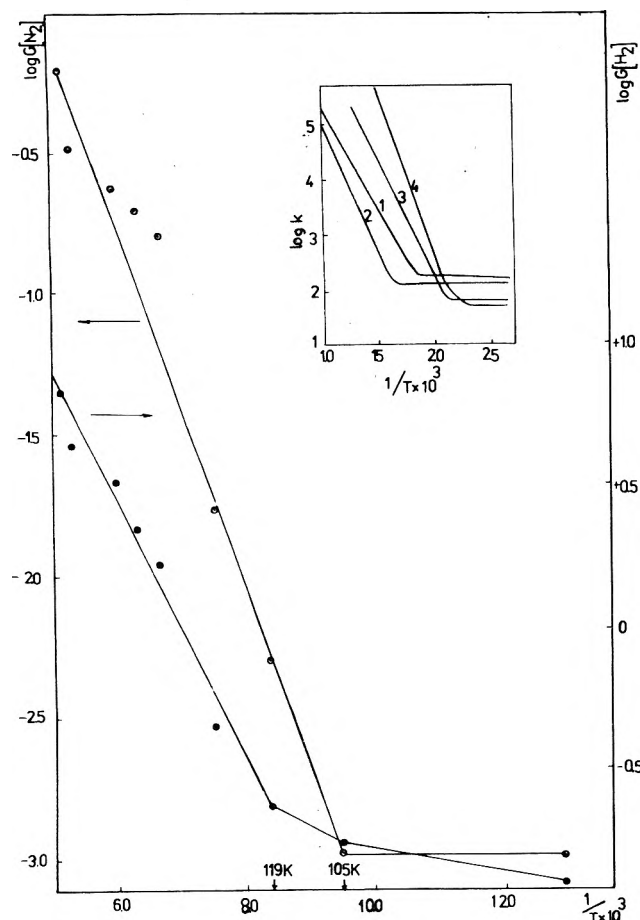
Figure 1. Arrhenius type dependence of crystalline ammonia radiolysis yields (H$_2$(●) and N$_2$(○)) on irradiation temperature. The insert shows the results[1] of Pikaev et al. for the similar Arrhenius type dependence of the F-centers decay in the alkali halide crystals: (1) KCl; (2) NaCl; (3) KBr; (4) CsI.

To check the analogy assumption, a comparison of T_{lim} and E_A for both cases was performed, taking into account the discrepancy in lattice energy (E_{lat}) and melting temperature (T_M). The calculated E_A/E_{lat} and T_{lim}/T_M ratios are shown in Table I.

The E_A/E_{lat} and T_{lim}/T_M for H$_2$ and N$_2$ formation during crystalline ammonia radiolysis fit into the scatter of results for different alkali halides although the energy of the ammonia lattice is only 4–5% of the alkali halides lattice energy. This fact seems to confirm the postulated analogy.

According to that, the temperature governed electron–hole recombination process in the fccub crystals is more influenced by the defects dynamics and the temperature disorder of crystal lattice than by the difference between ionic and molecular crystal character. It is likely that the neutral electron–hole pair may not distinguish between ionic and molecular lattices.

References and Notes

(1) A. Pikaev, B. G. Ershov, and I. E. Makarov, *J. Phys. Chem.*, **79**, 3025 (1975).
(2) A. I. Prokvatilov and D. N. Bolskutkin, *Fiz. Tverd. Tela*, **10**, 1218 (1968).
(3) A. Blum, *J. Chem. Soc., Faraday, Trans. 1*, **71**, 2299 (1975).
(4) A. Blum, *Int. J. Radiat. Phys. Chem.*, submitted for publication.
(5) L. W. Hobbs, A. E. Hughes, and D. Pooley, *Proc. R. Soc. London, Ser. A*, **332**, 167 (1973).
(6) We observed bubbles in transparent ammonia crystals irradiated at 193 K with a 13-MeV electron beam (5-μs pulses repeated 1 per second) from the liniac.
(7) P. Whaley, "Sodium, Potassium, Rubidium, Cesium and Francium, Comprehensive Inorganic Chemistry", Vol. 1, Pergamon Press, New York, N.Y., 1973, pp 410–412.
(8) A. F. Wells, "Structural Inorganic Chemistry", 4th ed, Clarendon Press, Oxford, 1975, p 249.

Institute of Nuclear Chemistry **A. Blum**
Department of Radiation Chemistry
Dorodna 16, 03-195 Warsaw, Poland

Responsible for environmental management and pollution control?

Here's how Environmental Science and Technology can help you!

ES&T brings you the *new technology*. These are the techniques to avoid contamination of air, water, and land. And it brings you up-to-the-minute information of the *economics, laws* and *feasibility* of many of these new techniques.

Utilizing the American Chemical Society's world-wide contacts, ES&T includes each month:

☐ Current government pollution legislation and guidelines.
☐ More efficient engineering techniques.
☐ Important fundamental research.
☐ First word of more productive equipment coming on the market.
☐ Case history studies of how others are overcoming the same problems as yours.

Complete the form and mail it back today. You can start benefiting from ES&T's coverage immediately!

AVAILABLE IN HARD COPY OR MICROFICHE.

Environmental Science & Technology
American Chemical Society   **1977**
1155 Sixteenth Street, N.W.
Washington, D.C. 20036

Yes . . . . I do want to subscribe to ES&T for the rate checked below:

	U.S.	PUAS	Canada and Foreign
ACS Member—1 Yr.	☐ $10.00	☐ $14.50	☐ $15.00
ACS Member—3 Yrs.	☐ $24.00	☐ $37.50	☐ $39.00
Nonmember (Personal)—1 Yr.	☐ $15.00	☐ $19.50	☐ $20.00
Nonmember (Personal)—3 Yrs.	☐ $36.00	☐ S49.50	☐ $51.00
Libraries, Institutions, Companies—1 Yr.	☐ $30.00	☐ S34.50	☐ $35.00

Name _____   Specific Title _____

Mailing Address ☐ Home ☐ Office _____

City _____   State _____   Zip _____

Billing Address _____

City _____   State _____   Zip _____

☐ Check enclosed   ☐ Bill Company   ☐ Bill Me   Allow 60 days for your first copy to be mailed.

1. Progress in Surface and Membrane Science

VOLUME 11

edited by D. A. CADENHEAD and J. F. DANIELLI
CONTENTS: *J. Koutecky*, Quantum Theory of Surface Phenomena.
E. B. Budevski, Some Fundamental Aspects of Electrocrystallization.
J. A. Ramsey, Exoelectric Emission. *G. D. Parfitt*, The Surface of
Titanium Dioxide. *W. Baumeister and M. Hahn*, Prospects for Atomic
Resolution Electron Microscopy in Membranology.
1976, 358 pp., $21.50/£ 15.25 ISBN: 0-12-571811-X

2. Atmospheric Chemistry

by JULIAN HEICKLEN

This marks one of the first major summaries of atmospheric
chemistry since Philip Leighton's highly acclaimed "Photochemistry
of Air Pollution." Although recent books have appeared on various
aspects of upper atmospheric chemistry, *Atmospheric Chemistry*
represents one of the first books to discuss both upper and lower
atmospheres, unifying them in such a way that obtains a compre-
hensive picture of the atmospheric chemical cycles. Topics covered
in this discussion include: the structure and chemistry of the at-
mosphere; pollutants in urban areas; emission rates, concentrations,
effects and influence on the chemistry of urban atmospheres; control
methods.
1976, 430 pp., $38.00/£27.00 ISBN: 0-12-336740-9

3. Theory of Simple Liquids

by JEAN-PIERRE HANSEN and IAN R. McDONALD

Recent years have shown an upsurge of interest in the statistical
mechanics of liquids which has been marked by a number of im-
portant advances. In discussing the present status of the theory, this
book emphasizes modern developments such as perturbation
methods (in equilibrium theory) and the ideas of generalized hy-
drodynamics (in the theory of transport processes). Since both au-
thors have a special interest in computer simulation, constant ref-
erence is made to this area, and one chapter is devoted to a de-
scription of the techniques of these calculations—so-called com-
puter 'experiments'. By and large, the work focuses on classical
one-component monatomic systems, known as the 'simple' liquids,
but attention is paid to aspects of the theory of molecular liquids,
liquid mixtures and quantum fluids. There are also sections on the
theory of charged liquids. Since the book is intended to be self-
contained, and a certain knowledge of statistical mechanics is re-
quired, an introductory chapter covers its basic theory; in addition,
the more difficult mathematical problems which arise are treated
in some detail.
1976, 412 pp., $29.75/£ 14.00 ISBN: 0-12-323850-1

Send payment with order and save postage plus 50¢ handling charge.
Prices are subject to change without notice.

Forensic Science

ACS Symposium Series No. 13

Geoffrey Davies, *Editor*

***A symposium sponsored by the Divisions of
Analytical Chemistry and Chemical Education
of the American Chemical Society.***

A fascinating volume that reflects the growing public
interest in forensic science as a key analytical tool in
establishing criminal guilt or innocence.

Nineteen chapters give an up-to-date status report on
educational preparation as well as new applications
and refinements of research techniques.

This wide-appeal book will be of special interest to
the analytical chemist, police officer, law enforcement
program head, college instructor, and general reader
alike, with its comprehensive coverage of the latest
developments in:

- forensic science education and research; LEAA's research
  program
- materials science methods; SEM analysis; bullet search
  systems; firearm residue detection; arson debris analysis;
  differential scanning calorimetry
- ink, bloodstain, and physiological fluid analysis; forensic
  toxicology; heroin sample comparison

204 pages (May 1975) $17.95 clothbound